frontiers | Research Topics

DAMP-sensing pattern recognition receptors in digestive tract inflammatory responses

Edited by
Daming Zuo, Zhi-Bin Zhao, Chunqing Guo and Jingbo Wang

Published in
Frontiers in Immunology

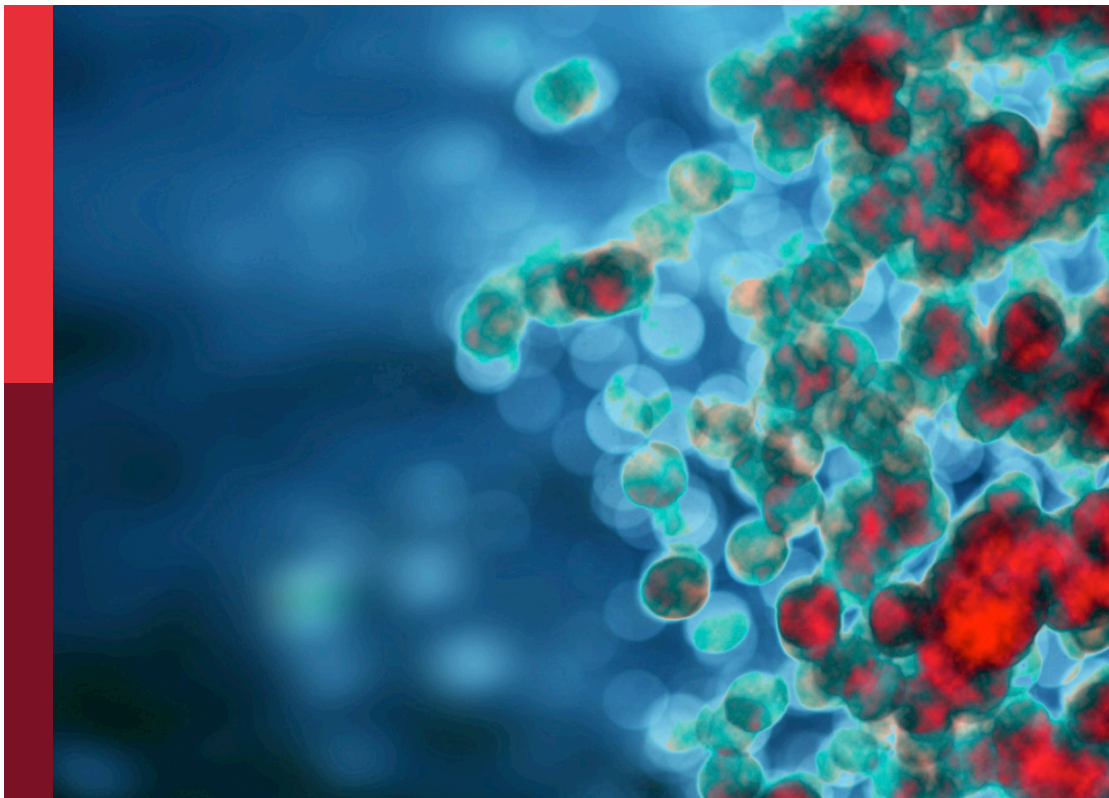

ISSN 1664-8714
ISBN 978-2-83251-163-3
DOI 10.3389/978-2-83251-163-3

About Frontiers

Frontiers is more than just an open access publisher of scholarly articles: it is a pioneering approach to the world of academia, radically improving the way scholarly research is managed. The grand vision of Frontiers is a world where all people have an equal opportunity to seek, share and generate knowledge. Frontiers provides immediate and permanent online open access to all its publications, but this alone is not enough to realize our grand goals.

Frontiers journal series

The Frontiers journal series is a multi-tier and interdisciplinary set of open-access, online journals, promising a paradigm shift from the current review, selection and dissemination processes in academic publishing. All Frontiers journals are driven by researchers for researchers; therefore, they constitute a service to the scholarly community. At the same time, the *Frontiers journal series* operates on a revolutionary invention, the tiered publishing system, initially addressing specific communities of scholars, and gradually climbing up to broader public understanding, thus serving the interests of the lay society, too.

Dedication to quality

Each Frontiers article is a landmark of the highest quality, thanks to genuinely collaborative interactions between authors and review editors, who include some of the world's best academicians. Research must be certified by peers before entering a stream of knowledge that may eventually reach the public - and shape society; therefore, Frontiers only applies the most rigorous and unbiased reviews. Frontiers revolutionizes research publishing by freely delivering the most outstanding research, evaluated with no bias from both the academic and social point of view. By applying the most advanced information technologies, Frontiers is catapulting scholarly publishing into a new generation.

What are Frontiers Research Topics?

Frontiers Research Topics are very popular trademarks of the *Frontiers journals series*: they are collections of at least ten articles, all centered on a particular subject. With their unique mix of varied contributions from Original Research to Review Articles, Frontiers Research Topics unify the most influential researchers, the latest key findings and historical advances in a hot research area.

Find out more on how to host your own Frontiers Research Topic or contribute to one as an author by contacting the Frontiers editorial office: frontiersin.org/about/contact

DAMP-sensing pattern recognition receptors in digestive tract inflammatory responses

Topic editors

Daming Zuo — Southern Medical University, China
Zhi-Bin Zhao — Guangdong Provincial People's Hospital, China
Chunqing Guo — Virginia Commonwealth University, United States
Jingbo Wang — Fourth Military Medical University, China

Citation

Zuo, D., Zhao, Z.-B., Guo, C., Wang, J., eds. (2023). *DAMP-sensing pattern recognition receptors in digestive tract inflammatory responses*. Lausanne: Frontiers Media SA. doi: 10.3389/978-2-83251-163-3

Table of contents

frontiers in Immunology

ORIGINAL RESEARCH
published: 24 January 2022
doi: 10.3389/fimmu.2022.816037

Neutrophils Culture in Collagen Gel System

*Ru Li[1], Ziqing Wang[1], Junhao Huang[1], Sixiao He[1], Yanmei Peng[2], Yong Wan[3] and Qiang Ma[1]**

[1] Department of Biopharmaceutics, School of Laboratory Medicine and Biotechnology, Southern Medical University, Guangzhou, China, [2] Department of General Surgery, Nanfang Hospital, Southern Medical University, Guangzhou, China, [3] Research and Development Department, Guangzhou Darui Biotechnology Co., Ltd, Guangzhou, China

Neutrophils (Neu) migrate rapidly to damaged tissue and play critical roles in host defense and tissue homeostasis, including the intestinal epithelia injuries and immune responses. Although their important roles in these diseases, they are challenging to study due to their short life span and the inability to cryopreserve or expand them *in vitro*. Moreover, the standard cell culturing on plastic plates (two-dimensional (2D) cultures) does not represent the actual microenvironment where cells reside in tissues. In this study, we developed a new three-dimensional (3D) culture system for human and mouse peripheral blood Neu, which is made of hydrogel. The Neu showed much better cell integrity and less cell debris in the 3D culture system compared to that in 2D culture system. Moreover, the 3D culture system was more suitable for the observation of neutrophil extracellular traps (NETs) stimulated by the classical stimulation phorbol ester (PMA), and other damage associated molecular patterns (DAMPs) such as Lipopolysaccharide (LPS)/ATP, interleukin-1 β (IL-1β) and tumor necrosis factor α (TNFα) than the 2D culture system. Moreover, NETs phenomenon in 3D culture system is similar to that *in vivo*. In addition, the 3D culture system was evaluated to co-culturing Neu and other parenchymal cells, such as colon mucosal epithelial cell lines. In conclusion, the 3D culture system could maintain better properties of Neu than that in 2D culture system and it may reduce the gap between *in vitro* an *in vivo* experimentations.

Keywords: neutrophils, 3D culture system, hydrogel, NETs, co-culture

OPEN ACCESS

Edited by:
Zhi-Bin Zhao, Guangdong Provincial People's Hospital, China

Reviewed by:
Wei Zhu, South China University of Technology, China
Federica Foglietta, University of Turin, Italy
Yuan Ping, Zhejiang University, China

***Correspondence:**
Qiang Ma
mq@smu.edu.cn

Specialty section:
This article was submitted to Molecular Innate Immunity, a section of the journal Frontiers in Immunology

Received: *16 November 2021*
Accepted: *03 January 2022*
Published: *24 January 2022*

Citation:
Li R, Wang Z, Huang J, He S, Peng Y, Wan Y and Ma Q (2022) Neutrophils Culture in Collagen Gel System. Front. Immunol. 13:816037. doi: 10.3389/fimmu.2022.816037

INTRODUCTION

Neu play crucial roles in elimination of pathogens and damaged tissue and cells, Neu depletion exacerbated colitis in the intestinal epithelia injury mode, and it plays a critical role in regulating the intestinal immune responses (1, 2). Once the Neu enters the tissue, it kills the bacteria through degranulation, phagocytosis, or extracellular traps (3, 4) that release DNA strands and bactericidal proteins. Although their important roles in these diseases, Neu have a relatively short lifespan and they will undergo apoptosis within 24 hours *in vivo* (5, 6). Moreover, the research on Neu is mainly based on fresh isolation (3), but they can only be kept alive within a short time frame *in vitro* (7). So prolonging the survival time of Neu and maintaining their activity *in vitro* is thus an important and urgent challenge (8).

The classical 2D monolayer cell culturing on flat and rigid substrate is a prevalent model system used to study immunological processes *in vitro*. But the 2D system was challenged in recent years by findings from the studies which revealed that the 2D-cultured cells are unable to simulate the exact phenomena observed *in vivo*, including topography, mechanics, and hierarchical tissue assembly, possibly resulting in non-physiological cell behavior (9–12). The drawbacks of the 2D system are also related to the investigations of inflammatory processes. During inflammation, Neu infiltrate tissues where they perform their effector functions. The tissues are three-dimensional and thus performance of the cells might also be different than in the 2D conditions (13). Some scholars have studied the 3D culture of neutrophil-like cell line HL-60 or primary Neu co-culture with other cells in collagen gels for improve the viability of Neu (12, 14–16), however, the detailed phenomena of Neu in 3D culturing system have never evaluated.

Hydrogels are composed of cross-linked hydrophilic polymer chains and can be used to form a scaffold for the construction of three-dimensional cell culture models. They are in a liquid state at 4°C and solidify at 37°C. They have good permeability, allowing a variety of nutrients, gases, and metabolites to pass through them freely and resembling the extracellular environment of the body's tissues (17). The exiting studies have showed that the hydrogels were used for hepatocytes, cardiac cells, breast cancer cells, islet beta-cells, and colon cancer cells culturing (15, 18–22), and for organoid culture, providing models for disease research (23–26), however, the 3D culture system has never been used to cultivate Neu.

In this study, we have established their 3D culturing system with hydrogels and evaluated the detailed phenomena of Neu. We cultured human and mouse derived peripheral blood Neu in the 3D hydrogel, demonstrating better morphological activity, oxidation, more chemotaxis, higher activity and more generation of NETs with incubation in PMA, LPS/ATP, IL-1β and TNFα than those in 2D culture system. Furthermore, when stimulated by PMA, Neu exhibited still better NETs characteristics, similar to those seen in animal experiments. When co-cultured with colon mucosal epithelial cell lines, Neu could still maintain good characteristics, which provides a model for studying the inflammation of skeletal muscle innate immunity. Overall, the results suggest that this 3D system is suitable for culturing Neu, hoping to provide convenient simulation for *in vitro* studies on Neu.

MATERIALS AND METHODS

Reagents

Adult male C57BL/6 mice, 8–10 weeks of age, were purchased from the Guangdong Medical Laboratory Animal Center (Guangzhou, China). The animals were housed in the animal center of the Southern Medical University, according to the criteria outlined in the Institutional Animal Care and Utilization Committee (IACUC). The mice (4 per cage) were housed under controlled environmental conditions (12 h light/dark cycle, 55% ± 5% humidity, 23°C ambient temperature) with free access to standard chow and water. All experimental protocols involving animals were approved by the Animal Care and Use Committee of the Southern Medical University in accordance with the Guide for the Care and Use of Laboratory Animals of the National Institutes of Health.

The hydrogel we got was Nitta Gelatin's Type I collagen, and the concentrated medium was composed of Ham's F-12 medium, MEM with Hanks' balanced salt solution DF medium (DME: F-12 = 1: 1) and Medium 199, reconstitution buffer was composed of sodium hydroxide (50 mM), sodium bicarbonate (260 mM) and HEPES (200 mM). I-PC and I-AC collagen were purchased from KOKEN. Collagen type I was purchased from Sigma. Cells disperse enzymes from Kit for Cell Premedium which were gifts from DARUI BIO (Guangzhou, China). EGTA (Cat#324626) was purchased from Merk. PMA was purchased from Sigma-Aldrich. MTT assay kit (KGA312)was purchased from Keygenbiotech. The apoptosis kit (Cat#70-AP101) was purchased from MultiSciences. Z-VAD-FMK (V116) was purchased from Sigma and WKYMVm (ab141811), LY6G-APC-750 antibody (ab46754) and NE (ab68672) were purchased from Abcam. Quant-iT™ PicoGreen™ dsDNA Reagent, SYTOX® green nucleic acid stain (S7020), SYTO® 13 (S7575) and CD11b-FITC antibody (53-0112-82) were purchased from Invitrogen. Tubulin beta antibody (AF7011) was purchased from Affinity Biosciences. DNA ladder detection kit (KGA112) was purchased from Keygenbiotech. Dextran T-500 (D8270) was purchased from Solarbio. SuperRed/GelRed (BS354B) was purchased from Biosharp Life Science and DNA marker was purchased from Dongsheng Biotech.

Murine Bone Marrow Neu Isolation

Neu were obtained from mouse bone marrow according to standard techniques. Briefly, mice were sacrificed by cervical dissection, the femur and tibia of the mice were taken, and the end of the bone was excised and the medullary cavity exposed, followed by the bone being washed with phosphate-buffered saline (PBS) with an 1 mL syringe and a 27-gauge needle, three times per bone. The washed suspension was filtered through a 100 μm filter, centrifuged at 400 xg for 10 min, and resuspended in 1 mL PBS. A Percoll stock solution (9 mL Percoll, 1 mL 9% NaCl) was diluted with 0.9% NaCl to give 54%, 64%, and 72% Percoll working solutions. After centrifugation (1000 xg, 30 min), the interface between the 64% and 72% layers containing Neu was harvested, with purity more than 95%.

Mouse Peripheral Blood Neu Isolation

Mouse peripheral blood Neu were isolated from peripheral blood by density gradient centrifugation (Beijing Solarbio, P9201). Briefly, heparinized blood was sedimented with 6% dextran T500 in PBS for 30 min at 37°C, the top clear layer containing leukocytes was transferred to a fresh tube and the cells were underlaid with 2 mL of Agent C in the middle and Agent A down here, and centrifuged at 1000 xg for 30 min. Neu between Agent A and C were obtained, resulting in cell populations containing at least 90% Neu.

Human Peripheral Blood Neu Isolation

Human blood was taken from healthy individuals following informed and written consent in a qualified institution. Human Neu were isolated from peripheral blood by density gradient centrifugation. Briefly, heparinized blood was sedimented with 6% dextran T500 in PBS for 30 min at 37°C, the top clear layer containing leukocytes was transferred to a fresh tube and the cells were underlaid with 10 mL of Ficoll Paque Plus, and centrifuged at 750 xg for 20 min. The Neu and erythrocytes were treated erythrocyte lysis solution (155 mM NH_4Cl, 10 mM $KHCO_3$, 0.1 mM EDTA, pH 7.3), resulting in cell populations containing at least 95% Neu.

Gel Transparency and Adhesion Evaluation

To prepare a hydrogel for the 3D culture system, 0.1 mL of concentrated medium was added to the cooled 0.8 mL of Cellmatrix type I collagen which was at pH 3 with a concentration of 3 mg/mL on ice, mixing well to become light yellow, then additional 0.1 mL of reconstitution buffer was mixed well to become light pink. Last, the mixture was added to the six-well plate (100 μL/well), which was then was placed in a 37°C incubator for 45 min, followed by culture at 37°C in 2 mL of complete medium containing 10% FBS. For comparison, I-PC collagen and I-AC collagen from KOKEN and Collagen type I from Sigma were executed in the same way. In order to evaluate the transparency of the gel, we observed and compared the transparency of the four collagen. In order to evaluate the adhesion of the gel, we placed the six-well plate on a horizontal shaker and oscillated for 1 hour at a rotation speed of 100 rpm/min and observe whether the glue drops in the wells of the plate fell off.

Cell Culture

To prepare a hydrogel for the 3D culture system, human Normal-Derived Colon Mucosa (NCM) Cell Lines NCM460 or mouse skeletal muscle cells C2C12 (2.5×10^6/mL each) together with corresponding species Neu or Neu alone were mixed in 0.8 mL hydrogel, 0.1 mL buffer, and 0.1 mL 10 x fetal bovine serum (FBS) on ice. The gel was placed in a six-well plate (100 μL/well), which was then was placed in a 37°C incubator for 45 min, followed by culture at 37°C in complete medium containing 10% FBS. For the 2D culture system, Neu together with NCM460 or C2C12 were cultured according to traditional culture methods.

If digestion needed, the hydrogel was washed once with pre-chilled neutral PBS and incubated with cell dispersase (diluted 10-fold with basic medium) at 37°C incubator for about 30 min until the hydrogel was completely digested. Finally, the digestion was stopped with the same amount of complete medium. After remove the supernatant at 250 xg for 5 min centrifugation, we stopped digestion again with 5 mL of 0.38 mg/mL EGTA and centrifuge at 250 xg for 5 min to obtain cell pellets.

MTT Assay

The MTT colorimetric method was used to measure cell viability to quantify cells in small droplets of collagen. According to the standard operation in the manual, 100 μL per well (about 1×10^5) of cells for 2D culture and 3D culture (2 μL of collagen) were added to a 96-well plate, and incubated in a 37°C with 5% CO_2 cell incubator for 24 h. The Neu cultured in hydrogel system were digested and then suspended in 100 μL medium. Then 5 × MTT was diluted to 1 × MTT by Dilution Buffer. Followed by adding 50 μL 1 × MTT to each well and incubating at 37°C for 4 h to reduce MTT to formazan. After the supernatant was aspirated, 150 μL of DMSO were added to each well to dissolve formazan, and shaked well with a plate shaker. The microplate reader detected the optical density of each well at a wavelength of 490 nm.

Analysis of Cell Activity and Nuclear Morphology

Human or mouse peripheral blood Neu ($5 \times 10^{6/}$mL) were cultured for 6 days in 2D and 3D culture systems with or without the inhibition of apoptosis z-vad-fmk (10 μM), stained with PI at room temperature in the dark for 15 min, and stained then with SYTO 13 for 15 min. The cells were washed twice with PBS, examined and immediately photographed under a fluorescence microscope. Dead cells were defined on the basis of positive PI staining and nuclear morphology changes such as chromatin condensation and fragmentation.

Isolation of Genomic DNA and Gel Electrophoresis

Genomic DNA was isolated from mouse Neu according to the manufacturer's protocol (DNA ladder detection kit, Keygenbiotech). Briefly, 5×10^5 cells collected by centrifugation at 280 xg for 5min were treated with 50 μL lytic buffer and mixed vigorously, followed by added 5 μL RNase A (37°C, 30 min) and proteinase K (50°C,1 h). DNA in the aqueous phase was precipitated at -20°C in 40 μL sodium acetate and 200 μL 100% ethanol. Precipitates were pelleted by centrifugation (12,000 xg, 10 min, 4°C), washed with ice-cold 70% ethanol, and dried.

For electrophoresis, DNA samples were dissolved in 10 μL of Tris-EDTA buffer. Gel loading buffer was added, and the samples were subjected to electrophoresis in 2% agarose gel containing SuperRed/GelRed (1:10000) at 4 V/cm for 2 h. DNA was visualized by UV light and photographed. The analyzed DNA fragments in the samples were compared with standard size fragments of the DNA marker LM1061.

ROS Measurements

For the detection of intracellular ROS level, ROS-sensitive probe H2DCFDA was used. Neu obtained from 2D culture system by direct centrifugation or 3D culture system by digestion (as shown in Cell Culture part) were incubated with 5 μM staining solution in PBS in the dark for 30 min at 37°C. Cells were centrifuged to remove supernatant, suspended in a fresh medium and immediately analyzed with flow cytometer (CytoFLEX, BECKMAN).

Detection of Chemotaxis

Migration assays were conducted using a 24-well Transwell chamber (Corning, New York, US) with 4 μm pores. One × 10^6

Neu cultured for 3 days in 2D and 3D culture systems were loaded (200 μL of a 5 × 10^6/mL solution) into the top chamber, with 300 μL WKYMVm (100 nM) for mouse peripheral blood Neu, fMLF (1 μM) for human peripheral blood Neu or DMEM contained 1% bovine serum albumin, as control, in the lower chamber, and then the assay system was incubated for 3 h at 37°C. Migrating cells dropped from the filters to the bottom of the lower chamber. After 350 xg for 10 min centrifugation, the cells on the chamber were counted in five fields (magnification × 200) using a light microscopy equipped with a image analyser.

Detection of NETs

Neu cultured in 2D and 3D systems for 3 days were stimulated with 20 μM PMA (1:810) for 4 h and then fixed with 4% paraformaldehyde for 15 min, permeabilized with 0.25% TritonX-100 for 10 min, blocked with PBS containing 5% bovine serum albumin for 1h, stained with NE (1:100), Sytox green (1:5000), DAPI (1:100), or SYTO 13 (1:5000) before being examined under a confocal or fluorescence microscope. To observe the production of NETs in live LPS-induced mice, we labeled Neu with LY6G-APC-750 (10 μg) and the DNA of NETs with Sytox green (10 nmol) *via* tail vein injection in advance, and NETs were observed under a two-photon fluorescence microscope (FV1200MPE, Olympus).

In order to determine the content of the above-mentioned NETs, dsDNA in the supernatants was evaluated by adding 100 μL Quant-iTTM PicoGreen®dsDNA Reagent (Invitrogen, 1:200 in 1× TE) to 100 μL sample as recommended by the manufacturer, followed by immediate measurement of fluorescence at 485 nm excitation, 520 nm emission with fluorescence plate reader FluoStar.

For the measurement of neutrophil elastase coupled dsDNA release, NE antibody (100 ng per well) was coated on the 96-well plate overnight, then 100 μL sample and 100 μL Quant-iTTM PicoGreen®dsDNA Reagent (Invitrogen, 1:200 in 1 × TE) were added as recommended by the manufacturer, followed by immediate measurement of fluorescence at 485 nm excitation, 520 nm emission with fluorescence plate reader FluoStar.

Statistical Analysis

Neu apoptosis and functional results are given as mean ± SD. Differences were analyzed by the Two-way ANOVA with Tukey post-test using Prism version 7 (GraphPad). A *p*-value of 0.05 was considered to indicate a significant difference.

RESULTS

Evaluation of Properties of the Cellmatrix Type I

As shown in **Figure 1**, we evaluated the performance of the gel and the Neu embedded in it. Cellmatrix type I collagen has been used to culture mesenchymal stem cells by other researchers before (27). We examined the characteristics of the four collagen gels before exploring the role of collagen gels in the cultivation of Neu. As shown in **Figure 2A**, the shape of the gel droplets were full and round hemispheres, obviously, Cellmatrix type I, I-AC and collagen type I showed better transparency, but I-PC did not, I-AC. Collagen type I was easy to fall off after shock, and the adhesion was poor. So we chose Cellmatrix type I for Neu culture to ensure we could observe the hydrogel with microscope.

The cytotoxicity of Cellmatrix type I collagen was evaluated by MTT assay to compare Neu activity after cultured in 2D culture medium or in 3D hydrogel with the same culture medium for 24 h. As shown in **Figure 2B**, there was no significant difference in Neu activity in 2D and 3D cultures after 24 h.

Morphology of the Fresh Neu in the 3D Culture System

Mouse peripheral blood Neu had round shape and were in a full state during the first day, but developed incomplete shapes with large amounts of cell debris on the second day in the 2D system. By contrast, cells remained intact in the 3D system (**Figure 2C**).

In order to evaluate the cell status more intuitively, we stained the human Neu nucleus with SYTO 13 which stained DNA in both live and dead eukaryotic cells and observed it under a fluorescence microscope (**Figure 2D**). Neu in all groups maintained intact multilobed nuclear structure on the first day, but nuclear condensation and loss of chromatin appeared on day2 in 2D culture system, while this phenomenon was not observed in the group with the addition of apoptosis inhibitor z-vad-fmk. Neu still had intact multilobed nuclear structure until day 4 in 3D culture system, which suggested that 3D culture may protect Neu from apoptosis.

Function of the Fresh Neu in the 3D Culture System

The intracellular ROS level was detected by the fluorescent probe H2DCFDA. As shown in **Figures 3A, B**, under the same LPS stimulation, 3D cultured mouse peripheral blood Neu produced more ROS than that in 2D culture system, although lower than the first day.

To evaluated the chemotaxis of Neu in 2D and 3D culture systems, we conducted the migration assays. As expected, Neu in 3D culture system migrated more to the lower chamber stimulated by WKYMVm (100 nM) for mouse peripheral blood Neu and fMLF (1 μM) for human peripheral blood Neu for 3 h than that in 2D culture (**Figures 3C, D**).

In addition, Neu capture microorganisms, activate myeloid cells, and promote coagulation through NETs, which contain chromatin decorated with specific proteins (28, 29). Studies have shown that Neu produced NETs when stimulated by PMA (30). As shown in **Figure 3E**, human peripheral blood Neu released large amounts of dsDNA and NE when stimulated by 20 μM PMA for 4 h. Surprisingly, we found that more NETs were produced (white arrow) in 3D than that in 2D culture, a similar phenomenon in mouse peripheral blood Neu (**Supplementary Figure 1A**). To quantify dsDNA with a general method (31), we measured the fluorescence of supernatants which were from PMA stimulated mouse Neu binding with PicoGreen®dsDNA Reagent. As for the NE-coupled dsDNA, we coated NE antibody

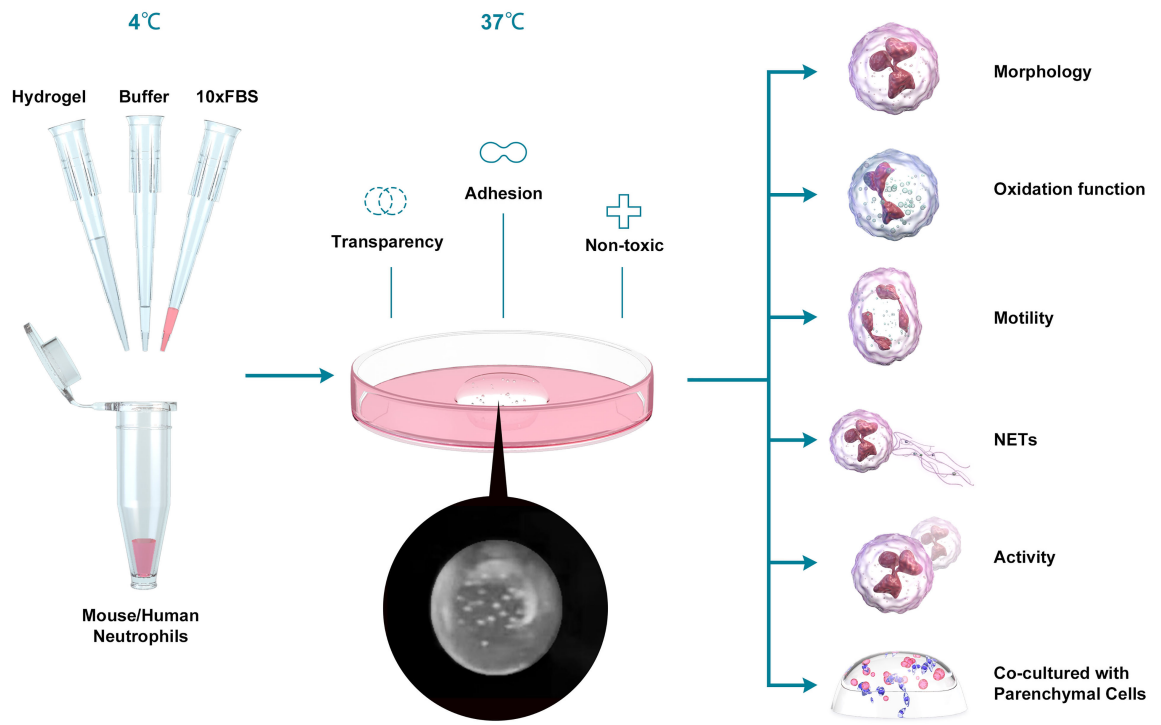

FIGURE 1 | Schematic depiction of the experiment. We mixed hydrogel, buffer, FBS and Neu, incubated at 37 °C for 30 min and added the medium to culture the cells. Then we tested the oxidation function, the motility, the NETs production, activity and the ability to co-culture with Parenchymal cells between Neu in 2D and 3D culture systems.

(100 ng per well) on the 96-well plate overnight in advance. Obviously, Neu in 3D culture system released more dsDNA and NE-coupled dsDNA, which were significantly different (**Figures 3F, G**).

A significant increase of NETs were seen following stimulation of mouse peripheral blood Neu with LPS/ATP, IL-1β and TNFα (**Supplementary Figures 1B, C**). Similarly, 3D cultured Neu produced more NETs than 2D cultures.

Activity of the Fresh Neu in the 3D Culture System

The activity of mouse bone marrow-derived Neu evaluated by MTT assay in the 2D culture system decreased rapidly, which was significantly slower than that of the 3D culture system (**Figures 4A, B**).

It is well known that caspase or other proteins activated early in apoptosis will activate degrading enzymes, which begin to cut DNA in the linker region, forming nucleosome and oligonucleosome DNA fragments (180 bp and multiples of 180 bp) (32). To assess the degree of Neu apoptosis during culture in 2D and 3D systems, we detected the classic approach of DNA fragmentation of 180 bp and multiples thereof (33). The characteristic "DNA ladder" pattern can be observed in **Figure 4C**. And apoptosis occurred on the 2nd day in 2D culture system, but on the 4th day in 3D culture system, which could be consistent with the appearance of nuclear condensation in **Figure 2D**.

We also detected cell viability by observing the co-localization of SYTO 13 (stain DNA in both live and dead eukaryotic cells) and PI (stain DNA in dead eukaryotic cells) under a fluorescence microscope (**Supplementary Figures 2, 3**), and the ratio of PI to SYTO 13 was used to evaluate the percentage of dead cells. As shown in **Figures 4D, E**, the Neu of mouse or human in 2D culture system behaved more apoptosis than that in 3D culture system taken for comparison on the same day. The inhibition of apoptosis z-vad-fmk could easily alleviate the death of cells in 2D culture systems (***$p<0.001$). Interestingly, the cell viability of human peripheral blood Neu was higher than that of mice with the same culture time and culture system (**Figures 4D, E**).

Status of the Fresh Neu When Co-Cultured With Parenchymal Cells in 3D Culture System

We tested the production of NETs by human peripheral blood Neu when co-cultured with mucosal epithelial cells lines NCM460. Neu produced fuller NETs when stimulated by LPS/ATP (**Figure 5A**, white arrow, **Supplementary Video 1**). At the same time, we showed that 2D cultured cells adhered and grew on a flat surface, while 3D cultured cells contact with other cells in three-dimensional space (**Supplementary Figure 4A**, white arrow, **Supplementary Video 2**).

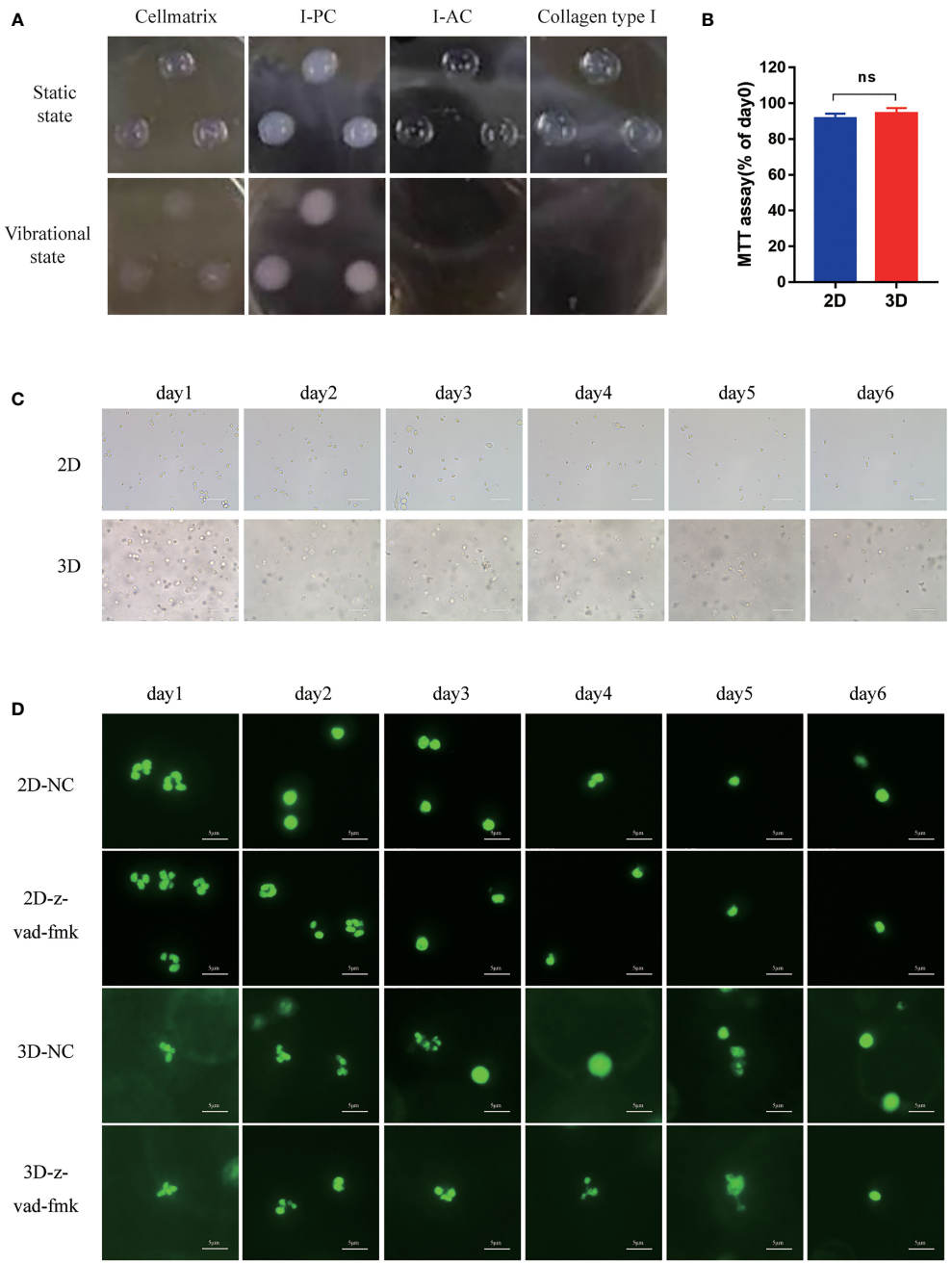

FIGURE 2 | The morphology of Neu in 2D and 3D culture systems. **(A)** Morphology of Cellmatrix Type I, I-PC collagen and I-AC and Collagen type I in a static state or vibrational under light microscope. **(B)** Toxicity testing was evaluated by the MTT assay. Mouse bone marrow-derived Neu were embedded in Cellmatrix Type I and cultured for 24 h. MTT reagent was used to detect the survival rate of the cells. **(C)** The morphology of mouse peripheral blood Neu representative light microscopy photographs (600x). **(D)** Representative fluorescence micrograph of human peripheral blood Neu dyed by SYTO 13 (stain DNA in both live and dead eukaryotic cells) during 6 days in 2D and 3D culture systems with or without the inhibition of apoptosis z-vad-fmk. Error bars represent mean ± S.D. n = 3, ns, not statistically significantly different by One-way ANOVA.

When co-cultured with C2C12, mouse Neu produced NETs when stimulated with PMA as usual. However, more NETs seemed to be produced (**Figure 5B**, white arrow), and a lot of blebbing (**Figure 5B**, white arrowhead) was observed on C2C12 cells, but not in the negative control group. As shown in the **Supplementary Figure 4B** and **Supplementary Video 3**, we could observe that in the 3D culture system Neu and co-cultured C2C12 stretched deeper, but limited to the culture surface in the 2D culture system.

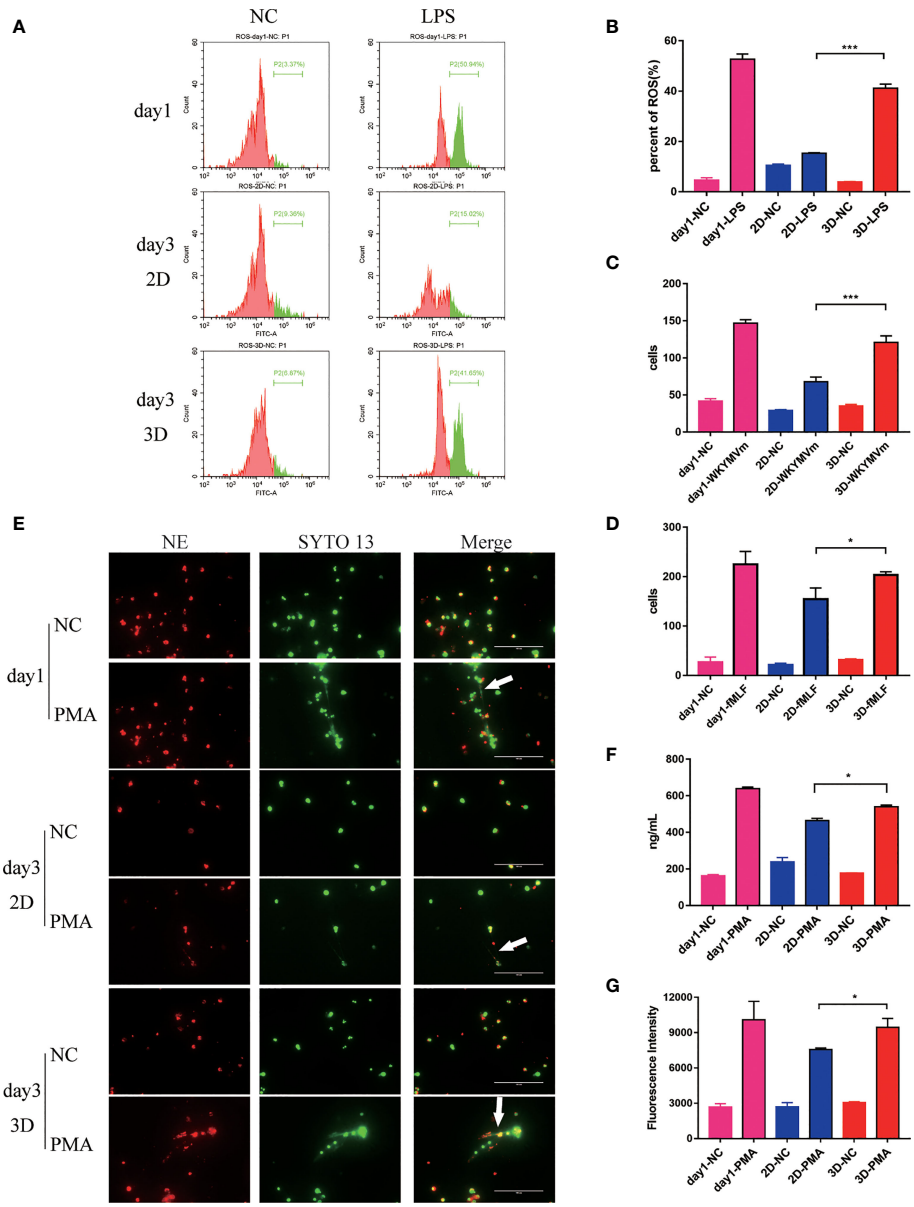

FIGURE 3 | The evaluation of function of Neu during 6 days in 2D and 3D culture system. **(A)** Flow cytometry analysis of ROS produced by mouse peripheral blood Neu cultured in 2D and 3D systems and corresponding statistical results **(B)**. Chemotactic ability of mouse peripheral blood Neu shown as the number of cells per high power field on the Petri dish bottom in 2D culture and 3D culture systems for control (randomly migrating) and WKYMVm (100 nM) stimulated mouse peripheral blood Neu **(C)** or control and fMLF (1 μM) stimulated human peripheral blood Neu **(D)**. **(E)** Human Neu released NETs marked by NE (Alexa Fluor 594 dye, red) and nuclear (SYTO 13, green) when stimulated by 20 μM PMA for 4 h in 2D and 3D culture systems under a confocal microscope *in vitro*. **(F)** A significantly different dsDNA release was detected using fluorescent-based Picogreen assay. **(G)** Meanwhile, a significantly different release of neutrophil elastase coupled dsDNA was measured using fluorescent-based Picogreen assay coated with NE antibodies. Error bars represent mean ± S.D. n = 3, *p < 0.05, **p < 0.01, ***p < 0.001, ****p < 0.0001, ns, not statistically significantly different by Two way ANOVA.

We also observed the production of a large number of NETs (**Figure 5C**, white box) in live mice under two-photon fluorescence microscopy. It can be observed that the production of NETs labeled with LY6G and sytox green in mouse liver increased after 3h of LPS injection in the tail vein. And dsDNA and NE-coupled dsDNA also increased accordingly (**Figures 5D, E**).

DISCUSSION

Neu have a short life span and are prone to apoptosis with characteristic morphological changes of nuclear condensation and cell shrinkage *in vitro* (34, 35). So it is great challenging to study the detailed molecular biological role of Neu due to their short life span and the inability to cryopreserve or expand them

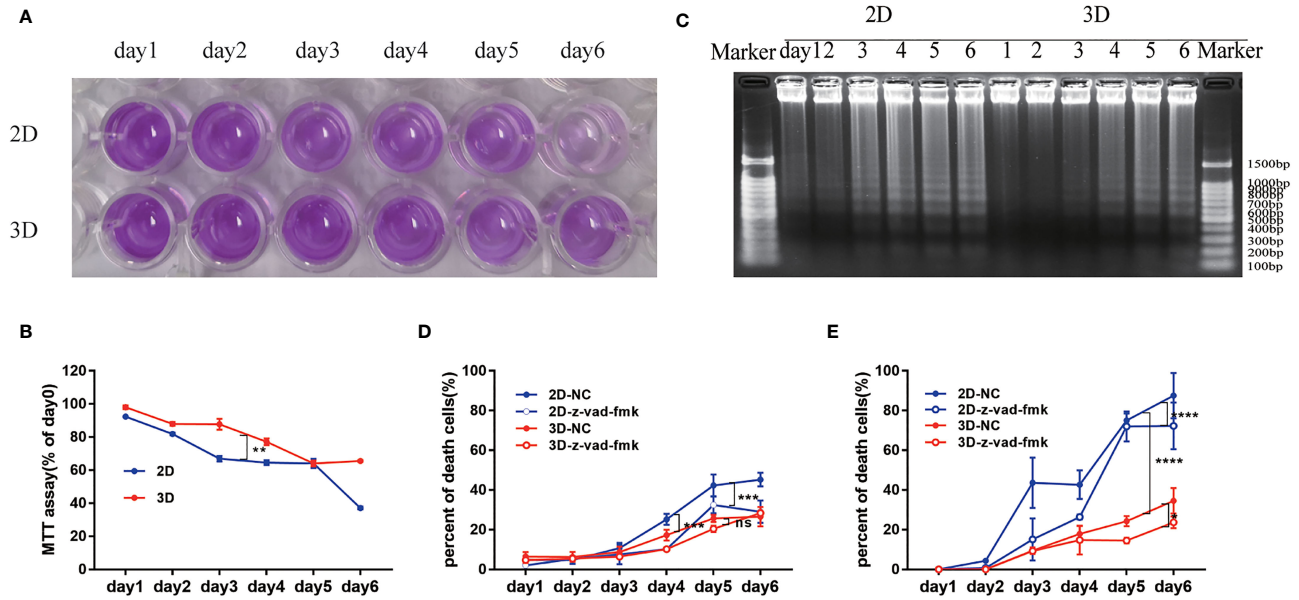

FIGURE 4 | The activity of Neu in 2D and 3D culture systems. **(A)** Survival rate was evaluated by the MTT assay. **(B)** Percentage of the absorbance value relative to the cells on day 1 was used to indicate the active cells. **(C)** DNA integrity was determined by electrophoresis of DNA isolated from cultured mouse Neu for 1-6 days. Each slot was loaded with 50 μg of genomic DNA (corresponding to $5x10^5$ Neu used for preparation). Percentage of PI positive in the total mouse **(D)** and human **(E)** peripheral blood Neu which were dyed by SYTO 13 during 6 days in 2D and 3D culture systems with or without the inhibition of apoptosis z-vad-fmk was used to indicate the dead cells. Data from one of three experiments performed are shown. Error bars represent mean ± S.D. n = 3, *p < 0.05, **p < 0.01, ***p < 0.001, ****p < 0.0001, ns, not statistically significantly different by Two way ANOVA.

in vitro (36). Prolonging the lifespan of Neu and keeping them active is very important for the outbreak of inflammation. Moreover, the standard 2D cell culturing does not represent the actual microenvironment where cells reside in tissues. Especially during inflammation, the Neu infiltrate tissues where they perform their effector functions. However, the tissues are three-dimensional (3D) and thus performance of the cells might also be different than that in the 2D conditions (12). In the current study, mainly using the hydrogel, we estalished a 3D culture system for human and mouse peripheral blood Neu. We demonstrated that the 3D culture system was more suitable for Neu. The NETs phenomenon of Neu induced by PMA, and other DAMPs in the 3D culture system is similar to that *in vivo*, and the the 3D culture system could maintain better properties of Neu than the classcial 2D culture system.

Although the 3D culture of neutrophil-like cell line or primary Neu co-culture with other cells have been used for improving the viability of Neu (15, 16), however, the detailed phenomena of Neu in 3D culturing system have never evaluated. The hydrogel is a biodegradable and biocompatible porous material with the ability to maintain high water content, used in a wide range of medical applications (15, 37, 38), including the drug release carriers, corneal contact lenses, in bone and soft tissue regeneration, in reconstruction and in the treatment of burns (39). They have good permeability, allowing a variety of nutrients, gases, and metabolites to pass through them freely and resembling the extracellular environment of the body's tissues (17). So It might be suitable for oberving the exact phenomena of Neu.

In current study, we characterized the morphology and activity of the human and mouse Neu cultured in the 3D culutring system based on hydrogel. Obviously, Neu showed better activity in 3D culture which was consistent with others' study of other cells (18–21, 40). The human-derived Neu are the most frequent nucleated cells in the circulation (50-70% Neu), but the mouse-derived Neu are significantly less frequent in the blood (10-25% Neu) and exhibit functional differences, for mouse-derived Neu are resistant to intravenous immunoglobulin (IVIG)-mediated cell death (41). The two origins of Neu were used to evalute their activities and function in the 2D and 3D culture system, and the results demonstrated that the human-derived peripheral blood Neu were more active than mice under the same culture time and culture system.

According to the existing study, the apoptotic Neu displayed a loss of background functions: ability to spread and change shape, random migration and chemotaxis (41). As the cultivation time increases, Neu gradually undergo apoptosis after 24 hours, but the 3D culture system slowed down this process. It is well known that apoptotic Neu display profound loss of capacity to generate and release histotoxic products under external stimulation (42) ROS production is one of the mechanisms by which Neu kill microorganisms. In our results, the amount of ROS produced by Neu in 2D and 3D was lower than that in the first day, may be because the two groups had different degrees of apoptosis. As shown in **Figure 2D**, Neu had apoptosis after the first day with characteristic morphological changes of nuclear condensation and cell shrinkage.

NETs are web-like chromatin based structures that are released into the extracellular environment to aid in pathogen

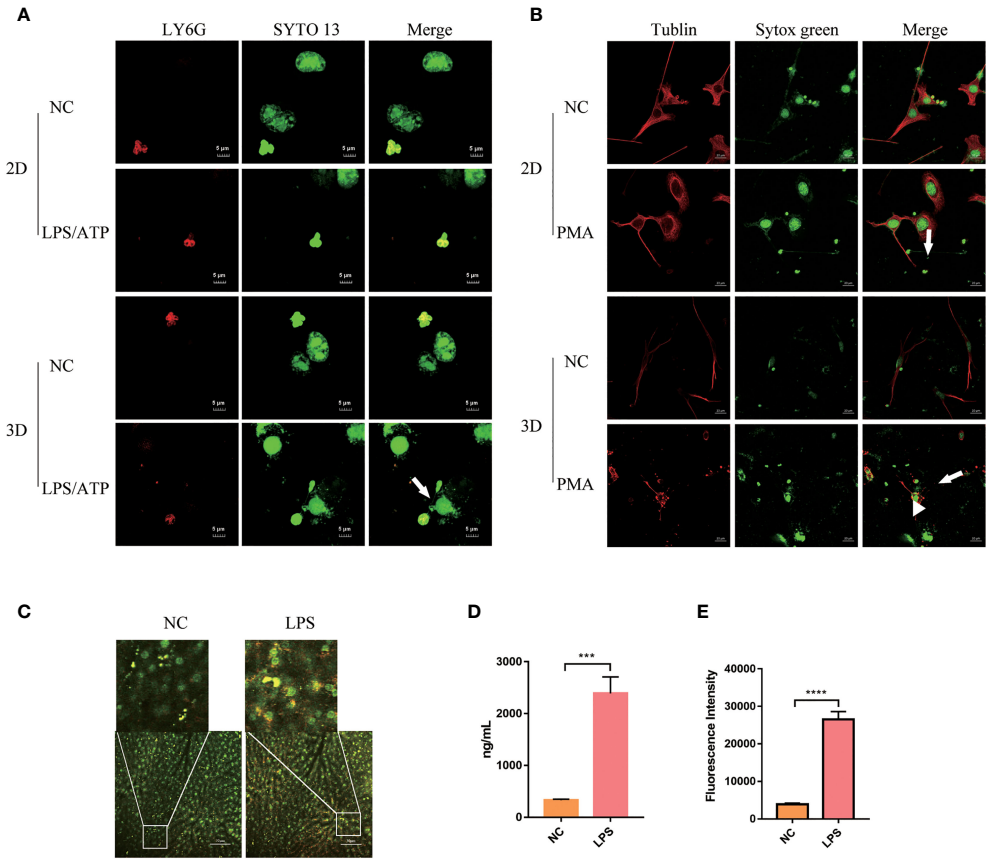

FIGURE 5 | Peripheral blood Neu co-cultured with parenchymal cells in 2D and 3D culture systems. **(A)** The formation of NETs (white arrow) of human peripheral blood Neu co-culture with NCM460 were observed under a confocal microscope. LY6G, PE (red) and nuclear, SYTO 13 (green). **(B)** The formation of NETs (white arrow) of Neu and blebbing (white arrowhead) of C2C12 were observed under a confocal microscope. Tublin, Alexa Fluor 594 dye (red) and nuclear, sytox green (green). **(C)** The formation of NETs (white box) produced by Neu in LPS-treated mouse was observed under a two-photon confocal microscope (APC-750-LY6G, red and nuclear-sytox green, green) *in vivo*. Quantification of NETs formation in the plasma was assessed by dsDNA **(D)** and neutrophil elastase coupled dsDNA **(E)**. Error bars represent mean ± S.D. n = 3, ***$p < 0.001$,****$p < 0.0001$ by Two-way ANOVA. Each experiment was repeated three times.

clearance, but they have also been implicated in excessive inflammation with resultant tissue damage, potentiation of autoimmunity, and promotion of vascular thrombosis (43). NETs were released when the Neu were simulated with PMA, LPS (28) or other DAMPs (44). In current study, our results showed the 3D systems could indeed assist Neu to maintain the function of NETs induced by LPS/ATP, IL-1β, IFN-γ, PMA and TNFα, respectilvey. We compared the differences of Neu between the 2D and 3D culture systems stimulated by IL-1β, TNFα, and LPS/ATP separately. Similar to the results of PMA, Neu stimulated by LPS/ATP, IL-1β and TNFα displayed more NETs in 3D culture and this suggests that our 3D culture of Neu may reduce the gap between *in vitro* an *in vivo* experimentations.

pt?>The 3D culture system could better simulated the interaction between cells and cells, cells and matrix *in vivo*, which may disappear in 2D culture, and provide more accurate depiction of cell polarization since in 2D the cells can only be partially polarized (11). When co-cultured with the colon mucosal epithelial cell line NCM460, Neu showed full NETs, and NCM460 showed membrane damage in 3D culture, while not in 2D culture. In the 3D culture movie, we can observed that the contact area between NCM460 and Neu was spatially multiplied in the 3D culture, while adjacent cells in 2D culture. The results were also confirmed in the co-culture of Neu and skeletal muscle cell C2C12.

In summary, the current study developed a better 3D culture system for Neu, and the 3D culture of Neu provides an opportunity to mimic the *in vivo* experiments.

DATA AVAILABILITY STATEMENT

The original contributions presented in the study are included in the article/**Supplementary Material**. Further inquiries can be directed to the corresponding authors.

ETHICS STATEMENT

Ethical review and approval was not required for the study on human participants in accordance with the local legislation and

institutional requirements. The patients/participants provided their written informed consent to participate in this study. The animal study was reviewed and approved by Animal Care and Use Committee of the Southern Medical University.

AUTHOR CONTRIBUTIONS

RL performed most of the experiments and contributed to planning the work, to the interpretation of data, and to writing the paper. ZW, JH, SH, YP, and YW contributed to the interpretation of data. QM supervised the study. All authors contributed to the article and approved the submitted version.

FUNDING

This work was supported by the following funding sources: the National Natural Science Foundation of China (81772133, 82072100, and 81902444), the Guangdong Natural Science Fund (2020A1515011367 and 2020A1515010269), the Guangzhou Citizen Health Science and Technology Research Project (201803010034 and 201903010072).

ACKNOWLEDGMENTS

We thank YW for technical assistance with the 3D culture system.

SUPPLEMENTARY MATERIAL

The Supplementary Material for this article can be found online at: https://www.frontiersin.org/articles/10.3389/fimmu.2022.816037/full#supplementary-material

Supplementary Figure 1 | (A) The formation of NETs when stimulated by PMA for 4 h in 2D and 3D culture systems which marked by NE (Alexa Fluor 488 dye, green) and nuclear (DAPI, blue) were observed in mouse peripheral blood Neu under a fluorescence microscope *in vitro*. **(B)** Mouse peripheral blood Neu released NETs marked by LY6G (PE, red) and nuclear (SYTO 13, green) when stimulated by LPS (2.5 μg/mL)/ATP (3 mM), IL-1β (20 ng/mL) and TNFα (20 ng/mL) for 4 h in 2D and 3D culture systems under a confocal microscope *in vitro*. **(C)** A significantly different dsDNA release was detected using fluorescent-based Picogreen assay. Error bars represent mean ± S.D. n = 3, $^{****}p < 0.0001$ by Two-way ANOVA.

Supplementary Figure 2 | Mouse peripheral blood Neu which were dyed by SYTO 13 (stain DNA in both live and dead eukaryotic cells) and PI (stain DNA in dead eukaryotic cells) during 6 days in 2D and 3D culture systems with or without the inhibition of apoptosis z-vad-fmk.

Supplementary Figure 3 | Human peripheral blood Neu which were dyed by SYTO 13 and PI during 6 days in 2D and 3D culture systems with or without the inhibition of apoptosis z-vad-fmk.

Supplementary Figure 4 | Immunofluorescence analysis using confocal laser microscopy of human peripheral blood Neu co-culture with NCM460 in 2D and 3D systems. **(A)** The location (white arrow) of cells in XZ and YZ view of the cell model were observed. Z-stacks were acquired using confocal fluorescence microscopy and were reconstructed using Olympus FV31S. **(B)** Three-dimensional reconstruction of C2C12 and Neu co-culture, and the cross-section of monolayer cells (white lines).

Supplementary Video 1 | Three-dimensional image of human peripheral blood Neu co-culture with NCM460 in 2D and 3D culture systems. Neu produced NETs under LPS (2.5 μg/mL)/ATP (3 mM) for 4 h stimulation.

Supplementary Video 2 | Three-dimensional image of human peripheral blood Neu co-culture with NCM460 in 2D and 3D culture systems and the location of cells in Z-stacks.

Supplementary Video 3 | Three-dimensional image of Neu and C2C12 co-culture in 2D and 3D culture systems. Neu produced NETs (white arrows) under 20 μM PMA for 4 h stimulation, and the depth of cells spanned during culture (white lines).

REFERENCES

1. Wang X, Cai J, Lin B, Ma M, Tao Y, Zhou Y, et al. GPR34-Mediated Sensing of Lysophosphatidylserine Released by Apoptotic Neutrophils Activates Type 3 Innate Lymphoid Cells to Mediate Tissue Repair. *Immunity* (2021) 54 (6):1123–36 e8. doi: 10.1016/j.immuni.2021.05.007
2. Li Z, Peirasmaki D, Svard S, Abrink M. Serglycin-Deficiency Causes Reduced Weight Gain and Changed Intestinal Cytokine Responses in Mice Infected With Giardia Intestinalis. *Front Immunol* (2021) 12:677722. doi: 10.3389/fimmu.2021.677722
3. Papayannopoulos V, Metzler KD, Hakkim A, Zychlinsky A. Neutrophil Elastase and Myeloperoxidase Regulate the Formation of Neutrophil Extracellular Traps. *J Cell Biol* (2010) 191(3):677–91. doi: 10.1083/jcb.201006052
4. Kolaczkowska E, Kubes P. Neutrophil Recruitment and Function in Health and Inflammation. *Nat Rev Immunol* (2013) 13(3):159–75. doi: 10.1038/nri3399
5. Duffin R, Leitch AE, Fox S, Haslett C, Rossi AG. Targeting Granulocyte Apoptosis: Mechanisms, Models, and Therapies. *Immunol Rev* (2010) 236:28–40. doi: 10.1111/j.1600-065X.2010.00922.x
6. Athens JW, Haab OP, Raab SO, Mauer AM, Ashenbrucker H, Cartwright GE, et al. Leukokinetic Studies. IV. The Total Blood, Circulating and Marginal Granulocyte Pools and the Granulocyte Turnover Rate in Normal Subjects. *J Clin Invest* (1961) 40:989–95. doi: 10.1172/JCI104338
7. Blanter M, Gouwy M, Struyf S. Studying Neutrophil Function *In Vitro*: Cell Models and Environmental Factors. *J Inflammation Res* (2021) 14:141–62. doi: 10.2147/JIR.S284941
8. Prince LR, Prosseda SD, Higgins K, Carlring J, Prestwich EC, Ogryzko NV, et al. NR4A Orphan Nuclear Receptor Family Members, NR4A2 and NR4A3, Regulate Neutrophil Number and Survival. *Blood* (2017) 130(8):1014–25. doi: 10.1182/blood-2017-03-770164
9. Short AR, Czeisler C, Stocker B, Cole S, Otero JJ, Winter JO. Imaging Cell-Matrix Interactions in 3D Collagen Hydrogel Culture Systems. *Macromol Biosci* (2017) 17(6). doi: 10.1002/mabi.201600478
10. Marwick JA, Dorward DA, Lucas CD, Jones KO, Sheldrake TA, Fox S, et al. Oxygen Levels Determine the Ability of Glucocorticoids to Influence Neutrophil Survival in Inflammatory Environments. *J Leukoc Biol* (2013) 94 (6):1285–92. doi: 10.1189/jlb.0912462
11. Antoni D, Burckel H, Josset E, Noel G. Three-Dimensional Cell Culture: A Breakthrough *In Vivo*. *Int J Mol Sci* (2015) 16(3):5517–27. doi: 10.3390/ijms16035517
12. Gonzalez Gonzalez M, Cichon I, Scislowska-Czarnecka A, Kolaczkowska E. Challenges in 3D Culturing of Neutrophils: Assessment of Cell Viability. *J Immunol Methods* (2018) 457:73–7. doi: 10.1016/j.jim.2018.02.015
13. Edmondson R, Broglie JJ, Adcock AF, Yang L. Three-Dimensional Cell Culture Systems and Their Applications in Drug Discovery and Cell-Based Biosensors. *Assay Drug Dev Technol* (2014) 12(4):207–18. doi: 10.1089/adt.2014.573
14. Heydarian M, Schweinlin M, Schwarz T, Rawal R, Walles H, Metzger M, et al. Triple Co-Culture and Perfusion Bioreactor for Studying the Interaction Between Neisseria Gonorrhoeae and Neutrophils: A Novel 3D Tissue Model for Bacterial Infection and Immunity. *J Tissue Eng* (2021) 12:2041731420988802. doi: 10.1177/2041731420988802
15. SenGupta S, Hein LE, Xu Y, Zhang J, Konwerski JR, Li Y, et al. Triple-Negative Breast Cancer Cells Recruit Neutrophils by Secreting TGF-Beta

and CXCR2 Ligands. *Front Immunol* (2021) 12:659996. doi: 10.3389/fimmu.2021.659996
16. Surendran V, Rutledge D, Colmon R, Chandrasekaran A. A Novel Tumor-Immune Microenvironment (TIME)-on-Chip Mimics Three Dimensional Neutrophil-Tumor Dynamics and Neutrophil Extracellalar Traps (Nets)-Mediated Collective Tumor Invasion. *Biofabrication* (2021) 13. doi: 10.1088/1758-5090/abe1cf
17. Tibbitt MW, Anseth KS. Hydrogels as Extracellular Matrix Mimics for 3D Cell Culture. *Biotechnol Bioeng* (2009) 103(4):655–63. doi: 10.1002/bit.22361
18. Zuppinger C. 3D Culture for Cardiac Cells. *Biochim Biophys Acta* (2016) 1863 (7 Pt B):1873–81. doi: 10.1016/j.bbamcr.2015.11.036
19. Imamura Y, Mukohara T, Shimono Y, Funakoshi Y, Chayahara N, Toyoda M, et al. Comparison of 2D- and 3D-Culture Models as Drug-Testing Platforms in Breast Cancer. *Oncol Rep* (2015) 33(4):1837–43. doi: 10.3892/or.2015.3767
20. McReynolds J, Wen Y, Li X, Guan J, Jin S. Modeling Spatial Distribution of Oxygen in 3d Culture of Islet Beta-Cells. *Biotechnol Prog* (2017) 33(1):221–8. doi: 10.1002/btpr.2395
21. Yue X, Lukowski JK, Weaver EM, Skube SB, Hummon AB. Quantitative Proteomic and Phosphoproteomic Comparison of 2D and 3D Colon Cancer Cell Culture Models. *J Proteome Res* (2016) 15(12):4265–76. doi: 10.1021/acs.jproteome.6b00342
22. Godoy P, Hewitt NJ, Albrecht U, Andersen ME, Ansari N, Bhattacharya S, et al. Recent Advances in 2D and 3D *In Vitro* Systems Using Primary Hepatocytes, Alternative Hepatocyte Sources and non-Parenchymal Liver Cells and Their Use in Investigating Mechanisms of Hepatotoxicity, Cell Signaling and ADME. *Arch Toxicol* (2013) 87(8):1315–530. doi: 10.1007/s00204-013-1078-5
23. Gjorevski N, Sachs N, Manfrin A, Giger S, Bragina ME, Ordonez-Moran P, et al. Designer Matrices for Intestinal Stem Cell and Organoid Culture. *Nature* (2016) 539(7630):560–4. doi: 10.1038/nature20168
24. Cruz-Acuna R, Quiros M, Farkas AE, Dedhia PH, Huang S, Siuda D, et al. Synthetic Hydrogels for Human Intestinal Organoid Generation and Colonic Wound Repair. *Nat Cell Biol* (2017) 19(11):1326–35. doi: 10.1038/ncb3632
25. Saheli M, Sepantafar M, Pournasr B, Farzaneh Z, Vosough M, Piryaei A, et al. Three-Dimensional Liver-Derived Extracellular Matrix Hydrogel Promotes Liver Organoids Function. *J Cell Biochem* (2018) 119(6):4320–33. doi: 10.1002/jcb.26622
26. Fong ELS, Toh TB, Lin QXX, Liu Z, Hooi L, Mohd Abdul Rashid MB, et al. Generation of Matched Patient-Derived Xenograft *In Vitro-In Vivo* Models Using 3D Macroporous Hydrogels for the Study of Liver Cancer. *Biomaterials* (2018) 159:229–40. doi: 10.1016/j.biomaterials.2017.12.026
27. Morishita A, Kumabe S, Nakatsuka M, Iwai Y. A Histological Study of Mineralised Tissue Formation Around Implants With 3D Culture of HMS0014 Cells in Cellmatrix Type I-a Collagen Gel Scaffold *In Vitro*. *Okajimas Folia Anat Jpn* (2014) 91(3):57–71. doi: 10.2535/ofaj.91.57
28. Brinkmann V, Reichard U, Goosmann C, Fauler B, Uhlemann Y, Weiss DS, et al. Neutrophil Extracellular Traps Kill Bacteria. *Science* (2004) 303 (5663):1532–5. doi: 10.1126/science.1092385
29. Jorch SK, Kubes P. An Emerging Role for Neutrophil Extracellular Traps in Noninfectious Disease. *Nat Med* (2017) 23(3):279–87. doi: 10.1038/nm.4294
30. Liu S, Su X, Pan P, Zhang L, Hu Y, Tan H, et al. Neutrophil Extracellular Traps are Indirectly Triggered by Lipopolysaccharide and Contribute to Acute Lung Injury. *Sci Rep* (2016) 6:37252. doi: 10.1038/srep37252
31. Neumann A, Brogden G, Jerjomiceva N, Brodesser S, Naim HY, von Kockritz-Blickwede M. Lipid Alterations in Human Blood-Derived Neutrophils Lead to Formation of Neutrophil Extracellular Traps. *Eur J Cell Biol* (2014) 93(8-9):347–54. doi: 10.1016/j.ejcb.2014.07.005
32. Riccardi C, Nicoletti I. Analysis of Apoptosis by Propidium Iodide Staining and Flow Cytometry. *Nat Protoc* (2006) 1(3):1458–61. doi: 10.1038/nprot.2006.238
33. Majtnerova P, Rousar T. An Overview of Apoptosis Assays Detecting DNA Fragmentation. *Mol Biol Rep* (2018) 45(5):1469–78. doi: 10.1007/s11033-018-4258-9
34. Kennedy AD, DeLeo FR. Neutrophil Apoptosis and the Resolution of Infection. *Immunol Res* (2009) 43(1-3):25–61. doi: 10.1007/s12026-008-8049-6
35. Barth ND, Vendrell M, Dorward DA, Rossi AG, Dransfield I. Assessment of Neutrophil Apoptosis. *Methods Mol Biol* (2020) 2087:167–90. doi: 10.1007/978-1-0716-0154-9_13
36. Nicolas-Avila JA, Adrover JM, Hidalgo A. Neutrophils in Homeostasis, Immunity, and Cancer. *Immunity* (2017) 46(1):15–28. doi: 10.1016/j.immuni.2016.12.012
37. Kuehlbach C, Hensler S, Mueller MM. Recapitulating the Angiogenic Switch in a Hydrogel-Based 3D *In Vitro* Tumor-Stroma Model. *Bioengineering (Basel)* (2021) 8(11). doi: 10.3390/bioengineering8110186
38. Jannat RA, Robbins GP, Ricart BG, Dembo M, Hammer DA. Neutrophil Adhesion and Chemotaxis Depend on Substrate Mechanics. *J Phys Condens Matter* (2010) 22(19):194117. doi: 10.1088/0953-8984/22/19/194117
39. Haidari H, Bright R, Strudwick XL, Garg S, Vasilev K, Cowin AJ, et al. Multifunctional Ultrasmall Agnp Hydrogel Accelerates Healing of s. Aureus Infected Wounds. *Acta Biomater* (2021) 128:420–34. doi: 10.1016/j.actbio.2021.04.007
40. Salvermoser M, Pick R, Weckbach LT, Zehrer A, Lohr P, Drechsler M, et al. Myosin 1f is Specifically Required for Neutrophil Migration in 3D Environments During Acute Inflammation. *Blood* (2018) 131(17):1887–98. doi: 10.1182/blood-2017-10-811851
41. Schneider C, Wicki S, Graeter S, Timcheva TM, Keller CW, Quast I, et al. IVIG Regulates the Survival of Human But Not Mouse Neutrophils. *Sci Rep* (2017) 7(1):1296. doi: 10.1038/s41598-017-01404-0
42. Whyte MK, Meagher LC, MacDermot J, Haslett C. Impairment of Function in Aging Neutrophils is Associated With Apoptosis. *J Immunol* (1993) 150 (11):5124–34.
43. Papayannopoulos V. Neutrophil Extracellular Traps in Immunity and Disease. *Nat Rev Immunol* (2018) 18(2):134–47. doi: 10.1038/nri.2017.105
44. Maugeri N, Capobianco A, Rovere-Querini P, Ramirez GA, Tombetti E, Valle PD, et al. Platelet Microparticles Sustain Autophagy-Associated Activation of Neutrophils in Systemic Sclerosis. *Sci Transl Med* (2018) 10(451). doi: 10.1126/scitranslmed.aao3089

Conflict of Interest: YW was employed by Guangzhou Darui Biotechnology Co., Ltd.

The remaining authors declare that the research was conducted in the absence of any commercial or financial relationships that could be construed as a potential conflict of interest.

frontiers | Frontiers in Immunology

ORIGINAL RESEARCH
published: 07 April 2022
doi: 10.3389/fimmu.2022.877650

D-Mannose Regulates Hepatocyte Lipid Metabolism *via* PI3K/Akt/mTOR Signaling Pathway and Ameliorates Hepatic Steatosis in Alcoholic Liver Disease

Mengyao Hu[1†], Yu Chen[1,2†], Fan Deng[1,2], Bo Chang[1], Jialiang Luo[1,2], Lijun Dong[1,2], Xiao Lu[1], Yi Zhang[2], Zhengliang Chen[1] and Jia Zhou[1*]*

[1] Department of Immunology, School of Basic Medical Sciences, Southern Medical University, Guangzhou, China, [2] Department of Medical Laboratory, School of Laboratory Medicine and Biotechnology, Southern Medical University, Guangzhou, China

OPEN ACCESS

Edited by:
Chunqing Guo,
Virginia Commonwealth University,
United States

Reviewed by:
Anjian Xu,
Capital Medical University, China
Fanlei Hu,
Peking University People's Hospital,
China

***Correspondence:**
Zhengliang Chen
zhlchen@smu.edu.cn
Jia Zhou
yuguomm@smu.edu.cn

[†]These authors share first authorship

Specialty section:
This article was submitted to Molecular Innate Immunity, a section of the journal Frontiers in Immunology

Received: 17 February 2022
Accepted: 17 March 2022
Published: 07 April 2022

Citation:
Hu M, Chen Y, Deng F, Chang B, Luo J, Dong L, Lu X, Zhang Y, Chen Z and Zhou J (2022) D-Mannose Regulates Hepatocyte Lipid Metabolism via PI3K/Akt/mTOR Signaling Pathway and Ameliorates Hepatic Steatosis in Alcoholic Liver Disease. Front. Immunol. 13:877650. doi: 10.3389/fimmu.2022.877650

This study investigated the protective properties and mechanisms of D-mannose against hepatic steatosis in experimental alcoholic liver disease (ALD). Drinking-water supplementation of D-mannose significantly attenuated hepatic steatosis in a standard mouse ALD model established by chronic-binge ethanol feeding, especially hepatocyte lipid deposition. This function of D-mannose on lipid accumulation in hepatocytes was also confirmed using ethanol-treated primary mouse hepatocytes (PMHs) with a D-mannose supplement. Meanwhile, D-mannose regulated lipid metabolism by rescuing ethanol-mediated reduction of fatty acid oxidation genes (PPARα, ACOX1, CPT1) and elevation of lipogenic genes (SREBP1c, ACC1, FASN). PI3K/Akt/mTOR signaling pathway was involved in this effect of D-mannose on lipid metabolism since PI3K/Akt/mTOR pathway inhibitors or agonists could abolish this effect in PMHs. Overall, our findings suggest that D-mannose exhibits its anti-steatosis effect in ALD by regulating hepatocyte lipid metabolism *via* PI3K/Akt/mTOR signaling pathway.

Keywords: D-mannose, hepatic steatosis, alcoholic liver disease, hepatocyte, lipid metabolism, PI3K/Akt/mTOR

INTRODUCTION

Alcoholic liver disease (ALD) is a significant health concern that causes considerable morbidity and mortality worldwide, which has become an increasingly prevalent liver disorder caused by chronic and excessive alcohol intake (1). Continued alcohol consumption can lead to a broad spectrum of hepatic lesion changes, including hepatic steatosis, inflammation, and liver injury that represent the main characteristics of ALD (2). Hepatic steatosis is the earliest form of ALD characterized by excessive fat accumulation in the liver, further developing into more severe forms of ALD, including hepatitis, fibrosis/cirrhosis, and eventually hepatocellular carcinoma and liver failure without effective treatment (3). While alcohol abstinence is the most valid therapy, targeted therapies are vital for patients who do not withdraw alcohol or with severe ALD (4). Unfortunately, there have remained no efficient therapies for ALD provided over the past few decades (5). Lipogenesis during

the initial stages of ALD has been considered a significant risk factor for disease progression, suggesting that the prevention and reversal of hepatic steatosis is a potential targeted therapeutic strategy for treating ALD (6).

Although how chronic alcohol consumption causes hepatic lipid accumulation remains elusive, accumulating evidence has indicated that alcohol could affect key transcription factors that modulate lipid metabolism, such as peroxisome proliferator-activated receptor α (PPARα) and sterol regulatory element-binding protein 1c (SREBP1c), which play a crucial role in the pathogenesis of ALD (5, 7). Furthermore, alcohol exposure significantly inhibits fatty acid oxidation by inactivating PPARα, a nuclear transcription factor that regulates the mRNA expression of genes that participate in fatty-acid transportation and oxidation, such as carnitine palmitoyl transferase 1 (CPT-1), peroxisomal acyl-CoA oxidases 1 (ACOX1) (8, 9). Meanwhile, alcohol exposure can promote hepatic fatty acid synthesis by activating SREBP1c, a major transcription factor affecting *de novo* lipogenesis through up-regulation of lipogenic enzymes, including acetyl-CoA carboxylase 1 (ACC1) and fatty acid synthase (FASN) (10, 11). Additionally, emerging evidence showed that phosphatidylinositol-3-kinase (PI3K)/protein kinase B (Akt)/mammalian target of rapamycin (mTOR) signaling pathway, including PI3K/Akt pathway and its primary downstream target mTOR, plays a critical role in regulating lipid metabolism (12, 13). Furthermore, several recent studies indicated that PI3K/Akt/mTOR pathway could regulate the PPARα expression (14, 15) and SREBP1c-mediated lipogenesis (16, 17). It also reported that PI3K/Akt pathway could participate in alcohol consumption-induced fatty liver (18), and mTOR is necessary for alcohol-regulated lipid metabolism in ALD (19).

D-mannose (hereafter referred to as mannose), a 2-epimer of glucose, is present in many plants and also exists in human blood (~50 μM). It can be transported into mammalian cells but does not contribute significantly to cell bioenergetics such as glucose (20, 21). Mannose supplementation at safe supraphysiological concentrations has become an effective therapeutic strategy for patients with mannose phosphate isomerase-congenital disorder of glycosylation (MPI-CDG) (22) and recurrent urinary tract infection (UTI) (23). Emerging evidence has shown that mannose possesses potential anti-cancer (24), anti-diabetic (25), anti-fibrotic (26), anti-obesity (27), and anti-inflammation (28) bioactivities. Furthermore, mannose can be transported into mammalian cells, which further suppress proliferation/survival of tumor cells (24), promote differentiation of regulatory T cells (Tregs) (25), regulate activation of hepatic stellate cells (HSCs) (26) and macrophages (28), partially *via* tuning glucose utilization (24, 28). In addition, Jaime Chu et al. demonstrated that mannose supplementation could attenuate hepatic fibrosis induced by MPI deficiency in zebrafish and the activation of ethanol-treated human HSCs. These findings indicate the potential functions of mannose for alleviating ALD, prompting us to explore the exact role and the underlying mechanism of mannose in ALD.

In this study, we performed drinking-water supplementation of mannose in a mouse model of ALD established by chronic and binge ethanol feeding, as well as mannose treatment on primary mouse hepatocytes (PMHs) in the presence of ethanol, aimed to elucidate the potential role and underlying mechanisms of mannose in ALD *in vivo* and *in vitro*. Our findings uncover a previously unrecognized protective role of mannose against hepatic steatosis in ALD. Furthermore, mannose can exert this function by regulating ethanol-induced lipid deposition in hepatocytes *via* tuning key transcription factors that control lipid metabolism, attenuating hepatic steatosis, thus alleviating ALD progression. Therefore, these data provide a whole new insight into utilizing mannose supplementation for improving fatty liver, thus ameliorating ALD progression.

MATERIALS AND METHODS

Chemicals and Reagents

D-mannose (purity ≥ 99%, Cat.#M2069) and ethanol (purity≥ 99.8%, 51976) were purchased from Sigma-Aldrich (St. Louis, MO, USA). Rapamycin (purity = 99.30%, S1039), LY294002 (purity = 99.84%, S1105), 740 Y-P (purity = 98.38%, S7865) and MHY1485 (purity = 99.09%, S7811) were purchased from Selleck Chemicals (Houston, Texas, USA). Liquid Standard Diet (TP4020C), Lieber-DeCarli Control Liquid Diet (TP4030C), and Lieber-DeCarli Ethanol Liquid Diet (TP4030D) were supplied by TROPHIC Animal Feed High-Tech Co. Ltd (Hai'an, Jiangsu, China). The antibodies against SREBP1c (AF-6283), PPARα (AF5301), ACC1 (AF6421), P110 of PI3K (AF-5112) were all from Affinity (Ancaster, ON, Canada). Anti-CPT1A (15184-1-AP), anti-ACOX1 (10957-1-AP), anti-FASN (10624-1-AP), anti-P85 (60225-1-Ig), anti-PPARγ (16643-1-AP), anti-PPARα (15540-1-AP) used in **Figure 6D** were obtained from Proteintech (Chicago, IL, USA). The antibodies against Akt (4691), phosphor-Akt (4060), mTOR (2983), phosphor-mTOR (5536) were from Cell Signaling Technology (Danvers, MA, USA).

Animals Experiments

C57BL/6 mice (male, 8-10 weeks old) were purchased from the Experimental Animal Center of Southern Medical University (Guangzhou, China). All mice were housed under a 12-h light/dark cycle in a specific pathogen-free animal condition with a controlled temperature (20-25°C) and humidity (50 ± 5%). All animal experiments in this study were approved by the Southern Medical University Experimental Animal Ethics Committee (No. L2020128).

The chronic-binge mouse model was established based on the methods of previous studies with minor modifications (29). Briefly, mice were fed a standard liquid diet for 3 days, then randomly divided into different groups as follows: Pair (Lieber-DeCarli control liquid diet); EtOH (Lieber-DeCarli ethanol liquid diet; ALD group); Pair+Man (Lieber-DeCarli control liquid diet supplemented with 3% (w/v) mannose); EtOH+Man [Lieber-DeCarli ethanol liquid diet supplemented with 1%, 2%, 3% (w/v) mannose (27)]. The mice in the EtOH and EtOH+Man groups were fed the Lieber-DeCarli liquid diet containing increasing 1% to 4% (w/v) ethanol for the first 6 days and then

the diet with 5% ethanol for 10 days. On day 11, mice fed ethanol before were gavaged a single dose of ethanol (5 g/kg body weight, 31.5% ethanol), while mice fed control diet were gavaged isocaloric dextrin maltose. Subsequently, the mice were sacrificed nine hours post gavage. Blood samples were obtained from the eye socket. A portion of the liver tissues was fixed in 4% neutral buffered formalin solution, and the remaining liver sections were immediately stored at -80°C.

Isolation and Culture of Primary Mouse Hepatocytes (PMHs)

Isolated primary hepatocytes from WT C57BL/6 mice (male, 8-12 weeks old) were obtained using a classical two-step *in situ* collagenase perfusion method as described previously with slight modifications (30). Briefly, the perfused liver was immediately excised and placed in a sterile dish containing RPMI 1640 medium (Gibco, United States). Then the cell suspension was filtered through a 70-μm nylon filter (BD Biosciences) and washed thrice by centrifugation at 50 × g for 3 min at 4°C. Subsequently, the cells were resuspended in the growth medium containing William's E medium (Thermo Fisher, Carlsbad, CA, USA) supplied with 10% fetal bovine serum (FBS, Gibco, United States), 10 ng/mL epidermal growth factor (EGF, GenScript, Nanjing, China), 2 nM L-glutamine (Macklin, Shanghai, China), 200 nM insulin (Macklin, Shanghai, China) and 100 nM dexamethasone (Macklin, Shanghai, China), and then seeded on type I collagen-coated dish. After incubation at 37°C for 4 h, PMHs were collected and washed twice, and the medium was replaced with the fresh growth medium.

Cultured PMHs were treated with 200 mM ethanol (EtOH) (31, 32) or cell growth medium only (Ctrl), in the presence of different concentrations (1 mM, 2.5 mM, 5 mM, 10 mM) of mannose (Man) (26) or not for 24 h. In some experiments, inhibitors (33) or agonists (34, 35) of PI3K or mTOR (Dimethyl sulfoxide (DMSO) as control) was added two hours before ethanol exposure or mannose treatment.

Biochemical Analysis

Serum alanine aminotransferase (ALT), aspartate aminotransferase (AST), triglyceride (TG), total cholesterol (TC), high-density lipoprotein-cholesterol (HDL-C), low-density lipoprotein-cholesterol (LDL-C) levels, and hepatic triglyceride (TG), total cholesterol (TC) contents were all measured according to the instructions of commercial assay kits from the manufacturer (Jiancheng Biotech, Nanjing, China).

Histopathological and Immunohistochemical Staining

The paraffin-embedded liver tissue blocks (n = 3 for each group) were cut into 5 μm slices sections and stained with hematoxylin and eosin (H&E). The frozen liver tissues (n = 3 for each group) were cut into 8 μm thick sections and then stained with Oil Red O. For immunohistochemical staining, liver tissue sections were deparaffinized and placed in a citrate buffer (pH 6.0) at 100°C for 10 min to antigen repair and then exposed to 3% H_2O_2 for 15 min to block endogenous peroxidase activity. Subsequently, sections were blocked with 5% normal goat serum for another 1 h at room temperature followed by incubated with primary antibodies at 4°C overnight. Immuno-reactivity was detected using the corresponding HRP-conjugated secondary antibody and visualized using a diaminobenzidine kit (Beyotime Institute of Biotechnology, Shanghai, China).

BODIPY Staining

The cellular content of neutral lipids was detected according to the manufacturer's instructions using lipophilic fluorescence dye BODIPY 493/503 (Invitrogen, Carlsbad, CA, USA). Briefly, cells were seeded on the 12-well culture plates containing cell-climbing slices pre-coated with collagen and incubated overnight. Cells were washed with Phosphate Buffered Saline (PBS) and fixed with 4% paraformaldehyde for 20 min at room temperature. Subsequently, cells were stained with 1 μg/mL BODIPY 493/503 dye for 30 min at 37°C, the nuclei were counterstained with 1 μg/mL Hoechst (CST) for 10 min. Then the slices were mounted on microscope glass slides and imaged immediately with a laser scanning microscope system (Nikon Eclipse Ni, Tokyo, Japan).

Western Blotting Analysis

The protein of PMHs was homogenized in RIPA buffer containing protease inhibitor (Beyotime Institute of Biotechnology, Shanghai, China). Subsequently, the protein concentrations were measured using a BCA protein assay kit (Beyotime Institute of Biotechnology). Equivalent amounts of protein were separated by SDS-PAGE and then transferred onto polyvinylidene fluoride membranes (Millipore, Billerica, MA, USA). The membrane was blocked with 5% bovine albumin (BSA) in Tris-buffered saline containing 0.05% Tween 20 and then incubated with the specific primary antibodies, followed by HRP-conjugated secondary antibody incubation. And the target proteins were visualized with enhanced chemiluminescence (Thermo Fisher, Carlsbad, CA, USA). The intensity of the protein band was quantified using ImageJ software.

Quantitative Real-Time PCR Analysis

The total RNA was extracted using TRIzol reagent (TransGene Biotech, Beijing, China) and then transcribed into cDNA using TranScript All-in-One First-Strand cDNA Synthesis SuperMix (TransGene Biotech), as instructed by the manufacturer. Real-time PCR was performed with an Eppendorf Realplex PCR system using TransStart Tip Green qPCR SuperMix (TransGene Biotech). The mRNA expression was normalized to the expression of the housekeeping gene β-actin. All primer sequences presented in **Table 1** were from PrimerBank (36) and synthesized by Huada Gene Technology Co., Ltd (Shenzhen, China).

Statistical Analysis

All data were expressed as mean ± SEM. Statistical significance was determined by the unpaired two-tailed *t*-test using GraphPad Prism 8.0 software (San Diego, CA, USA). Differences were considered statistically significant at $p < 0.05$.

TABLE 1 | Primers used for real-time qRT-PCR.

Gene	Primer	Sequence (5'-3')
PPARα	Forward	AACATCGAGTGTCGAATATGTGG
	Reverse	CCGAATAGTTCGCCGAAAGAA
CPT1	Forward	TGGCATCATCACTGGTGTGTT
	Reverse	GTCTAGGGTCCGATTGATCTTTG
ACOX1	Forward	TAACTTCCTCACTCGAAGCCA
	Reverse	AGTTCCATGACCCATCTCTGTC
SREBP1c	Forward	TGACCCGGCTATTCCGTGA
	Reverse	CTGGGCTGAGCAATACAGTTC
ACC1	Forward	CTCCCGATTCATAATTGGGTCTG
	Reverse	CTCCCGATTCATAATTGGGTCTG
FASN	Forward	GGAGGTGGTGATAGCCGGTAT
	Reverse	TGGGTAATCCATAGAGCCCAG
β-actin	Forward	GTGACGTTGACATCCGTAAAGA
	Reverse	GCCGGACTCATCGTACTCC

RESULTS

Mannose Supplement Alleviates Hepatic Steatosis in ALD

To address the role of mannose supplement in ALD, we investigated the degree of liver injury and hepatic steatosis in pair-fed mice (Pair) or a chronic-binge ethanol feeding mouse model of ALD (EtOH), along with drinking-water supplemented with different concentrations of mannose (Man). As shown in **Figure 1A** and **Table S1**, enzymatic assays demonstrated that mannose administration significantly reduced serum ALT and AST levels that elevated in chronic-binge ethanol-fed mice. The H&E staining of liver sections showed that ethanol-fed mice displayed extensive hepatic injuries and steatosis, which were markedly attenuated by mannose administration (**Figure 1B**). Furthermore, alcohol consumption substantially elevated TG, TC, and LDL-C levels but reduced HDL-C level in serum or liver tissue, which could be significantly inhibited by oral mannose (3%) supplement (**Figures 1C–E** and **Table S1**). Further Oil Red O staining of liver tissue sections revealed that mannose remarkably reduced ethanol-induced hepatic lipid deposits, and 3% mannose has the most significant effect (**Figure 1F**). Additionally, we performed immunofluorescence staining of liver tissue sections with BODIPY and found that mannose co-administration markedly reduced lipid deposits that present predominantly in hepatocytes upon ethanol administration (**Figure 1G**). Collectively, these results indicated a potential protective role of mannose against hepatic steatosis in ALD.

Mannose Treatment Attenuates Ethanol-Induced Lipid Accumulation in Primary Mouse Hepatocytes

Building upon the above findings in the mouse ALD model, we explored the exact role of mannose on hepatocytes *in vitro*. Therefore, we utilize an *in vitro* model of ALD established using ethanol-treated PMHs (32, 37, 38). Since most of the studies about the mannose supplement, mannose was added concurrently with other drugs or stimuli (24, 25), we simultaneously treated the PMHs with ethanol and indicated concentrations of mannose. Consistent with the above results *in vivo*, we demonstrated that mannose treatment significantly reduced serum ALT and AST activities and intracellular TG and TC levels in PMHs, which notably increased upon ethanol stimulation (**Figures 2A, B** and **Table S2**). Moreover, this effect was dose-dependent but with an effective plateau or saturation at concentrations higher than 5 mM (**Figures 2A, B** and **Table S2**). Further cellular staining with BODIPY 493/503 lipophilic fluorescent dye showed that ethanol notably elevated cellular neutral lipid contents deposited within lipid droplets in cultured PMHs, which significantly reduced upon mannose treatment (**Figure 2C**). These findings indicated that mannose could attenuate ethanol-induced lipid accumulation in PMHs.

Mannose Suppresses Ethanol-Mediated Reduction of Hepatocyte Fatty Acid Oxidation

Considering the above results showing that mannose attenuates ethanol-induced hepatocyte lipid accumulation in ALD, we were intrigued to clarify the underlying mechanisms. Firstly, we examined the mRNA levels and protein expression of crucial fatty acid oxidation (FAO)-related genes associated with lipid metabolism. As shown in **Figures 3A, B**, we observed notably reduced protein and mRNA levels of PPARα, a key controller of FAO (39), and its downstream FAO-related genes (ACOX1, CPT1) in isolated PMHs from ethanol-fed mice than that from pair-fed controls. However, oral mannose supplement significantly increased PPARα, ACOX1 and CPT1 levels in freshly isolated PMHs from ethanol-fed mice (**Figures 3A, B**). Further immunohistochemistry analysis also showed marked elevation of PPARα expression in liver sections from ethanol-fed mice upon mannose administration, although its expression notably decreased during ethanol feeding (**Figure 3C**). Similar results showed that mannose significantly increased protein and mRNA levels of PPARα, ACOX1 and CPT1 in PMHs upon ethanol treatment *in vitro* (**Figures 3D, E**). We also evaluated the effect of mannose on PPARγ, a nuclear receptor superfamily of ligand-inducible transcription factors involved in fatty acid uptake (40, 41). While the protein and mRNA levels of PPARγ in PMHs elevated upon ethanol stimulation, they were comparable between the mannose treated or untreated PMHs *in vitro* (**Figure 3D**). These data suggest that

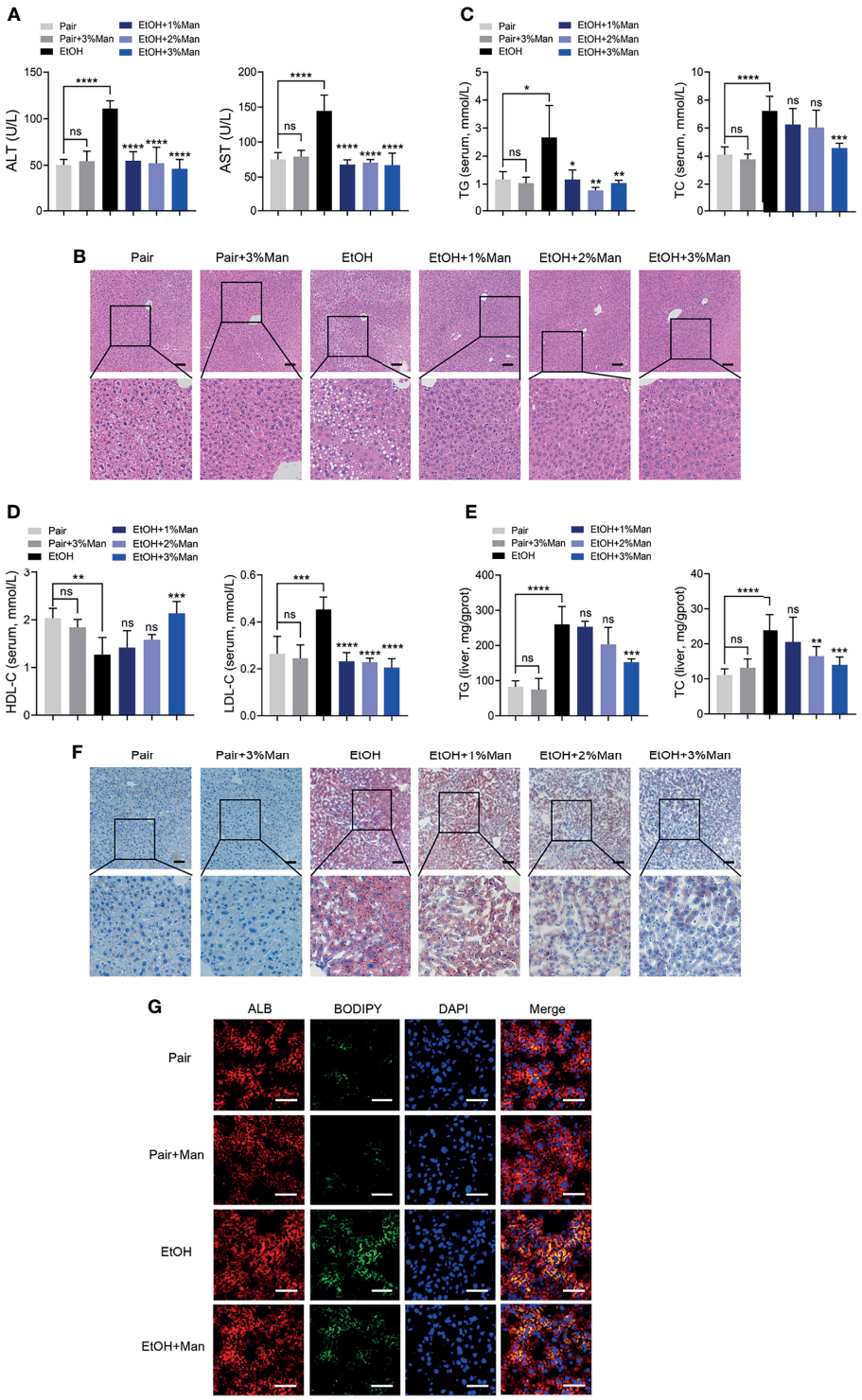

FIGURE 1 | Mannose supplement alleviates hepatic steatosis in ALD. Mice were fed control diet (Pair) or ethanol diet (EtOH) supplemented with/without 1%, 2%, 3% (w/v) mannose (Man) (n = 6 for each group). **(A)** Serum ALT and AST activities were assessed. **(B)** Histologic analysis of liver sections using H&E staining. Scale bars = 100 μm. **(C, D)** Serum TG, TC, HDL-C and LDL-C levels, and **(E)** hepatic TG and TC contents were determined. **(F)** Representative images of Oil Red O staining on liver sections. Scale bars = 100 μm. **(G)** Co-localization of neutral lipids (Green) and hepatocyte markers ALB (Red) in the liver sections were evaluated by immunofluorescence staining (n = 3). Scale bars = 25μm. Data are presented as the means ± SEM and analyzed with the unpaired two-tailed *t*-test. $^{*}p < 0.05$, $^{**}p < 0.01$, $^{***}p < 0.001$, $^{****}p < 0.0001$, ns, not significant, compared with the EtOH group.

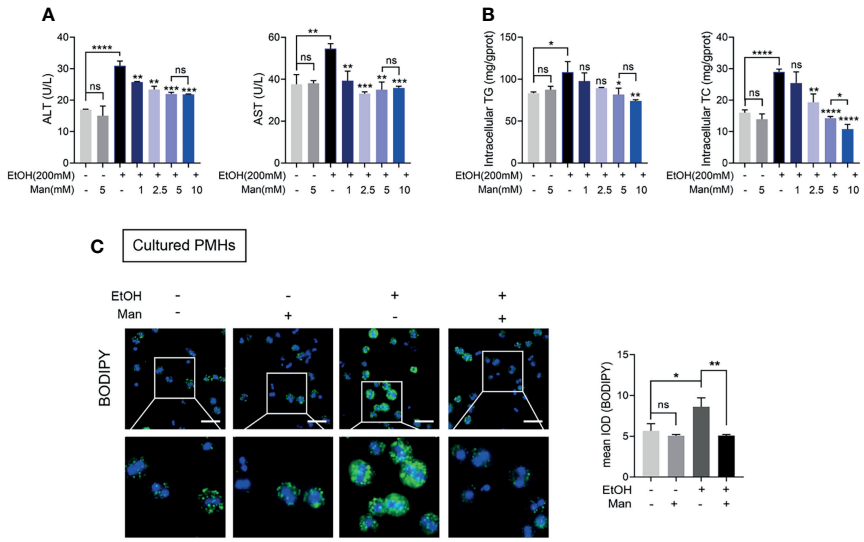

FIGURE 2 | Mannose treatment attenuates ethanol-induced lipid accumulation in PMHs. PMHs isolated from WT mice were stimulated by 200 mM ethanol (EtOH) with different concentrations of mannose (Man) for 24 h (n = 3). **(A)** The ALT and AST activities in the culture supernatant were measured. **(B)** The intracellular TG and TC contents were determined. **(C)** The content of neutral lipids was detected by double staining with BODIPY 493/503 dye and Hoechst in PMHs (cultured with 5 mM mannose). Scale bars = 50 μm. Data are presented as the mean ± SEM of three independent experiments and analyzed with the unpaired two-tailed t-test. $^{*}p < 0.05$, $^{**}p < 0.01$, $^{***}p < 0.001$, $^{****}p < 0.0001$, ns, not significant, compared with the EtOH group.

mannose might attenuate ethanol-induced lipid accumulation in hepatocytes *via* regulating lipid metabolism by upregulating fatty acid β-oxidation.

Mannose Inhibits Ethanol-Induced Hepatocyte Lipogenesis

Besides fatty acid oxidation, alcohol-induced hepatic lipid accumulation is also regulated by lipogenesis (42). Therefore, we next investigated whether mannose disturbs the alcohol-induced *de novo* lipogenesis in hepatocytes. As shown in **Figures 4A, B**, oral mannose supplementation could reverse the alcohol-induced elevation of protein and mRNA levels of crucial lipogenic enzyme SREBP1c and its downstream lipogenic genes (ACC1, FASN) in isolated PMHs. Further immunohistochemistry staining determined notably reduced SREBP1c expression in liver tissue sections from ethanol-fed mice upon mannose administration compared to that without mannose supplement (**Figure 4C**). Accordantly, we demonstrated that *in vitro* mannose treatment could eliminate the ethanol-induced increased protein and mRNA levels of SREBP1c, ACC1 and FASN in cultured PMHs (**Figures 4D, E**). Therefore, these data suggest that mannose might ameliorate ethanol-induced hepatocyte lipid accumulation in ALD by regulating lipid metabolism by inhibiting lipogenesis.

Mannose Suppresses Ethanol-Induced Activation of PI3K/Akt/mTOR Signaling Pathway in Hepatocytes

Given that PI3K/Akt/mTOR signaling pathway plays a crucial role in regulating the lipid metabolic process (12, 43), we subsequently investigated whether mannose affected PI3K/Akt/mTOR signaling pathway activation. Western blotting analysis demonstrated that mannose supplement significantly downregulated alcohol-induced elevation of PI3K expression (subunit p85, p110), as well as Akt and mTOR phosphorylation in isolated PMHs from ethanol-fed mice (**Figure 5A**). Additionally, we also observed that mannose notably downregulated the ethanol-induced increased levels of PI3K (subunit p85, p110), as well as Akt and mTOR phosphorylation in PMHs upon ethanol treatment *in vitro* (**Figure 5B**). Therefore, these data indicate that mannose suppresses the ethanol-induced PI3K/Akt/mTOR signaling pathway activation in ALD.

Mannose Improves Ethanol-Induced Lipid Accumulation in PMHs *via* The PI3K/Akt/mTOR Pathway

Our data above point to the potential involvement of the PI3K/Akt/mTOR signaling pathway in mannose-mediated alleviation of lipid accumulation driven by ethanol-mediated imbalanced lipid metabolism in hepatocytes. To test this, we pretreated PMHs with specific inhibitors or agonists of the PI3K/Akt/mTOR signaling pathway ahead of mannose with/without ethanol treatment. Western blotting analysis showed that pretreatment with the mTOR-specific inhibitor, rapamycin, did suppress mTOR phosphorylation, whereas its agonist MHY1485 could trigger mTOR phosphorylation (**Figure 6A**). However, these pretreatments could eliminate the differences of ethanol-induced hepatocyte lipid accumulation between mannose treated or untreated PMHs,

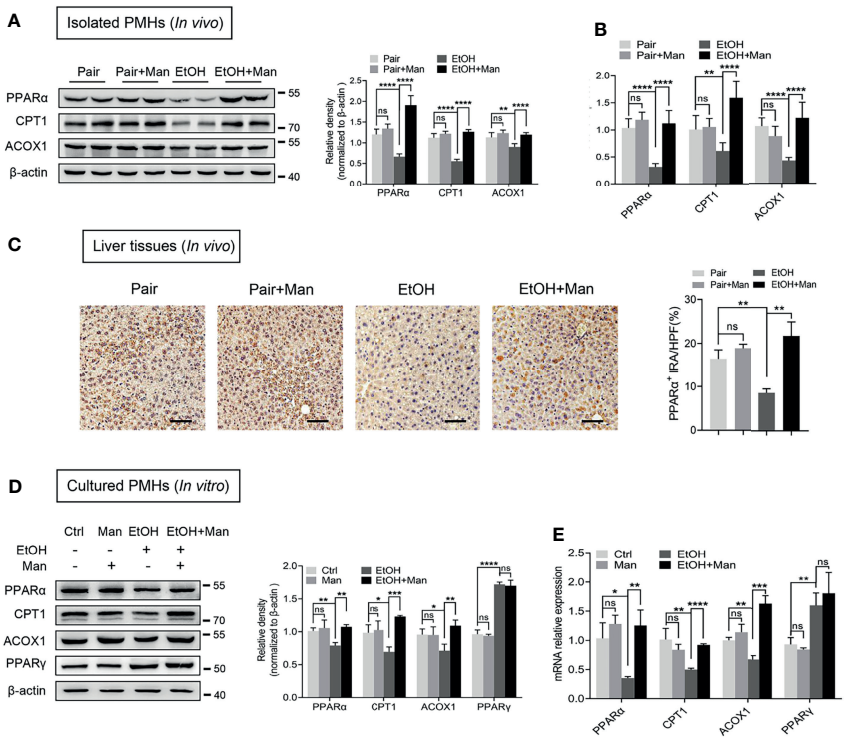

FIGURE 3 | Mannose suppresses ethanol-mediated reduction of hepatocyte fatty acid oxidation. **(A–C)** PMHs were extracted from mice (n = 6 for each group) fed the control diet (Pair) or ethanol diet (EtOH) supplemented with/without 3% (w/v) mannose (Man). The protein **(A)** and mRNA **(B)** levels of PPARα, CPT1, ACOX1 were evaluated by Western blotting and qRT-PCR, respectively. **(C)** Representative images of PPARα staining on the liver sections (n = 3). Scale bars = 100 μm. **(D, E)** PMHs from WT mice were stimulated by 200 mM ethanol (EtOH) with/without 5 mM mannose (Man) for 24 h, PMHs with cell culture medium as control (Ctrl). The protein **(D)** and mRNA **(E)** levels of PPARα, CPT1, ACOX1 and PPARγwere determined (n = 3). Data are expressed as the mean ± SEM of three independent experiments. $^{*}p < 0.05$, $^{**}p < 0.01$, $^{***}p < 0.001$, $^{****}p < 0.0001$, ns, not significant, unpaired two-tailed *t*-test.

as determined by comparable intracellular TG and TC levels, cellular neutral lipid contents, protein and mRNA levels of FAO-related genes (PPARα, CPT1, ACOX1) and lipogenic genes (SREBP-1, ACC1, FASN) in these cells (**Figures 6B–G**). Similar results were observed when using the PI3K inhibitor LY294002 or its agonist 740 Y-P instead of the inhibitor and agonist of mTOR (**Figure 7**). Overall, these results confirmed that PI3K/Akt/mTOR singling is responsible for the inhibitory effect of mannose on lipid accumulation in hepatocytes.

DISCUSSION

- Hepatic steatosis is recognized as an early symptom and a critical event during the progression of ALD, which can progress to severer liver diseases without efficient therapy (44). Thus developing effective therapeutic interventions for treating hepatic steatosis is critical to prevent further deterioration of ALD, whereas available effective target drugs are lacking (45). D-mannose, a monosaccharide widely distributed in nature, can be extracted from many plants and fruits, becoming a supplement for effective therapeutic strategies in various diseases (46). Recently, mannose supplements have been reported to treat liver-related diseases (26, 27, 47). Therefore, we were intrigued to explore the potential application of mannose supplements to prevent ALD deterioration. In the present study, while utilizing a widely used chronic-binge ethanol feeding mouse model of ALD, we discovered that oral mannose supplementation did alleviate ALD. This effect was evidenced by considerable improvement in liver injury and particular hepatic steatosis, which represented the main characteristics of ALD (1) in ethanol-fed mice upon mannose administration. A previous report indicated that mannose supplementation attenuated the liver steatosis induced by a high-fat diet when initiated early in life, suggesting a potential protective role of mannose against hepatic steatosis, which partially supports our current results (27). Consistently, we observed a similar effect of mannose in an *in vitro* model of ALD established using ethanol to stimulate primary mouse hepatocytes (32, 37, 38). Overall, our findings did emphasize the hepatoprotective role of mannose in ALD.

As we know, mannose is a 2-epimer of glucose present throughout nature, even in mammal cells (20, 21). Although

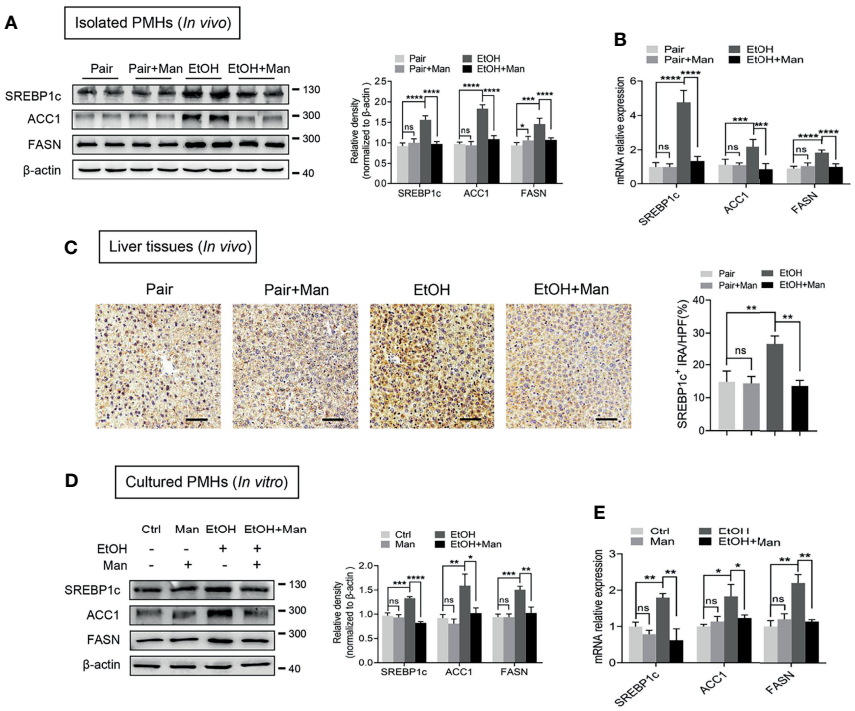

FIGURE 4 | Mannose inhibits ethanol-induced hepatocyte lipogenesis. **(A-C)** Isolated PMHs were obtained from mice fed the control diet (Pair) or ethanol diet (EtOH) supplemented with or without 3% (w/v) mannose (Man). The protein **(A)** and mRNA **(B)** levels of SREBP1c, ACC1 and FASN were evaluated (n = 6). **(C)** Representative images of SREBP1c staining on the liver sections (n = 3). Scale bars = 100 μm. **(D, E)** PMHs from WT mice were stimulated by 200 mM ethanol (EtOH) with/without 5 mM mannose (Man) for 24 h, PMHs with cell culture medium as control (Ctrl). The protein **(D)** and mRNA **(E)** levels of lipogenic enzyme genes SREBP1c, ACC1, and FASN were evaluated (n = 3). Data are expressed as the means ± SEM of three independent experiments. $^{*}p < 0.05$, $^{**}p < 0.01$, $^{***}p < 0.001$, $^{****}p < 0.0001$, ns, not significant, unpaired two-tailed *t*-test.

most mannose is derived from glucose and further catabolized to glycosylation precursors in the cells, it can also be uptook or released by various cell types (48). It has been reported that circulating mannose levels could be influenced by metabolic disorders (21). Accumulating evidence indicated that plasma mannose levels increased in subjects with insulin resistance (IR), including diabetics (49, 50). Furthermore, several studies demonstrated that blood mannose levels are closely linked to glucose metabolism or IR and insulin secretion (50–52). However, drinking-water supplementation of supraphysiological levels of D-mannose suppressed immunopathology in mouse models of diabetes, partially by its Treg-promoting effect mediated by upregulation of integrin $\alpha_v\beta_8$ and reactive oxygen species generated by increased fatty acid oxidation (25). IR and lipid metabolism dysfunction are common disorders in ALD (53, 54). Furthermore, alcohol consumption could impair the insulin signaling pathway in the liver, leading to glucose and lipid metabolism disorders, becoming vital drivers of hepatic steatosis in ALD (55, 56). Alcohol consumption also leads to defective glycosylation of lipid-carrying apolipoproteins, resulting in impaired intracellular lipid and lipoprotein transport, which in turn may contribute to alcoholic hepatic steatosis (57). These data suggest potential interactions of mannose and hepatic steatosis in ALD. However, the mechanisms need to be further explored.

Excessive lipid accumulation in hepatocytes and further hepatic steatosis are critical risk factors for ALD deterioration (58). Although previous studies indicated the potential functions of mannose for alleviating ALD (26), the exact role and the underlying mechanism of mannose in this context are still unknown. In this study, we did investigate that mannose did notably attenuate the ethanol-induced elevation of lipid deposits in hepatocytes both *in vivo* and *in vitro*, indicated by reduced ethanol-induced elevation of TG and TC levels and cellular neutral lipid contents. Intriguingly, *in vitro* experiments suggest that this effect of mannose is dose-dependent, reaching a plateau at concentrations above 5 mM. Of note, this effective working concentration is much lower than that in treating cancer cells as a supplement (24). This result was partially supported by a previous study showing that mannose attenuates hepatic stellate cell activation in a dose-dependent manner with an effective plateau (26). Furthermore, we found that mannose supplement hardly changed the transcription of the principal enzymes responsible for ethanol metabolism, alcohol dehydrogenase 1 (ADH1) and aldehyde dehydrogenase 2 (ALDH2) (59), indicating that mannose might not affect

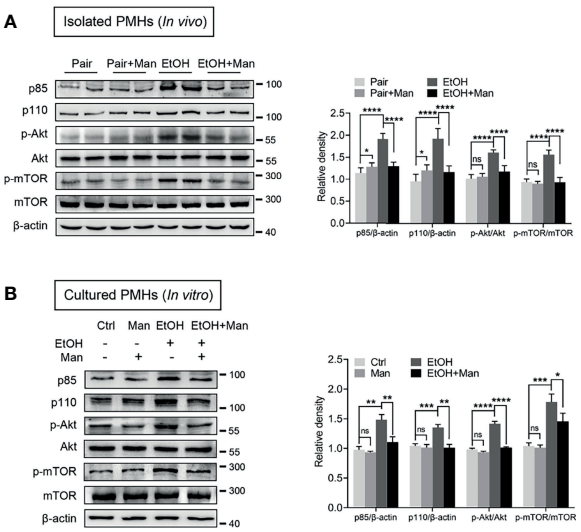

FIGURE 5 | Mannose suppresses ethanol-induced activation of PI3K/Akt/mTOR signaling pathway. **(A)** Isolated PMHs were obtained from mice fed the control diet (Pair) or ethanol diet (EtOH) supplemented with or without 3% (w/v) mannose (Man). The expression levels of PI3K-p85, PI3K-p110, p-Akt, Akt, p-mTOR and mTOR in isolated PMHs were analyzed by Western blotting (n = 6). **(B)** PMHs from WT mice were stimulated by 200 mM ethanol (EtOH) with/without 5 mM mannose (Man) for 24 h, PMHs with culture medium as control (Ctrl). PI3K-p85, PI3K-p110, Akt, p-Akt, mTOR and p-mTOR levels in cultured PMHs were determined (n = 3). Data are expressed as the mean ± SEM of three independent experiments. $^{*}p < 0.05$, $^{**}p < 0.01$, $^{***}p < 0.001$, $^{****}p < 0.0001$, ns, not significant, unpaired two-tailed *t*-test.

ethanol metabolism (**Figure S1**). Thus, these present results suggest that mannose alleviates lipid accumulation in hepatocytes not by affecting ethanol metabolism, thus improving hepatic steatosis in ALD.

Hepatic steatosis is characterized by excessive lipid accumulation in hepatocytes due to imbalanced lipid metabolism, driven mainly by reduced FAO, whereas increased *de novo* lipogenesis (60). PPARs, as ligand-activated transcription factors belonging to the nuclear receptor (NR) superfamily, play pivotal roles in liver diseases (61). PPARα, a subtype of PPARs, is widely expressed in the liver and regulates the mRNA expression of FAO-related genes (62). CPT1 and ACOX1, representative FAO-related genes, are the rate-limiting enzymes in the mitochondrial fatty acid oxidation and peroxisomal fatty acid β-oxidation, respectively (63). Emerging data have also demonstrated that alcohol consumption reduced fatty acid oxidation in hepatocytes through inhibiting PPARα (64). Therefore, these data prompt us to investigate whether mannose affects FAO in hepatocytes in ALD models. Our present findings indicated that ethanol did inhibit FAO in PMHs, evidenced by significantly reduced transcription and expression of PPARα and its target CPT1 and ACOX1 upon alcohol treatment. However, this ethanol-induced reduction of FAO was significantly inhibited after mannose treatment. Moreover, mannose could not significantly affect the expression of PPARγ involved in fatty acid uptake (40, 41, 65), although the PPARγ levels did elevate upon alcohol exposure as reported before (66–68). Therefore, these data imply that mannose might regulate lipid metabolism *via* upregulating fatty acid β-oxidation in ALD.

Except for fatty acid β-oxidation in cells, our current study also took *de novo* lipogenesis into account. SREBP1c is a crucial transcription factor modulating *de novo* lipogenesis *via* regulating the transcriptions of lipogenic genes such as ACC1, FASN (69). It has been reported that both acute and chronic ethanol exposure results in increased expression of SREBP1c and its target lipid synthesis enzymes (70). Furthermore, SREBP1c null mice are protected from ethanol-induced hepatic steatosis (71). Indeed, our present results confirmed that alcohol treatment significantly increased SREBP1c, ACC1 and FASN levels. As expected, we found that mannose could suppress the increased transcription and expression of lipogenic genes induced by ethanol. Therefore, our present *in vivo* and *in vitro* study suggests that mannose can regulate lipid metabolism *via* inhibiting alcohol-induced *de novo* lipogenesis in ALD. Overall, our current finding provided preliminary evidence that mannose prevented the imbalanced lipid metabolism induced by ethanol intake.

Although the exact mechanism of imbalanced lipid metabolism upon chronic alcohol consumption remains elusive, several signaling pathways might be involved where their crosstalk is complicated (45). Emerging evidence shows that the PI3K/Akt/mTOR pathway plays a critical role in lipid metabolism *via* regulating FAO and lipogenesis (12, 33, 72). Furthermore, a previous study about hepatocellular carcinoma suggests that activation of the Akt/mTOR pathway could elevate the expression of FAO regulator SREBP1c and then reprogram hepatic lipid metabolism (73). Additionally, Hanqing et al. observed that the mechanistic target of rapamycin complex 1 (mTORC1, mTOR complex 1) is necessary for ethanol-induced

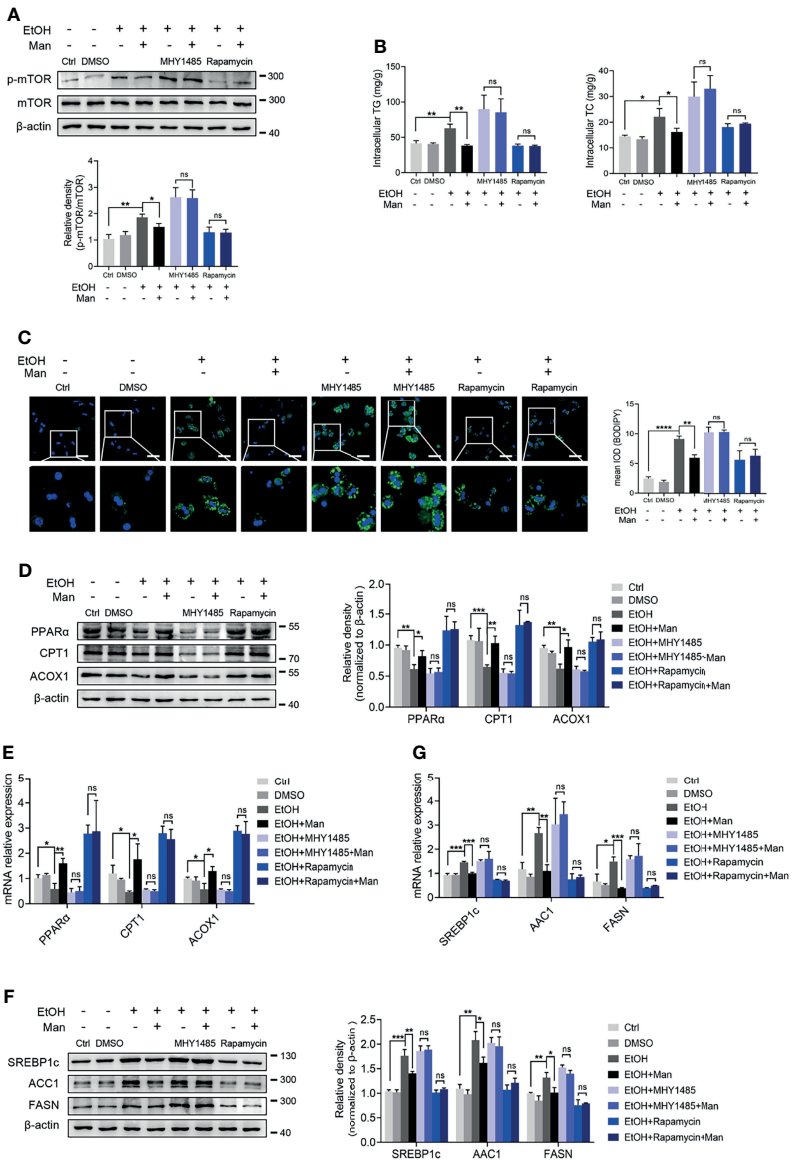

FIGURE 6 | mTOR activation is involved in the mannose-mediated improvement of ethanol-induced lipid accumulation in PMHs. PMHs were pretreated with MHY1485 (mTOR agonist, 10 μM) or Rapamycin (mTOR inhibitor, 10 nM) for 2 h (DMSO as control), ahead of treatment with 200 mM ethanol (EtOH) and 5 mM mannose (Man) or culture medium (Ctrl) for 24 h (n = 3). **(A)** Western blotting was used to evaluate the p-mTOR expression in cultured PMHs. **(B)** Cellular content of TG and TC levels were determined. **(C)** The intracellular levels of neutral lipids were evaluated by BODIPY 493/503 staining assay. **(D–G)** Western blotting and qRT-PCR analysis for protein and mRNA levels of lipid-regulating genes in PMHs. Scale bars = 50 μm. Data are expressed as the mean ± SEM of three independent experiments. *$p < 0.05$, **$p < 0.01$, ***$p < 0.001$, ****$p < 0.0001$, ns, not significant, unpaired two-tailed *t*-test.

imbalanced metabolism, driven by induction of hepatic *de novo* lipogenesis whereas suppressing fatty acid oxidation in alcohol liver disease (19). Given our current finding showing that mannose treatment markedly upregulated the ethanol-induced PI3K/Akt/mTOR signaling pathway activation, we proposed that this pathway is involved in the mannose-mediated improvement of imbalanced lipid metabolism in hepatocytes. To confirm this hypothesis, we subsequently pretreated PMHs with both inhibitors and agonists of PI3K or mTOR, ahead of ethanol exposure with/without mannose. The present results demonstrated that these inhibitors or agonists did inhibit or activate the PI3K/Akt/mTOR pathway and regulate the expression of downstream lipid metabolism-related genes, which was in line with a previous report (33). Our current results indicated that mannose treatment suppressed lipogenesis whereas enhanced fatty acid oxidation, which further attenuated lipid accumulation in PMHs exposed to ethanol. Intriguingly, these effects of mannose were abolished upon pretreatment with

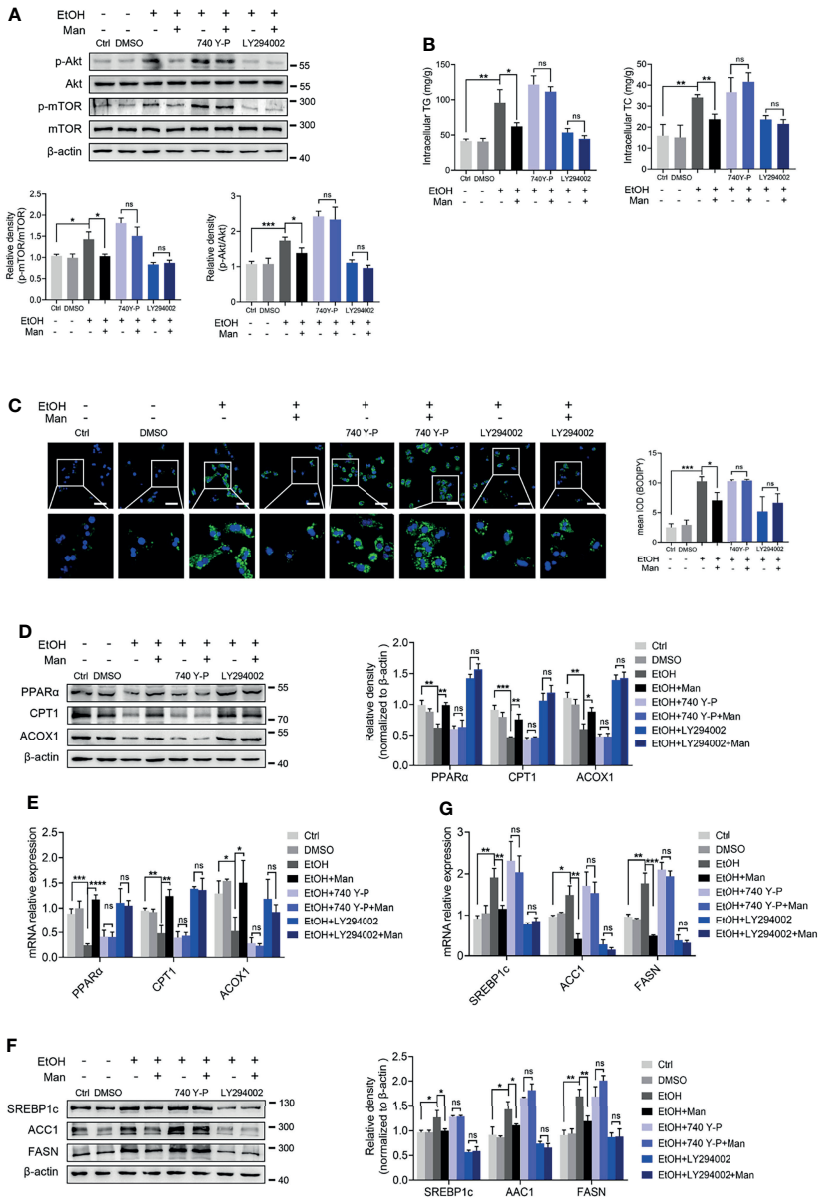

FIGURE 7 | PI3K-mediated Akt/mTOR activation involves mannose-mediated improvement of ethanol-induced lipid accumulation in PMHs. PMHs from WT mice were pretreated with 740 Y-P (PI3K agonist, 20 μg/ml) or LY294002 (PI3K inhibitor, 20 μM) for 2 h (DMSO as control), ahead of treatment with 200 mM ethanol (EtOH) and 5 mM mannose (Man) or culture medium (Ctrl) for 24 h (n = 3). **(A)** Akt, p-Akt, mTOR and p-mTOR expressions were evaluated. **(B)** Cellular content of TG and TC levels were determined. **(C)** The intracellular levels of neutral lipids were determined by BODIPY 493/503 staining assay. **(D–G)** Western blotting and qRT-PCR analysis for protein and mRNA levels of lipid-regulating genes. Scale bars = 50 μm. Data are expressed as the mean ± SEM of three independent experiments. *$p < 0.05$, **$p < 0.01$, ***$p < 0.001$, ****$p < 0.0001$, ns, not significant, unpaired two-tailed *t*-test.

these inhibitors or agonists, confirming that PI3K/Akt/mTOR signaling pathway is responsible for the inhibitory effect of mannose on lipid accumulation in hepatocytes. However, it should be noted that other signaling pathways involved in lipid metabolism could not be excluded.

In summary, this study elucidates a previously unknown hepatoprotective role of mannose against hepatic steatosis in ALD progression. Additionally, mannose can exert this protective effect by reversing imbalanced lipid metabolism to alleviate hepatocyte lipid accumulation. Furthermore, mannose can modulate lipid metabolism by upregulating fatty acid oxidation whereas damping *de novo* lipogenesis *via* inhibiting PI3K/Akt/mTOR signaling pathway activation. Thus, our present data indicate that mannose might be a potential candidate to treat alcoholic liver steatosis, providing novel insights for its application in hepatic steatosis-related liver diseases.

DATA AVAILABILITY STATEMENT

The original contributions presented in the study are included in the article/**Supplementary Material**. Further inquiries can be directed to the corresponding authors.

ETHICS STATEMENT

The animal study was reviewed and approved by the Southern Medical University Experimental Animal Ethics Committee (No. L2020128).

AUTHOR CONTRIBUTIONS

MH and YC are the primary investigators in this study. FD, JL, and LD participated in part of *in vivo* experiments. FD and BC participated in part of *in vitro* experiments. XL and YZ participated in part of the statistical analysis. JZ and ZC designed the study. JZ and MH wrote the manuscript. All authors contributed to the article and approved the submitted version.

FUNDING

This work was supported by the National Natural Science Foundation of China (NO.81971550 and NO.82171745).

SUPPLEMENTARY MATERIAL

The Supplementary Material for this article can be found online at: https://www.frontiersin.org/articles/10.3389/fimmu.2022.877650/full#supplementary-material

REFERENCES

1. Seitz HK, Bataller R, Cortez-Pinto H, Gao B, Gual A, Lackner C, et al. Alcoholic Liver Disease. *Nat Rev Dis Primers* (2018) 4(1):16. doi: 10.1038/s41572-018-0014-7
2. Osna NA, Donohue TM Jr, Kharbanda KK. Alcoholic Liver Disease: Pathogenesis and Current Management. *Alcohol Res* (2017) 38(2):147–61.
3. Singal AK, Bataller R, Ahn J, Kamath PS, Shah VH. ACG Clinical Guideline: Alcoholic Liver Disease. *Am J Gastroenterol* (2018) 113(2):175–94. doi: 10.1038/ajg.2017.469
4. Singh S, Osna NA, Kharbanda KK. Treatment Options for Alcoholic and Non-Alcoholic Fatty Liver Disease: A Review. *World J Gastroenterol* (2017) 23 (36):6549–70. doi: 10.3748/wjg.v23.i36.6549
5. Louvet A, Mathurin P. Alcoholic Liver Disease: Mechanisms of Injury and Targeted Treatment. *Nat Rev Gastroenterol Hepatol* (2015) 12(4):231–42. doi: 10.1038/nrgastro.2015.35
6. Fujii H, Kawada N. Fibrogenesis in Alcoholic Liver Disease. *World J Gastroenterol* (2014) 20(25):8048–54. doi: 10.3748/wjg.v20.i25.8048
7. Seitz HK, Bataller R, Cortez-Pinto H, Gao B, Gual A, Lackner C, et al. Publisher Correction: Alcoholic Liver Disease. *Nat Rev Dis Primers* (2018) 4 (1):18. doi: 10.1038/s41572-018-0021-8
8. Pawlak M, Lefebvre P, Staels B. Molecular Mechanism of Pparα Action and Its Impact on Lipid Metabolism, Inflammation and Fibrosis in Non-Alcoholic Fatty Liver Disease. *J Hepatol* (2015) 62(3):720–33. doi: 10.1016/j.jhep.2014.10.039
9. Bougarne N, Weyers B, Desmet SJ, Deckers J, Ray DW, Staels B, et al. Molecular Actions of Pparα in Lipid Metabolism and Inflammation. *Endocr Rev* (2018) 39(5):760–802. doi: 10.1210/er.2018-00064
10. Xu X, So JS, Park JG, Lee AH. Transcriptional Control of Hepatic Lipid Metabolism by SREBP and ChREBP. *Semin Liver Dis* (2013) 33(4):301–11. doi: 10.1055/s-0033-1358523
11. Linden AG, Li S, Choi HY, Fang F, Fukasawa M, Uyeda K, et al. Interplay Between ChREBP and SREBP-1c Coordinates Postprandial Glycolysis and Lipogenesis in Livers of Mice. *J Lipid Res* (2018) 59(3):475–87. doi: 10.1194/jlr.M081836
12. Du C, Wu M, Liu H, Ren Y, Du Y, Wu H, et al. Thioredoxin-Interacting Protein Regulates Lipid MetabolismVia Akt/mTOR Pathway in Diabetic Kidney Disease. *Int J Biochem Cell Biol* (2016) 79:1–13. doi: 10.1016/j.biocel.2016.08.006
13. Krycer JR, Sharpe LJ, Luu W, Brown AJ. The Akt-SREBP Nexus: Cell Signaling Meets Lipid Metabolism. *Trends Endocrinol Metab* (2010) 21 (5):268–76. doi: 10.1016/j.tem.2010.01.001
14. Jin M, Feng H, Wang Y, Yan S, Shen B, Li Z, et al. Gentiopicroside Ameliorates Oxidative Stress and Lipid Accumulation Through Nuclear Factor Erythroid 2-Related Factor 2 Activation. *Oxid Med Cell Longev* (2020) 2020:2940746. doi: 10.1155/2020/2940746
15. Gu H, Jiang W, You N, Huang X, Li Y, Peng X, et al. Soluble Klotho Improves Hepatic Glucose and Lipid Homeostasis in Type 2 Diabetes. *Mol Ther Methods Clin Dev* (2020) 18:811–23. doi: 10.1016/j.omtm.2020.08.002
16. Yi J, Zhu J, Wu J, Thompson CB, Jiang X. Oncogenic Activation of PI3K-AKT-mTOR Signaling Suppresses FerroptosisVia SREBP-Mediated Lipogenesis. *Proc Natl Acad Sci USA* (2020) 117(49):31189–97. doi: 10.1073/pnas.2017152117
17. Porstmann T, Santos CR, Griffiths B, Cully M, Wu M, Leevers S, et al. SREBP Activity Is Regulated by Mtorc1 and Contributes to Akt-Dependent Cell Growth. *Cell Metab* (2008) 8(3):224–36. doi: 10.1016/j.cmet.2008.07.007
18. Zeng T, Zhang CL, Song FY, Zhao XL, Yu LH, Zhu ZP, et al. PI3K/Akt Pathway Activation Was Involved in Acute Ethanol-Induced Fatty Liver in Mice. *Toxicology* (2012) 296(1-3):56–66. doi: 10.1016/j.tox.2012.03.005
19. Chen H, Shen F, Sherban A, Nocon A, Li Y, Wang H, et al. DEP Domain-Containing mTOR-Interacting Protein Suppresses Lipogenesis and Ameliorates Hepatic Steatosis and Acute-on-Chronic Liver Injury in Alcoholic Liver Disease. *Hepatology* (2018) 68(2):496–514. doi: 10.1002/hep.29849
20. Alton G, Hasilik M, Niehues R, Panneerselvam K, Etchison JR, Fana F, et al. Direct Utilization of Mannose for Mammalian Glycoprotein Biosynthesis. *Glycobiology* (1998) 8(3):285–95. doi: 10.1093/glycob/8.3.285
21. Sharma V, Ichikawa M, Freeze HH. Mannose Metabolism: More Than Meets the Eye. *Biochem Biophys Res Commun* (2014) 453(2):220–8. doi: 10.1016/j.bbrc.2014.06.021
22. Girard M, Douillard C, Debray D, Lacaille F, Schiff M, Vuillaumier-Barrot S, et al. Long Term Outcome of MPI-CDG Patients on D-Mannose Therapy. *J Inherit Metab Dis* (2020) 43(6):1360–9. doi: 10.1002/jimd.12289
23. Kranjčec B, Papeš D, Altarac S. D-Mannose Powder for Prophylaxis of Recurrent Urinary Tract Infections in Women: A Randomized Clinical Trial. *World J Urol* (2014) 32(1):79–84. doi: 10.1007/s00345-013-1091-6
24. Gonzalez PS, O'Prey J, Cardaci S, Barthet VJA, Sakamaki JI, Beaumatin F, et al. Mannose Impairs Tumour Growth and Enhances Chemotherapy. *Nature* (2018) 563(7733):719–23. doi: 10.1038/s41586-018-0729-3
25. Zhang D, Chia C, Jiao X, Jin W, Kasagi S, Wu R, et al. D-Mannose Induces Regulatory T Cells and Suppresses Immunopathology. *Nat Med* (2017) 23 (9):1036–45. doi: 10.1038/nm.4375
26. DeRossi C, Bambino K, Morrison J, Sakarin I, Villacorta-Martin C, Zhang C, et al. Mannose Phosphate Isomerase and Mannose Regulate Hepatic Stellate Cell Activation and Fibrosis in Zebrafish and Humans. *Hepatology* (2019) 70 (6):2107–22. doi: 10.1002/hep.30677
27. Sharma V, Smolin J, Nayak J, Ayala JE, Scott DA, Peterson SN, et al. Mannose Alters Gut Microbiome, Prevents Diet-Induced Obesity, and Improves Host

Metabolism. *Cell Rep* (2018) 24(12):3087–98. doi: 10.1016/j.celrep.2018.08.064
28. Liu H, Gu R, Zhu Y, Lian X, Wang S, Liu X, et al. D-Mannose Attenuates Bone Loss in MiceVia Treg Cell Proliferation and Gut Microbiota-Dependent Anti-Inflammatory Effects. *Ther Adv Chronic Dis* (2020) 11:2040622320912661. doi: 10.1177/2040622320912661
29. Bertola A, Mathews S, Ki SH, Wang H, Gao B. Mouse Model of Chronic and Binge Ethanol Feeding (the NIAAA Model). *Nat Protoc* (2013) 8(3):627–37. doi: 10.1038/nprot.2013.032
30. Severgnini M, Sherman J, Sehgal A, Jayaprakash NK, Aubin J, Wang G, et al. A Rapid Two-Step Method for Isolation of Functional Primary Mouse Hepatocytes: Cell Characterization and Asialoglycoprotein Receptor Based Assay Development. *Cytotechnology* (2012) 64(2):187–95. doi: 10.1007/s10616-011-9407-0
31. Jiang W, Bian Y, Wang Z, Chang TM. Hepatoprotective Effects of Poly-[Hemoglobin-Superoxide Dismutase-Catalase-Carbonic Anhydrase] on Alcohol-Damaged Primary Rat Hepatocyte CultureIn Vitro. *Artif Cells Nanomed Biotechnol* (2017) 45(1):46–50. doi: 10.1080/21691401.2016.1191229
32. Cheng Q, Li YW, Yang CF, Zhong YJ, He H, Zhu FC, et al. Methyl Ferulic Acid Attenuates Ethanol-Induced Hepatic Steatosis by Regulating AMPK and FoxO1 Pathways in Rats and L-02 Cells. *Chem Biol Interact* (2018) 291:180–9. doi: 10.1016/j.cbi.2018.06.028
33. Liu DD, Han CC, Wan HF, He F, Xu HY, Wei SH, et al. Effects of Inhibiting PI3K-Akt-mTOR Pathway on Lipid Metabolism Homeostasis in Goose Primary Hepatocytes. *Animal* (2016) 10(8):1319–27. doi: 10.1017/s1751731116000380
34. Liu B, Deng X, Jiang Q, Li G, Zhang J, Zhang N, et al. Scoparone Improves Hepatic Inflammation and Autophagy in Mice With Nonalcoholic Steatohepatitis by Regulating the ROS/P38/Nrf2 Axis and PI3K/AKT/mTOR Pathway in Macrophages. *BioMed Pharmacother* (2020) 125:109895. doi: 10.1016/j.biopha.2020.109895
35. Zha LH, Zhou J, Li TZ, Luo H, Zhang MQ, Li S, et al. NLRC3 Inhibits MCT-Induced Pulmonary Hypertension in RatsVia Attenuating PI3K Activation. *J Cell Physiol* (2019) 234(9):15963–76. doi: 10.1002/jcp.28255
36. Spandidos A, Wang X, Wang H, Seed B. PrimerBank: A Resource of Human and Mouse PCR Primer Pairs for Gene Expression Detection and Quantification. *Nucleic Acids Res* (2010) 38(Database issue):D792–9. doi: 10.1093/nar/gkp1005
37. You Y, Li WZ, Zhang S, Hu B, Li YX, Li HD, et al. SNX10 Mediates Alcohol-Induced Liver Injury and Steatosis by Regulating the Activation of Chaperone-Mediated Autophagy. *J Hepatol* (2018) 69(1):129–41. doi: 10.1016/j.jhep.2018.01.038
38. Zhou B, Jiang Z, Li X, Zhang X. Kaempferol's Protective Effect on Ethanol-Induced Mouse Primary Hepatocytes Injury Involved in the Synchronous Inhibition of SP1, Hsp70 and CYP2E1. *Am J Chin Med* (2018) 46(5):1093–110. doi: 10.1142/s0192415x1850057x
39. Kang Z, Fan R. PPARalpha and NCOR/SMRT Corepressor Network in Liver Metabolic Regulation. *FASEB J* (2020) 34(7):8796–809. doi: 10.1096/fj.202000055RR
40. Semple RK, Chatterjee VK, O'Rahilly S. PPAR Gamma and Human Metabolic Disease. *J Clin Invest* (2006) 116(3):581–9. doi: 10.1172/jci28003
41. Le TNH, Choi HJ, Jun HS. Ethanol Extract of Liriope Platyphylla Root Attenuates Non-Alcoholic Fatty Liver Disease in High-Fat Diet-Induced Obese MiceVia Regulation of Lipogenesis and Lipid Uptake. *Nutrients* (2021) 13(10):3338. doi: 10.3390/nu13103338
42. Geisler CE, Renquist BJ. Hepatic Lipid Accumulation: Cause and Consequence of Dysregulated Glucoregulatory Hormones. *J Endocrinol* (2017) 234(1):R1–R21. doi: 10.1530/JOE-16-0513
43. Soliman GA. The Integral Role of mTOR in Lipid Metabolism. *Cell Cycle* (2011) 10(6):861–2. doi: 10.4161/cc.10.6.14930
44. Lívero FA, Acco A. Molecular Basis of Alcoholic Fatty Liver Disease: From Incidence to Treatment. *Hepatol Res* (2016) 46(1):111–23. doi: 10.1111/hepr.12594
45. Yan J, Nie Y, Luo M, Chen Z, He B. Natural Compounds: A Potential Treatment for Alcoholic Liver Disease? *Front Pharmacol* (2021) 12:694475. doi: 10.3389/fphar.2021.694475
46. Scaglione F, Musazzi UM, Minghetti P. Considerations on D-Mannose Mechanism of Action and Consequent Classification of Marketed Healthcare Products. *Front Pharmacol* (2021) 12:636377. doi: 10.3389/fphar.2021.636377
47. Wei Z, Huang L, Cui L, Zhu X. Mannose: Good Player and Assister in Pharmacotherapy. *Biomed Pharmacother* (2020) 129:110420. doi: 10.1016/j.biopha.2020.110420
48. Sharma V, Freeze HH. Mannose Efflux From the Cells: A Potential Source of Mannose in Blood. *J Biol Chem* (2011) 286(12):10193–200. doi: 10.1074/jbc.M110.194241
49. Lee S, Zhang C, Kilicarslan M, Piening BD, Bjornson E, Hallstrom BM, et al. Integrated Network Analysis Reveals an Association Between Plasma Mannose Levels and Insulin Resistance. *Cell Metab* (2016) 24(1):172–84. doi: 10.1016/j.cmet.2016.05.026
50. Mardinoglu A, Stancakova A, Lotta LA, Kuusisto J, Boren J, Bluher M, et al. Plasma Mannose Levels Are Associated With Incident Type 2 Diabetes and Cardiovascular Disease. *Cell Metab* (2017) 26(2):281–3. doi: 10.1016/j.cmet.2017.07.006
51. Sone H, Shimano H, Ebinuma H, Takahashi A, Yano Y, Iida KT, et al. Physiological Changes in Circulating Mannose Levels in Normal, Glucose-Intolerant, and Diabetic Subjects. *Metabolism* (2003) 52(8):1019–27. doi: 10.1016/s0026-0495(03)00153-7
52. Mori A, Sato T, Lee P, Furuuchi M, Tazaki H, Katayama K, et al. Clinical Significance of Plasma Mannose Concentrations in Healthy and Diabetic Dogs. *Vet Res Commun* (2009) 33(5):439–51. doi: 10.1007/s11259-008-9190-3
53. Boyle M, Masson S, Anstee QM. The Bidirectional Impacts of Alcohol Consumption and the Metabolic Syndrome: Cofactors for Progressive Fatty Liver Disease. *J Hepatol* (2018) 68(2):251–67. doi: 10.1016/j.jhep.2017.11.006
54. Parker R, Kim SJ, Gao B. Alcohol, Adipose Tissue and Liver Disease: Mechanistic Links and Clinical Considerations. *Nat Rev Gastroenterol Hepatol* (2018) 15(1):50–9. doi: 10.1038/nrgastro.2017.116
55. Correnti J, Lin C, Brettschneider J, Kuriakose A, Jeon S, Scorletti E, et al. Liver-Specific Ceramide Reduction Alleviates Steatosis and Insulin Resistance in Alcohol-Fed Mice. *J Lipid Res* (2020) 61(7):983–94. doi: 10.1194/jlr.RA119000446
56. Cheng Q, Li YW, Yang CF, Zhong YJ, Li L. Ethanol-Induced Hepatic Insulin Resistance is Ameliorated by Methyl Ferulic Acid Through the PI3K/AKT Signaling Pathway. *Front Pharmacol* (2019) 10:949. doi: 10.3389/fphar.2019.00949
57. Gong M, Castillo L, Redman RS, Garige M, Hirsch K, Azuine M, et al. Down-Regulation of Liver Galbeta1, 4glcnac Alpha2, 6-Sialyltransferase Gene by Ethanol Significantly Correlates With Alcoholic Steatosis in Humans. *Metabolism* (2008) 57(12):1663–8. doi: 10.1016/j.metabol.2008.07.021
58. Carr RM, Ahima RS. Pathophysiology of Lipid Droplet Proteins in Liver Diseases. *Exp Cell Res* (2016) 340(2):187–92. doi: 10.1016/j.yexcr.2015.10.021
59. Ren T, Mackowiak B, Lin Y, Gao Y, Niu J, Gao B. Hepatic Injury and Inflammation Alter Ethanol Metabolism and Drinking Behavior. *Food Chem Toxicol* (2020) 136:111070. doi: 10.1016/j.fct.2019.111070
60. Jeon S, Carr R. Alcohol Effects on Hepatic Lipid Metabolism. *J Lipid Res* (2020) 61(4):470–9. doi: 10.1194/jlr.R119000547
61. Han X, Wu Y, Yang Q, Cao G. Peroxisome Proliferator-Activated Receptors in the Pathogenesis and Therapies of Liver Fibrosis. *Pharmacol Ther* (2021) 222:107791. doi: 10.1016/j.pharmthera.2020.107791
62. Reyes-Gordillo K, Shah R, Varatharajalu R, Garige M, Leckey LC, Lakshman MR. Low-ω3 Fatty Acid and Soy Protein Attenuate Alcohol-Induced Fatty Liver and Injury by Regulating the Opposing Lipid Oxidation and Lipogenic Signaling Pathways. *Oxid Med Cell Longevity* (2016) 2016:1840513. doi: 10.1155/2016/1840513
63. Mandard S, Müller M, Kersten S. Peroxisome Proliferator-Activated Receptor Alpha Target Genes. *Cell Mol Life Sci* (2004) 61(4):393–416. doi: 10.1007/s00018-003-3216-3
64. Lu C, Zhang F, Xu W, Wu X, Lian N, Jin H, et al. Curcumin Attenuates Ethanol-Induced Hepatic Steatosis Through Modulating Nrf2/FXR Signaling in Hepatocytes. *IUBMB Life* (2015) 67(8):645–58. doi: 10.1002/iub.1409
65. Berger J, Moller DE. The Mechanisms of Action of PPARs. *Annu Rev Med* (2002) 53:409–35. doi: 10.1146/annurev.med.53.082901.104018
66. Cui ZY, Han X, Jiang YC, Dou JY, Yao KC, Hu ZH, et al. Allium Victorialis L. Extracts Promote Activity of FXR to Ameliorate Alcoholic Liver Disease: Targeting Liver Lipid Deposition and Inflammation. *Front Pharmacol* (2021) 12:738689. doi: 10.3389/fphar.2021.738689
67. Xu MJ, Cai Y, Wang H, Altamirano J, Chang B, Bertola A, et al. Fat-Specific Protein 27/CIDEC Promotes Development of Alcoholic Steatohepatitis in

Mice and Humans. *Gastroenterology* (2015) 149(4):1030–41.e6. doi: 10.1053/j.gastro.2015.06.009
68. Zhang W, Sun Q, Zhong W, Sun X, Zhou Z. Hepatic Peroxisome Proliferator-Activated Receptor Gamma Signaling Contributes to Alcohol-Induced Hepatic Steatosis and Inflammation in Mice. *Alcohol Clin Exp Res* (2016) 40(5):988–99. doi: 10.1111/acer.13049
69. Foufelle F, Ferré P. New Perspectives in the Regulation of Hepatic Glycolytic and Lipogenic Genes by Insulin and Glucose: A Role for the Transcription Factor Sterol Regulatory Element Binding Protein-1c. *Biochem J* (2002) 366(Pt 2):377–91. doi: 10.1042/bj20020430
70. Yin HQ, Kim M, Kim JH, Kong G, Kang KS, Kim HL, et al. Differential Gene Expression and Lipid Metabolism in Fatty Liver Induced by Acute Ethanol Treatment in Mice. *Toxicol Appl Pharmacol* (2007) 223(3):225–33. doi: 10.1016/j.taap.2007.06.018
71. Ji C, Chan C, Kaplowitz N. Predominant Role of Sterol Response Element Binding Proteins (SREBP) Lipogenic Pathways in Hepatic Steatosis in the Murine Intragastric Ethanol Feeding Model. *J Hepatol* (2006) 45(5):717–24. doi: 10.1016/j.jhep.2006.05.009
72. Muthukumaran P, Thiyagarajan G, Rajendran AB, Lakshmi BS. Raffinose From Costus Speciosus Attenuates Lipid Synthesis Through Modulation of PPARs/SREBP1c and Improves Insulin Sensitivity Through PI3K/AKT. *Chem Biol Interact* (2018) 284:80–9. doi: 10.1016/j.cbi.2018.02.011
73. Li J, Huang Q, Long X, Zhang J, Huang X, Aa J, et al. CD147 Reprograms Fatty Acid Metabolism in Hepatocellular Carcinoma Cells Through Akt/mTOR/SREBP1c and P38/Pparα Pathways. *J Hepatol* (2015) 63(6):1378–89. doi: 10.1016/j.jhep.2015.07.039

Conflict of Interest: The authors declare that the research was conducted in the absence of any commercial or financial relationships that could be construed as a potential conflict of interest.

Publisher's Note: All claims expressed in this article are solely those of the authors and do not necessarily represent those of their affiliated organizations, or those of the publisher, the editors and the reviewers. Any product that may be evaluated in this article, or claim that may be made by its manufacturer, is not guaranteed or endorsed by the publisher.

frontiers | Frontiers in Immunology

ORIGINAL RESEARCH
published: 20 April 2022
doi: 10.3389/fimmu.2022.884462

Serum Antigenome Profiling Reveals Diagnostic Models for Rheumatoid Arthritis

Peng Han[1], Chao Hou[2], Xi Zheng[1,3], Lulu Cao[1], Xiaomeng Shi[4], Xiaohui Zhang[4], Hua Ye[1], Hudan Pan[5], Liang Liu[5], Tingting Li[2], Fanlei Hu[1,4,6]* and Zhanguo Li[1,3,4]**

[1] Department of Rheumatology and Immunology, Peking University People's Hospital and Beijing Key Laboratory for Rheumatism Mechanism and Immune Diagnosis (BZ0135), Beijing, China, [2] Department of Biomedical Informatics, School of Basic Medical Sciences, Peking University, Beijing, China, [3] Peking-Tsinghua Center for Life Sciences, Peking University, Beijing, China, [4] State Key Laboratory of Natural and Biomimetic Drugs, School of Pharmaceutical Sciences, Peking University, Beijing, China, [5] State Key Laboratory of Dampness Syndrome of Chinese Medicine, The Second Affiliated Hospital of Guangzhou University of Chinese Medicine, Guangzhou, China, [6] Department of Integration of Chinese and Western Medicine, School of Basic Medical Sciences, Peking University, Beijing, China

OPEN ACCESS

Edited by:
Daming Zuo,
Southern Medical University, China

Reviewed by:
Teng Ma,
Capital Medical University, China
Huanfa Yi,
Jilin University, China

***Correspondence:**
Zhanguo Li
li99@bjmu.edu.cn
Fanlei Hu
fanleihu@bjmu.edu.cn
Tingting Li
litt@hsc.pku.edu.cn

Specialty section:
This article was submitted to Molecular Innate Immunity, a section of the journal Frontiers in Immunology

Received: *26 February 2022*
Accepted: *21 March 2022*
Published: *20 April 2022*

Citation:
Han P, Hou C, Zheng X, Cao L, Shi X, Zhang X, Ye H, Pan H, Liu L, Li T, Hu F and Li Z (2022) Serum Antigenome Profiling Reveals Diagnostic Models for Rheumatoid Arthritis. Front. Immunol. 13:884462. doi: 10.3389/fimmu.2022.884462

Objective: The study aimed to investigate the serum antigenomic profiling in rheumatoid arthritis (RA) and determine potential diagnostic biomarkers using label-free proteomic technology implemented with machine-learning algorithm.

Method: Serum antigens were captured from a cohort consisting of 60 RA patients (45 ACPA-positive RA patients and 15 ACPA-negative RA patients), together with sex- and age-matched 30 osteoarthritis (OA) patients and 30 healthy controls. Liquid chromatography-tandem mass spectrometry (LC-MS/MS) was then performed. The significantly upregulated and downregulated proteins with fold change > 1.5 ($p < 0.05$) were selected. Based on these differentially expressed proteins (DEPs), a machine learning model was trained and validated to classify RA, ACPA-positive RA, and ACPA-negative RA.

Results: We identified 62, 71, and 49 DEPs in RA, ACPA-positive RA, and ACPA-negative RA, respectively, as compared to OA and healthy controls. Typical pathway enrichment and protein–protein interaction networks were shown among these DEPs. Three panels were constructed to classify RA, ACPA-positive RA, and ACPA-negative RA using random forest models algorithm based on the molecular signature of DEPs, whose area under curve (AUC) were calculated as 0.9949 (95% CI = 0.9792–1), 0.9913 (95% CI = 0.9653–1), and 1.0 (95% CI = 1–1).

Conclusion: This study illustrated the serum auto-antigen profiling of RA. Among them, three panels of antigens were identified as diagnostic biomarkers to classify RA, ACPA-positive, and ACPA-negative RA patients.

Keywords: rheumatoid arthritis, antigenome, biomarkers, mass spectrometry, random forest

INTRODUCTION

Rheumatoid arthritis (RA) is a chronic autoimmune disease that leads to joint damage, systemic inflammation, and early mortality (1). The prevalence of RA was approximately 0.5%–1% worldwide and 0.28% in China (2, 3). The joint inflammation, combined with extra-articular complications, causes disability and reduces quality of life (4). Early diagnosis and subsequent treatment can substantially slow the progression of joint damage, thereby preventing irreversible disability (5).

Though the precise molecular mechanism in the triggering and progression of systemic immune response is not fully understood, the emergence of antibodies against self-antigens marks the loss of self-tolerance and can serve as a diagnostic biomarker (6). Among these are rheumatoid factor (RF) and anti-citrullinated protein antibodies (ACPAs), which are currently used as biomarkers for diagnostics, and other anti-modified protein antibodies (AMPAs) (7–9). The combination of autoantibody and self-antigen could form immune complexes that significantly augment the immune response and contribute to the inflammatory process of RA (10). Multiple antigens have been confirmed such as α-enolase, fibrinogen, filaggrin, vimentin, and type II collagen (11, 12). However, the profiling of serum antigen, antigenome, remains poorly known.

For decades, research has focused on single antigen identified as biomarkers (13). However, none of those achieves better specificity and sensitivity than ACPA alone. In this study, we broadened the focus by addressing the entire repertoire, aiming to capture the enormous biodiversity of antigens, with the goal to find a panel of diagnostic biomarkers instead of a single candidate. Moreover, the approach allows for finding differences of immune response by clustering the antigen repertoire that share certain function and pathway, providing further evidence in understanding of RA pathophysiology.

The robust growth of quantitative proteomic methods enables researchers to discover indicator proteins for diagnosis and treatment of diseases. There has been a recent expansion in proteomics research on a number of different rheumatic diseases (14–16). Due to the large datasets generated by proteomics, it requires informatic approaches such as machine learning techniques to analyze and interpret data, which have been exploited to predict biomarkers to accurate classify different diseases (17–19). We employed a robust mass spectrometry (MS)-based proteomics strategy to delineate the serum antigenomic profiling. By applying a widely used machine-learning algorithm, random forest, we described 3 panels of biomarkers to distinguish RA, ACPA-positive RA, and ACPA-negative RA. These biomarkers were further validated in a cohort using proteomic data. These findings provided knowledge about serum antigen in RA and might reveal potential therapeutic targets.

MATERIALS AND METHODS

Study Population and Serum Sample Collection

Serum from 60 RA patients, as well as sex- and age-matched 30 osteoarthritis (OA) patients and 30 healthy controls were collected at the Department of Rheumatology and Immunology, Peking University People's Hospital, Beijing, China. The study was approved by the Research Ethics Committee of Peking University People's Hospital. Informed consent was obtained from all patients and healthy donors. The study population was randomly split into a test cohort (36 RA, 18 OA, and 18 HC) and a validation cohort (24 RA, 12 OA, and 12 HC). Detailed clinical and demographic characteristics are summarized in **Table 1**.

All RA patients met the 2010 American College of Rheumatology (ACR)/European League Against Rheumatism (EULAR) classification criteria (20). The exclusion criteria include active infection, malignancy, and other known autoimmune or immune-mediated diseases, such as systemic lupus erythematosus, Sjogren's syndrome, and type I diabetes.

TABLE 1 | Clinical and laboratory characteristics of RA patients and controls in the study.

Characteristics	RA (*n* = 60)	OA (*n* = 30)	HC (*n* = 30)
Age, mean (range), years	61.77 (44–78)	64.27 (46–81)	62.37 (52–69)
Gender, no. male/female	11/49	7/23	8/22
Duration, mean (range), years	12.37 (1–42)	–	–
ESR, mean (range), mm/h	39.28 (5–106)	–	–
CRP, median (range), mg/L	23.85 (0.22–172)	–	-
RF, median (range), IU/ml	327.4 (2–3750)	–	–
Anti-CCP, median (range), U/ml	147.4 (1.93–296.9)	–	–
WBC, median (range), 10^9/L	5.793 (2.6–12.3)	–	-
TJC, median (range)	7 (0–22)	–	-
SJC, median (range)	5 (0–21)	–	-
DAS28, median (range)	4.258 (1.15–6.93)	–	-
Medication, no (%)			
Steroids	25 (41.67%)	–	–
NSAIDs	13 (21.67%)	–	–
DMARDs	59 (98.3%)	–	–
Biologics	31 (51.67%)	–	–

HC, healthy controls; ESR, erythrocyte sedimentation rate; CRP, C-reactive protein; RF, rheumatoid factor; Anti-CCP, anti-cyclic citrullinated peptide antibody; WBC, white blood cell; TJC, tender joint count; SJC, swollen joint count; DAS28, disease activity score 28; NSAIDs, nonsteroidal anti-inflammatory drugs; DMARDs, disease-modifying anti-rheumatic drugs.

The individuals (n = 10 in each group) selected for IgG purification were required to be free from monoclonal antibody treatment in at least 6 months.

Sample Preparation and Tryptic Digestion

IgG from human serum was purified using protein G spin kit (Catalog No.22852, Thermo Fisher Scientific). IgG was purified from 500 µl of pooled serum of ten patients according to the manufacturer's instrument, representing the repertoire of antibodies of each group. The eluted IgG was then washed and concentrated using 30-kDa MWCO filters (Catalog No. UFC803096, Amicon, Millipore). To capture serum antigen, 5 mg of IgG was coupled to 1 ml of CNBr-activated Sepharose 4B column (Catalog No.17043001, GE). By pretreating the IgG column with acidic elution buffer (10 mmol/L Gly-HCl, pH = 2.8), the antigens bound to IgG were eluted. Then, the diluted serum of one patient was incubated at room temperature with end-over-end mixing for 1 h. Bound antigens were eluted with acidic elution buffer (10 mmol/L Gly-HCl, pH = 2.8) and immediately neutralized by Tris-HCl (1 mmol/L, pH = 9.1). The concentration of the protein was determined by Bradford protein assay (Catalog No. DQ101-01, Transgen Biotech) and then stored at −80°C .

LC-MS/MS and Data Analysis

Protein (10 µg) was hydrolyzed with trypsin. Digested products were separated by a 120-min gradient elution at a flow rate of 0.300 µL/min with the Thermo Ultimate 3000 nano-UPLC system, which was directly interfaced with the Thermo Fusion LUMOS mass spectrometer. The analytical column was an Acclaim PepMap RSLC column (75 µm ID, 250 mm length, C18). Mobile phase A consisted of 0.1% formic acid, and mobile phase B consisted of 100% acetonitrile and 0.1% formic acid. The single full-scan mass spectra were acquired in a data-dependent manner in the Orbitrap at a mass resolution of 60,000 at 375–1500 m/z. Xcalibur 4.1.50 software was used for data acquisition. Protein identification was carried out using Mascot and Sequest search algorithms through the Proteome Discovery software (version 2.4). Searches were carried against Human RefSeq protein database. MS tolerance was set to 10 ppm while MS/MS tolerance was set to 0.02 Da. The peptide-spectrum match allowed 1% target false discovery rate (strict). We used label-free quantification (LFQ) algorithm to quantify protein expression and peptide-spectrum matching. Normalization was performed against the total peptide amount. Immunoglobulins and post-translational modifications are not analyzed in the study, but could be potentially analyzed in the future.

Bioinformatic Analysis

To obtain the intersection of antigen among RA, OA, and healthy controls, we used the Venn diagram software (http://bioinformatics.psb.ugent.be/webtools/Venn/). Pathway enrichment analysis was performed to classify proteins based on molecular function and biological processes by Metascape web-based platform (21). Protein–protein interaction of differentially expressed proteins was performed using Search tool for the retrieval of interaction gene/protein (STRING) database (PPI enrichment p-value < 1.0e-16) and visualized by Cytoscape plug-in Cytohubba (22, 23).

Statistical Analysis and Machine Learning

Missing values were imputed with the minimal values for each feature. To get differentially expressed proteins, the fold change and t-test p-value were calculated between RA, ACPA-positive RA, ACPA-negative RA, and control (OA and healthy controls). The protein whose p-value < 0.05 and fold change > 1.5 was defined as differentially expressed protein. The heatmaps were drawn using the R package "pheatmap" (version 1.0.12), the sum of z-scores of log-transformed values were displayed, and the rows were sorted by fold changes. The PCA was performed using the function "decomposition.PCA" in scikit-learn (version 0.23.1) with default parameters. The log-transformed values were used as input for PCA.

The random forest classifiers were build using the function "ensemble.RandomForestClassifier" in scikit-learn (version 0.23.1), with 101 trees, and the max depth for the trees was set to 4 to avoid overfitting. The log-transformed values of differentially expressed proteins were used as input features, and the number of features to consider in each tree was sqrt (number of features). We deleted SAA (D3DQX7) as the sequence was very similar to SAA1 and SAA2. The importance of proteins was calculated using the build-in function "feature_importances_", which provides the impurity-based feature importance. The train-test split and classification process were repeated 500 times to calculate the AUC and feature importance.

RESULTS

Patients and Study Design

We procured a cohort of patients containing 60 RA, 30 OA, and 30 healthy controls. The detailed clinical and demographic characteristics are shown in **Table 1**. The median age was 61.77 years and 81.7% of the patients were female. Thirty OA patients and 30 healthy controls were all age- and sex-matched. The disease duration ranged from 1 to 42 years, with a mean duration of 12.37 years. Seventy-five percent (45 of 60) of RA patients were ACPA-positive. The mean ESR (erythrocyte sedimentation rate) and CRP (C-reactive protein) were 39.28 mm/h and 23.85 mg/dl, respectively. The mean DAS28 score (Disease Activity Score-28) was 4.258.

The workflow employed for this study is shown in **Figure 1**. Briefly, IgGs were purified from 500 µl of pooling mixture serum of 10 individuals in each group, respectively. These IgGs were bound to the Protein G column and then were treated to remove the antigens potentially bound to the antibodies first. After that, serum antigens from 120 samples were purified and collected individually. The antigen peptide mixture of each sample was then analyzed and quantified by high-resolution liquid chromatography with tandem mass spectrometry (LC-MS/MS) (24).

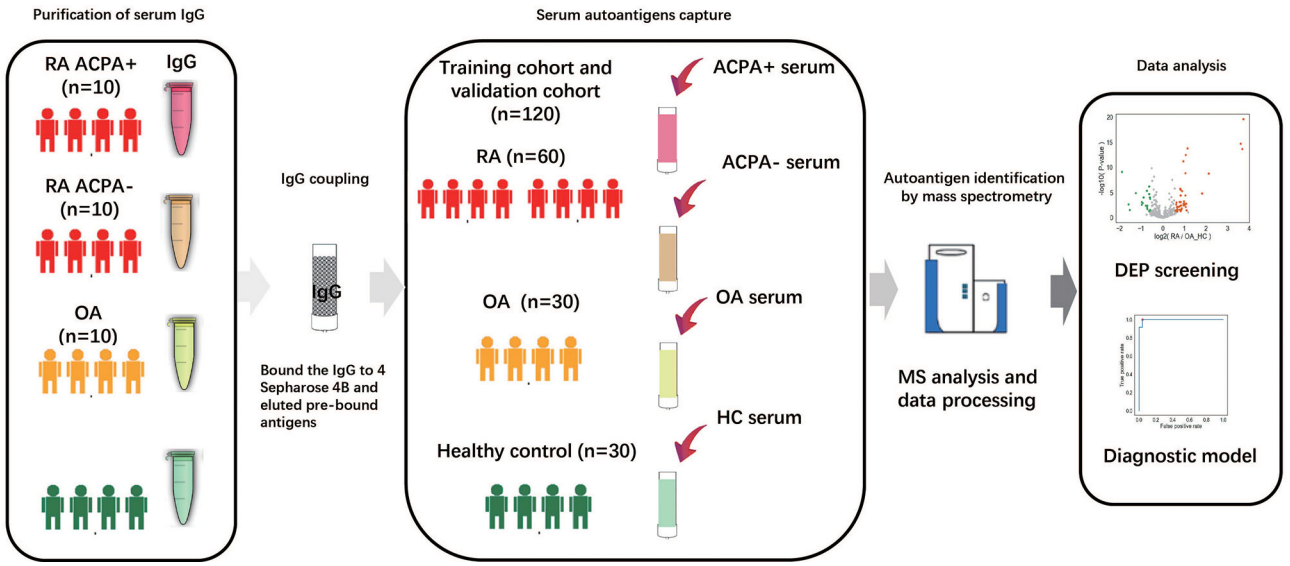

FIGURE 1 | Study overview and antigenome characterization. Overview of the study cohort and schematic workflow. RA, rheumatoid arthritis; OA, osteoarthritis; ACPA, anti-citrullinated protein antibody; HC, healthy control; MS, mass spectrometry; DEP, differentially expressed protein.

Serum Antigenomic Profiling of RA Patients

Applying this workflow, we quantified 4,475 proteins and 12,217 peptides from 120 samples. With immunoglobulins excluded, 461 proteins in ACPA-positive RA, 409 proteins in ACPA-negative RA, 427 proteins in OA patients, and 422 proteins in healthy control were identified. A total of 360 proteins were in common among the 3 groups, while 35 proteins were specific for ACPA-positive RA and 15 for ACPA-negative RA. Eight proteins were found only in the ACPA-negative group and 28 in the ACPA-positive group (**Figure 2A**). Proteins with high confidence and could be detected in more than 20% in a particular patient group were chosen for further analyses.

The principal component analysis (PCA) showed that the clustering of samples is clearly classified into different groups as RA, OA, and healthy controls (**Figure 2B**). However, PCA analysis could not distinguish ACPA-negative RA from ACPA-positive RA patients, demonstrating their similar antigenome pattern. Taken together, these data presented a deep antigenome coverage, a promising basis for discovery of biomarkers.

Analysis of Differentially Expressed Proteins

We next assessed significant quantitative differences between RA, OA, and healthy controls. We selected significantly upregulated and downregulated proteins by >1.5-fold ($p < 0.05$). A total of 62 differentially expressed proteins (DEPs) such as fibrinogen alpha chain, lipopolysaccharide-binding protein, and serum amyloid protein in RA were identified and shown in the volcano plot (**Figure 3A**). Heatmap analysis was performed to visualize those proteins (**Figure 3A**). We next found 71 proteins differentially expressed in ACPA-positive and 49 proteins differentially expressed in ACPA-negative patients, using the same filter criteria (**Figures 3B, C**).

The DEPs were then subjected to enrichment analysis (**Figure 4**). The analysis revealed that DEPs of these 3 groups were significantly enriched in pathways associated with immunology and inflammatory response, "acute inflammatory response", "activation of complement system", and "humoral immune response". DEPs in RA were enriched in pathways including "cell-cell adhesion" and "IL-4 and IL-13 signaling". The pathways of DEPs in ACPA-positive RA were enriched in processes involved in "binding and uptake of ligand of scavenger receptors" and "IL-6 pathway". Some pathways associated with metabolic process were enriched in DEPs of ACPA-negative RA, such as "folate metabolism", which might be interesting in future studies.

As shown by protein–protein interaction (PPI) analysis of DEPs by the STRING database, the antigenome possessed abundant interactions. To recognize the key antigens lying in an essential position, we exploited Cytoscape plugin Cytohubba, which identified hub proteins in the networks. As shown in **Figure 5**, DEPs such as haptoglobin and ITIH4 were screened out as top hub proteins based on the connectivity degree. Both haptoglobin and ITIH4 could function as acute-phase reactants (25, 26). It was previously reported that the levels of haptoglobin were elevated in RA serum (27). ITIH4 was found to be a serum biomarker for a variety of malignancies including gastric cancer and hepatocellular carcinoma (28, 29). However, there is limited research investigating their detailed role in RA. These proteins might be essential in the pathogenesis of RA and utilized as biomarkers after rigorous validation.

Machine Learning for Identification of RA Patients

Next, we attempted to discriminate RA from OA and healthy controls based on the DEPs. A widely used machine learning algorithm, random forest, was used to classify the patients. The

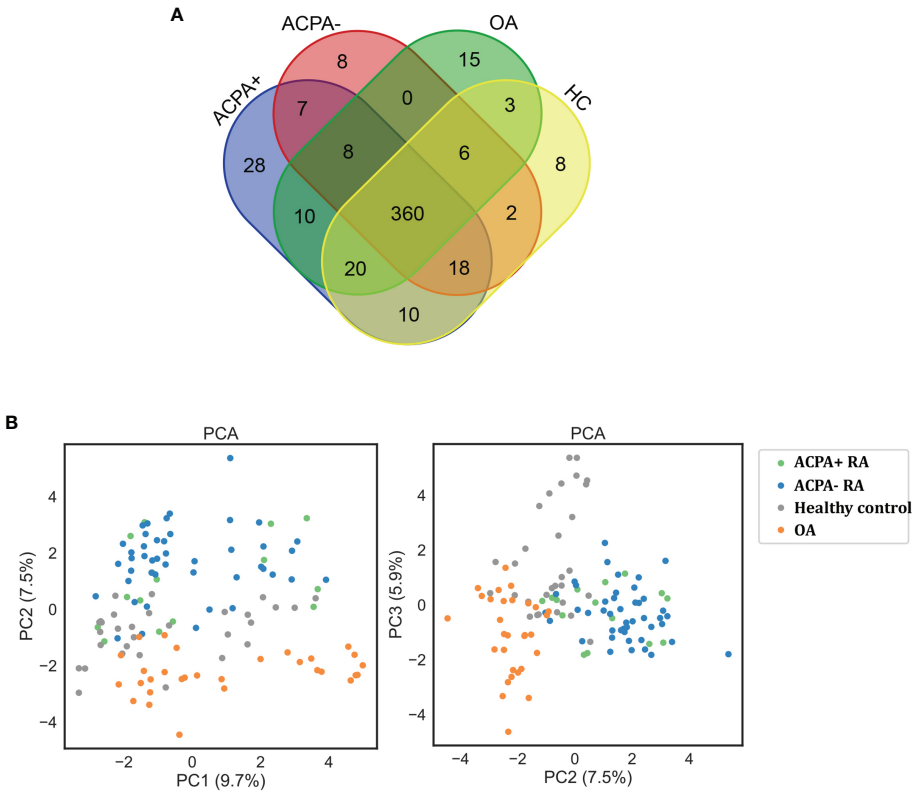

FIGURE 2 | Protein quantification through LC-MS/MS. **(A)** Venn diagram of the identified proteins among RA patients and controls. **(B)** Clustering analysis of differentially expressed proteins on PCA analysis. ACPA+, ACPA-positive RA; ACPA-, ACPA-negative RA; PCA, principal component analysis.

model was trained on 60% of the samples (36 RA, 18 OA, and 18 healthy controls) and evaluated on the remaining 40% of the samples (24 RA, 12 OA, and 12 healthy controls). We repeated this process 500 times to calculate the area under the curve (AUC) of the receiver operating characteristic curve and feature importance for each antigen.

For the classification of RA, the AUC of the random forest model reached 0.9949 (95% confidence interval [CI] = 0.9792–1) (**Figure 6A**), and the top 15 dominant antigens in the model were SAA2, C-reactive protein (CRP), leucine-rich alpha-2-glycoprotein, fibrinogen alpha chain, annexin A1, complement component C9, complement C4-A, SAA1, carbonic anhydrase, testicular tissue protein Li 70, ficolin-3, ACX136, hemoglobin subunit alpha, paired like homeobox 2B, and beta-actin-like protein 2 (**Figure 6A**).

Next, we investigated the possibility of discriminating ACPA-positive and ACPA-negative RA patients from OA patients and healthy controls based on the DEPs. Random forest algorithm was employed as well; 60% of the samples were used to train and 40% of the samples were used to evaluate. For ACPA-positive RA patients, the model reached an AUC of 0.9913 (95% CI = 0.9653–1) (**Figure 6B**), and the top 15 best-performing proteins were leucine-rich alpha-2-glycoprotein, SAA2, CRP, complement component C9, fibrinogen alpha chain, annexin A1, C4a anaphylatoxin, arfaptin-1, testicular tissue protein Li 70, SAA1, ITIH4 protein, ficolin-3, carbonic anhydrase, hemoglobin subunit alpha, and complement C4-A (**Figure 6B**). Moreover, for the classification of ACPA-negative RA patients, the AUC was calculated as 1.0 (95% CI = 1–1) (**Figure 6C**). The top 15 proteins were SAA2, fibrinogen alpha chain, SAA2-SAA4 readthrough, alpha-1-antitrypsin MBrescia variant, platelet glycoprotein V, SAA1, Fc-gamma receptor IIIb, beta-actin-like protein 2, testicular tissue protein Li 70, complement C1r subcomponent-like protein, AEP4D11, CRP, procollagen C-endopeptidase enhancer, Keratin type II cytoskeletal 6B, and caspase 14 (**Figure 6C**).

DISCUSSION

Our study presented a serum antigenomic investigation of RA using label-free global proteome strategy, which offered a landscape view of antigens. Using random forest, an ensemble, supervised machine learning algorithm, 3 diagnostic signatures were built to classify RA, ACPA-positive RA, and ACPA-negative RA patients. Our findings might help to understand the pathogenesis of RA and provide novel and specific diagnostic targets for the disease.

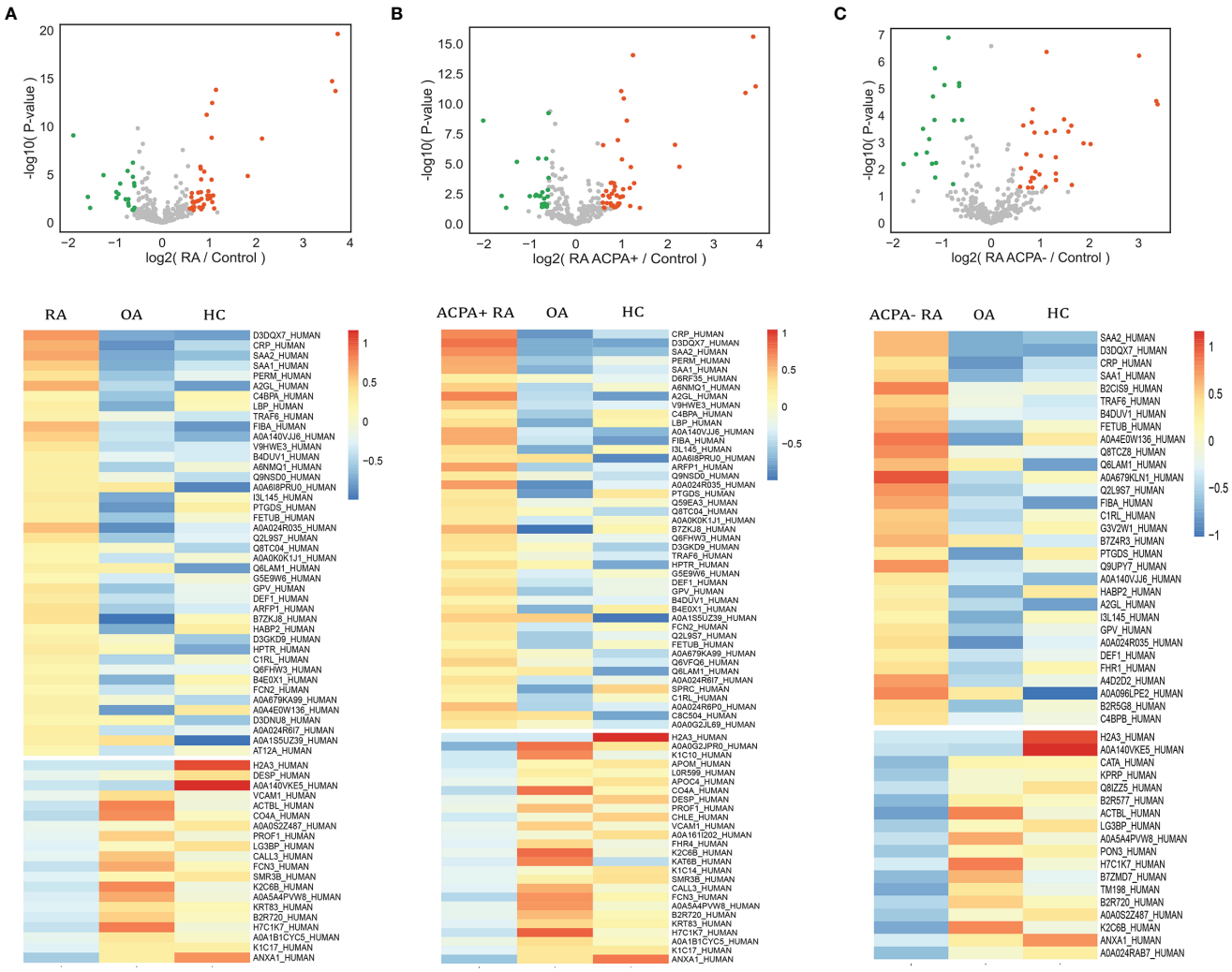

FIGURE 3 | Analysis of differential expressed proteins. Volcano plots compare RA **(A)**, ACPA-positive RA **(B)**, ACPA-negative RA **(C)**, and controls. Heatmap analysis of proteins that differ significantly ($p < 0.05$, fold change > 1.5) in abundance in RA **(A)**, ACPA-positive RA **(B)**, and ACPA-negative RA **(C)**.

Early diagnosis and immediate, effective therapy are crucial to gain control of inflammation and prevent deterioration, functional disability, and unfavorable progression in RA patients. To carry out personalized medicine for RA, clinical practice requires the use of biomarkers to ensure diagnosis, accurate stratification, and the high efficacy of treatment. Current clinically used biomarkers including anti-CCP and RF only shows a modest discriminating power due to the lack of sensitivity and specificity (30). Searching biomarkers for diagnosis is a continuous effort, but none of those translate into routine clinical use (31). Therefore, searching reliable biomarkers for RA in a large population is highly desirable. To address the problem, we have combined cutting-edge mass spectrometry hardware, MS data processing, and bioinformatic analysis to build a high-performance serum antigenomic workflow.

Other groups have also performed proteomic studies for RA. Mun et al. performed a quantitative proteomic study and identified 5 biomarkers using RA serum, which were quantitively verified by multiple reaction monitoring (MRM) (32). Colasanti et al. discovered that anti-Hcy-A1AT (homocysteinylated alpha 1 antitrysin) autoantibody could be considered as a potential biomarker for RA by using matrix-assisted laser desorption/ionization-time of flight (MALDI-TOF/TOF) (33). However, we used a novel approach to capture the set of serum antigens, which was advantageous as it focused on a more targeted set of proteins, compared to entire serum proteome. We identified confirmed and putative antigens as candidates of novel potential biomarkers. In total, 4,475 proteins were identified by label-free comparative proteomic analysis of antigen profiling of RA, OA, and healthy control serum. Compared to OA and healthy controls, we found 62 DEPs (FC > 1.5, $p < 0.05$) in RA, 71 DEPs that were specific in ACPA-positive patients, and 49 DEPs specific in ACPA-negative

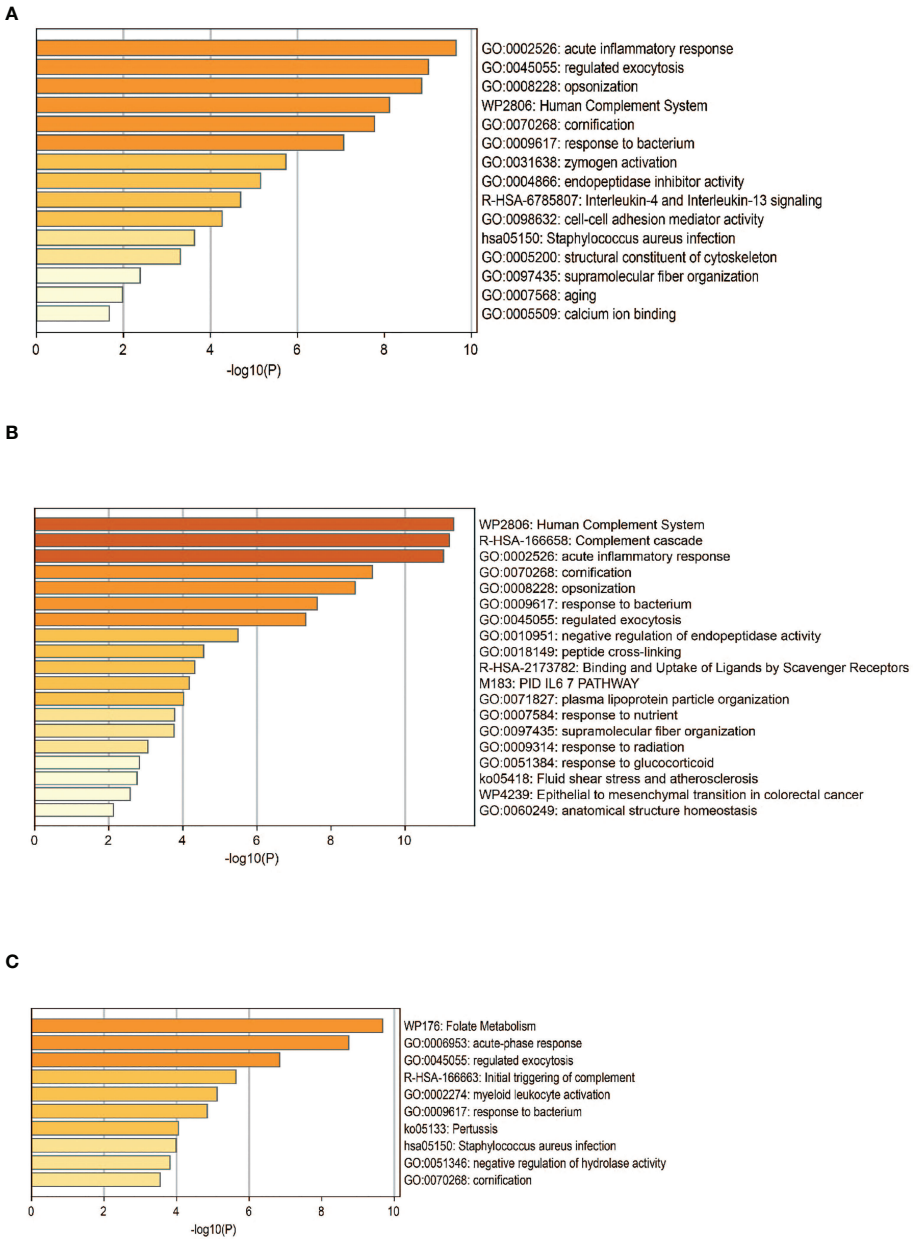

FIGURE 4 | Functional analysis of DEPS. Pathway analysis of DEPs in patients with RA **(A)**, ACPA-positive RA **(B)**, and ACPA-negative RA **(C)**. GO, gene ontology.

patients. We tried to gain insight into the functional roles of these DEPs associated with RA *via* pathway enrichment analysis. The interaction of DEPs was shown based on PPI networks. Moreover, we identified hub proteins in the interaction networks. These avenues of enquiry may provide insight into the underlying mechanisms of RA.

As a single biomarker may hardly achieve satisfactory discriminating power, seeking multiple biomarkers and developing a combinatorial model is a compromising strategy. By virtue of comprehensive antigenome profiling and random forest algorithm, we revealed 3 predictive models for RA, ACPA-positive RA, and ACPA-negative RA. The models have achieved low classification errors and resulted in very high AUC levels.

Compared to ACPA-positive RA, ACPA-negative RA is poorly understood in etiology and pathogenesis. Lack of effective biomarkers impedes early diagnosis and treatment, highlighting the importance of identifying specific antigens in this subset (34). It is worth noting that several antigens are unique in the ACPA-negative model, such as SAA2-SAA4 readthrough, platelet glycoprotein V, Fc-gamma receptor IIIb, complement C1r subcomponent-like protein, procollagen C-endopeptidase enhancer, and caspase 14 (**Figure 6C**). These

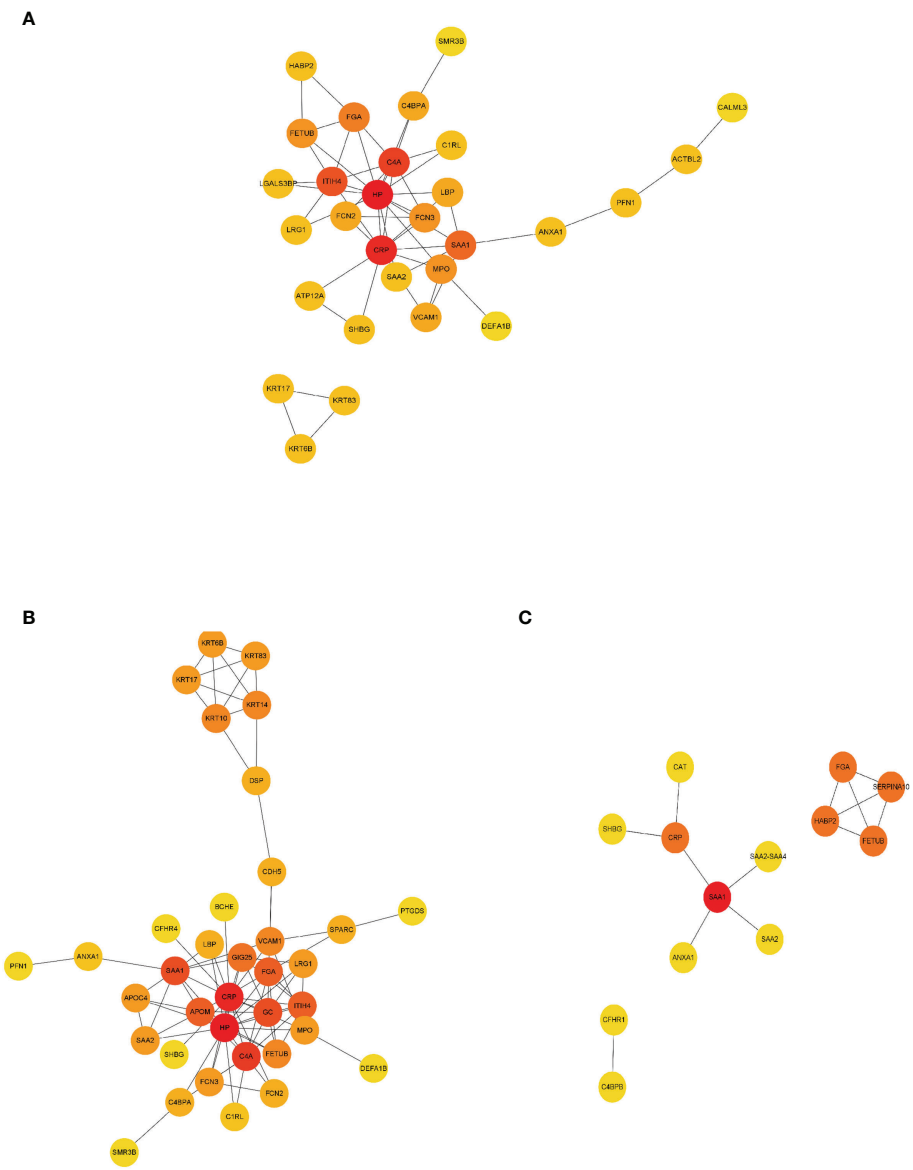

FIGURE 5 | PPI network construction of DEPs. Interaction network analysis of DEPs in RA **(A)**, ACPA-positive RA **(B)**, and ACPA-negative RA **(C)** by STRING and Cytoscape. Cytohubba plug-in was applied to identify the hub proteins in the network by protein degrees. Red indicated DEPs were at the center of the network and possessing 5–10 edges. Orange indicated DEPs possessing 3–5 edges. Yellow indicated DEPs possessing 1 to 2 edges. PPI, protein–protein interaction.

proteins participate in various biological processes including acute phase response, cornification, complement activation, innate immune response, platelet activation, and collagen binding (35, 36). There is limited research investigating their function and association with autoimmune or inflammatory diseases (37). Validation by ELISA in larger ACPA-negative RA cohorts and exploration of their detailed functions in the disease are needed. Hopefully, these newly identified antigens may help early diagnosis and hint underlying mechanism of ACPA-negative RA.

Though assay results were promising, this study does have limitations. First, we utilized IgG purified from ACPA-positive patients to capture antigens rather than anti-CCP2 antibody, which resulted in an incomplete reactivity pattern of ACPA-IgG due to its lower affinity toward citrullinated antigens. Besides, by using an IgG column to capture serum antigens from the corresponding group of patients, the DEPs identified between groups might be partially due to the differences of IgG binding ability from various patients rather than antigens that were purely from the capture. Second, if the model is to be applied in clinic, more rigorous quantification and extensive validation by targeted protein quantification or ELISA are still needed. The detailed roles of antigens in the pathogenesis of RA should be

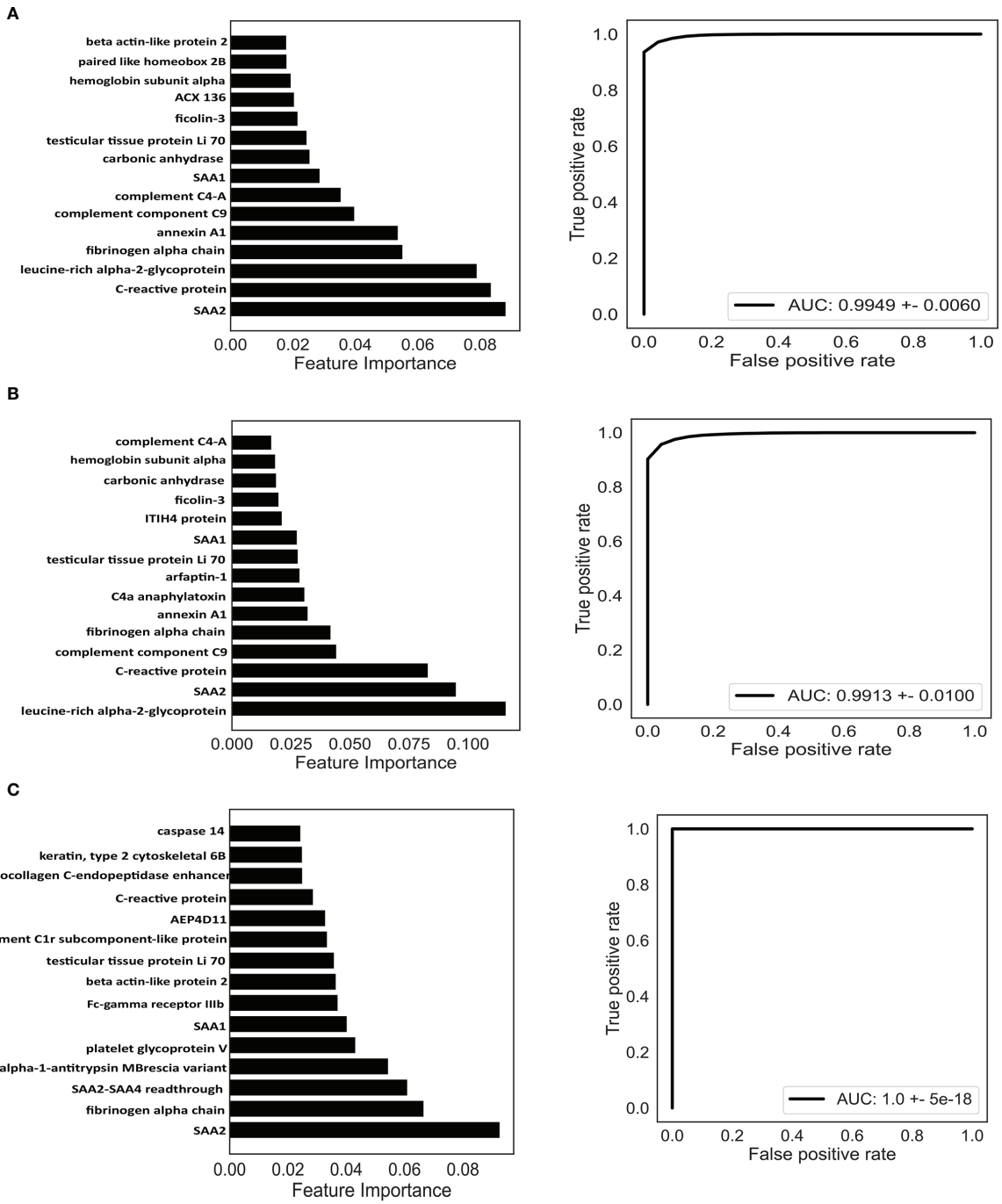

FIGURE 6 | Identification of potential biomarkers based on machine learning. Classification of RA **(A)**, ACPA-positive RA **(B)**, and ACPA-negative RA **(C)**. Top 15 proteins prioritized by random forest analysis (left). ROC of the random forest model in the test cohort (right). AUC, area under curve.

further elucidated or experimentally validated. Third, this was a single-center study, and the results merit validation in a larger, multicenter study that involve OA, systemic lupus erythematosus (SLE), ankylosing spondylitis (AS), psoriatic arthritis (PsA), gout patients, etc. Lastly, this work establishes the foundation for longitudinal studies geared toward the development of models predictive of disease onset or progression, and efficacy after treatment. The sera samples were collected at a single time point in both RA patients and control, and future studies of sera from more time points along the disease course are required, which could be potentially utilized to explore molecular dynamics during disease progression.

In summary, we employed label-free global proteomics technology to analyze serum antigenome profiling of RA. The study increased our understanding of RA antigens and identified potential biomarkers to provide novel and specific diagnostic targets for the disease. We suggest that these panels identified here could be utilized as multiplex protein microarray platforms that have potential for scalability and contribute toward improved decision-making.

DATA AVAILABILITY STATEMENT

The datasets presented in this study can be found in online repositories. The names of the repository/repositories and accession number(s) can be found at: http://www.proteomexchange.org/, PXD031498.

ETHICS STATEMENT

The studies involving human participants were reviewed and approved by the Research Ethics Committee at Peking University of People's Hospital. The patients/participants provided their written informed consent to participate in this study.

AUTHOR CONTRIBUTIONS

FH and ZL designed the research. PH, XZ, and LC collected blood sample and PH summarized clinical data. PH, XS, and XHZ performed LC-MS/MS. PH, CH, XS, XHZ, XZ, LC, TL, and FH analyzed and interpreted the data. CH and TL performed machine learning. PH and CH wrote the manuscript. HY, FH, HP, LL and ZL edited the manuscript. All authors contributed to the article and approved the submitted version.

FUNDING

This work was supported by grants from Guangdong Basic and Applied Basic Research Foundation (2020B1515130005 to LL), the National Natural Science Foundation of China (U1903210 to ZL, 82171773 and 81971523 to FH), the Beijing Nova Program (Z181100006218044 and Z211100002121163 to FH), the Beijing Science and Technology Planning Project (Z191100006619109 to HY), Macao Science and Technology Development Fund (0094/2018/A3 to ZL), as well as by the Fundamental Research Funds for the Central Universities: Peking University Clinical Medicine Plus X-Young Scholars Project (PKU2021LCXQ014 to FH) and the Peking University People's Hospital Research and Development Funds (RDX2020-01 to FH).

REFERENCES

1. Smolen JS, Aletaha D, McInnes IB. Rheumatoid Arthritis. *Lancet (London England)* (2016) 388:2023–38. doi: 10.1016/S0140-6736(16)30173-8
2. Tobón GJ, Youinou P, Saraux A. The Environment, Geo-Epidemiology, and Autoimmune Disease: Rheumatoid Arthritis. *J Autoimmun* (2010) 35:10–4. doi: 10.1016/j.jaut.2009.12.009
3. Li R, Sun J, Ren LM, Wang HY, Liu WH, Zhang XW, et al. Epidemiology of Eight Common Rheumatic Diseases in China: A Large-Scale Cross-Sectional Survey in Beijing. *Rheumatol (Oxford England)* (2012) 51:721–9. doi: 10.1093/rheumatology/ker370
4. Scott DL, Steer S. The Course of Established Rheumatoid Arthritis. *Best Pract Res Clin Rheumatol* (2007) 21:943–67. doi: 10.1016/j.berh.2007.05.006
5. Aletaha D, Smolen JS. Diagnosis and Management of Rheumatoid Arthritis: A Review. *JAMA* (2018) 320:1360–72. doi: 10.1001/jama.2018.13103
6. Weyand CM, Goronzy JJ. The Immunology of Rheumatoid Arthritis. *Nat Immunol* (2021) 22:10–8. doi: 10.1038/s41590-020-00816-x
7. De Rycke L, Peene I, Hoffman IE, Kruithof E, Union A, Meheus L, et al. Rheumatoid Factor and Anticitrullinated Protein Antibodies in Rheumatoid Arthritis: Diagnostic Value, Associations With Radiological Progression Rate, and Extra-Articular Manifestations. *Ann Rheum Dis* (2004) 63:1587–93. doi: 10.1136/ard.2003.017574
8. van Venrooij WJ, van Beers JJ, Pruijn GJ. Anti-Ccp Antibodies: The Past, the Present and the Future. *Nat Rev Rheumatol* (2011) 7:391–8. doi: 10.1038/nrrheum.2011.76
9. Kampstra ASB, Dekkers JS, Volkov M, Dorjée AL, Hafkenscheid L, Kempers AC, et al. Different Classes of Anti-Modified Protein Antibodies are Induced on Exposure to Antigens Expressing Only One Type of Modification. *Ann Rheum Dis* (2019) 78:908–16. doi: 10.1136/annrheumdis-2018-214950
10. McInnes IB, Schett G. The Pathogenesis of Rheumatoid Arthritis. *N Engl J Med* (2011) 365:2205–19. doi: 10.1056/NEJMra1004965
11. Chandra PE, Sokolove J, Hipp BG, Lindstrom TM, Elder JT, Reveille JD, et al. Novel Multiplex Technology for Diagnostic Characterization of Rheumatoid Arthritis. *Arthritis Res Ther* (2011) 13:R102. doi: 10.1186/ar3383
12. Pratesi F, Tommasi C, Anzilotti C, Puxeddu I, Sardano E, Di Colo G, et al. Antibodies to a New Viral Citrullinated Peptide, Vcp2: Fine Specificity and Correlation With Anti-Cyclic Citrullinated Peptide (Ccp) and Anti-Vcp1 Antibodies. *Clin Exp Immunol* (2011) 164:337–45. doi: 10.1111/j.1365-2249.2011.04378.x
13. Maksymowych WP, Naides SJ, Bykerk V, Siminovitch KA, van Schaardenburg D, Boers M, et al. Serum 14-3-3η is a Novel Marker That Complements Current Serological Measurements to Enhance Detection of Patients With Rheumatoid Arthritis. *J Rheumatol* (2014) 41:2104–13. doi: 10.3899/jrheum.131446
14. Liao W, Li Z, Li T, Zhang Q, Zhang H, Wang X. Proteomic Analysis of Synovial Fluid in Osteoarthritis Using Swath–Mass Spectrometry. *Mol Med Rep* (2018) 17:2827–36. doi: 10.3892/mmr.2017.8250
15. Peffers MJ, Smagul A, Anderson JR. Proteomic Analysis of Synovial Fluid: Current and Potential Uses to Improve Clinical Outcomes. *Expert Rev Proteomic* (2019) 16:287–302. doi: 10.1080/14789450.2019.1578214
16. Cai A, Qi S, Su Z, Shen H, Yang Y, He L, et al. Quantitative Proteomic Analysis of Peripheral Blood Mononuclear Cells in Ankylosing Spondylitis by Itraq. *Clin Trans science* (2015) 8:579–83. doi: 10.1111/cts.12265
17. Swan AL, Mobasheri A, Allaway D, Liddell S, Bacardit J. Application of Machine Learning to Proteomics Data: Classification and Biomarker Identification in Postgenomics Biology. *Omics J Integr Biol* (2013) 17:595–610. doi: 10.1089/omi.2013.0017
18. Xiao Q, Zhang F, Xu L, Yue L, Kon OL, Zhu Y, et al. High-Throughput Proteomics and Ai for Cancer Biomarker Discovery. *Adv Drug Deliv Rev* (2021) 176:113844. doi: 10.1016/j.addr.2021.113844
19. Shen B, Yi X, Sun Y, Bi X, Du J, Zhang C, et al. Proteomic and Metabolomic Characterization of Covid-19 Patient Sera. *Cell* (2020) 182:59–72. doi: 10.1016/j.cell.2020.05.032
20. Aletaha D, Neogi T, Silman AJ, Funovits J, Felson DT, Bingham CO, et al. 2010 Rheumatoid Arthritis Classification Criteria: An American College of Rheumatology/European League Against Rheumatism Collaborative Initiative. *Ann Rheum Dis* (2010) 69:1580–8. doi: 10.1136/ard.2010.138461
21. Zhou Y, Zhou B, Pache L, Chang M, Khodabakhshi AH, Tanaseichuk O, et al. Metascape Provides a Biologist-Oriented Resource for the Analysis of

Systems-Level Datasets. *Nat Commun* (2019) 10:1523. doi: 10.1038/s41467-019-09234-6
22. Franceschini A, Szklarczyk D, Frankild S, Kuhn M, Simonovic M, Roth A, et al. String V9.1: Protein-Protein Interaction Networks, With Increased Coverage and Integration. *Nucleic Acids Res* (2013) 41:D808–15. doi: 10.1093/nar/gks1094
23. Shannon P, Markiel A, Ozier O, Baliga NS, Wang JT, Ramage D, et al. Cytoscape: A Software Environment for Integrated Models of Biomolecular Interaction Networks. *Genome Res* (2003) 13:2498–504. doi: 10.1101/gr.1239303
24. Cox J, Hein MY, Luber CA, Paron I, Nagaraj N, Mann M. Accurate Proteome-Wide Label-Free Quantification by Delayed Normalization and Maximal Peptide Ratio Extraction, Termed Maxlfq. *Mol Cell Proteomics MCP* (2014) 13:2513–26. doi: 10.1074/mcp.M113.031591
25. Petersen HH, Nielsen JP, Heegaard PM. Application of Acute Phase Protein Measurements in Veterinary Clinical Chemistry. *Vet Res* (2004) 35:163–87. doi: 10.1051/vetres:2004002
26. Kashyap RS, Nayak AR, Deshpande PS, Kabra D, Purohit HJ, Taori GM, et al. Inter-Alpha-Trypsin Inhibitor Heavy Chain 4 is a Novel Marker of Acute Ischemic Stroke. *Clinica Chimica Acta; Int J Clin Chem* (2009) 402:160–3. doi: 10.1016/j.cca.2009.01.009
27. Charles-Schoeman C, Watanabe J, Lee YY, Furst DE, Amjadi S, Elashoff D, et al. Abnormal Function of High-Density Lipoprotein is Associated With Poor Disease Control and an Altered Protein Cargo in Rheumatoid Arthritis. *Arthritis Rheumatism* (2009) 60:2870–9. doi: 10.1002/art.24802
28. Sun Y, Jin J, Jing H, Lu Y, Zhu Q, Shu C, et al. Itih4 is a Novel Serum Biomarker for Early Gastric Cancer Diagnosis. *Clinica Chimica Acta; Int J Clin Chem* (2021) 523:365–73. doi: 10.1016/j.cca.2021.10.022
29. Li X, Li B, Li B, Guo T, Sun Z, Li X, et al. Itih4: Effective Serum Marker, Early Warning and Diagnosis, Hepatocellular Carcinoma. *Pathol Oncol Res POR* (2018) 24:663–70. doi: 10.1007/s12253-017-0285-4
30. Nishimura K, Sugiyama D, Kogata Y, Tsuji G, Nakazawa T, Kawano S, et al. Meta-Analysis: Diagnostic Accuracy of Anti-Cyclic Citrullinated Peptide Antibody and Rheumatoid Factor for Rheumatoid Arthritis. *Ann Intern Med* (2007) 146:797–808. doi: 10.7326/0003-4819-146-11-200706050-00008
31. Mahler M, Martinez-Prat L, Sparks JA, Deane KD. Precision Medicine in the Care of Rheumatoid Arthritis: Focus on Prediction and Prevention of Future Clinically-Apparent Disease. *Autoimmun Rev* (2020) 19:102506. doi: 10.1016/j.autrev.2020.102506
32. Mun S, Lee J, Park A, Kim HJ, Lee YJ, Son H, et al. Proteomics Approach for the Discovery of Rheumatoid Arthritis Biomarkers Using Mass Spectrometry. *Int J Mol Sci* (2019) 20:4368. doi: 10.3390/ijms20184368
33. Colasanti T, Sabatinelli D, Mancone C, Giorgi A, Pecani A, Spinelli FR, et al. Homocysteinylated Alpha 1 Antitrypsin as an Antigenic Target of Autoantibodies in Seronegative Rheumatoid Arthritis Patients. *J Autoimmun* (2020) 113:102470. doi: 10.1016/j.jaut.2020.102470
34. Li K, Mo W, Wu L, Wu X, Luo C, Xiao X, et al. Novel Autoantibodies Identified in Acpa-Negative Rheumatoid Arthritis. *Ann Rheum Dis* (2021) 80:739–47. doi: 10.1136/annrheumdis-2020-218460
35. Markiewicz A, Sigorski D, Markiewicz M, Owczarczyk-Saczonek A, Placek W. Caspase-14-From Biomolecular Basics to Clinical Approach. A Review of Available Data. *Int J Mol Sci* (2021) 22:5575. doi: 10.3390/ijms22115575
36. Ligoudistianou C, Xu Y, Garnier G, Circolo A, Volanakis JE. A Novel Human Complement-Related Protein, C1r-Like Protease (C1r-Lp), Specifically Cleaves Pro-C1s. *Biochem J* (2005) 387:165–73. doi: 10.1042/BJ20041196
37. Walsh DS, Borke JL, Singh BB, Do NN, Hsu SD, Balagon MV, et al. Psoriasis is Characterized by Altered Epidermal Expression of Caspase 14, a Novel Regulator of Keratinocyte Terminal Differentiation and Barrier Formation. *J Dermatol Sci* (2005) 37:61–3. doi: 10.1016/j.jdermsci.2004.10.003

Conflict of Interest: The authors declare that the research was conducted in the absence of any commercial or financial relationships that could be construed as a potential conflict of interest.

frontiers | Frontiers in Immunology

ORIGINAL RESEARCH
published: 29 April 2022
doi: 10.3389/fimmu.2022.856463

PreS/2-21-Guided siRNA Nanoparticles Target to Inhibit Hepatitis B Virus Infection and Replication

Lixia Gao[1†], Jie Yang[1†], Jutao Feng[2†], Ziying Liu[3], Ying Dong[4], Jiangyan Luo[1], Liangzhentian Yu[1], Jiamei Wang[1], Hongying Fan[1], Weifeng Ma[1] and Tiancai Liu[4*]*

[1] Department of Microbiology, School of Public Health, Southern Medical University, Guangzhou, China, [2] Department of Hepatobiliary Surgery, The First Affiliated Hospital of Guangzhou Medical University, Guangzhou, China, [3] State Key Laboratory of Organ Failure Research, Guangdong Provincial Key Laboratory of Viral Hepatitis Research, Department of Infectious Diseases, Nanfang Hospital, Southern Medical University, Guangzhou, China, [4] Institute of Antibody Engineering, School of Laboratory Medicine & Biotechnology, Southern Medical University, Guangzhou, China

OPEN ACCESS

Edited by:
Chunqing Guo,
Virginia Commonwealth University,
United States

Reviewed by:
Zheng Liu,
Virginia Commonwealth University,
United States
Xupeng Hong,
The Pennsylvania State University,
United States

***Correspondence:**
Tiancai Liu
liutc@smu.edu.cn
Weifeng Ma
maweifeng919@163.com

[†]These authors have contributed equally to this work

Specialty section:
This article was submitted to Molecular Innate Immunity, a section of the journal Frontiers in Immunology

Received: 17 January 2022
Accepted: 04 April 2022
Published: 29 April 2022

Citation:
Gao L, Yang J, Feng J, Liu Z, Dong Y, Luo J, Yu L, Wang J, Fan H, Ma W and Liu T (2022) PreS/2-21-Guided siRNA Nanoparticles Target to Inhibit Hepatitis B Virus Infection and Replication. Front. Immunol. 13:856463. doi: 10.3389/fimmu.2022.856463

A viable therapy is needed to overcome the deadlock of the incurable chronic hepatitis B (CHB). The prolonged existence of covalently closed circular DNA (cccDNA) and integrated HBV DNA in the nucleus of hepatocytes is the root cause of CHB. As a result, it is critical to successfully suppress HBV DNA replication and eliminate cccDNA. RNA interference has been proven in recent research to silence the expression of target genes and thereby decrease HBV replication. However, siRNA is susceptible to be degraded by RNA enzymes *in vivo*, making it difficult to deliver successfully and lacking of tissue targeting. To exploit the advantages of siRNA technology while also overcoming its limitations, we designed a new strategy and prepared biomimetic nanoparticles that were directed by PreS/2-21 peptides and precisely loaded HBV siRNA. Experiments on these nanoparticles *in vitro* and *in vivo* revealed that they are tiny, stable, safe and highly targetable, with high inhibitory effects on HBV DNA, pgRNA, cccDNA, HBeAg and HBsAg. PreS/2-21-directed nanoparticles loaded with HBV gene therapy drugs are expected to be promising for the treatment of CHB.

Keywords: HBV, siRNA, peptide, liposomal nanoparticles, targeting

INTRODUCTION

Hepatitis B virus (HBV) is a hepatophilic DNA virus and its persistent infection leads to chronic hepatitis B (CHB). HBV is now infecting over 250 million people globally (1), with over 600,000 people dying each year due to progression to cirrhosis, liver failure and hepatocellular carcinoma (HCC) (2). It is clear that there is still no effective response to hepatitis B virus infection. Despite the availability of a highly effective hepatitis B vaccination, hepatitis B virus infection remains a global public health problem. To improve the condition, a more methodical treatment technique must be identified (3). The nucleoside/nucleotide analogues (NAs) and interferon alpha (IFN-α)/pegylated interferon (PEG-IFN), which are currently utilized to treat chronic HBV infection, both have significant drawbacks. Interferon treatment has a wide range of in individual responses, as well as a

slew of adverse side effects and drug resistance. NAs inhibit HBV replication directly by suppressing viral reverse transcription, which are well tolerated, promote viral clearance and adherence to treatment (4), as well. However, NAs are unable to provide a cure because they do not remove covalently closed circular DNA (cccDNA). Therefore, developing an effective NAs hepatitis B therapy is critical.

RNA interference (RNAi) is a gene therapy that can be used to inhibit HBV replication and treat hepatitis B by mediating targeted mRNA degradation or mRNA translation inhibition to silence the expression of target genes in a specific manner (5). Clinical studies with siRNA drugs targeting the Pre-C, Pre-S1, Pre-S2, and X genes of HBV are now underway, with promising results (6, 7). Since all five mRNAs transcribed by HBV contain the X gene sequence, siRNA targeting the X gene can simultaneously inhibit the *in vivo* replication of HBV by inhibiting the formation of pregenomic RNA (pgRNA). Silencing the X gene of HBV fundamentally inhibits the translation of viral antigens and prevents liver injury from T-cell immune responses caused by viral antigen accumulation (8, 9). In this study, RNAi-mediated X gene silencing played an important inhibitory role in HBV replication in hepatocytes. *In vivo*, however, siRNA is susceptible to degradation by RNA enzymes, making it challenging to ensure successful delivery of siRNA. Viral vectors, non-viral vectors and chemically modified siRNAs have all been shown to help with this problem to some extent (10), but given the lack of tissue targeting of nanoparticles (11), further special modifications are needed to achieve active targeting of liposomal nanoparticles and thus increasing drug concentrations in liver tissue.

Studies have confirmed that HBV infects hepatocytes *via* attaching its PreS1 protein to the sodium taurocholate cotransporting polypeptide (NTCP) receptor of the latter (12, 13). Due to the critical function of PreS1 protein in HBV infection, the HBVpreS/2-21^{myr} (the binding region of PreS1) modified long-acting liposomal nanoparticles prepared by Han et al. (14) can specifically deliver fluorescein sodium into hepatocytes with high NTCP expression. Drawing on this, in this paper, PreS/2-21 is employed as a guide peptide, and linked to the surface of siRNA-encapsulated liposomal nanoparticles, which increased the targeting ability of the nanoparticles and competitively inhibited extracellular HBV invasion. Theoretically, the PreS/2-21-modified siRNA nanoparticles (PSN) can exert inhibitory effects on both extracellular and intracellular viruses. On the one hand, PreS/2-21 on the surface of the nanoparticles can target and bind to NTCP receptors on the surface of hepatocytes, acting as both an entry inhibitor to inhibit viral invasion into host cells and a guider for the nanoparticle specific entry into hepatocytes with high NTCP expression. On the other hand, the siRNA drug released *via* endocytosis has the ability to selectively block intracellular viral replication and expression. **Figure 1** depicts the working principles of this system. Through *in vitro* and *in vivo* studies, the anti-HBV viral efficacy, targeting and safety of PSN were comprehensively investigated and evaluated in this work.

MATERIALS AND METHODS

Cells and Animals

HepG2.2.15 cells, HepG2-N6 cells and pHBV1.3 plasmid were donated by Prof. Xiaoyong Zhang from the Department of Infectious Diseases, Nanfang Hospital. In particular, HepG2.2.15 cells, which can stably express HBsAg, HBV DNA and other substances in cell supernatant, are liver tumor cell lines of HepG2 cells with HBV genome integrated on their chromosomes (15), and HepG2-N6 cells are HepG2-derived cell lines that retain the characteristics of polarized

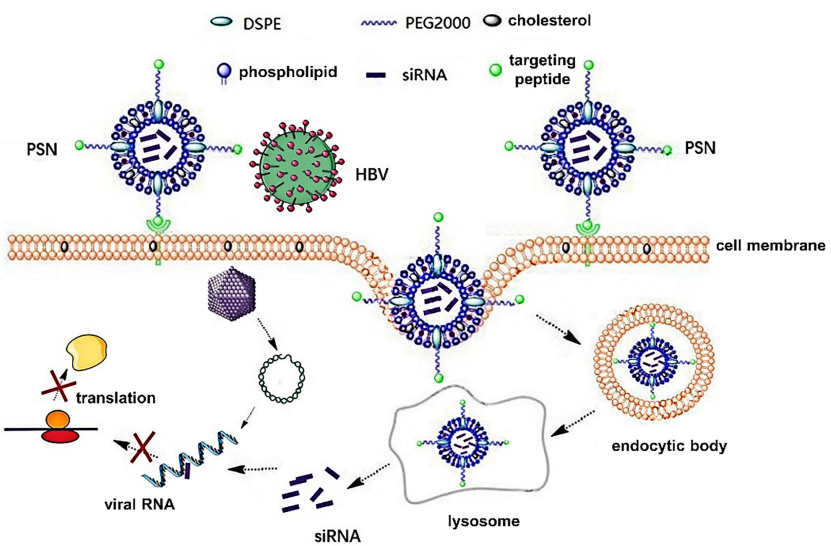

FIGURE 1 | Principles of PreS/2-21-conjugated nanoparticle with siRNA on targeted inhibition of hepatitis B virus.

hepatocytes, but display the morphology of a single columnar epithelium, enabling routine studies of virus transmission and release (16). In addition, HepG2-N6 cells highly express human NTCP (hNTCP) receptor, which is applicable for HBV targeting research. Mouse macrophage RAW 264.7 was donated by Prof. Longying Zha from the School of Public Health, Southern Medical University; HepG2 cells were kept in our laboratory; HBV/pMD18-T plasmid containing HBV DNA was constructed in our laboratory. HepG2 cells, HepG2-N6 cells, and RAW 264.7 cells were cultured in dulbecco's modified eagle medium (DMEM) containing 10% serum, and HepG2.2.15 cells were cultured in 1640 medium containing 10% fetal bovine serum, non-essential amino acids, and G418 (200 μg/mL).

Six to eight weeks-old SPF grade C57BL/6J male mice were purchased from the Animal Experiment Centre of Southern Medical University and housed in a sterile SPF grade laminar flow chamber. The mice were given regular mouse chow and ad libitum under controlled conditions of temperature (20-25°C) and humidity (40-45%) using a 12:12 h light/dark cycle. All animal experiments were performed after receiving consent from Southern Medical University's ethics review committee for animal experimentation.

Cellular Assay of HBV Inhibition by siRNA

The siRNA-X (1646-1664, GGUCUUACAUAAGAGGACU), siRNA-P (411-429, UCCUGCUGCUAUGCCUCAU), siRNA-C (2019-2039, AAGCCUUAGAGUCUCCUGAGC) against HBV X, P, and C genes respectively were selected by referring literature (17–20) and validated with cellular experiments, and synthesized by Guangzhou RiboBio, Co., Ltd.

The pHBV1.3 plasmid containing 1.3 times of the HBV genome was used for the construction of HBV infection models *in vitro* (21). To produce a cellular model of HBV infection, the pHBV1.3 plasmid was transfected into HepG2 cells using Lipofectamine 3000 (Gibco, Co., Ltd). siRNA was transfected simultaneously with the pHBV1.3 plasmid into HepG2 cells; HepG2.2.15 cells exclusively transfected with siRNA; the control group consisted of cells transfected with non-targeted control siRNA, and three replicate wells were set up for each cell line. After 72 h, the culture supernatants were collected and the levels of HBV DNA and HBsAg in the supernatants were measured. The HBV/pMD18-T plasmid containing HBV DNA was used as the standard of DNA levels. After fold dilution, quantitative real-time polymerase chain reaction (qPCR) was performed according to SYBR Premix Ex TaqTM II instructions (YEASEN, Co., Ltd). The lysis curve was the system default. The standard curve for HBV DNA was plotted using Ct values and the copy number was converted to international unit IU/mL. After centrifuging the supernatant, 50 μL was transferred to a new PCR tube, heated at 100°C for 2 min, then 1 μL was taken into the qPCR system (7), and the level of HBV DNA was calculated using the standard curve. After centrifugation to remove cell debris, the supernatant was obtained and HBsAg ELISA kits (Keygen Biotech, Co., Ltd) were used to detect HBV antigen levels according to the kit instructions.

Preparation of PSN

The experimental approach described in reference (22) was partially improved to prepare PSN and its controls, PreS/2-21-modified nanoparticles (PN), siRNA nanoparticles (SN), and lipid-like nanoparticles (LLN). TT3 is an organic compound produced the stepwise reaction with addition of propylene diamine, di-tert-butyl dicarbonate, sodium bicarbonate, 1,3,5-benzenetricarbonyl chloride, pyridine, trifluoroacetic acid, ethyl acetate, triethylamine, dodecaldehyde, and triacetyl, and was synthesized by WuXi AppTec. 1,2-distearoyl-sn-glycero-3-phosphocholine (DSPC) was purchased from Shanghai yuanye Bio-Technology, Co., Ltd. 1,2-distearoyl-sn-glycero-3-phosphoethanolamine-N[maleimide(polyethyleneglycol)-2000] (Mal-PEG2000-DSPE) was purchased from Shanghai Aladdin Biochemical Technology, Co., Ltd. The target peptide HBV PreS/2-21 and the lipid were synthesized by ChinaPeptides, Co., Ltd. The sequence of the target peptide is: NH_2-GTNLSVPNPLGFFPDHQLDP-COOH, synthesized with a stearylation modification at the N-terminal end and a cysteine (Cys) coupled at the C-terminal end. PreS/2-21 was dissolved in PBS solution (pH=7.0), Mal-PEG2000-DSPE was dissolved in N, N-Dimethylformamide (DMF), the two were combined at a molar ratio of Mal-PEG2000-DSPE: PreS/2-21 = 1:1.2 and the dehydration-condensation reaction was carried out slowly at 4°C for 8 h. PreS/2-21-Mal-PEG2000-DSPE (PMD) was obtained by lyophilizing the reaction products, followed by re-solubilizing it with anhydrous ethanol. The extrusion approach was used to synthesize PSN by TT3, cholesterol, DSPC, and PMD in a molar ratio of 50:10:38.5:1.5 (23). The aforementioned ingredients were also partially or completely used to make PN, SN, and LLN (**Table 1**). The above liposomal nanoparticle extrusions were concentrated using an ultrafiltration tube and decontaminated using a 0.22 μm filter membrane.

Encapsulation Rate and Characterization of Liposomal Nanoparticles

The concentrations of siRNA were measured using an ultra-micro UV spectrophotometer (Denovix, Co., Ltd) and the number of moles of siRNA was calculated from the volume.

TABLE 1 | The molar ratio of each component in the synthesis of liposomal nanoparticles.

	TT3	DSPC	Cholesterol	PEG2000-DSPE	PMD	siRNA
PSN	50	10	38.5	No	1.5	Yes
PN	50	10	38.5	No	1.5	No
SN	50	10	38.5	1.5	No	Yes
LLN	50	10	38.5	1.5	No	No

The encapsulation rate was calculated as EE% = (moles of siRNA before packaging - moles of siRNA after packaging)/moles of siRNA before packaging × 100%. PSN was naturally dried on aluminum foil and plated with gold, and then the ultrastructural morphology was observed by scanning electron microscope (Hitachi, Co., Ltd). The particle size and zeta potential of liposomal nanoparticles were measured by Zetasizer Nano (Malvern, Co., Ltd): the liposomal nanoparticles diluted with ddH_2O from 1 μL to 1000 μL were placed in a potentiometric cuvette and then assayed and scanned 100 times in duplicate. The liposomal nanoparticles were stored at 4°C analyzed for the particle size every 5 days, and monitored continuously for 30 days to examine the temporal stability. 10 μL of liposomal nanoparticles were added to 90 μL of PBS containing 10% FBS and shaken at 37°C at 100 rpm/min. The particle size was measured at 0, 3, 6, 12, 24, and 48 h to observe the serum stability. In addition, we monitored the temporal stability of activity by storing the liposomal nanoparticles at 4°C and analyzed the inhibition of HBV DNA by PSN using HepG2.2.15 cells once a week for a month.

In Vitro Safety and Efficacy Testing of Liposomal Nanoparticles

HepG2.2.15, HepG2-N6 and RAW263.7 cells (1×10^4 cells/well) were grown for 24 h in 96-well plates, then incubated with varying dosages of PSN for 48 h. To assess cytotoxicity, MTT was applied to the samples, and the absorbance values at OD 490 nm were measured to calculate the 50% cytotoxic concentration (CC50) of PSN on different cells. Experiments were performed using the cell models of HepG2.2.15, HepG2 transfected with pHBV1.3 (pHBV1.3-HepG2), and HepG2-N6 cells. Treatment groups consisted of five PSN concentration gradient subgroups, as well as a negative control and a blank control group, each with three replicate wells. The cell supernatant was collected after 72 h of incubation to detect the level of HBV DNA, the inhibition rate of PSN against HBV was calculated, and the half effective concentration (EC50) was estimated by GraphPad Prism 7 software (GraphPad Software, Inc., San Diego, CA, USA). Therapeutic Index (TI) was calculated by the ratio of CC50 against EC50. RAW264 cells were seeded on 6-well plates at a density of 2×10^5 per well and co-cultured with 25 μg/mL PSN. The cells and culture supernatants were collected respectively after co-cultivation for 12 h, and the expression of cytokines IFN-α, TNF-α, and IL-6 was detected by reverse transcription qPCR (RT-qPCR) and ELISA kits (MULTI SCIENCES(LIANKE) BIOTECH, CO., LTD.).

In Vitro Targeting Assay of PSN on NTCP Receptors

First, the expression of NTCP receptors on the surface of HepG2 cells, HepG2-N6 cells were detected by flow cytometry, fluorescence microscopy, and western blot. The binding ability of PSN to NTCP receptors were detected by flow cytometry and fluorescence microscopy. HepG2 cells and HepG2-N6 cells were plated in six-well plates and incubated for 12 hours followed by a 30 min incubation with PBS or PSN (40 μL), then were stained with FITC-labeled NTCP antibody (ImmunoClone, IC03828F), and an equal amount of cells stained with FITC-labeled isotype control antibody was used as a negative control and analyzed by flow cytometry and fluorescence microscopy. HepG2-N6 cells and HepG2 cells were seeded in six-well plates. After 12-hours incubation, the cells were processed for total protein extraction, concentration determination, and western blot analysis. The protein concentration was measured with Pierce™ BCA Protein Assay Kit (ThermoFisher #23225) following instructions. Western blot was done according to standard methods. The expression level of β-actin was used as an internal control. The primary antibodies used in western blot were NTCP polyclonal antibody (Signalway Antibody Co., United States) and β-actin antibody (Fude Biological Technology Co., Hangzhou, China), and the secondary antibody was horseradish peroxidase-conjugated goat anti-rabbit IgG (Bioworld, United States). Furthermore, liposomal nanoparticles PSN-Cy3 and SN-Cy3 were prepared by Cy3-labeled siRNA-X, and the targeting of PSN-Cy3 to NTCP receptors was detected by HepG2-N6 cells, HepG2 cells and Hela cells. The Cy3-labelled siRNA-X was synthesized by Guangzhou RiboBio, Co., Ltd., and the liposomal nanoparticles were prepared as before, light protection throughout the process. Cells were inoculated into six-well plates and incubated for 12 h, then 40 μL PSN-Cy3 or SN-Cy3 was added and incubated for 30 min protected from light, while PBS-treated cells were used as a negative control. The fluorescence was measured by flow cytometry, observed under a fluorescence microscope and photographed.

In Vitro Inhibition of HBV by PSN

Experiments were performed using the cell models of HepG2.2.15, pHBV1.3-HepG2, and HepG2-N6 cells. Among them, HepG2-N6 cell model was infected with HBV produced in HepG2.2.15 cell culture supernatant and concentrated using PEG8000, and the infection efficiency was verified by western blot. The experiments were divided into five groups: negative control, PSN, PN, SN, and LLN group. Approximately 12 h after the cells were inoculated onto the six-well plates, cells had attained 80% confluency, and 5 nM siRNA-containing nanoparticles or an equivalent amount of nanoparticles were introduced to the cells. Cell supernatants and cells were collected separately after 72 h of incubation, and the expression of HBxAg, pgRNA, HBV DNA and cccDNA were detected using RT-qPCR or qPCR. The primer sequences are shown in **Table S1**. The levels of HBsAg and HBeAg in cell supernatants were detected by ELISA kits (Keygen Biotech, Co., Ltd). The cells were processed for protein extraction, concentration determination, and western blot analysis. Antibody to hepatitis B core antigen (anti-HBc, a gift from Prof. Xiaoyong Zhang, the Department of Infectious Medicine, Nanfang Hospital, China) and horseradish peroxidase-conjugated goat anti-rabbit IgG (Zhongshan Golden Bridge Biotechnology Co., Beijing, China) were incubated as described previously.

Construction and Identification of CHB Model in Mice

The recombinant adeno-associated virus AAV-HBV-002 applied to construct the hepatitis B model was purchased from PackGene Biotech, Co., Ltd. AAV-HBV-002 containing 1.3× HBV genome, is characterized by the production of HBV DNA, HBeAg and HBsAg, and the genotype is C2 and serotype is adr. Sixteen mice were each injected with AAV-HBV-002 into the tail vein at a dose of 1×10^{11} vg. Another group of eight mice was injected with an equal volume of PBS as normal controls. Every four days, the mice's mental condition, nutrition, and water consumption were assessed, and their body weight was measured and recorded. During collection every four days, a total of nearly 500 μL of orbital blood were collected and stored at -80°C. On fifteenth day, the expression of HBV DNA, HBeAg and HBsAg in serum was measured to determine whether the model had been successfully constructed. **Figure 2** depicts the process of constructing a hepatitis B model in mice by injecting virus into the tail vein.

In Vivo Efficacy and Safety Trials of PSN

Fresh mouse blood was taken to prepare 2% erythrocyte suspension, to which different concentrations of PSN were added, and those with distilled water were used as the positive control group. After incubating at 37°C for 3 h, the colour of the supernatant was observed to monitor whether haemolysis had occurred. The 16 of mice who successfully constructed were randomly divided into PSN group and hepatitis B model group, and 8 untreated normal mice were selected as blank control group. The mice in the PSN group were given PSN and the other two groups were given saline in equal doses. In the PSN group, the effective dose of 5 mg/kg siRNA was administered every other day for 15 days, for a total of 8 doses. After completion of administration, the mice were anesthetized with 5% anhydrous ether, dissected, and perfused with PBS, then 1.5-2.0 mL of blood was collected. qPCR was used to detect the relative expression of HBV DNA (24). The primers and probe sequences were shown in **Table S1**. The levels of antigens HBeAg and HBsAg, transaminases of ALT and AST were detected by ELISA kits (NanJing JianCheng Bioengineering Institute). The expression of IFN-α, TNF-α, and IL-6 was detected by RT-qPCR and ELISA kits. The important organs of the mouse, such as heart, liver, kidney, spleen, lung and brain, were removed and fixed in 4% paraformaldehyde solution, before being embedded, sectioned, and HE staining. The procedure for administration of PSN intervention to mice is shown in **Figure 2**.

In Vivo Targeting Experiments for PSN

Six of 6-8 weeks C57BL/6J male mice were selected to construct a mouse hepatitis B virus model. After successful modelling, the mice were randomly divided into two groups with 3 mice in each group, and the experimental and control groups were treated with PSN-Cy7 and SN-Cy7, respectively, with a tail vein injection dose of 5 mg/kg. The fluorescence intensity in liver, kidney, lung, spleen and brain tissues was observed by a multi-modal small animal live imaging system at 1 and 3 h after injection.

Statistical Analysis

All data reported are representative of at least three independent experiments. The experimental results were statistically evaluated using SPSS v19.0 software and were reported as mean ± standard deviation (Mean ± SD). Comparisons between two groups of data were made using the t-test for two independent samples, and the Shapior-Wilk test for normality and chi-square test was used between multiple groups of data, with the test level $\alpha = 0.05$ (two-sided), and $P<0.05$ was considered a statistically significant difference.

RESULTS

Optimal Inhibitory Effect of siRNA-X on HBV DNA and HBsAg

The pHBV1.3-HepG2 and HepG2.2.15 cells were inoculated into six-well plates and the experiment was divided into five groups: PBS negative control group, siRNA-P, siRNA-C, siRNA-X, and siRNA-NC. As demonstrated in **Figure 3**, three of the siRNAs reduced HBV expression with statistically significant differences. For the inhibition of HBV DNA in the supernatant of HepG2.2.15 cells, siRNA-X was more effective than siRNA-C; for the inhibition of HBsAg, siRNA-X was the most effective (**Figures 3A–D**).

PSN is Stable

The particle sizes of nanoparticles ranged from (83.85 ± 11.99) nm to (116.30 ± 8.05) nm (**Figures 4A, D**). The zeta potential of

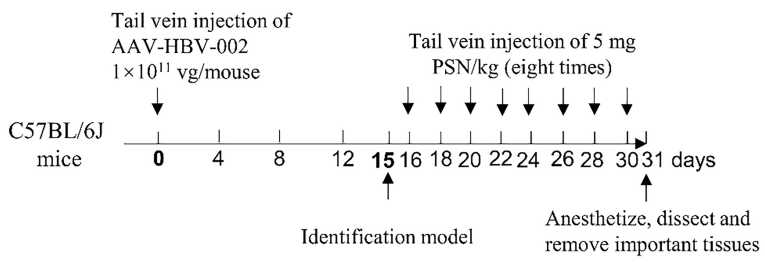

FIGURE 2 | Schematic diagram of mouse modelling and PSN administration.

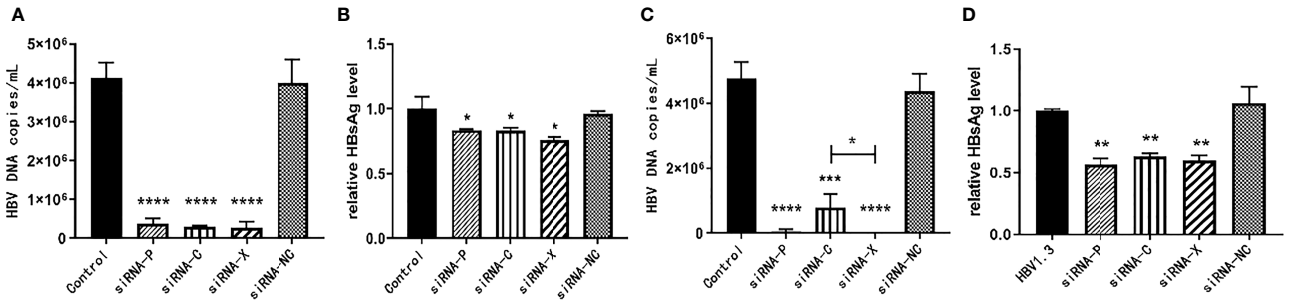

FIGURE 3 | *In vitro* inhibition of HBV by siRNA. **(A, B)** pHBV1.3-HepG2 cells; **(C, D)** HepG2.2.15 cells. Data are represented as the mean ± SD from at least three independent experiments. *$P < 0.05$, **$P < 0.01$, ***$P < 0.001$, ****$P < 0.0001$.

PSN was (-103.01 ± 2.61) mV at 37°C (**Figure 4B**). Under the scanning electron microscope, the PSNs were spherical, with smooth surface and uniform size distribution, and the diameters were mostly about 100 nm (**Figure 4C**). The siRNA concentration in the filtrate before and after encapsulation was measured to calculate the encapsulation rate. The results showed that PSN achieved an encapsulation rate of (84.75 ± 0.30) %, which was higher than the others. The encapsulation rates and particle sizes of the nanoparticles are shown in **Figure 4D**.

Liposomal nanoparticles were stored at 4°C and particle size was tested every 5 days. There were some fluctuations in particle size, but no fragmentation or fusion into large particles (**Figure 5A**). It was also mixed with 10% serum and incubated at 37°C for 48 h to test the stability in serum, showing little fluctuation in particle size and no fragmentation or fusion into large particles (**Figure 5B**). HepG2.2.15 cells were treated with PSN stored at 4°C for different periods of time, showing that more than 60% of HBV DNA inhibition was retained for at least 28 days, and the activity was relatively stable (**Figure 5C**).

PSN is Safe and Effective for Cells

We examined the CC50 and EC50 of PSN against three cell models and calculated the TI (CC50/EC50). The results (**Table 2**) showed that the TIs of PSN to three kinds of cells were close to or exceeded 100, indicating that PSN can specifically inhibit HBV with less damage to host cells and maintain good cell safety. RAW264 cells treated with 25 μg/mL PSN for 12 h did not cause significant changes in the

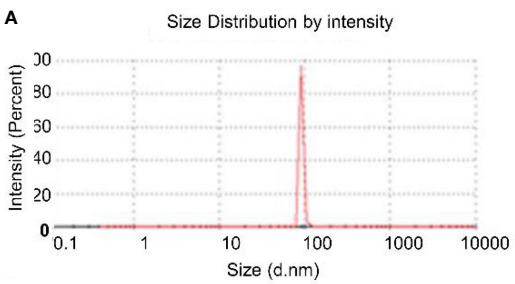

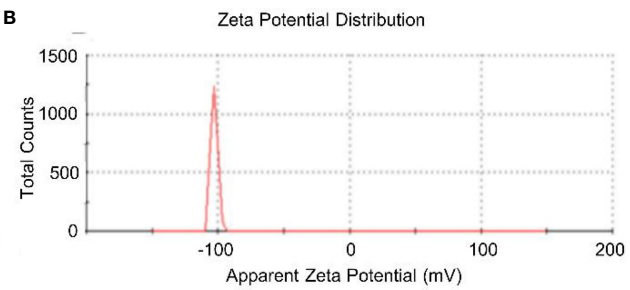

C

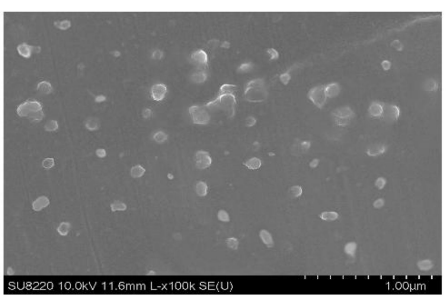

D

	Encapsulation rate	Particle size (nm)	Zeta (mV)
PSN	(84.75±0.3)%	91.72±2.49	-103±2.61
PN	-	93.71±9.87	-
SN	(78.29±3.53)%	116.3±8.05	-
LLN	-	83.85±11.99	-
PSN-Cy3	(79.80±0.73)%	91.86±15.20	-
SN-Cy3	(61.57±1.49)%	116.1±10.23	-

FIGURE 4 | Properties of liposomal nanoparticles. **(A)** Particle size of PSN. **(B)** Zeta potential of PSN. **(C)** The ultrastructural morphology of PSN detected by scanning electron microscope. **(D)** Data on encapsulation rates, particle sizes, and zeta potentials of liposomal nanoparticles.

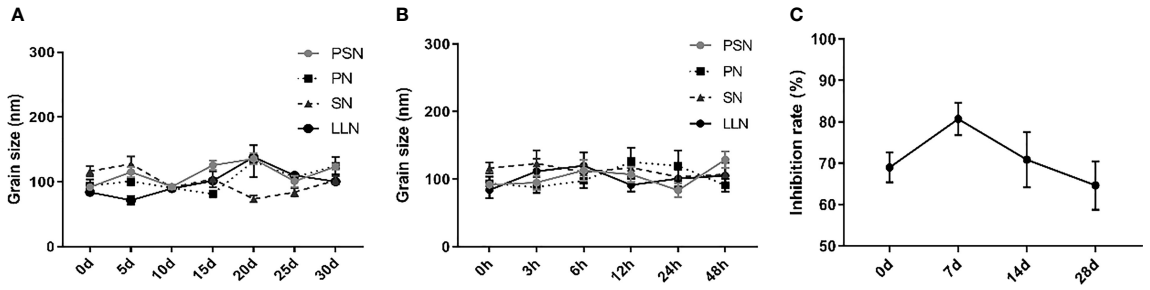

FIGURE 5 | The stability of liposomal nanoparticles. **(A)** Temporal stability. **(B)** Stability in serum. **(C)** PSN activity at different time points.

expression of cytokines IFN-α, TNF-α, and IL-6, either in the cells or culture supernatants (**Figure S1**).

PSN Precisely Targets NTCP Receptors

After labeling with NTCP-FITC antibody, the expression of NTCP on the surface of each cell was detected by flow cytometry. The results (**Figure 6A**) showed that the fluorescence intensity of HepG2-N6 cells was high, while HepG2-N6 cells was significantly lower after PSN treatment with statistically difference (P<0.0001) (**Figure 6G**). The fluorescence intensity of HepG2 cells incubated with NTCP-FITC antibody was lower (P<0.0001) (**Figure 6G**), and the fluorescence intensity of HepG2 cells did not change significantly after PSN treatment. The same results were obtained by fluorescence microscopy, as detailed in **Figures S2A–C**. The results indicate that HepG2-N6 cells have a high level of NTCP receptors on surface, and PSN specifically binds to NTCP and induces a reduction in its endocytosis. And the results (**Figure 6I**) by western blot analysis further indicated that HepG2-N6 cells have a high level of NTCP receptors.

The Cy3-labeled siRNA was used to quantify the targeting of PSN to various cells. Flow cytometry results showed that the fluorescence intensity of PSN-Cy3 in HepG2-N6 cells was significantly higher than that in HepG2 cells as well as Hela cells (P<0.0001, P<0.001) (**Figures 6B, C, H**); the fluorescence intensity in PSN-Cy3-treated HepG2-N6 cells was significantly higher than that in SN-Cy3 group (P<0.001) (**Figures 6D, H**); while the fluorescence intensity in PSN-Cy3-treated HepG2 cells and Hela cells had almost the same fluorescence intensity as the SN-Cy3 group (**Figures 6E, F**). Under the fluorescence microscope, PSN-Cy3 showed the highest brightness in HepG2-N6 cells, but weak fluorescent signal in HepG2 cells and Hela cells (**Figures S2D–I**). The results indicate that PSN has strong NTCP binding ability and can be endocytosed by HepG2-N6 cells with high NTCP expression, but less by HepG2 cells and Hela cells with low expression of NTCP receptor.

PSN Strongly Inhibits Intracellular HBV

The inhibitory effect of liposomal nanoparticles on HBV was examined using HepG2.2.15 cells. Except for LLN, all liposomal nanoparticles had a certain inhibitory effect on HBV with statistically significant difference. The inhibition rate of PSN on pgRNA and HBV DNA was stronger, reaching 95.81% and 83.53%, respectively, and on HBxAg, cccDNA, HBeAg, and HBsAg was around 40% (**Figures S3A–F**). The inhibitory impact of PSN on HBV was further investigated using HepG2 cells transfected with pHBV1.3 plasmid as a model of HBV-infected cells, which showed similarly result (**Figures S3G–L**).

In addition, we detected HBV core antigen in HepG2-N6 cells infected with HBV by western blot, and the results (**Figure 7F**) showed that the core antigen in HBV-infected HepG2-N6 cells was significantly reduced after PSN treatment. We also tested the anti-HBV effect of PSN using HepG2-N6 cells before, during and after HBV infection respectively, and found that adding PSN before or at the time of HBV infection had a better pgRNA, HBeAg inhibition effect than after HBV infection, and the results were statistically different (**Figures 7**, **S4**). It showed that PreS/2-21 on the surface of nanoparticles could compete with HBV to bind NTCP receptors and function as a certain HBV entry inhibitor.

PSN is Biocompatible Without Hemolysis and Tissue Damage

The results of the haemolytic assay showed no haemolysis in the PSN group, with all red blood cells sinking and the upper layer being a slightly cloudy yellow solution. In contrast, the distilled water group showed haemolysis and the solution was red (**Figure S5**). After 15 days of PSN treatment (5 mg/kg, qod, 8 time), all

TABLE 2 | The cytotoxicity, efficacy, and therapeutic index of liposomal nanoparticles.

	CC50 (μg/mL)	EC50 (μg/mL)	TI
pHBV1.3-HepG2	338.95 ± 5.48	3.19 ± 0.02	121.10
HepG2.2.15	450.11 ± 13.96	2.80 ± 0.26	160.81
HepG2-N6	273.34 ± 12.01	3.06 ± 0.02	97.66

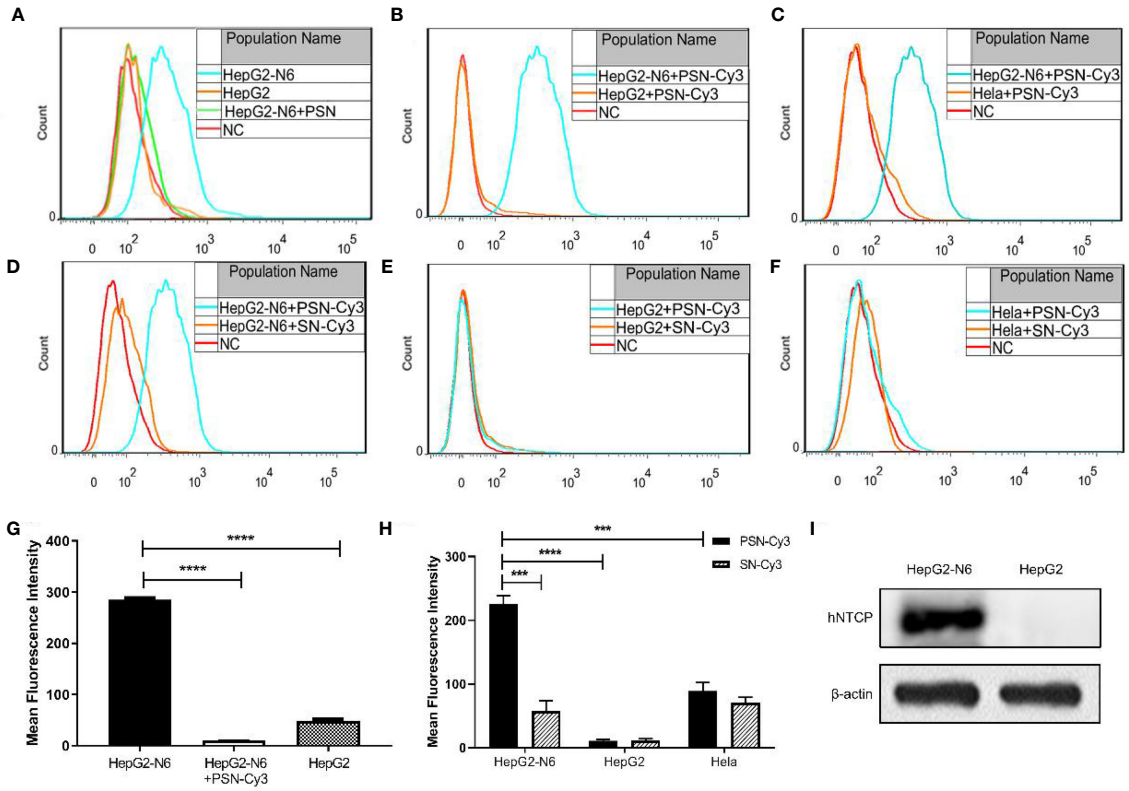

FIGURE 6 | Targeting detection of liposomal nanoparticles. **(A)** After NTCP-FITC antibody labeling, flow cytometry detects NTCP receptor expression on cells and PSN competition for receptor binding, NC is the same amount of cells stained with FITC-labeled isotype control antibody; **(B–F)** Flow cytometric detection of the targeting properties of siRNA-Cy3 loaded nanoparticles PSN and SN to HepG2-N6, HepG2 and Hela cells, NC is the corresponding cell added with the same amount of PBS; **(G)** Comparison of the fluorescence intensity of each treatment group in **Figure A**; **(H)** Comparison of fluorescence intensity of each experimental group in **Figure B**–**F**; **(I)** Western blot analysis of NTCP expression in HepG2-N6 and HepG2 cells. Data are represented as the mean ± SD from at least three independent experiments. ***$P < 0.001$, ****$P < 0.0001$.

mice were anaesthetized and dissected, and pathological sections were taken from liver, lung, heart, kidney, spleen and brain tissues for HE staining. During modeling and administration, the mental status and body weight of the mice did not fluctuate apparently (**Figure S6**). The hepatocytes in the blank control group were normal in structure, with the nucleus in the centre of the cell and normal in size (left side of **Figure 8A**). The liver tissue of the mice in the hepatitis B model group was diffusely edema, the liver cells were obviously enlarged with indistinct boundaries, and there were a large number of vacuoles (middle of **Figure 8A**). The hepatocytes in the PSN group had clear borders and no evident pathological changes were observed (right side of **Figure 8A**). The rest of the tissues in the hepatitis B model group and the PSN groups showed no abnormalities (**Figures 8B–F**).

PSN Reduces the Hepatitis B Viral Load *In Vivo*

After successful modelling, the experimental group was given PSN intervention for 15 days, while a model control group and a blank control group were set up and given an equal volume of saline. After 15 days of treatment, a high copy of HBV DNA could be detected in the hepatitis B model group at a concentration of $(49.13 \pm 2.68)\times10^5$ IU/mL. In the PSN group, the level of HBV DNA was lower than that in the hepatitis B model group, at $(37.13 \pm 3.35)\times10^5$ IU/mL (**Figure 9A**), with an inhibition rate of 24.43%. The relative expression of cccDNA was also lower in the PSN group compared to the hepatitis B model group (**Figure 9B**), and the inhibition rate of cccDNA by PSN was 28.93%. After PSN intervention, the expression of HBeAg decreased from (117.97 ± 38.14) PEI U/mL to (52.56 ± 17.55) PEI U/mL and the expression of HBsAg decreased from (112.38 ± 37.61) IU/mL to (68.79 ± 28.90) IU/mL with statistically significant difference (**Figures 9C, D**), and the inhibition rates of PSN on HBeAg and HBsAg were 55.45% and 38.79%, respectively.

PSN Reduces the Levels of Transaminases and Cytokines *in Vivo*

After 15 days of PSN treatment, the expression of ALT and AST were lower than those in the hepatitis B model group and close to those in the blank control group (**Figure 10A**). The mRNA expression of cytokines IFN-α, TNF-α and IL-6 was significantly reduced after PSN treatment, which appeared to be closer to the

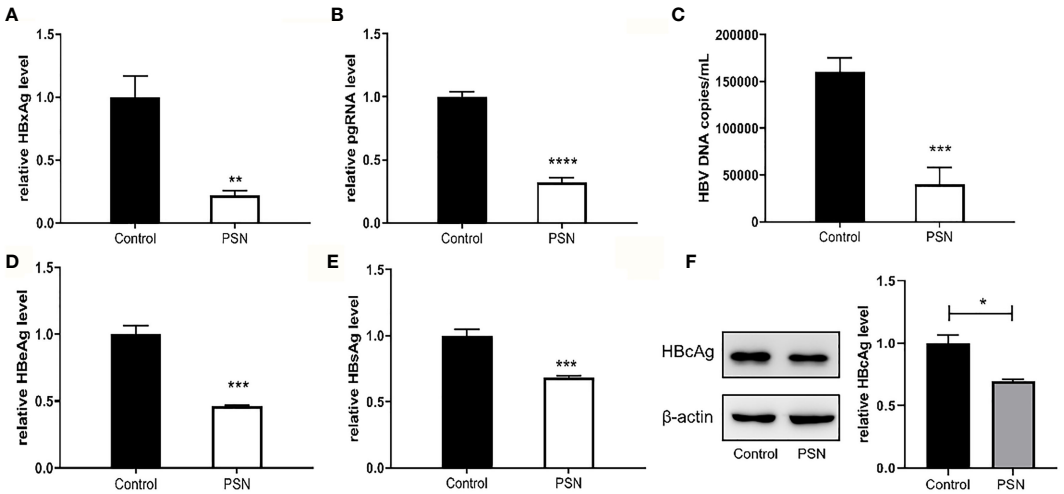

FIGURE 7 | Inhibitory effect of nanoparticles on HBV, when nanoparticles and HBV simultaneously act on HepG2-N6. **(A, B)** Inhibitory effect of nanoparticles on HBxAg mRNA and pgRNA in cells. **(C–E)** Inhibitory effect of nanoparticles on HBV DNA, HBeAg and HBsAg in supernatant. **(F)** Western blot analysis of HBcAg expression in HepG2-N6 cells infected HBV, and expression after PSN treatment. Data are represented as the mean ± SD from at least three independent experiments. *$P < 0.05$, **$P < 0.01$, ***$P < 0.001$, ****$P < 0.0001$.

levels of the control group (**Figure S7**). Compared with the model group, the protein expression of IL-6 and IFN-α in the serum of mice in the PSN group decreased, among which IL-6 decreased with statistical difference ($P < 0.01$), while the expression level of TNF-α appeared to be relatively low among the three groups (**Figure 10B**).

PSN Targets Liver Tissue *In Vivo*

After 1 h of injection of PSN-Cy7 and SN-Cy7, *in vivo* imaging of mice revealed that the fluorescence in the PSN group was concentrated in the liver and gastrointestinal tract, while in the SN group was concentrated in the gastrointestinal tract with only weak fluorescence in the liver (**Figures 11A, B**). After 3 h of injection, the fluorescence in the PSN group was concentrated in the gastrointestinal tract, while some mice in the control group only had fluorescence in the gastrointestinal tract or even no fluorescence in the body (**Figures 11C, D**).

DISCUSSION

The HBV genome is a 3.2 kb partial double-stranded circular DNA that can be transcribed into 3.5, 2.4, 2.1, and 0.7 kb viral transcripts containing four open reading frames (S, C, P, and X, respectively) (25). All HBV transcripts are encoded in an overlapping reading format with the same polyadenylation signal (PAS) and a shared 3' terminus (26). Among them, the gene X encodes HBx, which is a 17 kDa protein. In addition to acting as a trans-activating transcription factor for oncogenes, it is also a protein necessary for virus replication. It initiates and maintains the transcription of cccDNA template, which has an impact on apoptosis and metabolism. These effects may lead to chronic HBV infection (27, 28). And as the HBx sequence is expressed in all four viral mRNAs, it appears to be an attractive target for anti-HBV siRNA development (25). In contrast, several studies have shown that not only viral mRNA expression but also HBV replication were inhibited in cultured cells and in mice by using siRNAs targeting the P, S, C, and X genes (29–32). We tested siRNAs targeting different genes of HBV by cellular assays, siRNA-X showed the best inhibitory effect on HBV (**Figure 3**). Therefore, we chose to construct targeting nanoparticles on the basis of siRNA-X. The liposomal nanoparticles have the characteristics of safety, stability, efficiency, ease of targeting modifications, and the possibility of long circulation, which make them ideal as carriers for the delivery of gene drugs *in vivo*. Two kinds of siRNA drugs are currently on the market, Onpattro (patisiran) (33) and Givlaari (givosiran) (34), both encapsulated in liposomes, the former targeting transthyretin (TTR) as an injectable treatment for hereditary transforming amyloidosis (hATTR) (35), and the latter targeting a neurotoxic intermediate (ALAS1) for the treatment of acute hepatic porphyria (36). In view of this, and based on the important role that the PreS1 protein plays in HBV infection, PEG was used in this study to improve the stability of liposomes, and PreS/2-21 was added to the liposome surface to achieve active targeting, i.e., to reduce drug accumulation in normal tissues and increase drug concentrations in liver tissue.

In this study, PreS/2-21 modified siRNA nanoparticles were investigated *in vivo* and *in vitro* experiments, and were validated in terms of safety, targeting and antiviral effects, all of which achieved the expected results and were consistent with theory. In addition, PN only blocking extracellular HBV entry and SN only inhibiting intracellular HBV replication were designed as controls. Compared with PN and SN, PSN inhibited pgRNA, HBxAg, and HBeAg with significantly increased efficiency, indicating that nanoparticles modified with PreS/2-21

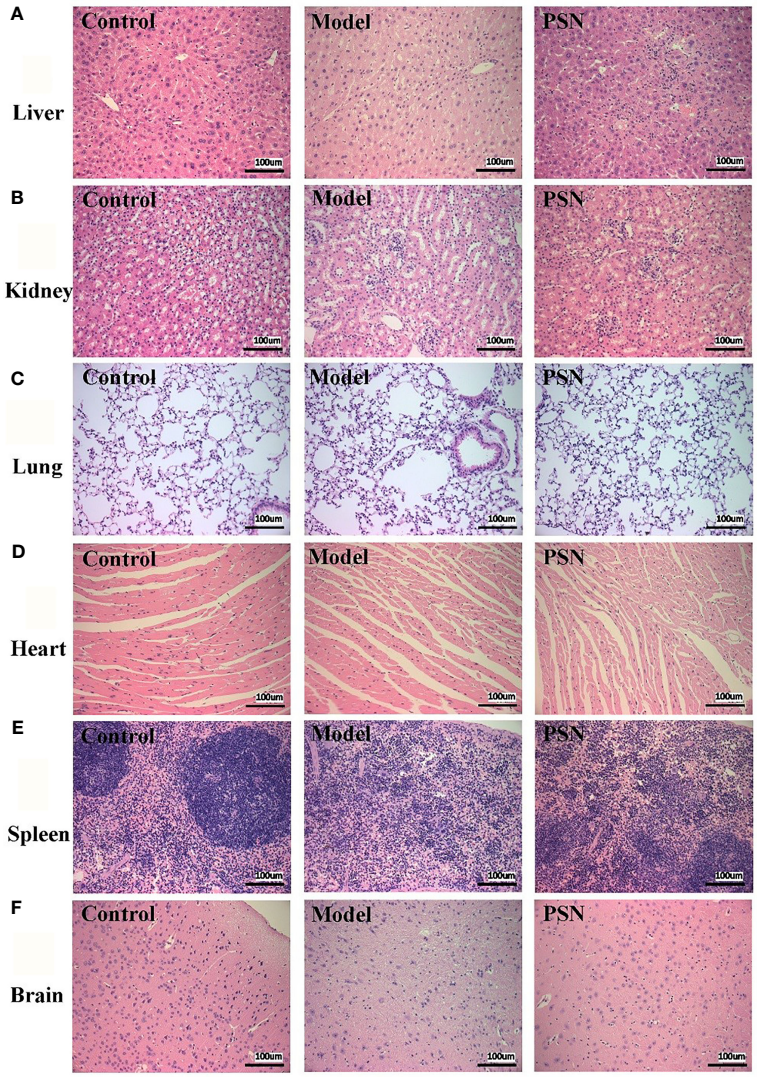

FIGURE 8 | HE staining of mice's tissue sections in control, HBV model, and PSN groups (×200). **(A–F)** Liver, kidney, lung, heart, spleen, and brain tissue in sequence.

specifically inhibit viral infection through competitive binding; while the nanoparticles loaded with siRNA specifically inhibit intracellular viral replication. The nanoparticles with the modification of PreS/2-21 on the surface, along with internal loading of siRNA, showed the highest anti-HBV activity. Such a combination design is quite beneficial to improve the drug effect. Also, PreS/2-21 has been proven to be an excellent HBV entry inhibitor, which can effectively inhibit HBV infection of cells (37). In this study, PreS/2-21 was coupled to the surface of nanoparticles, hoping that it would confer targeting ability to hepatocytes while also preventing HBV infection. NTCP is a receptor protein for HBV infection that is extensively expressed on the surface of hepatocytes. We confirmed that the NTCP receptor was abundantly expressed on the surface of HepG2-N6 cells by fluorescent antibody labeling, flow cytometry and western blot, and that PSN could compete with anti-NTCP-FITC antibody to bind NTCP receptor, initially confirming the targeting of NTCP by PSN. The siRNA in the nanoparticles was subsequently labelled with the fluorescent dye of Cy3 and detected by fluorescence microscopy and flow cytometry, demonstrating that PSN-Cy3 could be enriched in HepG2-N6 cells, while the fluorescent signal was weak in HepG2 cells and Hela cells with low NTCP expression, indicating that PSN has a strong targeting ability. Cytotoxicity assays further confirm that PSN specifically inhibits only viral replication, with TIs approaching or exceeding 100, without causing cytolysis and significant changes in cytokines, all of which indicate a high safety for PSN. In addition, the particle size of PSN does not change significantly with the addition of serum or temporarily storage, and PSN retains more than 60% of cellular activity even

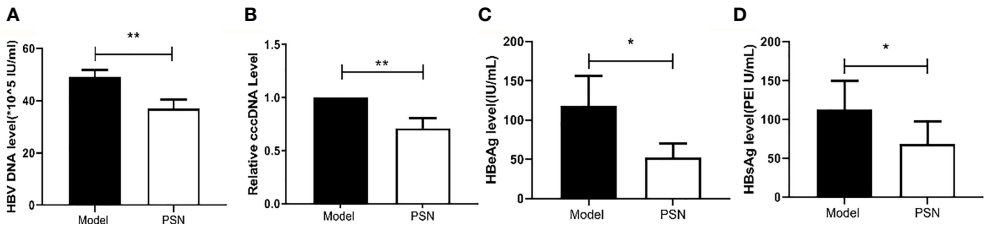

FIGURE 9 | Inhibition of HBV by PSN in mice. **(A–D)** qPCR or ELISA tests for the expression of HBV DNA, cccDNA, HBeAg and HBsAg in mice's serum. Data are representative of three independent experiments with n = 8 mice per group. *$P < 0.05$, **$P < 0.01$.

after one month of storage, indicating that PSN is stable and has excellent drug-forming properties.

Based on the *in vitro* experiments, this study further investigated the safety and efficacy of PSN through *in vivo* experiments. The hepatitis B model mice were successfully constructed and treated with PSN for 15 days, during which time the mental status and body weight of the mice did not change appreciably. The results of HE staining of the heart, liver, spleen, kidney, brain and lung sections from the PSN-treated mice showed that PSN intervention could improve liver injury in HBV-infected mice without other organ damage, which indicated that the efficacy and safety of PSN were not in doubt. For the antiviral effect of PSN, we found that the levels of HBV DNA, HBeAg and HBsAg in the PSN-treated hepatitis B mice group were significantly lower than those in the model group, which is consistent with the results of related studies that siRNA can significantly reduce the levels of HBeAg and HBsAg *in vivo* (7, 38). Furthermore, we discovered that PSN lowered ALT and AST levels in hepatitis B mice, confirming the antiviral action of PSN *in vivo* and improving liver function to some extent. The mice were then administered targeted PSN and non-targeted SN interventions and performed *in vivo* imaging after 1 and 3 h of the intervention in both groups. Thus, it was confirmed that PSN is equally liver tissue-targeting *in vivo*.

It is clear that the safety, targeting and anti-HBV efficacy of PSN have been validated and confirmed by *in vitro* and *in vivo* trials, which provides new ideas for the development of hepatitis B drugs and offers hope for the eradication of hepatitis B. This is the significance of this study. The two therapeutic agents currently approved for the treatment of CHB in adults are interferon-alpha (Peg-IFNα) and NAs: nucleosides (lamivudine, telbivudine, and entecavir) and nucleotides (adefovir and tenofovir). Although NAs are well tolerated and can suppress viral replication to undetectable levels, the long-term treatment required to maintain viralogical control frequently leads to drug resistance or serious side effects such as nephrotoxicity, reduced bone mass, or bone marrow failure. Although Peg-IFNα has a high probability of clearing HBsAg, it has restricted by expensive cost, a slew of adverse effects, or low response rates (39). The combination of Peg-IFNα and NAs improves functional cure rates, but it is only appropriate for a limited proportion of patients (40). The PSN is modified on the basis of RNA interference, and siRNA is encapsulated by liposomal nanoparticles coupled with PreS/2-21 to boost its stability and targetability. PreS/2-21 inhibits viral infection outside hepatocytes by blocking receptors, and RNAi inhibits viral replication in hepatocytes by mediating gene silencing. Thus, PSN has the advantages of siRNA antiviral agent, which reduces all measurable viral products as well as actively targets the hepatocyte NTCP receptor. Therefore, PSN is a drug with great potential for the treatment of hepatitis B.

Of course, the present study has certain limitations due to time restriction. On the one hand, we only selected one siRNA as the encapsulated drug for research *in vitro* and *in vivo*, and the

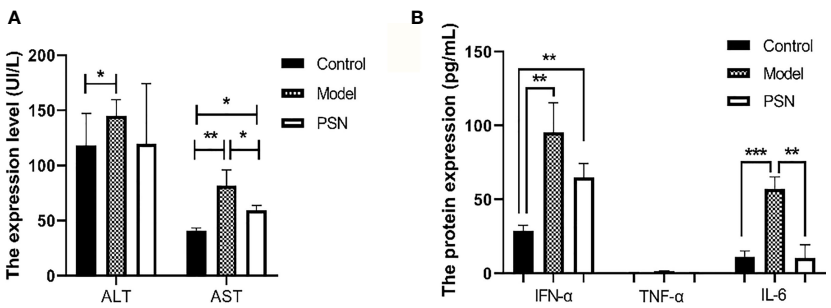

FIGURE 10 | ELISA tests for the expression of transaminases and cytokines in mices's serum after PSN treatment. **(A, B)** The relative expression of transaminases ALT and AST, cytokines IFN-α, TNF-α, and IL-6. Data are representative of three independent experiments with n = 8 mice per group. *$P < 0.05$, **$P < 0.01$, ***$P < 0.001$.

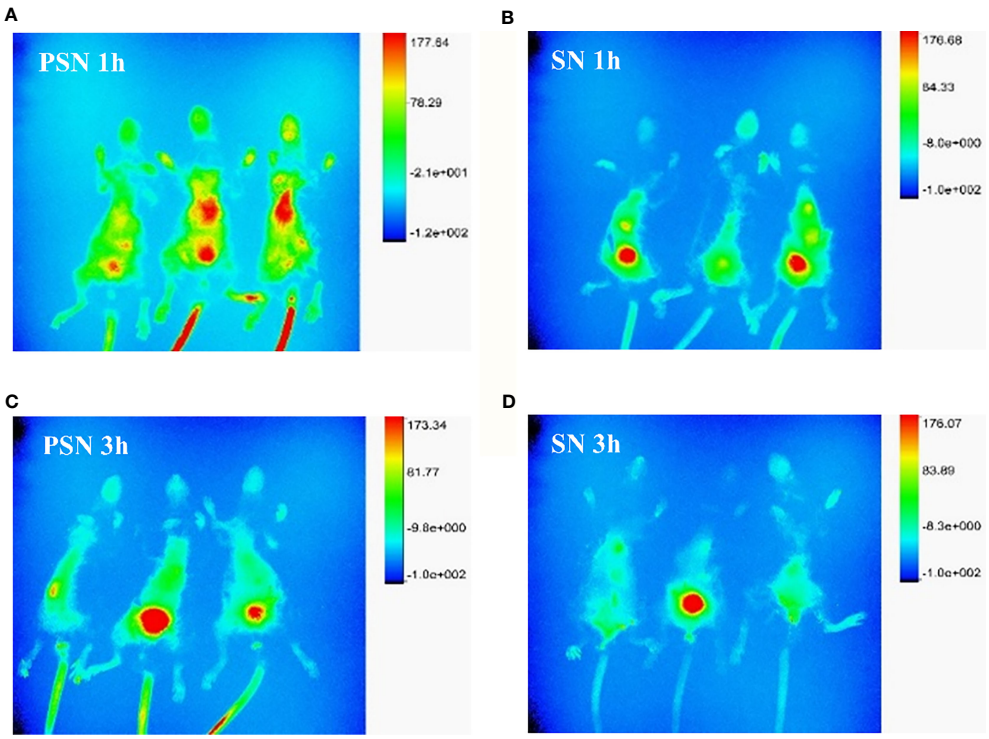

FIGURE 11 | Fluorescence distribution of live and *in vivo* mice tissues. **(A, B)**. Fluorescence distribution of 1 h *in vivo* imaging of mice after PSN-Cy7 and SN-Cy7 injection respectively; **(C, D)**. Fluorescence distribution of 3 h *in vivo* imaging of mice after PSN-Cy7 and SN-Cy7 injection respectively.

experimental results showed that the encapsulated drug played a crucial role in inhibiting HBV, but the encapsulated drug was not limited to just one, which suggested that we could select multiple gene therapeutic drugs and co-package them in liposomal nanoparticles to play a combined role but without interaction, thereby improving the inhibitory effect on HBV and contributing to the cure of acute and chronic hepatitis B. On the other hand, the NTCP receptor discoverer Li (41) further found that the mouse NTCP (mNTCP) was unable to support HBV infection, however, it can bind to pre-S1 of HBV L protein and is functional in transporting substrate taurocholate. When mNTCP residues 84 to 87 were substituted by human counterparts, mNTCP can effectively support viral infections, suggesting that 84–87 aa residues are determinants of NTCP's function as an HBV entry receptor (41). Although the reason why mNTCP does not support HBV infection remains to be further elucidated, mNTCP supports the specific binding of the pre-S1 lipopeptide on the cell surface, despite the binding ability of mNTCP to the pre-S1 region appears to be weaker than that of hNTCP. From this point of view, the *in vivo* targeting experiment in mice we designed is theoretically feasible. HBV binding to mNTCP may be insufficient and additional molecules or mechanisms are required to trigger the following early infection process (42). The fact that the liposome fuses with the cell membrane to deliver the drug into the cell compensates for the above deficiency, so PSN theoretically has the ability to mimic early infection. Importantly, the results in **Figures 8A** and **11A** are consistent with theory, showing that PSN indeed targets and enters mouse hepatocytes to exert inhibitory activity. Admittedly, the AAV-HBV-mouse model is not a natural infection process, whether it can form true cccDNA was still controversial. It is necessary to further study on the inhibitory effect of PSN on HBV through the natural infection model of hepatitis B virus constructed by human hepatocyte chimeric mice. In conclusion, PreS/2-21-directed nanoparticles loaded with HBV gene therapy drugs are expected to be promising for the treatment of CHB.

CONCLUSION

SiRNA nanoparticles guided by PreS/2-21 can target and inhibit the infection and replication of hepatitis B virus, which has been confirmed at the level of animal experiments. Compared with the conventional drugs used in clinical practice, it shows obvious advantages.This study also provides a new idea for the treatment of chronic hepatitis B.

DATA AVAILABILITY STATEMENT

The original contributions presented in the study are included in the article/**Supplementary Material**. Further inquiries can be directed to the corresponding author.

ETHICS STATEMENT

The animal study was reviewed and approved by Ethics Committee of Southern Medical University.

AUTHOR CONTRIBUTIONS

WM and TL conceived and designed the study. ZL, YD, JL, LY, and JW conducted the experiments. JF and HF analyzed the data. LG and JY wrote the paper. All authors reviewed and edited the manuscript. All authors contributed to the article and approved the submitted version.

FUNDING

This work was supported by the Natural Science Foundation of Guangdong Province (grant no. 2021A1515011828 and no. 2022A1515010985).

SUPPLEMENTARY MATERIAL

The Supplementary Material for this article can be found online at: https://www.frontiersin.org/articles/10.3389/fimmu.2022.856463/full#supplementary-material

REFERENCES

1. Collaborators PO. Global Prevalence, Treatment, and Prevention of Hepatitis B Virus Infection in 2016: A Modelling Study. *Lancet Gastroenterol Hepatol* (2018) 3:383–403. doi: 10.1016/S2468-1253(18)30056-6
2. Megahed F, Zhou X. The Interactions Between HBV and the Innate Immunity of Hepatocytes. *Viruses* (2020) 12:285. doi: 10.3390/v12030285
3. Revill PA, Chisari FV, Block JM, Dandri M, Gehring AJ, Guo H, et al. A Global Scientific Strategy to Cure Hepatitis B. *Lancet Gastroenterol Hepatol* (2019) 4:545–58. doi: 10.1016/S2468-1253(19)30119-0
4. Meng Z, Chen Y, Lu M. Advances in Targeting the Innate and Adaptive Immune Systems to Cure Chronic Hepatitis B Virus Infection. *Front Immunol* (2019) 10:3127. doi: 10.3389/fimmu.2019.03127
5. Nanna AR, Kel'in AV, Theile C, Pierson JM, Voo ZX, Garg A, et al. Generation and Validation of Structurally Defined antibody-siRNA Conjugates. *Nucleic Acids Res* (2020) 48:5281–93. doi: 10.1093/nar/gkaa286
6. Qureshi A, Tantray VG, Kirmani AR, Ahangar AG. A Review on Current Status of Antiviral siRNA. *Rev Med Virol* (2018) 28:e1976. doi: 10.1002/rmv.1976
7. Lan T, Wei Z, He Y, Wan S, Liu L, Cheng B, et al. Immunostimulatory siRNA With a Uridine Bulge Leads to Potent Inhibition of HBV and Activation of Innate Immunity. *Virol J* (2021) 18:37. doi: 10.1186/s12985-021-01509-z
8. Manzoor S, Saalim M, Imran M, Resham S, Ashraf J. Hepatitis B Virus Therapy: What's the Future Holding for Us? *World J Gastroenterol* (2015) 21:12558–75. doi: 10.3748/wjg.v21.i44.12558
9. Gane EJ. Future Anti-HBV Strategies. *Liver Int* (2017) 37 Suppl 1:40–4. doi: 10.1111/liv.13304
10. Wang Y, Xie Y, Kilchrist KV, Li J, Duvall CL, Oupicky D. Endosomolytic and Tumor-Penetrating Mesoporous Silica Nanoparticles for siRNA/miRNA Combination Cancer Therapy. *ACS Appl Mater Interfaces* (2020) 12:4308–22. doi: 10.1021/acsami.9b21214
11. Ichihara H, Nagami H, Yamamoto K, Matsumoto Y, Ueoka R. Chemotherapy With Hybrid Liposomes Without Any Drug *In Vivo*. *Yakugaku Zasshi* (2003) 123:25–34. doi: 10.1248/yakushi.123.25
12. Yan H, Zhong G, Xu G, He W, Jing Z, Gao Z, et al. Sodium Taurocholate Cotransporting Polypeptide is a Functional Receptor for Human Hepatitis B and D Virus. *Elife* (2012) 1:e00049. doi: 10.7554/eLife.00049
13. Li J, Tong S. From DCPD to NTCP: The Long Journey Towards Identifying a Functional Hepatitis B Virus Receptor. *Clin Mol Hepatol* (2015) 21:193–9. doi: 10.3350/cmh.2015.21.3.193
14. Han C, Liu HL, Li J, Lan Z, Wu YZ, Han JF. The Research of Nano-Liposome Targeting Hepatocyte Mediated by Pre S1 Peptide (2-21Aa). *Immunol J* (2014) 30:240–5. doi: 10.13431/j.cnki.immunol.j.20140052
15. Peng B, Xu GD, Wei WJ, Nong SQ, Chen XH, Xiao SR, et al. Antiviral Effect Of Antigene Olocked Nucleic Acid of HBV Pres1, Pres2 Coding Chain on HepG 2.2.15 Cells. *Lab Med Clin* (2020) 17:3106–9. doi: 10.3969/j.issn.1672-9455.2020.21.009
16. Bhat P, Snooks MJ, Anderson DA. Hepatocytes Traffic and Export Hepatitis B Virus Basolaterally by Polarity-Dependent Mechanisms. *J Virol* (2011) 85:12474–81. doi: 10.1128/JVI.05344-11
17. Klein C, Bock CT, Wedemeyer H, Wüstefeld T, Locarnini S, Dienes HP, et al. Inhibition of Hepatitis B Virus Replication *In Vivo* by Nucleoside Analogues and siRNA. *Gastroenterology* (2003) 125:9–18. doi: 10.1016/S0016-5085(03)00720-0
18. Wen WH, Liu JY, Qin WJ, Zhao J, Wang T, Jia LT, et al. Targeted Inhibition of HBV Gene Expression by Single-Chain Antibody Mediated Small Interfering RNA Delivery. *Hepatology* (2007) 46:84–94. doi: 10.1002/hep.21663
19. Han Q, Zhang C, Zhang J, Tian Z. Reversal of Hepatitis B Virus-Induced Immune Tolerance by an Immunostimulatory 3p-HBx-siRNAs in a Retinoic Acid Inducible Gene I-Dependent Manner. *Hepatology* (2011) 54:1179–89. doi: 10.1002/hep.24505
20. Soriano V, Barreiro P, Benitez L, Peña JM, De Mendoza C. New Antivirals for the Treatment of Chronic Hepatitis B. *Expert Opin Investig Drugs* (2017) 26:843–51. doi: 10.1080/13543784.2017.1333105
21. Wang J, Chen J, Liu Y, Zeng X, Wei M, Wu S, et al. Hepatitis B Virus Induces Autophagy to Promote its Replication by the Axis of miR-192-3p-XIAP Through NF Kappa B Signaling. *Hepatol (Baltimore Md)* (2019) 69:974–92. doi: 10.1002/hep.30248
22. Jiang C, Mei M, Li B, Zhu X, Zu W, Tian Y, et al. A non-Viral CRISPR/Cas9 Delivery System for Therapeutically Targeting HBV DNA and Pcsk9 *In Vivo*. *Cell Res* (2017) 27:440–3. doi: 10.1038/cr.2017.16
23. Richner JM, Himansu S, Dowd KA, Butler SL, Salazar V, Fox JM, et al. Modified mRNA Vaccines Protect Against Zika Virus Infection. *Cell* (2017) 168:1114–25.e10. doi: 10.1016/j.cell.2017.02.017
24. Hamada-Tsutsumi S, Naito Y, Sato S, Takaoka A, Kawashima K, Isogawa M, et al. The Antiviral Effects of Human microRNA miR-302c-3p Against Hepatitis B Virus Infection. *Aliment Pharmacol Ther* (2019) 49:1060–70. doi: 10.1111/apt.15197
25. Shin D, Kim SI, Kim M, Park M. Efficient Inhibition of Hepatitis B Virus Replication by Small Interfering RNAs Targeted to the Viral X Gene in Mice. *Virus Res* (2006) 119:146–53. doi: 10.1016/j.virusres.2005.12.012
26. Gish RG, Given BD, Lai CL, Locarnini SA, Lau JY, Lewis DL, et al. Chronic Hepatitis B: Virology, Natural History, Current Management and a Glimpse at Future Opportunities. *Antiviral Res* (2015) 121:47–58. doi: 10.1016/j.antiviral.2015.06.008
27. Slagle BL, Bouchard MJ. Role of HBx in Hepatitis B Virus Persistence and its Therapeutic Implications. *Curr Opin Virol* (2018) 30:32–8. doi: 10.1016/j.coviro.2018.01.007
28. Kornyeyev D, Ramakrishnan D, Voitenleitner C, Livingston CM, Xing W, Hung M, et al. Spatiotemporal Analysis of Hepatitis B Virus X Protein in Primary Human Hepatocytes. *J Virol* (2019) 93:e00248–19. doi: 10.1128/JVI.00248-19
29. Yao J, Yu W, Chang Y, Ren J, Xu D, Han S, et al. Targeted Screening of SiRNA Directed HBV Polymerase Gene for Effective Inhibition of HBV Expression. *J Huazhong Univ Sci Technol Med Sci* (2008) 28:266–71. doi: 10.1007/s11596-008-0308-1
30. Bian ZQ, Liu S, Liu MQ, Xiao A, Jiao Y, Yan WY, et al. PreC/C Gene-Targeting RNA Interference Suppresses Hepatitis B Virus Replication and Expression in Human Hepatoma Cells. *Zhonghua Yi Xue Za Zhi* (2012) 92:768–72. doi: 10.3760/cma.j.issn.0376-2491.2012.11.013

31. Huang W, Li X, Yi M, Zhu S, Chen W. Targeted Delivery of siRNA Against Hepatitis B Virus by Pres1 Peptide Molecular Ligand. *Hepatol Res* (2014) 44:897–906. doi: 10.1111/hepr.12189
32. Han Q, Hou Z, Yin C, Zhang C, Zhang J. 5′-Triphosphate siRNA Targeting HBx Elicits a Potent Anti-HBV Immune Response in pAAV-HBV Transfected Mice. *Antiviral Res* (2019) 161:36–45. doi: 10.1016/j.antiviral.2018.11.006
33. Saw PE, Song EW. siRNA Therapeutics: A Clinical Reality. *Sci China Life Sci* (2020) 63:485–500. doi: 10.1007/s11427-018-9438-y
34. Blanco MJ, Gardinier KM. New Chemical Modalities and Strategic Thinking in Early Drug Discovery. *ACS Med Chem Lett* (2020) 11:228–31. doi: 10.1021/acsmedchemlett.9b00582
35. Al Shaer D, Al Musaimi O, Albericio F, de la Torre BG. 2018 FDA Tides Harvest. *Pharmaceut (Basel)* (2019) 12:52. doi: 10.3390/ph12020052
36. Sardh E, Harper P, Balwani M, Stein P, Rees D, Bissell DM, et al. Phase 1 Trial of an RNA Interference Therapy for Acute Intermittent Porphyria. *N Engl J Med* (2019) 380:549–58. doi: 10.1056/NEJMoa1807838
37. Schulze A, Schieck A, Ni Y, Mier W, Urban S. Fine Mapping of Pre-S Sequence Requirements for Hepatitis B Virus Large Envelope Protein-Mediated Receptor Interaction. *J Virol* (2010) 84:1989–2000. doi: 10.1128/JVI.01902-09
38. Fu LL, Liu J, Chen Y, Wang FT, Wen X, Liu HQ, et al. In Silico Analysis and Experimental Validation of Azelastine Hydrochloride (N4) Targeting Sodium Taurocholate Co-Transporting Polypeptide (NTCP) in HBV Therapy. *Cell Prolif* (2014) 47:326–35. doi: 10.1111/cpr.12117
39. Spyrou E, Smith CI, Ghany MG. Hepatitis B: Current Status of Therapy and Future Therapies. *Gastroenterol Clinics North America* (2020) 49:215–38. doi: 10.1016/j.gtc.2020.01.003
40. Rybicka M, Bielawski KP. Recent Advances in Understanding, Diagnosing, and Treating Hepatitis B Virus Infection. *Microorganisms* (2020) 8:1416. doi: 10.3390/microorganisms8091416
41. Yan H, Peng B, He W, Zhong G, Qi Y, Ren B, et al. Molecular Determinants of Hepatitis B and D Virus Entry Restriction in Mouse Sodium Taurocholate Cotransporting Polypeptide. *J Virol* (2013) 87:7977–91. doi: 10.1128/JVI.03540-12
42. Watashi K, Urban S, Li W, Wakita T. NTCP and Beyond: Opening the Door to Unveil Hepatitis B Virus Entry. *Int J Mol Sci* (2014) 15:2892–905. doi: 10.3390/ijms15022892

Conflict of Interest: The authors declare that the research was conducted in the absence of any commercial or financial relationships that could be construed as a potential conflict of interest.

Publisher's Note: All claims expressed in this article are solely those of the authors and do not necessarily represent those of their affiliated organizations, or those of the publisher, the editors and the reviewers. Any product that may be evaluated in this article, or claim that may be made by its manufacturer, is not guaranteed or endorsed by the publisher.

frontiers | Frontiers in Immunology

ORIGINAL RESEARCH
published: 10 May 2022
doi: 10.3389/fimmu.2022.897835

Autophagy-Related Genes Are Involved in the Progression and Prognosis of Asthma and Regulate the Immune Microenvironment

Fan Yang[1,2†], Jingwei Kong[1,2†], Yuhan Zong[1,2†], Zhuqing Li[1,2], Mingsheng Lyu[3,4], Wanyang Li[5], Wenle Li[1,2], Haoyue Zhu[6], Shunqi Chen[1,2], Xiaoshan Zhao[7†] and Ji Wang[2*†]*

[1] College of Traditional Chinese Medicine, Beijing University of Chinese Medicine, Beijing, China, [2] National Institute of Traditional Chinese Medicine (TCM) Constitution and Preventive Medicine, Beijing University of Chinese Medicine, Beijing, China, [3] Center of Respiratory, Beijing University of Chinese Medicine Affiliated Dongzhimen Hospital, Beijing, China, [4] Department of Respiratory, The Third Affiliated Hospital, Beijing University of Chinese Medicine, Beijing, China, [5] Department of Clinical Nutrition, Chinese Academy of Medical Sciences - Peking Union Medical College, Peking Union Medical College Hospital, Beijing, China, [6] Beijing Hospital of Traditional Chinese Medicine (TCM), Capital Medical University, Beijing, China, [7] School of Chinese Medicine, Southern Medical University, Guangzhou, China

OPEN ACCESS

Edited by:
Chunqing Guo, Virginia Commonwealth University, United States

Reviewed by:
Bin Liu, Guangzhou Medical University, China
Li Rong Meng, Macau Polytechnic University, Macao SAR, China

***Correspondence:**
Ji Wang
doctorwang2009@126.com
Xiaoshan Zhao
zhaoxs0609@163.com

[†]These authors have contributed equally to this work

Specialty section:
This article was submitted to Molecular Innate Immunity, a section of the journal Frontiers in Immunology

Received: *16 March 2022*
Accepted: *14 April 2022*
Published: *10 May 2022*

Citation:
Yang F, Kong J, Zong Y, Li Z, Lyu M, Li W, Li W, Zhu H, Chen S, Zhao X and Wang J (2022) Autophagy-Related Genes Are Involved in the Progression and Prognosis of Asthma and Regulate the Immune Microenvironment. Front. Immunol. 13:897835. doi: 10.3389/fimmu.2022.897835

Background: Autophagy has been proven to play an important role in the pathogenesis of asthma and the regulation of the airway epithelial immune microenvironment. However, a systematic analysis of the clinical importance of autophagy-related genes (ARGs) regulating the immune microenvironment in patients with asthma remains lacking.

Methods: Clustering based on the k-means unsupervised clustering method was performed to identify autophagy-related subtypes in asthma. ARG-related diagnostic markers in low-autophagy subtypes were screened, the infiltration of immune cells in the airway epithelium was evaluated by the CIBERSORT, and the correlation between diagnostic markers and infiltrating immune cells was analyzed. On the basis of the expression of ARGs and combined with asthma control, a risk prediction model was established and verified by experiments.

Results: A total of 66 differentially expressed ARGs and 2 subtypes were identified between mild to moderate and severe asthma. Significant differences were observed in asthma control and FEV1 reversibility between the two subtypes, and the low-autophagy subtype was closely associated with severe asthma, energy metabolism, and hormone metabolism. The autophagy gene *SERPINB10* was identified as a diagnostic marker and was related to the infiltration of immune cells, such as activated mast cells and neutrophils. Combined with asthma control, a risk prediction model was constructed, the expression of five risk genes was supported by animal experiments, was established for ARGs related to the prediction model.

Conclusion: Autophagy plays a crucial role in the diversity and complexity of the asthma immune microenvironment and has clinical value in treatment response and prognosis.

Keywords: autophagy-related genes, asthma, immune cell, prognosis, diagnostic model

INTRODUCTION

Asthma is a chronic airway inflammatory disease involving a variety of cells and cellular components. At least 300 million patients have asthma worldwide, and the incidence is increasing yearly (1). Current studies showed that the Th1/Th2-mediated immune imbalance is the main mechanism of asthmatic airway inflammatory response (2), and a variety of immune cells are involved in the course of asthma. In addition, the Global Initiative for Asthma (2021) updated the definition of severe asthma. This group accounts for about 10% of the total number of patients but accounts for 60% of the expenditure on asthma medicine (3–5). Therefore, effective assessment tools are urgently needed for the early identification and management of this population to prevent the transition from mild to moderate asthma to severe asthma and develop drugs for severe, uncontrolled asthma (6).

Autophagy, also known as cell self-digestion, is a process in which the body relies on lysosomes to degrade excessive proteins and aging and damaged organelles for the recycling of body substances and maintenance of the balance of cell metabolism and homeostasis. A growing number of studies showed a close relationship between autophagy and asthma (7). For example, autophagy is a cellular mechanism of TGFβ1-dependent airway remodeling and loss of lung function in patients with asthma, and the single nucleotide polymorphism rs12212740 of autophagy-related gene 5 (ATG5) is significantly associated with lung function and airway remodeling in patients with asthma (8). In addition, in asthma, the regulation of immune cells by autophagy is extensive (9). Clinical studies showed that the autophagy marker LC3-II is highly expressed in neutrophils, T lymphocytes in sputum and neutrophils, and eosinophils and monocytes in the peripheral blood of patients with asthma, and the expression levels of autophagy pathway-related proteins Beclin-1, LC3B, and ATG5 are significantly increased in lung eosinophils compared with the control group (10–12). The dendritic cell-specific knockout of ATG5 can reduce the expression of cytokines (e.g., IL-6, TNF, and IL-1β) and aggravate the pulmonary inflammatory response in bronchial asthma mouse models (13). Although current studies preliminarily reported the role of autophagy and its related genes in the occurrence and development of asthma, most studies focused on specific ARGs and did not comprehensively analyze ARGs in combination with the clinical prognosis and immune imbalance of asthma. In order to clarify the relationship among autophagy, immune cells and asthma, and how these biological processes affect the progression and prognosis of asthma, in this study, based on a group of transcriptome data sets of airway epithelium of patients with asthma, we conducted a comprehensive analysis of ARGs to explore the diagnostic and prognostic value of ARGs in patients with asthma, and the accuracy of the diagnostic model was further verified by an asthma animal model.

MATERIALS AND METHODS

Data Source

We downloaded the asthma microarray data set GSE89809, including airway epithelial samples from 27 patients with mild to moderate asthma and 11 patients with severe asthma (14), from the GEO (https://www.ncbi.nlm.nih.gov/geo/) database from GPL13158 (Affymetrix HT HG-U133+ PM Array Plate). Raw data were background corrected and normalized by the RMA algorithm. Differentially expressed genes (DEGs) were screened using the "*limma*" software package (15), and $P < 0.05$ and $|\log2FC| > 0.585$ were considered to indicate significant differences. ARGs were extracted from the Human Autophagy Database (http://www.autophagy.lu/index.html) and the GO_AUTOPHAGY gene set in the Gene Set Enrichment Analysis (GSEA) website (http://software.broadinstitute.org/gsea/index.jsp). In accordance with Ref., these two gene sets were merged into one ARG set (16).

Classification and Functional Enrichment Analysis of ARG-Related Subtypes in Asthma

The unsupervised cluster analysis was performed to identify different subtypes on the basis of the differences in ARG expression in asthma (17, 18). A consensus clustering algorithm was used to evaluate cluster numbers and robustness. The R package "*ConsensuClusterPlus*" implemented the above steps for 1000 iterations to guarantee the robustness of classification (19). The protein–protein interaction (PPI) network was obtained from the STRING database (https://string-db.org/), and the MCODE was performed using the Metascape (http://metascape.org/gp/index.html#/main/step1) platform. We used the "*clusterProfiler*" and "*ggplot2*" packages to perform Gene Ontology (GO) and Kyoto Encyclopedia of Genes and Genomes (KEGG) enrichment analyses, respectively, on DEGs (20, 21). GSEA was performed on the gene expression matrix through the "*clusterProfiler*" package, and the "*c2.cp.kegg.v7.0.symbols.gmt*" was selected as the reference gene set. Genes associated with specific subtypes were identified by the weighted gene co-expression network analysis (WGCNA) by using the R package "*WGCNA*" (22). The topological overlap matrix (TOM) and the corresponding dissimilarity (1 – TOM) were transformed from the adjacency matrix. A hierarchical clustering dendrogram was further built, and similar gene expressions were divided into different modules. Finally, the expression profiles of each module were summarized by the module eigengene (ME), and the correlation between the ME and clinical features was determined.

Relationship Between the Screening and Validation of ARG-Related Diagnostic Markers and Immune Cell Infiltration

We used the least absolute shrinkage and selection operator (LASSO) logistic regression and the support vector machine–recursive feature elimination (SVM-RFE) to perform feature selection and screen diagnostic markers for asthma (23, 24). The LASSO algorithm was applied with the "*glmnet*" package (25). The SVM module was established to further identify the diagnostic value of these biomarkers in asthma by the "*e1071*" package (26). Subsequently, the degree of immune cell infiltration in the airway epithelium was assessed. The CIBERSORT algorithm is an excellent tool used to calculate the abundance of specific cells in the mixture matrix (27). The "*Corrplot*" software package was further used to draw relevant heatmaps and show the correlation

of 22 types of infiltrating immune cells (28), and the differences in infiltrating immune cells between groups were illustrated by the "*ggplot2*" package violin plot. Finally, the Spearman correlation analysis of diagnostic markers and infiltrating immune cells was performed using the "*ggstatsplot*" package, and results were visualized using the "*ggplot2*" package (29).

Construction of a Risk Signature Associated With Asthma Control

Univariate Cox regression models were used to select genes associated with asthma control. $P < 0.05$ was considered statistically significant. The LASSO regression was used to screen out the optimal gene combination and construct the risk characteristics, and the regression coefficient was linearly combined with the gene expression level to establish the risk characteristics. The risk score was calculated as follows: Risk score = (exprgene1 × Coefgene1) + (exprgene2 × Coefgene2) + … + (exprgene*n* × Coefgene*n*) (30). Patients with asthma were divided into low- and high-risk groups in accordance with the median risk score. The Kruskal test was used to compare the infiltrating immune cell abundance score and immune response score in the two risk models.

Gene Expression Regulation of Prognostic Genes, Autophagy-Related Diagnostic Markers, and Predictive Models

The transcriptional regulatory networks of prognosis-related genes were predicted from the ChEA3 database (https://maayanlab.cloud/chea3/). The database integrated ENCODE; ReMap; some independently published CHIP-seq data; and transcription factor co-expression data from GTEx, TCGA, and ARCHS4 RNA-seq data (31). The target miRNA was first predicted using the starBase (http://starbase.sysu.edu.cn/) database to predict the regulation of target genes by noncoding RNAs, and prediction results included the analysis of RNA22, miRanda, and TargetScan (32). Then, the target lncRNA of miRNA was predicted using the miRNet2.0 database (www.mirnet.ca/miRNet/home.xhtml) and starBase. Finally, the ceRNA network was established (33, 34).

Identification of Small Molecular Therapeutic Agents

The Broad Institutes Connectivity Map (cMAP) database (https://portals.broadinstitute.org/cmap) was used for the identification of small candidate molecules related to asthma (35). For the identification of small candidate chemical molecules, DEGs (log2FC > 0.585) were introduced into the cMAP database for GSEA. The PubChem (https://pubchem.ncbi.nml.gov) was used for the extraction of detailed information and 3D confirmation of the established small molecules. Then, molecular docking experiments were carried out, and the crystal structures of key targets were retrieved from the human (Human) database in the PDB (https://www.rcsb.org/) database. AutoDockTool software was used to dewater and hydrogenate the receptor protein, and Discovery Studio 4.5.0 software was used to perform molecular docking between small drug molecules and target proteins. A negative value indicates free binding. In this study, binding energy value less than − 5 kcal/mol (20.9 kj/mol) was set as significant binding.

Animal Experiment

BALB/c mice (female, 17–20 g, 6–8 weeks old) were obtained from Beijing Vital River Laboratory Animal Technology Co., Ltd in China. All animal studies were conducted in accordance with the institutional animal care regulations of Beijing University of Chinese Medicine and were conducted in accordance with AAALAC and IACUC guidelines. Keeping mice in specific pathogen-free conditions in Beijing University of Chinese Medicine. All mice were kept at a controlled room (25 ± 1°C, 45–60% humidity). The allergic asthma model of mice was established by OVA sensitization and atomization inhalation stimulation. Briefly, mice were intraperitoneally injected with 2 mg of OVA (Sigma-Aldrich, Cat#A5503) mixed with 2 mg Imject™Alum Adjuvant (Invitrogen, Cat#77161) and PBS on day 0 and day 14. The challenge phase was from the 21st day to the 25th day after injection, and the mice were atomized with 1% OVA for 30 minutes. Then, the animals were killed, and part of the lung tissue was taken and placed in 4% paraformaldehyde fixed solution for the preparation of histopathological sections. The remaining lung tissues were washed with PBS and stored in -80°C refrigerator for reverse transcription quantitative real-time polymerase chain reaction (RT - qPCR).

Immunohistochemical Analysis

Rabbit anti-PTK6 polyclonal antibody (abs117941), rabbit anti-MAP2K7 polyclonal antibody (abs136429) and rabbit anti-CD46 polyclonal antibody (abs136051) were purchased from Aibixin Biotechnology Co., Ltd. (Shanghai, China). Horseradish peroxidase-labeled goat anti-rabbit IgG antibodies (GB23303) were purchased from Wuhan Servicebio Technology Co., Ltd. After being dewaxed, the lung slices were subjected to antigen recovery with citrate buffer under microwave heating. The slices were cooled down to room temperature and then sealed with 3% bovine serum albumin (BSA) for 30min and were incubated overnight with primary antibody at 4°C. The primary antibodies used were rabbit anti-PTK6 antibody (diluted 1:200), rabbit anti-MAP2K7 antibody (diluted 1:200), and rabbit anti-CD46 antibody (diluted 1:200). The slices were then washed with PBS and incubated with goat anti-rabbit secondary antibody (diluted 1:200) at 37°C for 50 min. After being rinsed with PBS, the slices were visualized with diaminobenzidine and counterstained with hematoxylin.

Quantitative Real-Time Polymerase Chain Reaction

mRNA was extracted from the lung tissue using a universal RT-PCR Kit (Solarbio Science & Technology Co., Ltd., Shanghai, China) following the manufacturer's instructions. Samples were treated with DNase and then purified using an RNeasy kit (Qiagen, Hilden, Germany). Glyceraldehyde-3-phosphate dehydrogenase (GAPDH) was used as internal reference. PCR primer sequences included the following: ACBD5: forward primer: 5'-TCGC AGGCGAAATTATCTTTG-3'; reverse primer: 5'-GTGCC AACCACTGAGCAATAA-3', S100A9: forward primer: 5'-

CATAAATGACATCATGGAGGACC-3'; reverse primer: 5'-TTGCCATCAGCATCATACACTC-3', CD46: forward primer: 5'-TGGAAGGCAGTAGCATGGTGAT-3'; reverse primer: 5'-GAGGCTTGGTAGGATGAGTAGGC-3', MAP2K7: forward primer: 5'-CAATGACTTGGAGAACTTGGGTG-3'; reverse primer: 5'-CGCCGCATTTGCTTAACAG-3', PTK6: forward primer: 5'-CTGCGTGACTCTGATGAGAAAGC-3'; reverse primer: 5'-AGGTCACGGTGGATGTAATTCTG-3', GAPDH: forward primer: 5'-CCTCGTCCCGTAGACAAAATG-3'; reverse primer: 5'-TGAGGTCAATGAAGGGGTCGT-3'.

Statistical Analysis

Data were shown as mean ± standard deviation (SD). The differences between the two groups were evaluated by independent sample t-test and nonparametric test. A $P < 0.05$ was considered statistically significant. Statistical analyses and figures were obtained using IBM SPSS Statistics 23.0 (IBM SPSS Software, NY, USA) and GraphPad Prism Version 8.0 (GraphPad Software, San Diego, CA, USA).

RESULTS

Landscape of ARGs Between Mild to Moderate and Severe Asthma Samples

The study involved 531 ARGs. A total of 66 differentially expressed ARGs were observed in mild to moderate and severe asthma. Among these ARGs, SERPINB10 and ATG9B had the highest degree of difference ($P < 0.001$, **Figure 1A**). These ARGs had a PPI network (**Figure S1A**), and the MCODE analysis showed that this network had a key module (**Figure S1B**). Co-expression relationships were explored for 21 differentially expressed ARGs at $P < 0.01$, and a close correlation between genes was found (**Figure 1B**). These findings suggested that ARGs were involved in the disease process of asthma and might be related to the evolution of clinical symptoms or course of disease.

Differentially Expressed ARGs Between Mild to Moderate and Severe Asthma Divided Asthma Into Two Subtypes

To investigate the role of ARGs in asthma, we performed the unsupervised consensus cluster analysis on asthma samples based on the expression of 66 ARGs in combination with clinical data (**Figures 1C** and **2A, B**). Differences in the expression of 14 ARGs were observed in the two different asthma subtypes (C1 and C2), and the expression of ARGs was downregulated in C1-subtype samples, which were the low-autophagy subtype. The analysis of relevant clinical features showed a significant difference in the use of ICS between patients with C1 and C2 subtypes ($P < 0.05$). The C1 subtype was higher than the C2 subtype, suggesting the presence of glucocorticoid resistance, and patients with the C1 subtype had more severe symptoms than patients with the C2 subtype (**Figure 2C**). Other key clinical indicators also supported this result. The asthma control questionnaire (ACQ) is the most widely used standardized questionnaire for asthma control and can evaluate the control degree of patients stably and effectively (36–38). The FEV1 reversibility is a marker of airway hyperresponsiveness (AHR) and has traditionally been considered positively correlated with the severity of asthma (39, 40). A combined analysis of two key indicators, i.e., ACQ control and FEV1 reversibility, found that patients with the C1 subtype had higher FEV1 reversibility and more severe poor asthma control than those with the C2 subtype (**Figure 2D**). Even at the same level of FEV1 reversibility, patients with the C1 subtype had lower asthma control than those with the C2 subtype ($P = 0.011$). These results suggested that ARGs were involved in the disease exacerbation process of asthma, associated with clinical outcomes, and had a good classification function.

Biological Characteristics of the C1 Subtype

To explore the biological characteristics of the C1 subtype, we performed GO analysis on the DEGs of C1 subtype. Results showed that the generation of precursor metabolites and energy, hormone metabolic process, and cilium assembly were the main biological processes; ribosomes and mitochondria were the key cell components; and oxidoreductase activity was the main molecular function (**Figure S1C**). The KEGG analysis revealed that neurodegeneration, amino acid metabolism, and energy metabolism were core pathways in this group (**Figure 2E**). GSEA showed the difference of main signal pathways between C1 and C2 subtypes (**Figures 2F, G**), in which the C1 subtype was predominantly enriched in complement and coagulation cascades, hematopoietic cell lineage, and other pathways. We further constructed the WGCNA network and explored biomarkers in C1-subtype samples on the basis of clinical features. Gene modules were detected on the basis of the TOM, and 28 modules were detected (**Figures 3A, B**). Further analysis of the relationship between modules and clinical features showed that MEdarkslateblue modules had the highest correlation with asthma control (COR = 0.58, $P = 0.02$). Therefore, the MEdarkslateblue module was selected for subsequent analysis. GO analysis showed that the characteristic genes in the module were involved in the Wnt signaling pathway, positive regulation of nitric oxide biosynthetic process, and extracellular matrix organization, which were closely related to AHR and airway remodeling in asthma (**Figure 3C**) (41). Genes within the same cluster often shared common transcription factors, and we predicted and analyzed the transcription factors of genes in the MEdarkslateblue module and visualized the mutual regulatory relationships between the top 10 transcription factors in Mean Rank (**Figure 3D**). The association of these transcription factors with asthma was demonstrated. For example, histone deacetylase 4 can mediate KLF5 deacetylation to upregulate CXCL12, leading to airway remodeling and promoting the progression of asthma (42).

Correlation of Differentially Expressed ARGs Between Subtypes and Immune Cells

Based on the DEGs between C1 and C2 subtypes, we identified 12 genes as diagnostic markers for asthma by using the LASSO logistic regression algorithm (**Figure 4A**). Two genes were identified as diagnostic markers for asthma by using the SVM-

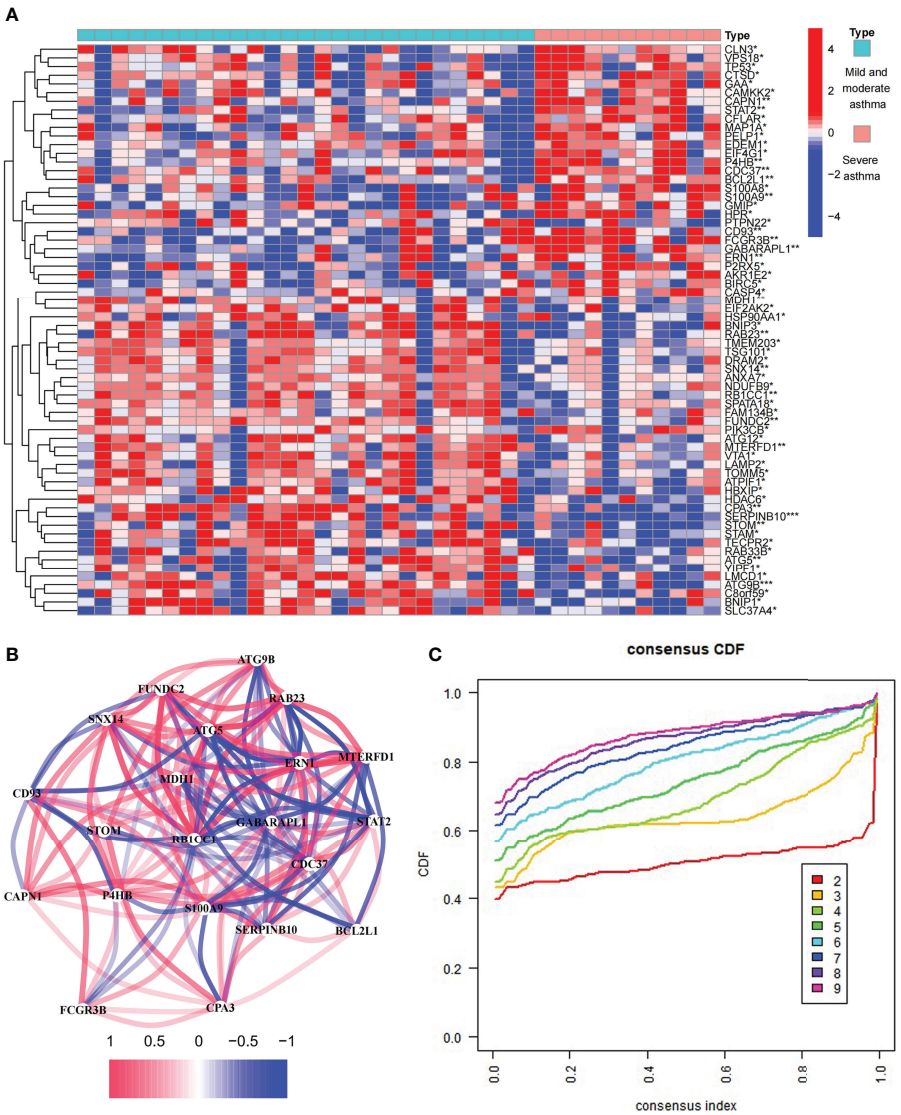

FIGURE 1 | Expression of autophagy-related genes (ARGs) in asthma. **(A)** 66 differentially expressed ARGs between mild to moderate and severe asthma. *P < 0.05, **P < 0.01, ***P < 0.001. **(B)** Co-expression network of 22 ARGs. **(C)** Consensus clustering cumulative distribution function (CDF) for k = 2–9.

RFE algorithm (**Figure 4B**). The genetic markers obtained by the two algorithms overlapped to obtain SERPINB10 as the diagnostic gene. The expression of SERPINB10, an ARG, in the C1 subtype was significantly lower than that in the C2 subtype (P < 0.01, **Figure 4C**). To assess the immune landscapes of C1 and C2 subtypes, we quantified the level of immune cell infiltration, and the ratios and differences of 22 types of immune cell infiltration between the two subtypes were presented as heatmaps and histograms (**Figures 4D** and **S1D**). The violin diagram of differences in immune cell infiltration showed that compared with the C2 subtype, the C1 subtype had less $CD8^+$ T cell, resting dendritic cell, and resting mast cell infiltrations and more activated mast cell and neutrophil infiltrations ($P \leq 0.05$, **Figure 4E**). A strong correlation was also observed between several types of immune cells closely associated with asthma. $CD8^+$ T cells was significantly negatively correlated with activated mast cells and M0 macrophages, whereas activated mast cells were significantly positively correlated with eosinophils and M2 macrophages (**Figure 5A**). The correlation analysis between SERPINB10 and immune cells showed that SERPINB10 was positively correlated with $CD8^+$ T cells (R = 0.34, P = 0.036), T follicular helper cells (R = 0.35, P = 0.03), resting dendritic cells (R = 0.5, P = 0.0013), resting mast cells (R = 0.53, P = 7e−0) and negatively correlated with activated mast cells (R = −0.36, P = 0.028) and neutrophils (R = −0.46, P = 0.0035; **Figure 5B**). Finally, to explore the gene expression regulatory network of SERPINB10, a key ARG, we explored the ceRNA mechanism of SERPINB10 and constructed a

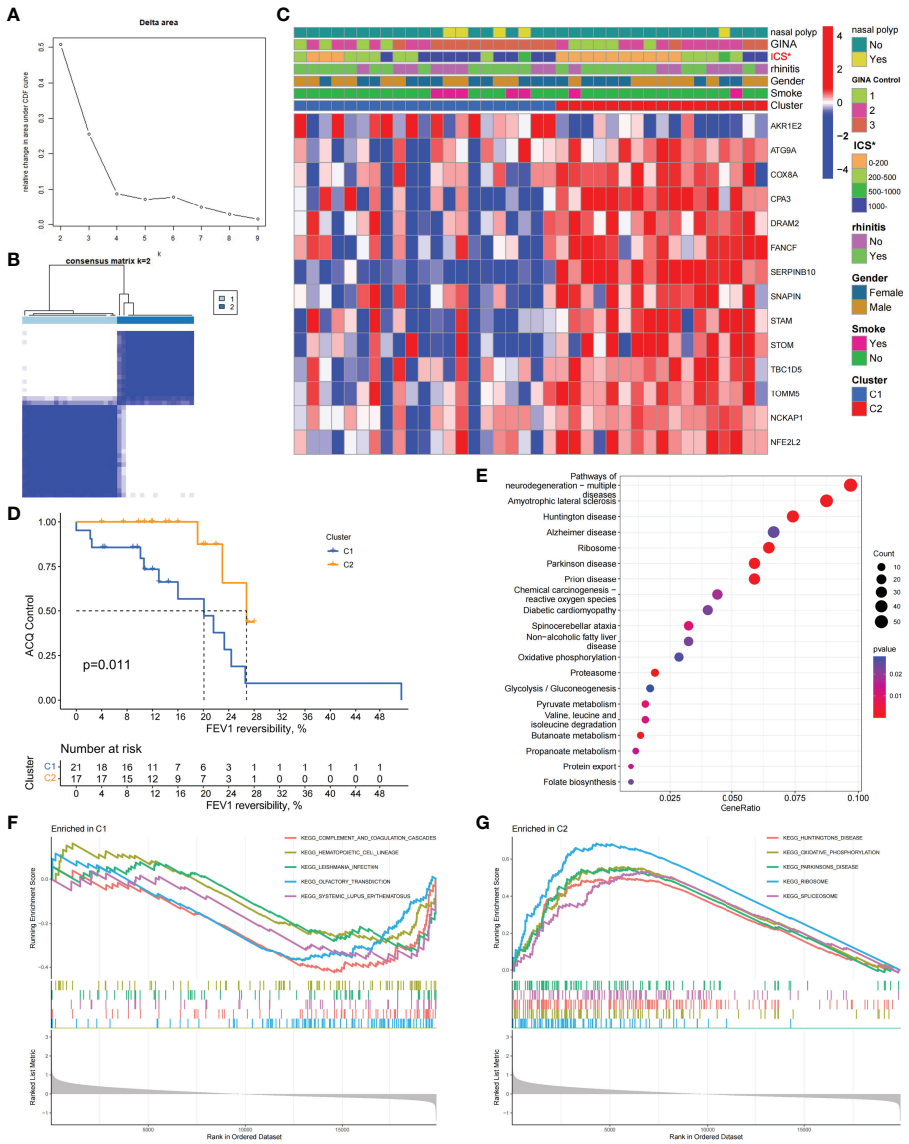

FIGURE 2 | Two different autophagy-related subtypes identified in asthma by unsupervised clustering of 66 ARGs. **(A)** Relative change in area under CDF curve for k = 2–9. **(B)** Heatmap of the matrix of co-occurrence proportions for asthma samples. **(C)** Composite heatmap showing the relationship between the expression characteristics of 14 ARGs and the incidence of nasal polyps, GINA control, ICS dosage, prevalence of allergic rhinitis, gender, and smoking. *$P < 0.05$. **(D)** Kaplan–Meier curves of different gene subtypes ACQ Control and FEV1 reversibility. **(E)** KEGG analysis revealing the key signal pathway of C1 subtype. **(F, G)** GSEA of C1 and C2 subtypes.

ceRNA network including 38 lncRNAs and 2 miRNAs (**Figure 5C**). The ERPINB10 gene is regulated by miR-876-5p and miR-2681-3p, and the downregulation of miR-876-5p and miR-2681-3p may lead to the upregulation of SERPINB10 gene in asthma.

Prognostic Model Classification, Immunological Characteristics, and Drug Prediction Based on Asthma Control

We analyzed ARGs and clinical data and found 61 ARGs associated with asthma control (**Figure 6A**). The LASSO Cox regression analysis was performed on ARGs, and a prediction model consisting of five ARGs (i.e., ACBD5, S100A9, CD46, MAP2K7, and PTK6) was further obtained (**Figure 6B**). The risk score for each patient was calculated as follows: Risk score = (−0.539 × ACBD5 expression level) + (0.016 × S100A9 expression level) + (−0.152 × CD46 expression level) + (0.934 × MAP2K7 expression level) + (0.182 × PTK6 expression level). Patients were divided into high- and low-risk groups on the basis of the median cutoff score. PCA based on genomic expression data showed significant distribution differences between the two groups (**Figure S1E**). We found that with increased FEV1 reversibility,

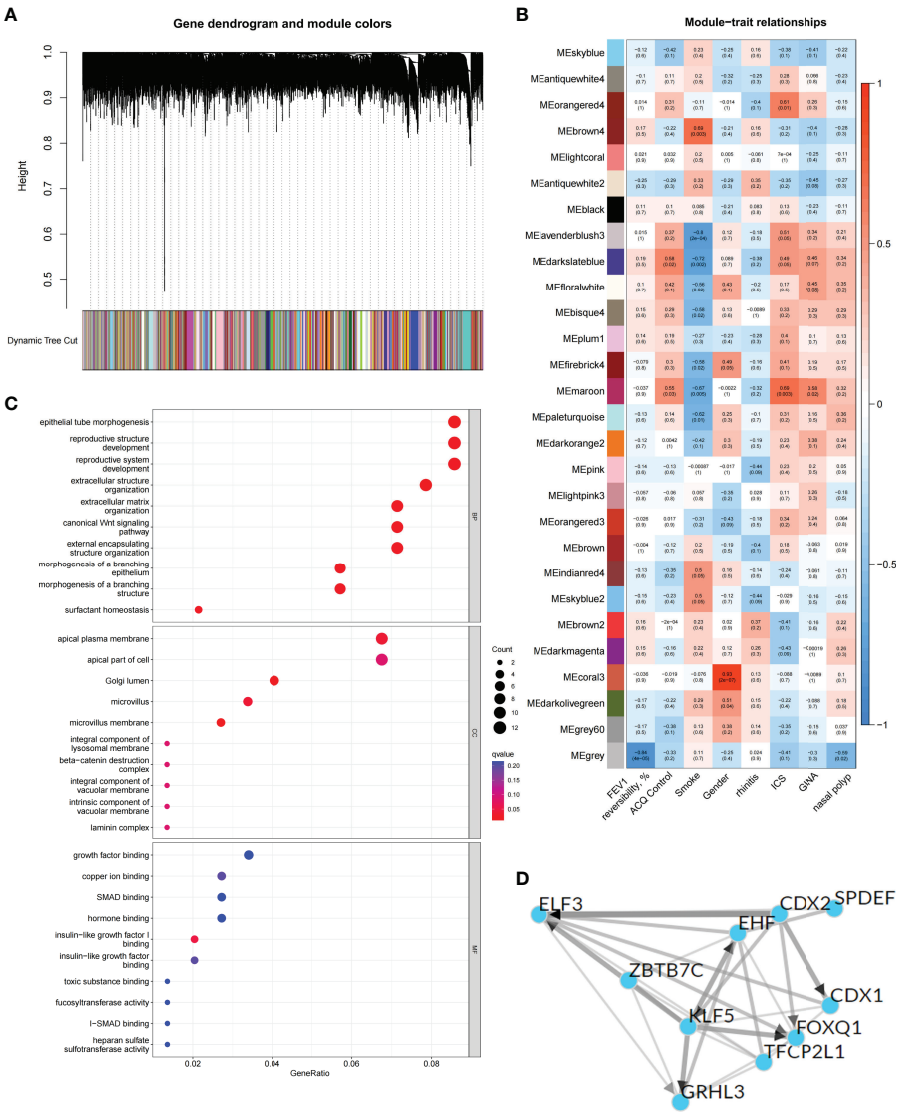

FIGURE 3 | Identification and functional analysis of C1 subtype phenotype-related genes. **(A)** WGCNA of the C1 subtype to obtain a cluster dendrogram of coexpressed genes. **(B)** Module–trait relationships for C1 subtypes. Each module contains the corresponding correlation and *P*-value. **(C)** GO analysis of genes represented by the MEdarkslateblue module revealing biological processes associated with prognosis. **(D)** Transcription factors that regulate the expression of genes represented by the MEdarkslateblue module and their interactions.

the level of asthma control decreased gradually. In addition, poor asthma control was more common in the high-risk group than in the low-risk group. At the same level of FEV1 reversibility, the high-risk group was more likely to be poorly controlled than the low-risk group (**Figure 6C**). This result suggested that risk models based on ARGs could be used as a promising indicator for assessing the control status of patients with asthma. To understand the differences of immune microenvironment characteristics among different risk groups mediated by ARGs, we used ssGSEA to analyze their immune function and immune cell abundance. The high-risk group had higher T cell co-inhibition and lower degrees of immune responses, such as types I and II IFN responses, than the low-risk group, but no statistical difference was observed between the two groups (**Figure 6D**). The immune cell infiltration analysis showed that the high-risk group had a higher degree of B-cell, pDC, and Tfh infiltrations than the low-risk group (**Figure 6E**). These cells were closely related to the occurrence and development of asthma, and the difference was statistically significant ($P < 0.05$). These findings confirmed the risk-predictive value of predictive models from an immunological perspective. The results of animal experiments were the same as those of the prediction model. ACBD5 and CD46 mRNA were down-regulated in asthmatic mice, while S100A9, MAP2K7 and PTK6 mRNA were up-regulated in asthmatic mice (**Figure 7A**). There was a statistically significant difference in CD46, MAP2K7 and PTK6 ($P < 0.05$). Further

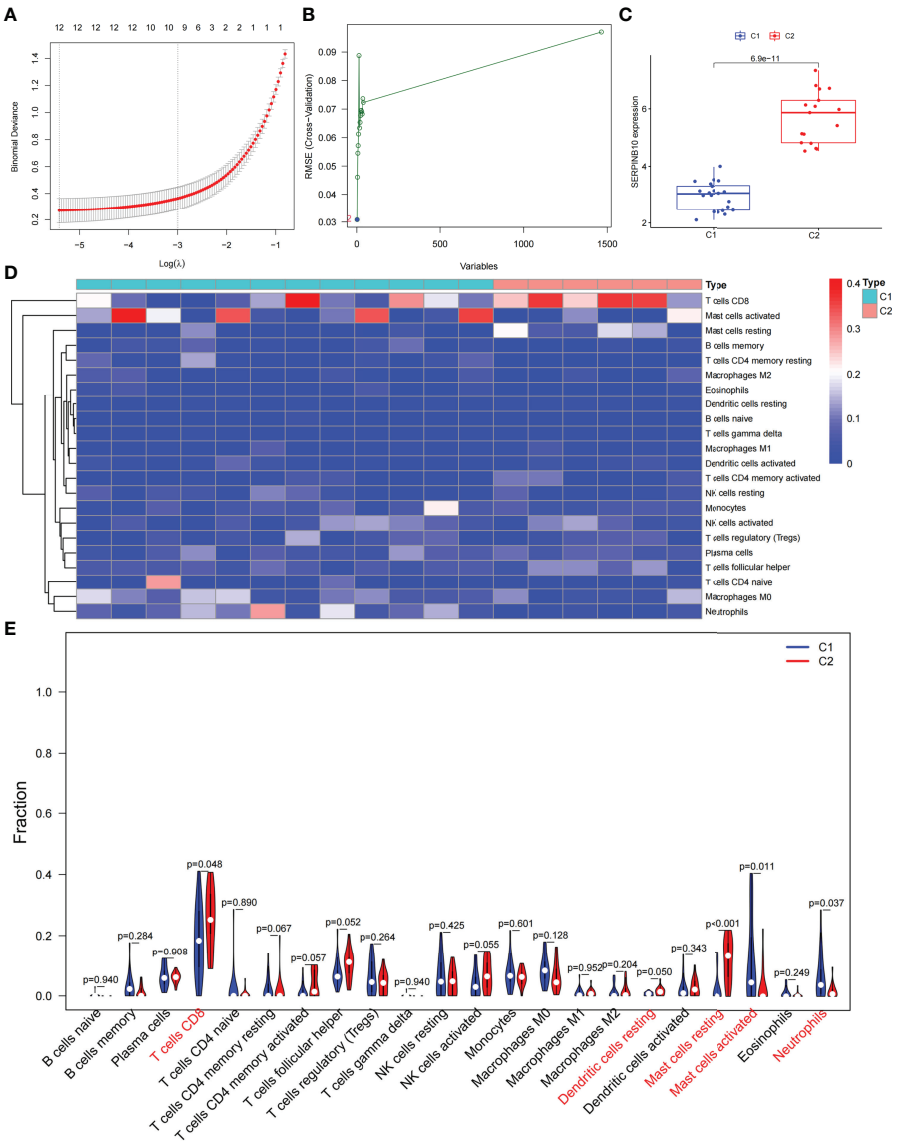

FIGURE 4 | Screening of autophagy-related diagnostic markers and differences in immune cell infiltration between C1 and C2 subtypes. **(A)** LASSO logistic regression algorithm to screen diagnostic markers. **(B)** SVM-RFE algorithm to screen diagnostic markers. **(C)** Difference of SERPINB10 gene expression between C1 and C2 subtypes. **(D)** Heatmap of the degree of infiltration of 22 immune cells in C1 subtype samples versus C2 subtype samples. **(E)** Violin diagram of the proportion of 22 kinds of immune cells. Markers in red indicate significant differences between the two subtypes.

immunohistochemical staining showed that compared with normal mice, CD46 was low expressed in the airway epithelium of asthmatic mice, while MAP2K7 and PTK6 were highly expressed (**Figure 7B**). The analysis of the ceRNA mechanism of the five risk genes in the model showed that S100A9, CD46, miR-328-3p, miR-20a-5p, NEAT1, MALAT1, and XIST occupied an important position and were closely associated with autophagy (**Figure 7C**). For example, miR-20a-5p, which is associated with CD46, is involved in autophagy-induced apoptosis and inflammation in asthma (43), but long-chain noncoding RNA can be used as "molecular sponge" of miR-20a-5p to participate in the regulation of target gene expression (44). Evidence showed that MALAT1 and XIST are involved in the process of autophagy of immune cells (45). Finally, eight potentially important small molecules targeting asthma were screened by the cMAP database, and seven of them had significant correlation with TBXA2R. These molecules were carbacylin, dinoprostone, fluprostenol, GR-32191, iloprost, picotamide, and U-46619, which were considered as PPAR, prostanoid, and thromboxane receptor agonists (**Figure 7D**). Carbacyclin, dinoprostone, fluprostenol, and iloprost were molecularly docked with TBXA2R to confirm their binding ability. Results showed that the affinity between them was all less than −5.0 kcal/mol. Their molecular docking patterns are shown in **Figures 7E–H**. Small molecules with high

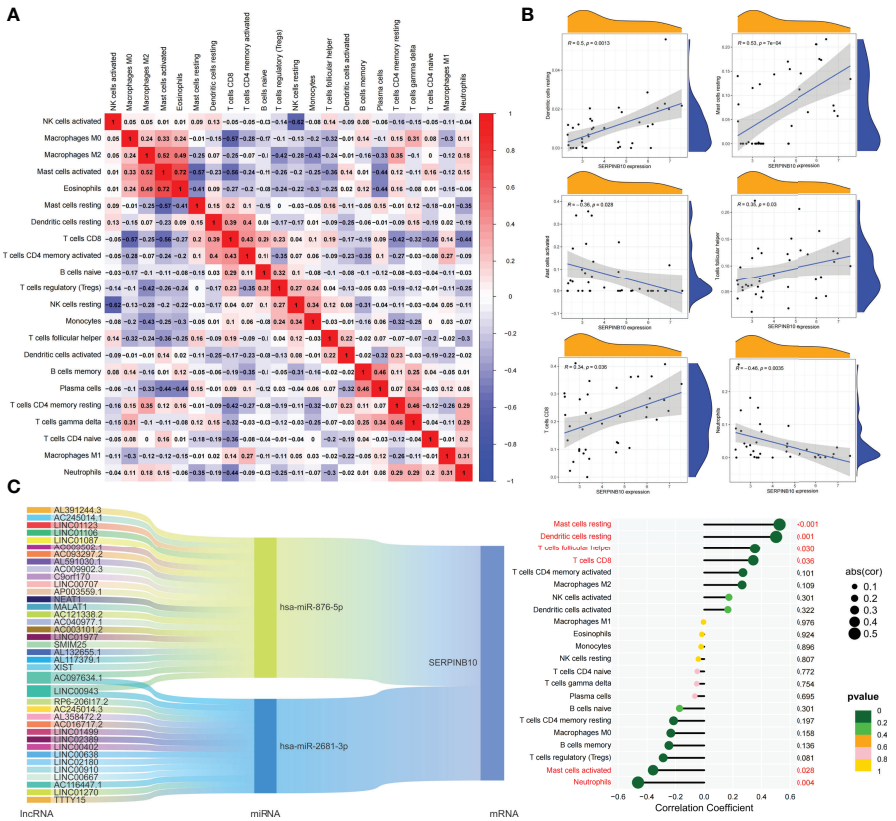

FIGURE 5 | Correlation of key ARGs with immune cell infiltration and its gene expression regulatory network. **(A)** Heatmap of correlations of 22 immune cells. The size of the colored square represents the strength of correlation, and red and blue colors indicate positive and negative correlations, respectively. A dark color indicates a strong correlation. **(B)** Mountain diagram showing the correlation between the SERPINB10 gene and resting dendritic cells, resting mast cells, activated mast cells, T follicular helper cells, CD8$^+$ T cells, and neutrophils. The lollipop diagram shows the correlation between SERPINB10 gene and 22 kinds of immune cells, and red marks indicate $P < 0.05$. **(C)** CeRNA networks involved in the regulation of SERPINB10 gene expression.

affinity might reverse or induce the biological state encoded by specific gene expression markers, thereby playing a potential therapeutic role in asthma.

DISCUSSION

Different types of asthma are caused by many different triggers. Th2-driven asthma is the most common and is typically characterized by elevated levels of type 2 inflammatory biomarkers, including type 2 cytokines (e.g., IL-4, IL-5, and IL-13), serum IgE, and blood eosinophils (6). However, these diagnostic markers are not specific. At present, the monoclonal antibodies approved for severe asthma have generally developed glucocorticoid resistance in patients with severe asthma, and the standard ICS–LABA treatment can no longer maintain control. In addition, monoclonal antibody drugs are often targeted for IgE or type 2 cytokines and their receptors but not for patients without allergy and noneosinophil phenotypes (3). Therefore, it is naturally inclined to poorly controlled severe asthma, and its clinical diagnosis and treatment are faced with severe challenges. Patients with severe asthma tendency should be identified early, and their evolution from mild and moderate to severe should be prevented.

The involvement of autophagy in the evolution of severe asthma has been widely explored. Studies focused on various immune cells involved in the process of asthma. Clinical observations show that NLRP3-mediated inflammatory response caused by circulating and pulmonary monocytes is a key driver of the pathogenesis of asthma. In the autophagy inhibition asthma model, NLRP3 induces monocyte activation. Autophagy inhibits NLRP3-induced monocyte activation in the asthma model. With the impaired autophagy level in circulating monocytes, the activation of NLRP3 inflammatory bodies increases. This process relies on the reprogramming of monocyte inflammatory response mediated by ARG transcription factor EB and is related to the severity of asthma (46). However, the specific role of autophagy in asthma is still controversial (47, 48). For example, neutrophils can increase the level of airway inflammation in severe asthma by destroying airway epithelial cells through autophagy (11), but the conditional knockout of ATG5 and lack of autophagy can induce neutrophil-infiltrated airway inflammation and AHR, further leading to hormone-resistant asthma (13). The

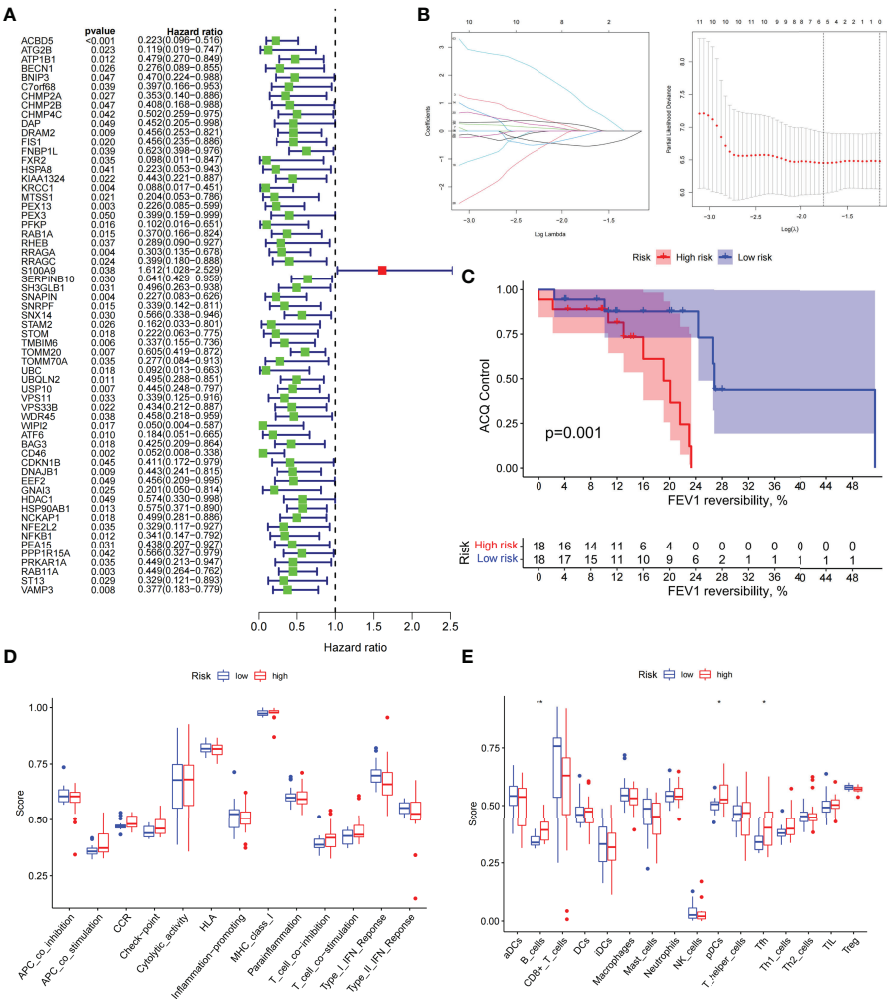

FIGURE 6 | The prognostic model constructed by differentially expressed genes of different autophagy patterns can distinguish between high- and low-risk patients with asthma. **(A)** DEGs associated with asthma control status. Red and green colors represent high- and low-risk genes, respectively. **(B)** Distribution of LASSO coefficients for DEGs. Tenfold cross-validation for tuning parameter selection in the LASSO regression. Dotted vertical lines are drawn at the optimal values by minimum criteria and 1 – SE criteria. **(C)** Kaplan–Meier curves of ACQ control and FEV1 reversibility in patients with different risk groups. **(D)** Differences in the degree of response to each immune function in high- and low-risk groups. **(E)** Differences in the abundance of infiltrating immune cells in the immune microenvironment between high- and low-risk groups. $^{*}P < 0.05$, $^{**}P < 0.01$.

difference in the results may be related to the type of immune cells and the function of specific ARGs. On the basis of the transcriptome data of patients with asthma, this study found that most of the high expression of ARGs is related to the good control of asthma. The key clinical indicators and functional enrichment analysis of patients with low-autophagy subtypes based on ARG typing point to the differences in dose and metabolism of glucocorticoids. Similar to the conclusions of previous studies (49), the present study proved that the ARG-based typing method is important in guiding the use of hormones in patients with potentially severe asthma. Future studies can focus on exploring the relationship between autophagy and glucocorticoid metabolism, and develop gene diagnosis models specially used to guide patients with severe asthma to choose glucocorticoids or monoclonal antibodies.

Gene markers are widely used in modern clinical diagnosis. In this study, SVM-RFE and LASSO logistic regression method found that SERPINB10 in ARGs is a diagnostic marker of low-autophagy subtypes. Studies showed that increased levels of SERPINB10 mRNA in epithelial cells of patients with asthma can lead to allergic airway inflammation, which is positively correlated with AHR, sputum eosinophil percentage, and exhaled nitric oxide content (50). Interestingly, the stimulation of T cell receptor with anti-CD3 antibody can upregulate the expression of SERPINB10 in Th2-polarized cells but has no effect on the expression of SERPINB10 in Th1-polarized cells, proving that it is a stable marker in non-Th2-type asthma (51). Severe asthma is dominated by Th1/Th17 cytokine responses and rarely has a Th2-mediated immune imbalance (52), whereas this phenomenon is consistent with our findings. A variety of

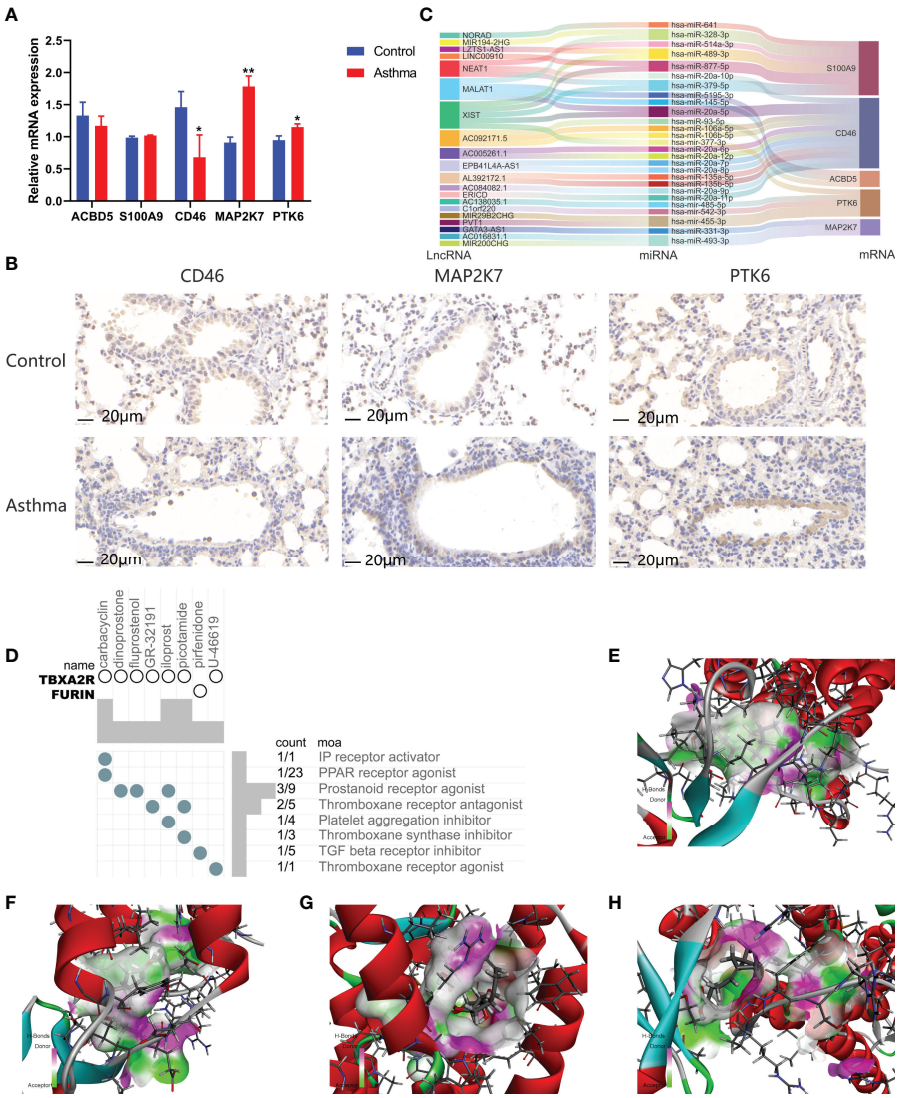

FIGURE 7 | Gene expression regulatory network based on prognostic model and prediction of potential therapeutic drugs for high-risk asthma (N=3, *$P < 0.05$, **$P < 0.01$). **(A)** mRNA expression of 5 risk genes in lung tissues of asthmatic mice and normal mice. **(B)** The expression of CD46, MAP2K7 and PTK6 in airway of asthmatic mice and normal mice. **(C)** CeRNA network involved in regulating the expression of five prognostic genes. **(D)** Correlation between potential therapeutic drugs and corresponding targets. **(E)** Binding conformation of TBXA2R and carbacyclin (binding energy = –59.29 kcal/mol). **(F)** Binding conformation of TBXA2R and dinoprostone (binding energy = –34.08 kcal/mol). **(G)** Binding conformation of TBXA2R and fluprostenol (binding energy = –16.13 kcal/mol). **(H)** Binding conformation of TBXA2R and iloprost (binding energy = – 64.50 kcal/mol).

immune cells associated with SERPINB10, such as neutrophils and dendritic cells, have also been shown to play an important role in asthma through autophagy. The enhancement of autophagy in neutrophils can activate the release of extracellular traps and aggravate asthma, whereas the enhancement of autophagy in dendritic cells can improve asthma induced by respiratory syncytial virus (53, 54). However, further research is needed to clarify the complex interaction between genes and immune cells.

Mild to moderate or severe asthma, poor control caused by environmental stimulation, medication differences, and activation of specific genes or pathways may run through the whole course of the patient (55). The analysis showed that the risk score model established in this study is a reliable index for predicting asthma control, and the role of five differentially expressed ARGs in asthma is partially supported by previous studies. Peripheral blood neutrophils in patients with asthma induce airway epithelial cells to produce S100A9 and further induce M1 macrophages to polarize through extracellular signal-regulated kinase pathway, which aggravates asthma (56). PTK6 is identified as a genetic susceptibility molecule for severe asthma (57). CD46 directly associates with autophagy, induces autophagy, and reduces oxidative stress-mediated apoptosis of

respiratory epithelial cells in patients with asthma (58). Based on the DEGs of high-risk patients, the cMAP database identified different small molecules that may be effective in asthma, predominantly prostaglandin receptor agonists. Some studies found that prostaglandin D2 inhibits mediator release and antigen-induced bronchoconstriction in the guinea pig trachea by the activation of DP 1 receptors (59). Transgenic mice overexpressing the PGE 2 receptor EP 2 on mast cells show protective phenotype in allergic asthma models (60). Therefore, the small molecule found may play an important role in the treatment of patients with asthma.

On the basis of the successful classification of asthma by ARGs, this study systematically revealed the significance of ARGs in the occurrence, development, and prognosis of asthma. The key diagnostic markers and five prognostic-related genes can be used as powerful biomarkers for the prognosis of asthma. However, this study has some limitations. First, the number of transcriptome datasets studied is relatively small, and no validation set is used. In addition, the clinical information contained in the data set is limited. For example, some lung function test data cannot be used in this study. Finally, as a regulatory factor in the occurrence and development of asthma, the biological function and molecular mechanism of ARGs need to be confirmed by further study.

CONCLUSION

In this study, we obtained ARGs associated with disease progression in patients with asthma. By evaluating the expression profiles of these genes, we distinguished the two subtypes and explored the relationship between autophagy, infiltrating immune cells, and asthma progression. An autophagy-related risk score model was constructed. This model is important in predicting the control of patients with asthma and can indicate the therapeutic targets and potential therapeutic drugs of asthma. Our findings can provide the predictions of individual course and control and promote the choice of better treatment strategies.

DATA AVAILABILITY STATEMENT

The datasets presented in this study can be found in online repositories. The names of the repository/repositories and accession number(s) can be found in the article/ **Supplementary Material**.

ETHICS STATEMENT

The animal study was reviewed and approved by Experimental animal ethics subcommittee of Academic Committee of Beijing University of traditional Chinese Medicine.

AUTHOR CONTRIBUTIONS

FY designed and conducted the whole research. JK and YZ applied for the GEO dataset analysis of asthma. WYL and ML carried out animal experiments and molecular biological analysis. ZL and WLL were responsible for the analysis of miRNAs associated with asthma. FY, HZ, and SC completed the data analysis and drafted the manuscript. XZ and JW revised and finalized the manuscript. All authors contributed to the article and approved the submitted version.

FUNDING

This work was supported by the National Key R&D Program of China (2020YFC2003100, 2020YFC2003101), National Natural Science Foundation of China (No. 82174243, No. 81973715), General project of Beijing Natural Science Foundation (No. 7202110), Innovation Team and Talents Cultivation Program of National Administration of Traditional Chinese Medicine (No. ZYYCXTD-C-202001).

ACKNOWLEDGMENTS

We thank the authors of the GSE89809 datasets for their contribution.

SUPPLEMENTARY MATERIAL

The Supplementary Material for this article can be found online at: https://www.frontiersin.org/articles/10.3389/fimmu.2022.897835/full#supplementary-material

REFERENCES

1. Li W, Gao RH, Xin T, Gao P. Different Expression Levels of Interleukin-35 in Asthma Phenotypes. *Respir Res* (2020) 21(1):9. doi: 10.1186/s12931-020-01356-6
2. Menzies-Gow A, Corren J, Bourdin A, Chupp G, Israel E, Wechsler ME, et al. Tezepelumab in Adults and Adolescents With Severe, Uncontrolled Asthma. *N Engl J Med* (2021) 384(19):1800–9. doi: 10.1056/NEJMoa2034975
3. Hinks TSC, Levine SJ, Brusselle GG. Treatment Options in Type-2 Low Asthma. *Eur Resp J* (2021) 57(1):21. doi: 10.1183/13993003.00528-2020
4. Bagnasco D, Paggiaro P, Latorre M, Folli C, Testino E, Bassi A, et al. Severe Asthma: One Disease and Multiple Definitions. *World Allergy Organ J* (2021) 14(11):10. doi: 10.1016/j.waojou.2021.100606
5. Sadatsafavi M, Lynd L, Marra C, Carleton B, Tan WC, Sullivan S, et al. Direct Health Care Costs Associated With Asthma in British Columbia. *Can Respir J* (2010) 17(2):74–80. doi: 10.1155/2010/361071
6. Pelaia C, Pelaia G, Crimi C, Maglio A, Gallelli L, Terracciano R, et al. Tezepelumab: A Potential New Biological Therapy for Severe Refractory Asthma. *Int J Mol Sci* (2021) 22(9):13. doi: 10.3390/ijms22094369

7. Racanelli AC, Kikkers SA, Choi AMK, Cloonan SM. Autophagy and Inflammation in Chronic Respiratory Disease. *Autophagy* (2018) 14 (2):221–32. doi: 10.1080/15548627.2017.1389823
8. Poon A, Eidelman D, Laprise C, Hamid Q. Atg5, Autophagy and Lung Function in Asthma. *Autophagy* (2012) 8(4):694–5. doi: 10.4161/auto.19315
9. Martinez J, Cook DN. What's the Deal With Efferocytosis and Asthma? *Trends Immunol* (2021) 42(10):904–19. doi: 10.1016/j.it.2021.08.004
10. McAlinden KD, Deshpande DA, Ghavami S, Xenaki D, Sohal SS, Oliver BG, et al. Autophagy Activation in Asthma Airways Remodeling. *Am J Respir Cell Mol Biol* (2019) 60(5):541–53. doi: 10.1165/rcmb.2018-0169OC
11. Pham DL, Ban GY, Kim SH, Shin YS, Ye YM, Chwae YJ, et al. Neutrophil Autophagy and Extracellular DNA Traps Contribute to Airway Inflammation in Severe Asthma. *Clin Exp Allergy* (2017) 47(1):57–70. doi: 10.1111/cea.12859
12. Liu JN, Suh DH, Trinh HK, Chwae YJ, Park HS, Shin YS. The Role of Autophagy in Allergic Inflammation: A New Target for Severe Asthma. *Exp Mol Med* (2016) 48(7):e243. doi: 10.1038/emm.2016.38
13. Suzuki Y, Maazi H, Sankaranarayanan I, Lam J, Khoo B, Soroosh P, et al. Lack of Autophagy Induces Steroid-Resistant Airway Inflammation. *J Allergy Clin Immunol* (2016) 137(5):1382. doi: 10.1016/j.jaci.2015.09.033
14. Singhania A, Wallington JC, Smith CG, Horowitz D, Staples KJ, Howarth PH, et al. Multitissue Transcriptomics Delineates the Diversity of Airway T Cell Functions in Asthma. *Am J Respir Cell Mol Biol* (2018) 58(2):261–70. doi: 10.1165/rcmb.2017-0162OC
15. Ritchie ME, Phipson B, Wu D, Hu Y, Law CW, Shi W, et al. Limma Powers Differential Expression Analyses for Rna-Sequencing and Microarray Studies. *Nucleic Acids Res* (2015) 43(7):e47. doi: 10.1093/nar/gkv007
16. Wang Y, Zhao W, Xiao Z, Guan G, Liu X, Zhuang M. A Risk Signature With Four Autophagy-Related Genes for Predicting Survival of Glioblastoma Multiforme. *J Cell Mol Med* (2020) 24(7):3807–21. doi: 10.1111/jcmm.14938
17. Zhang B, Wu Q, Li B, Wang D, Wang L, Zhou YL. M(6)a Regulator-Mediated Methylation Modification Patterns and Tumor Microenvironment Infiltration Characterization in Gastric Cancer. *Mol Cancer* (2020) 19(1):53. doi: 10.1186/s12943-020-01170-0
18. Zhang X, Zhang S, Yan X, Shan Y, Liu L, Zhou J, et al. M6a Regulator-Mediated Rna Methylation Modification Patterns Are Involved in Immune Microenvironment Regulation of Periodontitis. *J Cell Mol Med* (2021) 25 (7):3634–45. doi: 10.1111/jcmm.16469
19. Wilkerson MD, Hayes DN. Consensusclusterplus: A Class Discovery Tool With Confidence Assessments and Item Tracking. *Bioinformatics* (2010) 26 (12):1572–3. doi: 10.1093/bioinformatics/btq170
20. Ginestet C. Ggplot2: Elegant Graphics for Data Analysis. *J R Stat Soc Ser A-Stat Soc* (2011) 174:245–. doi: 10.1111/j.1467-985X.2010.00676_9.x
21. Yu G, Wang LG, Han Y, He QY. Clusterprofiler: An R Package for Comparing Biological Themes Among Gene Clusters. *Omics J Integr Biol* (2012) 16 (5):284–7. doi: 10.1089/omi.2011.0118
22. Zhang X, Wang Q, Yan X, Shan Y, Xing L, Li M, et al. Immune Landscape of Periodontitis Unveils Alterations of Infiltrating Immunocytes and Molecular Networks-Aggregating Into an Interactive Web-Tool for Periodontitis Related Immune Analysis and Visualization. *J Transl Med* (2020) 18(1):438. doi: 10.1186/s12967-020-02616-1
23. Tibshirani R. Regression Shrinkage and Selection *Via* the Lasso. *J R Stat Soc Ser B Methodol* (1996) 58(1):267–88. doi: 10.1111/j.2517-6161.1996.tb02080.x
24. Suykens JAK, Vandewalle J. Least Squares Support Vector Machine Classifiers. *Neural Process Lett* (1999) 9(3):293–300. doi: 10.1023/a:1018628609742
25. Friedman J, Hastie T, Tibshirani R. Regularization Paths for Generalized Linear Models *Via* Coordinate Descent. *J Stat Softw* (2010) 33(1):1–22. doi: 10.18637/jss.v033.i01
26. Huang ML, Hung YH, Lee WM, Li RK, Jiang BR. Svm-Rfe Based Feature Selection and Taguchi Parameters Optimization for Multiclass Svm Classifier. *Sci World J* (2014) 2014:795624. doi: 10.1155/2014/795624
27. Newman AM, Liu CL, Green MR, Gentles AJ, Feng WG, Xu Y, et al. Robust Enumeration of Cell Subsets From Tissue Expression Profiles. *Nat Methods* (2015) 12(5):453. doi: 10.1038/nmeth.3337
28. Friendly M. Corrgrams: Exploratory Displays for Correlation Matrices. *Am Stat* (2002) 56(4):316–24. doi: 10.1198/000313002533
29. Deng YJ, Ren EH, Yuan WH, Zhang GZ, Wu ZL, Xie QQ. Grb10 and E2f3 as Diagnostic Markers of Osteoarthritis and Their Correlation With Immune Infiltration. *Diagnostics* (2020) 10(3):13. doi: 10.3390/diagnostics10030171
30. Wang Y, Liu X, Guan G, Zhao W, Zhuang M. A Risk Classification System With Five-Gene for Survival Prediction of Glioblastoma Patients. *Front Neurol* (2019) 10:745. doi: 10.3389/fneur.2019.00745
31. Fu Z, Xu Y, Chen Y, Lv H, Chen G, Chen Y. Construction of Mirna-Mrna-Tf Regulatory Network for Diagnosis of Gastric Cancer. *BioMed Res Int* (2021) 2021:9121478. doi: 10.1155/2021/9121478
32. Li JH, Liu S, Zhou H, Qu LH, Yang JH. Starbase V2.0: Decoding Mirna-Cerna, Mirna-Ncrna and Protein-Rna Interaction Networks From Large-Scale Clip-Seq Data. *Nucleic Acids Res* (2014) 42(D1):D92–D7. doi: 10.1093/nar/gkt1248
33. Chang L, Zhou GY, Soufan O, Xia JG. Mirnet 2.0: Network-Based Visual Analytics for Mirna Functional Analysis and Systems Biology. *Nucleic Acids Res* (2020) 48(W1):W244–51. doi: 10.1093/nar/gkaa467
34. Liu XS, Gao Y, Wu LB, Wan HB, Yan P, Jin Y, et al. Comprehensive Analysis of Glut1 Immune Infiltrates and Cerna Network in Human Esophageal Carcinoma. *Front Oncol* (2021) 11:665388. doi: 10.3389/fonc.2021.665388
35. Lamb J, Crawford ED, Peck D, Modell JW, Blat IC, Wrobel MJ, et al. The Connectivity Map: Using Gene-Expression Signatures to Connect Small Molecules, Genes, and Disease. *Science* (2006) 313(5795):1929–35. doi: 10.1126/science.1132939
36. Rhee H, Love T, Mammen J. Comparing Asthma Control Questionnaire (Acq) and National Asthma Education and Prevention Program (Naepp) Asthma Control Criteria. *Ann Allergy Asthma Immunol* (2019) 122(1):58–64. doi: 10.1016/j.anai.2018.09.448
37. Schuler M, Faller H, Wittmann M, Schultz K. Asthma Control Test and Asthma Control Questionnaire: Factorial Validity, Reliability and Correspondence in Assessing Status and Change in Asthma Control. *J Asthma* (2016) 53(4):438–45. doi: 10.3109/02770903.2015.1101134
38. Nguyen JM, Holbrook JT, Wei CY, Gerald LB, Teague WG, Wise RA, et al. Validation and Psychometric Properties of the Asthma Control Questionnaire Among Children. *J Allergy Clin Immunol* (2014) 133(1):91. doi: 10.1016/j.jaci.2013.06.029
39. Thayyezhuth D, Venkataram R, Bhat VS, Aroor R. A Study of Spirometric Parameters in Non Asthmatic Allergic Rhinitis. *Heliyon* (2021) 7(11):3. doi: 10.1016/j.heliyon.2021.e08270
40. Ye Q, Liao A, D'Urzo A. Fev1 Reversibility for Asthma Diagnosis: A Critical Evaluation. *Expert Rev Respir Med* (2018) 12(4):265–7. doi: 10.1080/17476348.2018.1439741
41. Jia S, Guo P, Lu J, Huang X, Deng L, Jin Y, et al. Curcumol Ameliorates Lung Inflammation and Airway Remodeling *Via* Inhibiting the Abnormal Activation of the Wnt/B-Catenin Pathway in Chronic Asthmatic Mice. *Drug Design Dev Ther* (2021) 15:2641–51. doi: 10.2147/dddt.S292642
42. Wei WD, Chen WD, He NF. Hdac4 Induces the Development of Asthma by Increasing Slug-Upregulated Cxcl12 Expression Through Klf5 Deacetylation. *J Transl Med* (2021) 19(1):15. doi: 10.1186/s12967-021-02812-7
43. Yu YY, Men S, Zhang YH. Mir-20a-5p Ameliorates Ovalbumin (Ova)-Induced Mouse Model of Allergic Asthma Through Targeting Atg7-Regulated Cell Death, Fibrosis and Inflammation. *Int Immunopharmacol* (2021) 95:10. doi: 10.1016/j.intimp.2020.107342
44. Ma ZB, Zhang J, Xu XR, Qu YL, Dong H, Dang J, et al. Lncrna Expression Profile During Autophagy and Malat1 Function in Macrophages. *PloS One* (2019) 14(8):23. doi: 10.1371/journal.pone.0221104
45. Zhao X, Sun J, Yuan Y, Lin S, Lin J, Mei X. Zinc Promotes Microglial Autophagy Through Nlrp3 Inflammasome Inactivation *Via* Xist/Mir-374a-5p Axis in Spinal Cord Injury. *Neurochem Res* (2021) 47(2):372–81. doi: 10.1007/s11064-021-03441-8
46. Theofani E, Semitekolou M, Samitas K, Mais A, Galani IE, Triantafyllia V, et al. Tfeb Signaling Attenuates Nlrp3-Driven Inflammatory Responses in Severe Asthma. *Allergy* (2022). doi: 10.1111/all.15221
47. Reed M, Morris SH, Jang S, Mukherjee S, Yue Z, Lukacs NW. Autophagy-Inducing Protein Beclin-1 in Dendritic Cells Regulates Cd4 T Cell Responses and Disease Severity During Respiratory Syncytial Virus Infection. *J Immunol (Baltimore Md 1950)* (2013) 191(5):2526–37. doi: 10.4049/jimmunol.1300477
48. Liu HX, Yan HY, Qu W, Wen X, Hou LF, Zhao WH, et al. Inhibition of Thymocyte Autophagy-Associated Cd4(+)T Thymopoiesis Is Involved in

Asthma Susceptibility in Mice Exposed to Caffeine Prenatally. *Arch Toxicol* (2019) 93(5):1323–35. doi: 10.1007/s00204-019-02418-5
49. Al-Ramli W, Prefontaine D, Chouiali F, Martin JG, Olivenstein R, Lamiere C, et al. T(H)17-Associated Cytokines (Il-17a and Il-17f) in Severe Asthma. *J Allergy Clin Immunol* (2009) 123(5):1185–7. doi: 10.1016/j.jaci.2009.02.024
50. Mo YQ, Zhang K, Feng YC, Yi LL, Jiang YX, Wu WL, et al. Epithelial Serpinb10, a Novel Marker of Airway Eosinophilia in Asthma, Contributes to Allergic Airway Inflammation. *Am J Physiol-Lung Cell Mol Physiol* (2019) 316 (1):L245–L54. doi: 10.1152/ajplung.00362.2017
51. Mo YQ, Ye L, Cai H, Zhu GP, Wang J, Zhu MC, et al. Serpinb10 Contributes to Asthma by Inhibiting the Apoptosis of Allergenic Th2 Cells. *Respir Res* (2021) 22(1):12. doi: 10.1186/s12931-021-01757-1
52. Subramanian H, Hashem T, Bahal D, Kammala AK, Thaxton K, Das R. Ruxolitinib Ameliorates Airway Hyperresponsiveness and Lung Inflammation in a Corticosteroid-Resistant Murine Model of Severe Asthma. *Front Immunol* (2021) 12:786238. doi: 10.3389/fimmu.2021.786238
53. Guo Y, Gao F, Wang X, Pan ZZ, Wang Q, Xu SY, et al. Spontaneous Formation of Neutrophil Extracellular Traps Is Associated With Autophagy. *Sci Rep* (2021) 11(1):10. doi: 10.1038/s41598-021-03520-4
54. Chen X, Luo Y, Wang M, Sun L, Huang K, Li Y, et al. Wuhu Decoction Regulates Dendritic Cell Autophagy in the Treatment of Respiratory Syncytial Virus (Rsv)-Induced Mouse Asthma by Ampk/Ulk1 Signaling Pathway. *Med Sci Monit Int Med J Exp Clin Res* (2019) 25:5389–400. doi: 10.12659/msm.917692
55. Mulugeta T, Ayele T, Zeleke G, Tesfay G. Asthma Control and Its Predictors in Ethiopia: Systematic Review and Meta-Analysis. *PloS One* (2022) 17(1): e0262566. doi: 10.1371/journal.pone.0262566
56. Quoc QL, Choi Y, Bich TCT, Yang EM, Shin YS, Park HS. S100a9 in Adult Asthmatic Patients: A Biomarker for Neutrophilic Asthma. *Exp Mol Med* (2021) 53(7):1170–9. doi: 10.1038/s12276-021-00652-5
57. Zayed H. Novel Comprehensive Bioinformatics Approaches to Determine the Molecular Genetic Susceptibility Profile of Moderate and Severe Asthma. *Int J Mol Sci* (2020) 21(11):18. doi: 10.3390/ijms21114022
58. Tsai YG, Wen YS, Wang JY, Yang KD, Sun HL, Liou JH, et al. Complement Regulatory Protein Cd46 Induces Autophagy Against Oxidative Stress-Mediated Apoptosis in Normal and Asthmatic Airway Epithelium. *Sci Rep* (2018) 8:11. doi: 10.1038/s41598-018-31317-5
59. Safholm J, Abma W, Liu JL, Balgoma D, Fauland A, Kolmert J, et al. Prostaglandin D-2 Inhibits Mediator Release and Antigen Induced Bronchoconstriction in the Guinea Pig Trachea by Activation of Dp1 Receptors. *Eur J Pharmacol* (2021) 907:9. doi: 10.1016/j.ejphar.2021.174282
60. Urbano A, Plaza J, Turon S, Pujol A, Costa-Farré C, Marco A, et al. Transgenic Mice Overexpressing the Pge(2) Receptor Ep(2) on Mast Cells Exhibit a Protective Phenotype in a Model of Allergic Asthma. *Allergy* (2021) 76 (10):3196–9. doi: 10.1111/all.1498

Conflict of Interest: The authors declare that the research was conducted in the absence of any commercial or financial relationships that could be construed as a potential conflict of interest.

Publisher's Note: All claims expressed in this article are solely those of the authors and do not necessarily represent those of their affiliated organizations, or those of the publisher, the editors and the reviewers. Any product that may be evaluated in this article, or claim that may be made by its manufacturer, is not guaranteed or endorsed by the publisher.

frontiers | Frontiers in Immunology

REVIEW
published: 10 May 2022
doi: 10.3389/fimmu.2022.894445

The Role of C-Type Lectin Receptor Signaling in the Intestinal Microbiota-Inflammation-Cancer Axis

Muhan Li[1,2†], *Runfeng Zhang*[1,2†], *Ji Li*[1,2*‡] *and Jingnan Li*[1,2*‡]

[1] Department of Gastroenterology, Peking Union Medical College Hospital, Chinese Academy of Medical Sciences and Peking Union Medical College, Beijing, China, [2] Key Laboratory of Gut Microbiota Translational Medicine Research, Peking Union Medical College Hospital, Chinese Academy of Medical Sciences and Peking Union Medical College, Beijing, China

OPEN ACCESS

Edited by:
Chunqing Guo,
Virginia Commonwealth University,
United States

Reviewed by:
Chao Li,
Virginia Commonwealth University Health System, United States
Wenjie Liu,
Virginia Commonwealth University,
United States

***Correspondence:**
Ji Li
lijii0235@pumch.cn
Jingnan Li
lijn2008@126.com

[†]These authors have contributed equally to this work and share first authorship

[‡]These authors have contributed equally to this work

Specialty section:
This article was submitted to Molecular Innate Immunity, a section of the journal Frontiers in Immunology

Received: 11 March 2022
Accepted: 04 April 2022
Published: 10 May 2022

Citation:
Li M, Zhang R, Li J and Li J (2022) The Role of C-Type Lectin Receptor Signaling in the Intestinal Microbiota-Inflammation-Cancer Axis. Front. Immunol. 13:894445. doi: 10.3389/fimmu.2022.894445

As a subset of pattern recognition receptors (PRRs), C-type lectin-like receptors (CLRs) are mainly expressed by myeloid cells as both transmembrane and soluble forms. CLRs recognize not only pathogen associated molecular patterns (PAMPs), but also damage-associated molecular patterns (DAMPs) to promote innate immune responses and affect adaptive immune responses. Upon engagement by PAMPs or DAMPs, CLR signaling initiates various biological activities *in vivo*, such as cytokine secretion and immune cell recruitment. Recently, several CLRs have been implicated as contributory to the pathogenesis of intestinal inflammation, which represents a prominent risk factor for colorectal cancer (CRC). CLRs function as an interface among microbiota, intestinal epithelial barrier and immune system, so we firstly discussed the relationship between dysbiosis caused by microbiota alteration and inflammatory bowel disease (IBD), then focused on the role of CLRs signaling in pathogenesis of IBD (including Mincle, Dectin-3, Dectin-1, DCIR, DC-SIGN, LOX-1 and their downstream CARD9). Given that CLRs mediate intricate inflammatory signals and inflammation plays a significant role in tumorigenesis, we finally highlight the specific effects of CLRs on CRC, especially colitis-associated cancer (CAC), hoping to open new horizons on pathogenesis and therapeutics of IBD and CAC.

Keywords: C-type lectin receptor, pathogen-associated molecular patterns, damage-associated molecular patterns, inflammatory bowel disease, colitis associated cancer

INTRODUCTION

IBD consists of Crohn's disease (CD) and ulcerative colitis (UC). IBD majorly affects young adults, which substantially alters their life quality and causes enormous financial burden for health care (1, 2). The incidence of IBD in western countries has been high for decades, with over 1 million patients in the USA and 2.5 million in Europe (1). Many newly industrialized countries around the world also have a rapidly increasing incidence in recent years (1). Although the exact pathogenesis of IBD remains obscure, numerous evidence supports that aberrant innate and adaptive immune response against the intestinal pathogenic and commensal microbiota are responsible for IBD in genetically susceptible populations (3).

Fungus, as an indispensable component of intestinal microbiota, take a crucial part in maintaining the gut homeostasis, and its dysbiosis might contribute to the pathogenesis of IBD (4, 5). There are trillions of microorganisms resided in human gut, including bacteria, fungi, archaea and viruses (4), and metagenomic sequencing reveals that their collective genome are 100 times more than our own genome (6, 7). Over 99% of these genes belong to bacteria, and over 90% of intestinal bacteria belong to two phyla, *Firmicutes* and *Bacteroidetes (*7, 8). Whereas fungi only makes up 0.1% of the total human gut microorganisms, among which the phyla *Ascomycota*, *Basidiomycota* and *Chytridiomycota* are predominant (4). Bacteria have long been the focus of intestinal flora research, while the role of fungi have been undervalued due to their low proportion and relatively low infection rate. In recent years, the number of immunocompromised patients has largely expanded due to increasing prevalence of HIV and the wide use of chemotherapy, organ transplantation, and immunosuppressive agents. Opportunistic infections and mortality caused by fungi have attracted more and more attention, thus understanding immune responses against fungi is of great immediate significance. Now people have realized that both bacteria and fungi exert important functions in maintaining the intestinal homeostasis, and their dysbiosis have been indicated to take part in multiple diseases, including IBD (4, 9, 10).

The recognition of fungi are predominantly dependent on the C-type lectin receptor (CLR) family, an important family of pattern recognition receptors (11). The basic theory of the interplay between fungi and CLRs is the Janeway's theory that antigen presenting cells (APCs) recognize and respond to non-self molecules through PRRs binding to quite conserved pathogen-associated molecular patterns (PAMPs) (12). Upon ligation with conserved PAMPs expressed on a wide variety of fungal cell walls, CLRs initiate intricate downstream signal network and ultimately induce corresponding innate and adaptive immune responses. Distinct fungi have different cell wall composition thus expressing different PAMPs (13). The combination of many PAMPs is just like a fingerprint, which triggers the activation of specific signaling pathways to distinguish between different microorganisms and fine-tune the immune response against specific microorganism (13, 14). Although CLRs are at the very core of intestinal fungal immunity, it is unreasonable to ignore the crosstalk and collaboration between CLRs and other subsets of the PRR family, including well-studied Toll-like receptors (TLRs), inflammasome-related nucleotide-binding oligomerization domain (NOD)-like receptors (NLRs), and RNA-detecting retinoic acid-inducible gene-I(RIG-I)-like receptors (RLRs) (14, 15). Much more diverse immune responses can be induced by engaging several PRRs simultaneously to ensure the effectiveness of immune response (14).

However, PAMPs are still insufficient to explain many phenomena, such as tumor immunity, transplant rejection and autoimmunity. Matzinger's danger model supposes that APCs also recognize and respond to endogenous damage-associated molecular patterns(DAMP) derived from damaged or distressed tissues, which nicely complement Janeway's self-non-self model (16). The danger model is supported by mounting evidences. For example, many CLRs have been demonstrated to bind not only PAMP, but also DAMP, with different ligation to produce different responses. By recognizing DAMPs that are released by distressed tissues or expressed during malignant transformation, CLRs have been proven to participate in the pathogenesis of multiple inflammatory disorders and malignant tumors, with different CLRs playing different or even opposite roles (17–21).

In order to comprehensively understand the significance of CLRs family in the interplay among intestinal microbiota-inflammation-cancer axis, we selected several typical representatives from each of the four CLRs categories, including Mincle, Dectin-3, Dectin-1, DCIR, LOX-1, and DC-SIGN. In addition, there is a consistent core downstream molecule CARD9 in the downstream signaling pathways of various CLRs, therefore CARD9 also takes a central part in intestinal immunity. In this review, we summarized the cutting-edge research progress of these molecules in the field of intestinal inflammation and CRC, which is of great significance for understanding the pathogenesis of IBD and colitis associated cancer (CAC) and developing new therapeutic strategies.

THE C-TYPE LECTIN RECEPTOR FAMILY AND ITS SUBTYPE

Lectins can selectively bind to specific carbohydrate structures, which are extremely useful tools for understanding the information encoded in carbohydrates, studying the characterization of polysaccharides and glycoproteins, recognizing cell-molecule and cell-cell interactions, especially investigating the changes in malignancy (22, 23). In 1988, Drickamer organized numerous lectins into several categories, two of which are Ca^{2+}-dependent C-type and thiol-dependent S-type (24). The C-type lectin family has boomed since then, with a thousand identified members from diverse animal species (25). Through characterizing the structures and functions of different domains, their carbohydrate-binding activities were demonstrated to be mediated by special carbohydrate recognition domain (CRD), whose compact globular structure was not similar to any known protein fold (25).

The C-type lectin receptors have at least one C-type lectin-like domains (CTLD) in their extracellular region (C-terminus), which are homologous to CRD and responsible for recognizing specific carbohydrate structures mainly in a Ca^{2+}-dependent manner (14, 25). CLRs whose CRD contains Glu-Pro-Asn (EPN) tripeptide motifs could bind mannose, glucose, fucose and N-acetylglucosamine (GlcNAc), whereas CLRs whose CRD contains another tripeptide motif, Glu-Pro-Asp (QPD), bind galactose and N-acetylgalactosamine (GalNAc) (26). In fact, CLRs do not always bind carbohydrate structures or depend on Ca^{2+} (14, 25), for example, proteins and lipids can also act as ligands of CLRs (27). Most CLRs are transmembrane receptors, but some can be released as soluble proteins, such as mannose-binding-lectin (MBL) (28). A lot of CLRs were initially identified to be expressed on dendritic cells (DCs) including the well-

known Dectin-1and DC-SIGN (29–31). Following studies found that monocytes, macrophages, B cells, neutrophils, and intestinal epithelial cell (IEC) may also express certain CLRs (14, 32). Although CLRs are classically considered to be capable of recognizing carbohydrate structures in fungal cell wall, many evidences suggest that they are also involved in sensing a large range of pathogens including bacteria, viruses, and helminths, as well as DAMPs (14, 18, 33–38). Upon ligation, distinct CLRs can variably affect endocytic, phagocytic, proinflammatory or anti-inflammatory responses, which is determined by the extremely versatile CLR signaling system (27). Finally, CLRs connect innate immunity with adaptive immunity through antigen internalization, antigen presentation and T cell activation (27, 34, 39, 40).

CLRs can be roughly divided into four groups with different cytoplasmic signaling motifs (**Table 1**) (27, 41). Immunoreceptor tyrosine-based activating motif (ITAM)-coupled CLRs either have an evident ITAM motifs consisting of YxxL tandem repeats in their cytoplastic tail with Y representing tyrosine, or interacts with ITAM-containing adaptors. Fc receptor γ chain (FcRγ) is the most common ITAM-containing adaptor proteins for CLR-mediated downstream signal transduction, such as Mincle (18). Hemi-ITAM-(hemITAM)-bearing CLRs only contain a single tyrosine (Y) within their cytoplasmic YxxL motif, such as Dectin-1 (27, 42). After CLRs binding to ligands, tyrosine(s) within the ITAM or hemITAM are phosphorylated to recruit spleen tyrosine kinase (Syk) and subsequently assemble the CARD9/Bcl-10/MALT1 complex, thus leading to NF-κB activation, which affects many aspects of both innate and adaptive immunity (43, 44). Therefore, these ITAM or hemITAM CLRs generally function as activating receptors to trigger and potentiate immune responses, although they may also play an inhibiting role in some cases (45–48). Unlike ITAM or hemITAM-containing CLRs mentioned above, immunoreceptor tyrosine-based inhibitory motif (ITIM)-containing CLRs, such as DCIR, usually negatively regulate the signaling pathway of other PRRs, which is achieved by recruiting tyrosine phosphatases SHP-1 or SHP-2 instead of tyrosine kinase (27). ITAM-ITIM independent CLRs, such as human DC-SIGN and LOX-1, lack typical ITAM or ITIM signaling motifs (41).

It should be noted that although the intracellular structural motifs of CLRs are crucial to the molecular signaling pathways, they are still not enough to accurately characterize or predict downstream signaling transduction and following immune responses (41). Motif context, receptor location, multimerization of CLRs, ligand type and concentration, crosstalk with other PRR all contribute to the flexibility of signaling pathways (41).

THE ROLE OF CLRS IN THE INTERPLAY BETWEEN FUNGAL MICROBIOTA AND IBD

The intestinal bacterial microbiota is skewed in IBDs, whose dysbiosis has been thoroughly investigated and proven a substantial significance in IBD pathogenesis (49, 50). While the fungal microbiota is relatively poorly studied. In recent years, mounting clues suggest that fungi dysbiosis also take part in IBD pathogenesis. An early preliminary study showed changes in the intestinal fungal diversity and composition of IBD patients (51). Compared to the noninflamed mucosa, inflamed mucosa shows elevated fungal richness and diversity, which is characterized by expanded opportunistic pathogenic fungi including *Candida*

TABLE 1 | C-type lectin receptors and its immune recognition.

	Signal module	Other names	Expression	PAMP	DAMP
Dectin-1	hemITAM	CLECSF12, CLEC7A	Mo, Mϕ, DC, Neu, Eos, B cell, T cell, bronchial epithelial cell, intestinal epithelial cell	β-1, 3-glucan	Vimentin, carbohydrate on tumor
Mincle	ITAM	CLECSF9,CLEC4E	activated Mϕ, DC, Neu, B cell	α-mannan, various glycolipids, (TDM)	SAP130, cholesterol sulfate, cholesterol crystal, β-GlcCer
Dectin-3	ITAM	MCL, CLECSF8, Clec4d	Mϕ, Mo, Neu, DC	α-mannan, TDM	——
DCIR	ITIM	CLECSF6, Clec4a2	DCs, Mo, Mϕ, B cell, granulocyte, activated T cell	fucose, mannose	carbohydrate on tumor
DC-SIGN	ITAM-ITIM independent	CD209 murine homolog: SIGN-R1, SIGN-R3	Human DC, Mϕ	fucose, mannose	ICAM-3, ICAM-2, Mac-1, Mac-2BP, MSPL/ TMPRSS13, CEA, CEACAM1, carbohydrate on tumor
LOX-1	ITAM-ITIM independent	OLR1, Clec8a	endothelial cell, smooth muscle cell, cardiomyocyte, adipocyte, platelet, Mo, Mϕ, DC, B cell, chondrocyte, intestinal cell	G+ bacteria, G- bacteria	Ox-LDL, Ox-HDL, HSP, PS, apoptotic bodies, AGEs, platelets

ITAM, immunoreceptor tyrosine-based activating motif; hemITAM, hemi-ITAM; ITIM, immunoreceptor tyrosine-based inhibitory motif; Mϕ, macrophage; DC, dendritic cell; Neu, neutrophil; Mo, monocyte; Eos, eosinophil; TDM, trehalose-6,6′-dimycolate; G+, Gram-positive; G-, Gram-negative; SAP130, spliceosome-associated protein 130; β-GlcCer, β-glucosylceramides; ICAM-3, intercellular adhesion molecule-3; ICAM-2, intercellular adhesion molecule-2; Mac-2BP, Mac-2-binding protein; MSPL, mosaic serine protease large-form; TMPRSS13, transmembrane protease serine 13; CEA, carcinoembryonic antigen; CEACAM1, carcinoembryonic-antigen-related cell-adhesion molecule-1; Ox-LDL, oxidized low density lipoprotein; Ox-HDL, oxidized high density lipoprotein; HSP, heat shock protein; PS, phosphatidylserine; AGEs, advanced glycation end-products.

spp., *Gibberella moniliformis* and *Cryptococcus neoformans* (52). Subsequently, many studies consistently found that *Candida* spp. (e.g., *Candida tropicalis*) showed significantly increased abundance in IBD patients, suggesting its involvement in the pathogenesis of IBD (53–55). More recently, fungal composition and diversity in the feces of IBD patients and healthy subjects was identified and compared by ITS2 sequencing, and results showed fungal dysbiosis in IBD, with decreased *Saccharomyces cerevisiae*, increased *Candida albicans* and increased *Basidiomycota*/*Ascomycota* ratio (56). Interestingly, genotype–fungal microbiota analysis implied that genes could influence the intestinal fungal dysbiosis in IBD (56). A latest multi-omics study revealed fungi-related and bacteria-related metabolomics profiles in CD patients charactered by increased amino acid degradation and specific fecal volatile organic compounds (VOCs) (57). Murine colitis models, as a counterpart to human IBD, also showed alterations in intestinal fungal communities (58). Compared with normal controls, dextran sulfate sodium (DSS)-induced colitis mice showed increased *Candida*, *Penicillium*, *Wickerhamomyces*, *Alternaria* whereas decreased *Cryptococcus*, *Phialemonium*, *Wallemia* (58).

Intestinal fungi play a dual role in intestinal inflammation. The most commonly observed intestinal commensal fungal species *Candida albicans* has been shown to contribute to the development of IBD. *Candida albicans* could induce anti-*Saccharomyces cerevisiae* antibodies (ASCA), a biomarker of CD (59, 60). Other researchers then showed that gut inflammation greatly promoted *Candida albicans* colonization in mice, and *C. albicans* exacerbated DSS-colitis in turn (61). In fact, *Candida* could delay healing in trinitrobenzene sulphonic acid (TNBS)-induced mouse colitis model, and antifungal fluconazole therapy or probiotic lacidofil treatment during *Candida* infection could help the restoration of colonic damage during colitis (62). Besides, in chronic recurrent DSS-colitis, intestinal fungi can also harmfully translocate into abnormal sites (e.g., colonic mucosa, mesenteric lymph nodes and spleen) and aggravate disease (58). Intriguingly, gut fungal dysbiosis also had persistent effects on local and peripheral immunity and lead to exacerbated allergic airway disease (63), later study demonstrated the mechanism was mediated by $CX3CR1^{+}$ mononuclear phagocytes (64).

However, fungi also exhibit a protective function. For example, *Saccharomyces boulardii* acts as a probiotic yeast to suppress intestinal colonization by *Candida albicans*, suppress intestinal inflammation and facilitate mucosal restoration by regulating VEGFR signaling and angiogenesis (65, 66). What's more, fungi can interact with intestinal bacteria to ensure a balance between fungi and bacteria. Compared with normal control, the depletion of fungi lead to aggravated DSS-induced mouse colitis, which is associated with substantial alterations in mucosal bacterial composition, for example, *Bacteroides* and *Lactobacillus* increased while butyrate-producing *Clostridia* XIVa and *Anaerostipes* reduced (58). Some strains from clusters IV, XIVa and XVIII of *Clostridia* are benefical to the host, and oral administration of them can ameliorate mice colitis, because these bacteria lack prominent virulence and have been proven to provide a TGF-β-rich environment to promote the growth and differentiation of anti-inflammatory cells and the upregulation of anti-inflammatory molecules, especially regulatory T cells (Treg) and IL-10 (67). Interestingly, commensal bacteria depletion leads to susceptibility to colitis, and intestinal mono-colonization with single species of fungi (*Candida albicans* or *Saccharomyces cerevisiae*) can overturn this susceptibility (68). That means commensal fungi can exhibit equivalent protective benefits just as the commensal bacteria do, through providing tonic microbial stimulation, protecting against mucosal injury and elaborately tuning the responsiveness of circulating immune cells (68). Persistent fungal intestinal colonization and the mannans structure of fungal cell wall are required for the beneficial role of commensal fungi (68). The protective effects of commensal fungi may partly explain why antifungal treatment exacerbates colitis in wild-type mice (63).

As discussed above, CLRs function as the most important PRRs that regulate antifungal immunity. The maintenance of intestinal homeostasis requires the role of CLRs, thus responding to the pathogenic microorganisms and tolerating the normal intestinal commensal flora. The following will introduce the effects of several classic CLRs signaling pathways on intestinal immunity and IBD (**Figure 1**).

Dectin-1

As one of the most well-researched CLRs, Dendritic cell-associated C-type lectin-1 (Dectin-1) is a membrane protein, consisting of a hemITAM-containing cytoplasmic tail, transmembrane region, a stalk and extracellular CTLD (27, 29). Originally identified as a dendritic cell receptor in the mouse through subtractive cDNA cloning (29), Dectin-1 is now known to be present on various kinds of cells in human and mice, including monocytes, macrophages, neutrophils, eosinophils (69), B cells (69), some subgroups of T cells (69), bronchial epithelial cells (70), and intestinal epithelial cells (32), demonstrating that Dectin-1 is not a myeloid restricted CLRs (**Table 1**).

Atypically, Dectin-1 recognize carbohydrate in a Ca^{2+}-independent manner (71). Dectin-1 can recognize β-1, 3-glucans derived from diverse sources, including plants, bacteria and nearly all fungi (e.g., *Pneumocystis carinii*, *Candida albicans*, and *Aspergillus fumigatus*) (71–75). Particulate but not soluble β-glucans can activate Dectin-1 through forming Dectin-1-clustered synapse-like structures and excluding tyrosine phosphatases at β-glucan contact sites (76). Then Dectin-1 mediates signaling pathways through Syk, CARD9/Bcl-10/MALT1 complex and sometimes noncanonical caspase-8, to induce phagocytosis, production of reactive oxygen species (ROS) and maturation of IL-1β, which is important for protective immune responses (76, 77). In addition to be coupled with Syk, Dectin-1 can induce helper T cell (Th cell) differentiation and immune responses through another independent signaling pathways *via* serine-threonine kinase Raf1 (78). Besides, Dectin-1 also have endogenous ligand vimentin, which contributes to the pathogenesis of atherosclerosis (79).

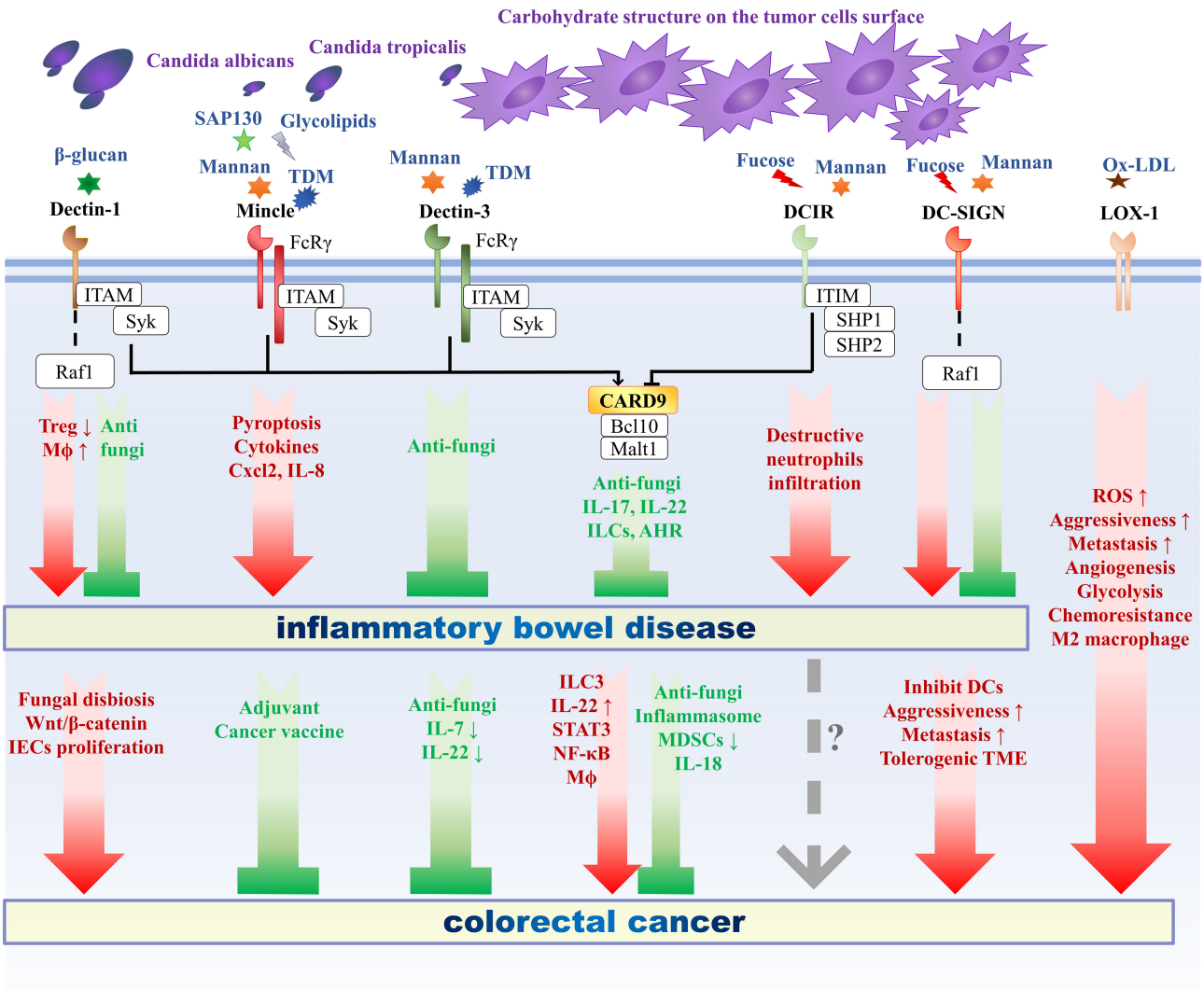

FIGURE 1 | The role of C-type lectin receptors in intestinal inflammation and oncogenesis. The role of C-type lectin receptors in intestinal inflammation and oncogenesis. CLRs include different categories, among which Mincle and Dectin-3 belong to ITAM-coupled CLRs, Dectin-1 belongs to hemITAM-bearing CLRs, DCIR belongs to ITIM-containing CLRs, and DC-SIGN and LOX-1 belong to ITAM-ITIM independent CLRs. CARD9 functions as a crucial adaptor molecule downstream of various CLRs. Upon ligation with ligands derived from fungi or cancer, different CLRs initiate different signal transduction pathway and following immune responses, thus exerts different roles in the pathogenesis of inflammatory bowel disease and colorectal cancer. Mincle and DCIR exacerbate IBD, Dectin-3 and CARD9 prevent IBD, while Dectin-1 and DC-SIGN can both exacerbate and ameliorate IBD. As for CRC, Mincle and Dectin-3 play a protective role against tumor progression, Dectin-1, DC-SIGN and LOX-1 deteriorate CRC, CARD9 plays a dual role, and the role of DCIR in CRC remains unclear. CLRs, C-type lectin receptors; ITAM, immunoreceptor tyrosine-based activating motif; hemITAM, hemi-ITAM; ITIM, immunoreceptor tyrosine-based inhibitory motif; TME, tumor microenvironment; AHR, aryl hydrocarbon receptor; Mϕ, macrophage; ROS, reactive oxygen species; DC, dendritic cell; MDSC, myeloid-derived suppressor cell; IEC, intestinal epithelial cell; ILC, innate lymphoid cell; Treg, regulatory T cell.

Dectin-1 plays pleiotropic functions in the intestinal mucosa barrier to defense against pathogens invasion. Intestinal epithelial cells (IECs) provide the biggest contact area to interact with luminal abundant antigens, and has been proven to express the β-glucan receptor Dectin-1 and other downstream adaptor proteins (32). Based on Dectin-1 dependent pathway, human IECs respond to intestinal β-glucans stimulation through secretion of multiple cytokines and chemokines (e.g., IL-8 and CCL2), emphasizing the significance of CLRs-mediated interactions between fungi and non-myeloid cells such as IEC (32). In addition to mechanical defense function, intestinal mucosa also contains many types of biologically active substances, such as mucin glycoproteins, secreted immunoglobulins (sIgA and IgG), which is also related to Dectin-1. Besides physically separating intestinal epithelia and the luminal microbiota or food to protect mucosa barrier, the dense mucus layer also prevents intestinal inflammation and enhances oral tolerance by mucin MUC2-mediated formation of

galectin-3 (Gal-3) -Dectin-1-FcγRIIB complex, which inhibits NF-κB activation, downregulates pro-inflammatory cytokine and imprints DCs with anti-inflammatory characters (80). The molecular basis is that the N-glycan structures of Dectin-1 as well as SIGN-R1 can be recognized by Gal-3 (81). Another study found that Dectin-1 that is expressed on microfold cells also mediate the intestinal reverse transcytosis of secretory IgA (SIgA) to transport from lumen to the gut-associated lymphoid tissue (GALT) (82).

Though it has not been fully studied, some researchers have recognized that Dectin-1 is also involved in adaptive immunity in the gastrointestinal tract. Both *in vitro* and *in vivo*, Dectin-1-Syk-CARD9 signaling has been implicated to connect the innate immunity and adaptive immunity *via* promoting the maturation of DCs, the secretion of proinflammatory IL-6, TNF, IL-23, and the differentiation of IL-17-producing Th-17 cells (83). It is noteworthy that Dectin-1-induced protective Th17 responses are critical in the human mucosal antifungal defense responses, for example distinguishing between colonizing and invasive *Candida* based on their morphological transition from yeast to hyphae (84). However, uncontrolled Th17 activation and polarization also contribute to pathogenic inflammatory conditions, such as IBD and colitis-associated cancer (85). In addition, Dectin-1 is required for driving intestinal fungal-specific $CD4^+$ T-cell immune responses during fungal infection in mice, and the deficiency of Dectin-1 leads to substantially aberrated $CD4^+$ T responses in the mesenteric lymph nodes with increased T cell apoptosis and defective T cell activation (86).

Dectin-1 exerts protective function, whose deficiency strongly influence susceptibility to intestinal inflammation. An early classic study demonstrated that Dectin-1-deficient mice showed more susceptibility to colitis when treated with DSS, as a result of impaired immune responses against specific commensal fungi companied by increased opportunistic pathogenic fungi such as *Candida* and *Trichosporon*, whereas decreased nonpathogenic *Saccharomyces* (87). After supplementing with an opportunistic pathogen *Candida tropicalis*, Dectin-1-deficient mice exhibited more aggravated colitis and increased pro-inflammatory molecules (such as IFN-γ, IL-17, IL-23p19, TNF-α) in contrast to wild-type mice, but supplementing with nonpathogenic fungus *Saccharomycopsis fibuligera* did not contribute to mouse colitis (87). Inhibiting fungal dysbiosis with antifungal treatment (fluconazole) could ameliorate colitis in Dectin-1-deficient mice (87). Interestingly, the altered gastrointestinal and vaginal mucosal antifungal immunity induced by Dectin-1 deficiency is also affected by the genetic background of the host, because of different canonical or noncanonical signaling pathways downstream of Dectin-1 in distinct mouse strains (C57BL/6 and BALB/c) leading to diverse immune responses (88). In humans, there is evidence that Dectin-1 expression is upregulated on various immune cells that take part in the intestinal inflammation, such as macrophages and neutrophils, which results in the overexpression of Dectin-1 in inflamed colon tissues in both IBD and diverticulitis patients (89). And the polymorphism of human Dectin-1 gene is strongly correlated to medically refractory UC (87). Besides, defective expression and function of Dectin-1 on monocyte also promote systemic lupus erythematosus, rheumatoid arthritis and many inflammatory diseases (90).

Intriguingly, Dectin-1 actually serves as a double-edged sword. In mouse arthritis model, the stimulation of Dectin-1 by β-glucan causes inflammatory cells and cytokines responses and is harmful to the host (91). What is more, because Dectin-1-induced anti-microbial peptides could inhibit *Lactobacillus murinus* growth, the deficiency of Dectin-1 can elevate the abundance of *Lactobacilli* in the mice gut, which promote regulatory T cell (Treg) development and consequently suppress the development of colitis induced by DSS or $CD45RB^{high}CD4^+$ T cell (92). Besides, there is a similar pattern existing in humans. *Lactobacillus salivarius*, which is closely related to *L. murinus*, has been demonstrated to decrease in the intestinal flora of IBD patients, and *L. salivarius* also induce the upregulation of anti-inflammatory TGF-β and IL-10 in intestinal immune cells just like the *L. murinus* do (92). These observations point out the important role of Dectin-1 in balancing intestinal proinflammatory immunity and anti-inflammatory immunity through adjustment of commensal microbiota. A latest study also found that experimental colitis was attenuated in mice with Dectin-1-deficient myeloid cells, while the deficiency of mannose receptor (MR) exacerbates colitis (93). Through the elevated production of chemokine CCL2, Dectin-1 promotes the enrichment of $Ly6C^{high}CCR2^{high}$ monocyte subset in the blood and their infiltration to the inflamed colon tissue, thus contributing to the proinflammatory profile of intestinal macrophages during colitis (93). Furthermore, both overexpression of Dectin-1 and reduction of MR expression are associated to colonic inflammation in IBD biopsy specimens (93).

In addition to intestinal microbiota, the ingredients in daily foods may contain ligands for Dectin-1, which also affects intestinal inflammation. Because of the Dectin-1/IL-17F/anti-microbial peptides (calprotectin) axis, β-glucans components from food can modulate the expansion of commensal bacterium *L. murinus* to influence the Treg expansion in mice (94). Therefore, β-glucan-free diet alleviates the mouse colitis, with significantly decreased infiltration of inflammatory cells in colonic epithelia or lamina propria compared to normal diet (94). While laminarin, a Dectin-1 antagonist derived from brown algae kombu, have been proven to ameliorate the mouse DSS-colitis through intestinal *L. murinus* expansion and Treg accumulation (92). Interestingly, the effects of Dectin-1 antagonist in experimental mouse colitis are similar to other observations of Dectin-1-deficiency and β-glucan-free food (92, 94). Therefore, these studies indicate the important role of diet and Dectin-1 in intestinal inflammation, which inspire a new idea to prevent IBD by developing beneficial foods.

Both excessive Dectin-1 inhibition and excessive Dectin-1 activation lead to aggravated colitis because of uncontrolled fungal invasion or the suppression of anti-inflammation responses respectively (92). Overall, a delicate balance between agonist and antagonist for Dectin-1 is important for intestinal homeostasis.

Mincle

After exposure to various stimuli, macrophage inducible C-type lectin (Mincle) is mainly upregulated on macrophages (18). Mincle commonly acts as an activating receptor that couples with the ITAM-containing FcRγ, and initiates a downstream signaling pathway through Syk recruitment, CARD9/Bcl-10/MALT1 complex formation, and NF-κB activation to induce immune responses including the production of cytokines and chemokines and the recruitment of inflammatory cells (18, 41, 95).

Mincle possesses the capacity to recognize plenty of PAMP and DAMP (**Table 1**) (95). PAMP, such as α-mannan and various glycolipid, can be derived from versatile microbial pathogens and commensals. For example, glycolipid in mycobacterial cell wall whose chemical structure is trehalose-6,6'-dimycolate (TDM), can be recognized by Mincle (96). After ligation, TDM can induce the upregulation of Mincle (97). Mincle is essential for TDM-induced immune responses, such as inflammatory cytokines production and granuloma formation (96). DAMP include cholesterol sulfate (19), cholesterol crystals (20), β-glucosylceramides (β-GlcCer) (98), and spliceosome-associated protein 130 (SAP130) (18), which is released upon cell death.

The role of Mincle in mucosal barrier function and intestinal immunity has only been revealed in recent years. Murine Mincle is responsible for the commensal-detecting function of the intestinal Peyer's patches to regulate interleukin-17 (IL-17) and interleukin-22 (IL-22) production from innate lymphoid cells (ILC) and T cells, ensure the production of many intestinal antimicrobial proteins (e.g., RegIIIγ, IgA), and eventually restrict aberrant microbial translocation (99). Besides, another study revealed the importance of a $CX3CR1^+$ gut-resident mononuclear phagocytes (MNPs), which are a subset of phagocytes equipped with a high expression of genes involved in fungal recognition (including Mincle, Dectin-1, and Dectin-2). It function as a novel mediator of the interactions between fungal community and host intestinal immunity in a Syk-dependent manner (100). Consistent with the observation that $CX3CR1^+$ MNPs-depleted mice exhibit gut microbiota alteration and severe DSS-induced colitis, the CX3CR1 gene missense mutation in CD patients is associated with impaired antifungal antibody responses (100). Furthermore, compared with CD remission patients and health controls, the serum levels of SAP130, a classic DAMP of Mincle, is significantly increased in active CD patients (101). Meanwhile, both SAP130 and Mincle in colon tissues of active CD patients is upregulated, which provide a promising biomarker to monitor the severity of CD and the clinical efficacy of treatment (101).

Then a latest study further illustrates a direct link between Mincle signaling and intestinal inflammation (102). Biopsies from CD patients, DSS-induced mouse colitis model and TNBS-induced mouse colitis model consistently suggest that increased expression of Mincle is correlated to inflammation severity. The immune cells that predominantly express Mincle during inflammation are proven to be macrophages in intestinal lamina propria. After damaged tissues produce SAP130, the activated Mincle signaling in macrophage not only leads to inflammatory cytokines release through macrophage pyroptosis, but also recruits neutrophils through the production of chemokines (e.g., Cxcl2 and IL-8). Deficiency of Mincle or inhibition of its downstream Syk both ameliorate experimental colitis by restricting macrophage pyroptosis and limiting the release of proinflammatory cytokines and chemokines. Conversely, when adding a synthetic analog of TDM to bind and activate Mincle, the disease is deteriorated, highlighting that the Mincle/Syk axis is a novel target for the therapeutics of CD. In addition to anti-Mincle neutralizing antibody which has been shown to improve experimental colitis, effective agent to inhibit Mincle hasn't been developed till now, which is worth exploring.

Dectin-3

Macrophage C-type lectin(MCL, Dectin-3) is a transmembrane CLR expressed on macrophages (103), monocytes, neutrophils and DCs. Tumor necrosis factor (TNF) can upregulate Dectin-3, Mincle, and Dectin-2 in macrophages (104). Dectin-3 is also linked to FcRγ (35), and acts as an activating receptor capable of initiating immune signaling pathway *via* Syk, CARD9 and NF-κB, which is important for antimicrobial defense, phagocytosis, cytokine expression, and respiratory burst (105, 106).

Dectin-3 can selectively bind α-mannans derived from diverse fungi (e.g., *Candida albicans*, *Paracoccidioides brasiliensis*) and lead to NF-κB activation and defense response (107, 108). Dectin-3 also recognizes TDM of *Mycobacterium tuberculosis* (**Table 1**) and induces Mincle expression upon TDM stimulation (35). Dectin-3 can cooperate with Dectin-2 to form a heterodimeric PRR, which binds α-mannans more potently comparted to their homodimers, thus inducing powerful inflammatory response against fungi (107). Besides, Dectin-3 can also form heterodimer with Mincle (109), implying that various heterodimers and homodimers formed by distinct CLRs greatly elevate the sensitivity and expand the diversity required for monitoring a wide range of microbial infections (107).

In addition to deteriorating experimental autoimmune encephalomyelitis (110) and systemic lupus erythematosus (111), Dectin-3 was initially found a limited role in regulating intestinal immunity (112), while later research revealed that Dectin-3 was also significant in intestinal homeostasis through interplaying with commensal fungi. The deficiency of Dectin-3 leads to more susceptibility to DSS-induced mouse colitis, with an obviously increase of specific fungal burden and microbial translocation, especially a common commensal *Candida tropicalis* (113). Administration with *Candida tropicalis* only worsens colitis in Dectin-3-deficient mice, because Dectin-3 deficiency impedes NF-κB activation, which leads to defects in cytokine production, epithelial restitution, macrophage phagocytosis during fungal invasion (113). When treated with antifungal therapy, intestinal inflammation can be effectively suppressed in Dectin-3 deficient mice (113). Furthermore, a latest study found that a negative regulatory factor downstream of Dectin-2 and Dectin-3 signaling pathways, E3 ubiquitin ligase c-Cbl, is also involved in regulating intestinal fungi-induced inflammation (114). Commensal fungi-derived mannans can

facilitate the transcription of gene *il10* and the expression of anti-inflammatory cytokine to decrease susceptibility to colitis in wild-type mice through activating Dectin-2, Dectin-3 and their downstream c-Cbl in DCs (114). However, c-Cbl deficiency leads to activation of noncanonical NF-κB subunit RelB during mannan stimulation, which suppresses canonical NF-κB subunit p65-mediated *il10* transcription, thus eventually exacerbating DSS-induced mouse colitis (114).

DCIR

Dendritic cell (DC) immunoreceptor (DCIR) is expressed on DCs, monocytes, macrophages, granulocytes, NK cells, B cells and activated T cells (**Table 1**) (38, 115, 116), and contains a single CRD and an intracellular ITIM (116). The expression of DCIR on DCs relies on their origin and developmental stage, for example, the down-regulation of DCIR is associated with stimuli that induce DCs maturation (e.g., LPS, TNF-α) (116).DCIR is mannose/fucose-binding lectin, which can interplay with both microbial and endogenous ligands (117). Interestingly, DCIR also interacts with HIV-1 and contributes to viral infection (118). The interaction between DCIR and ligands was substantially affected by the glycosylation of the CRD domain in DCIR (117, 119). The special cytoplasmic ITIM of DCIR is responsible for transducing immunoregulatory signals *via* recruiting SHP-1 and SHP-2 (27). DCIR signaling not only suppresses the TLR8-induced production of IL-12 and TNF-α in myeloid DCs but also inhibits the TLR9-induced expression of IFN-α in plasmacytoid DCs (120, 121). Besides, DCIR suppresses the function of $CD8\alpha^-$ conventional DCs (cDCs), and the deficiency of DCIR results in TLR-mediated hyperinflammation and reinforced T cell responses against microbes (122).

DCIR may play a different and even opposite role in different inflammatory processes. In addition to ameliorating autoimmune arthritis (123) and exacerbating brain inflammation (124), DCIR also take part in the pathogenesis of IBD. Compared to wild-type mice, there is only a little exacerbation of intestinal inflammation in DCIR-deficient mice in an early study using DSS-induced murine colitis model, hinting an insignificant role of DCIR in intestinal homeostasis (112). However, another murine experiment shows that DCIR1 deficiency is associated to decreased accumulation of neutrophils that shows destructive characteristics and reduced neutrophil-recruiting chemokine MIP-2 in DSS-induced colitis (125), and massive infiltration of neutrophils is known to be associated with the pathogenesis of ulcerative colitis (126) and DSS-induced mice colitis (127). In summary, current studies on the relationship between DCIR and colitis are not sufficient, and the results are not convincing, so further exploration is needed in this field.

DC-SIGN

Another well-studied CLRs, Dendritic cell-specific intercellular adhesion molecule-3-grabbing non-integrin (DC-SIGN) is mainly expressed on human DCs and macrophages. DC-SIGN on DCs and ICAM-3 on T cells mediate intercellular contact and stabilize their contact zone, which is important for T cell immune response (31). Unlike the CLRs described above, DC-SIGN don't contain evident ITAM or ITIM domains, but the stimulation of DC-SIGN by various pathogens can regulate TLR signaling *via* serine and threonine kinase Raf-1 and resulting in subsequent acetylation of the NF-κB subunit p65 (128). With prolonged NF-κB transcriptional activity and elevated *il10* transcription rate, acetylation of p65 facilitate anti-inflammatory cytokine responses (128).

DC-SIGN is Ca^{2+} dependent fucose/mannose binding lectin (**Table 1**), and these carbohydrate structures are abundantly expressed by many exogenous pathogens and endogenous ligands. Exogenous ligands consist of virus, helminths, bacteria and fungi, such as HIV-1 (129), *Schistosoma mansoni (*130), *Mycobacterium tuberculosis (*130), *Helicobacter pylori (*130), *Pseudomonas aeruginosa (*131), and *Candida albicans (*132). DC-SIGN is critical for DCs responses against pathogens, with different pathogens interacting with DC-SIGN to modulate different TLRs signaling (128). Interestingly, the recognition of mannans by host has been demonstrated to exhibit quite a few functional redundancies with various PRRs involved, such as TLR2, TLR4, Mincle, Dectin-3, Dectin-1 and DC-SIGN. While different *Candida* spp. rely on different kinds of mannan-detecting PRRs, because of disparate mannan composition in fungal cell wall (133).

In addition, various endogenous ligands, including ICAM-3 (31), ICAM-2 (134), Mac-1 (135, 136), Mac-2BP (137), MSPL/TMPRSS13 (138), CEA (139, 140) and CEACAM1 (136), have been reported to take part in intercellular recognition and interaction *via* DC-SIGN (**Table 1**). Interestingly, oncogenesis causes altered glycosylation in tumor cells and elevates the presence of DC-SIGN-binding carbohydrate on tumor associated antigens, such as carcinoembryonic antigen (CEA) (139, 140). Although many of these ligands of DC-SIGN also bind DCIR, there is DC-SIGN-specific ligands, such as *Candida albicans* and glycoproteins on certain cancer cells (117).

Several animal experiments have discovered that mouse homologs of human DC-SIGN take part in the development of colitis. After the administration with DSS, SIGN-R1-deficient mice are more resistant to colitis and exhibit less severe intestine injury and lower expressions of proinflammatory cytokines than wild-type mice, which is associated with defective macrophage responsiveness to commensal lipopolysaccharide (LPS) stimulation (141). Furthermore, SIGN-R1 and TLR4 acts synergistically to regulate intestinal inflammation (141). In contrast, another murine homolog SIGN-R3 can recognize carbohydrate ligands on commensal fungi, and the SIGN-R3-deficient mice exhibit more severe colitis symptoms (such as weight loss and diarrhea) with increased TNF-α production in colon compared to wild-type mice (142). Besides, it's worth noting that SIGN-R3 contains hemITAM signal motif, while both DC-SIGN and SIGN-R1 belong to ITAM-ITIM-independent CLRs (27). Interestingly, a recent finding shows that the interaction between surface layer protein A (SlpA) in food-grade probiotics *Lactobacillus acidophilus* and murine SIGN-R3 protects intestinal mucosal barrier, prevents dysbiosis, promotes colonic regulatory signaling and finally

helps to mitigate experimental colitis, while these protective roles don't exist in SIGN-R3-deficient mice (143).

THE ROLE OF CLRS IN INTESTINAL CARCINOGENESIS

Inflammation can facilitating neoplastic progression by contributing to multiple hallmark capabilities of tumor (144). To be specific, inflammation can supply various bioactive molecules to the tumor microenvironment (TME), including proangiogenic factors, growth factors, survival factors, mutagenic reactive oxygen species, epithelial-mesenchymal transition (EMT) activation signals, and extracellular matrix-modifying enzymes that facilitate metastasis. Furthermore, as an essential downstream signal of numerous CLRs, NF-κB also functions as an important bridge between inflammation and carcinogenesis (145).

The close relationship between inflammation and cancer is particularly prominent in colorectal cancer (CRC). As the third most common malignancy, CRC causes a vast amount of cancer-related death around the world (146). Chronic colonic inflammation in UC or CD patients is a well-recognized risk factor for colon carcinogenesis (147, 148). Unlike sporadic CRC that progresses based on precancerous lesion (i.e. colorectal adenomas), colitis-associated cancer (CAC) usually progresses in an order of indefinite dysplasia, low-grade dysplasia, high-grade dysplasia, and finally carcinoma (148). Many pro-inflammatory cells and molecules in chronic inflammation have also been confirmed to influence the progression of CAC. Besides, inflammation is also involved in sporadic CRC though less understood (149). In contrast to normal colon, inflamed colon exhibits higher mutation frequency of many genes(such as tumor suppressor gene p53) under the influence of reactive oxygen and nitrogen species even before there is any evident dysplasia in tissues (150). The risk of CRC is positively related to prolonged colitis duration, severity of inflammation, extensive anatomic extent of colitis and other inflammatory comorbidity (especially primary sclerosing cholangitis), for example, CRC rarely happens in patients whose duration of IBD is less than 7 years, but the CRC risk increases year by year with the prolonged IBD duration after diagnosis (148). Whereas the risk of CRC decreases when IBD patients take anti-inflammatory agents (such as steroids) (148). A better knowledge of the pathogenesis of CRC or CAC is of great significance to define preventive, diagnostic, and prognostic protocols.

Because the intestinal fungal dysbiosis is closely involved in the pathogenesis of IBD, fungi may be also involved in the development of CRC. More exactly, the pathogenesis of CRC including CAC is closely associated with the sophisticated interplay between intestinal immune system and flora (151–153). By comparing fecal fungal microbiota (i.e. mycobiota) of colon polyp patients, CRC patients, and healthy controls, obvious fungal dysbiosis is observed in polyp and CRC groups, including decreased fungal diversity, increased *Ascomycota*/*Basidiomycota* ratio, and an increased abundance of opportunistic pathogenic fungi *Trichosporon* and *Malassezia*, implying a role of fungi in CRC (153). It should be noted that fecal microbiota is not exactly equivalent to mucosal microbiota (154). Then deep sequencing characterized the fungal profile using biopsies of adenomas and paired adjacent tissues, but healthy biopsy samples are unavailable in this study because of ethical issues (155). The results revealed that three fungal phyla, *Ascomycota*, *Glomeromycota* and *Basidiomycota* were dominant in all biopsy samples, and two rare phyla, *Chytridiomycota* and *Neocallimastigomycota* are present in partial samples with relative abundance less than 1% (155). Although the fungal diversity was lower in adenomas than in adjacent tissues, two opportunistic pathogenic fungal genera, *Phoma* and *Candida*, were abundant both in adenomas and adjacent tissues (155). More importantly, the fungal dysbiosis is significantly related to the size and stage of adenomas (i.e. advanced and non-advanced) (155). Likewise, a similar tendency of fungal alteration is also present in the IBD study (51, 52, 56). Interestingly, by collecting fecal and mucosal samples from CRC patients, polyps patients and healthy controls, other researchers found that bacterial microbiota dysbiosis existed not only in cancerous tissues but also in noncancerous tissues, and exhibits differences between distal CRC and proximal CRC, though there is still some confounding factor behind this result (154). By transferring human fecal microbiota to germ-free mice, a recent study found CRC-associated microbiota dysbiosis contributed to oncogenic epigenetic alterations by inducing more hypermethylated genes in murine colonic mucosa, and cumulative methylation index is an independent risk factor for CRC (156). In addition, many mycotoxins and fungal metabolites also directly promote carcinogenesis, for example, *Candida albicans* can product nitrosamine, acetaldehyde and candidalysin (157). Furthermore, a latest study has just found that not only bacterial microbiota (e.g., *Fusobacterium*) but also fungal microbiota can affect chemotherapy resistance (158). Both in CRC patients and in animal experiments, the burden of *Candida tropicalis* is significantly elevated, which can increase the resistance to oxaliplatin treatment *via* facilitating the production of lactate and inhibiting the mismatch repair system (158).

Above all, both intestinal inflammation and fungal disorders have been confirmed important roles in the pathogenesis of CRC. As a key mediator of fungal recognition and immune response, CLRs also take part in the progression and development of CRC (**Figure 1**).

Dectin-3

The impact of Dectin-3 on CAC development has just been revealed. After administration with azoxymethane (AOM) and DSS, Dectin-3-deficient mice showed exacerbated CAC tumorigenesis, increased *Candida albicans* burden and impaired immune responses compared to wild type mice (159). Furthermore, germ-free mice that is colonized with *C. albicans* shows more severe colitis and CAC during AOM-DSS administration, and treatment with antifungal fluconazole ameliorates chemically induced-CAC in Dectin-3-deficient mice (159). By carrying out a variety of experiments such as

fecal microbiota transplantation, the putative mechanism behind this phenomenon is as follows (159). The impaired fungicidal abilities of Dectin-3 deficient macrophages lead to intestinal fungal dysbiosis, especially increased *C. albicans* burden, which triggers glycolysis in macrophage to produce IL-7, then promotes innate lymphoid cells ILC3 to produce IL-22 under the control of IL-7, *Stat3* and *AhR*, and IL-22-induced p-STAT3 in intestinal epithelial cells eventually promotes CAC tumorigenesis. Consistently, a similar mycobiota/Dectin-3/IL-22 regulatory axis exists in human CRC patients. Patients with more advanced CRC tumors show significantly lower Dectin-3 expressions, and CRC patients with higher fecal fungal burden exhibit lower Dectin-3 expression, higher levels of IL-22 in tumor tissues and poorer disease-free survival and overall survival (159). What's more, Dectin-3 and Dectin-2 can also act cooperatively to limit liver metastasis by promoting Kupffer cells to phagocytize cancer cells (160).

DC-SIGN

Long time ago, researchers have realized that DCs recognize tumor-specific antigen on CRC tumor cells through DC-SIGN to affect effective antitumor responses thus helping tumor escape immunosurveillance (139, 140, 161). Malignant transformation alters the glycosylation process and causes increased levels of Lewis X and Lewis Y on tumor-specific CEA in intestinal epithelial cells(IECs), which can be selectively recognized by DC-SIGN to mediate the interaction between DCs and tumor cells, while normal IECs contains low levels of Lewis antigens on CEA thus avoiding DC-SIGN binding (139). Besides, primary CRC tissues from some patients express a novel DC-SIGN ligand, Mac-2-binding protein (Mac-2BP), which also contained special glycosylated structures (137). The interactions between DC-SIGN and CRC-specific glycosylation inhibit functional maturation and differentiation of Monocyte-Derived Dendritic Cells (MoDCs) and enhance anti-inflammatory cytokine secretions (e.g., IL-6 and IL-10), which might supply a tolerogenic microenvironment for CRC (137, 161). Interestingly, except in a glycan-dependent manner, DC-SIGN can interact with Type II Serine Protease MSPL/TMPRSS13 on CRC cells in a glycan-independent manner (138). A case-control study found single nucleotide polymorphisms (SNPs) in DC-SIGN were associated with CRC risk (162). Furthermore, CRC patients exhibit decreased serum levels of soluble DC-SIGN, thus meaning a diagnostic significance (163). Additionally, compared to normal colon tissues, the levels of DC-SIGN are higher in the tumor stroma and the invasive margin of CRC tissues, and higher levels of DC-SIGN in CRC tissues are correlated with lower serum levels of DC-SIGN from the same patient (163). Then a systematic review also proves that DC-SIGN/DC-SIGNR is one of the most promising circulating markers for CRC diagnosis (164).

A recent study has shed more light on the mechanism of how DC-SIGN affects CRC. Both infiltrated DCs and cancer cells in colon tumor tissues can express DC-SIGN, whose overexpression was closely linked with more aggressive and invasive tumor, worse prognosis and shorter metastasis-free survival in CRC patients (165). The mechanism is that DC-SIGN activation promotes the transcription of MMP-9 and VEGF *via* PI3K/Akt/β-catenin pathway and suppresses the transcription of miR-185 *via* β-catenin/TCF1/LEF1 pathway, which eventually promotes metastasis of CRC (165). The DC-SIGN signaling pathway in metastatic CRC reveals a new pathogenesis of CRC and provides new targets for blocking the invasion and metastasis of CRC. Another study demonstrated that CRC craftily take advantage of the overexpression of complex branched N-glycans to help tumor cells escape immune recognition and construct immunosuppressive microenvironment with inhibited production of IFN-γ and increased frequency of Treg (166). Intriguingly, the removal of this branched N-glycans on CRC cells could expose immunogenic glycan epitopes to enhance recognition by immune cells *via* DC-SIGN and potentiate an effective antitumor immune response (166). Besides, another member of DC-SIGN family, DC-SIGNR, could promote colon carcinoma hepatic metastasis (167).

LOX-1

The lectin-like oxidized low-density lipoprotein receptor-1 (LOX-1) is expressed by vascular endothelial cells (168), vascular smooth muscle cells, cardiomyocytes, adipocytes, platelets, monocytes, macrophages, DCs, B cells, chondrocytes (169) and intestinal cells (170) (**Table 1**), and function as a scavenger receptor (171). The low expression of LOX-1 under physiological conditions can be up-regulated by many diseases-related stimuli, such as cytokines (e.g., TGF-β1 (172), TNF-α (173)), oxidized low-density lipoprotein (oxLDL) (174, 175), angiotensin II (176), endothelin (177), asymmetric dimethylarginine (178). There is no known ITAM or ITIM in LOX-1 cytoplasmic tail, but LOX-1 can also mediate NF-κB pathway, thus implying LOX-1 utilizes other molecules for intracellular signaling transduction, which needs further elucidation (27).

LOX-1 is responsible for the recognition and adhesion of exogenous Gram-positive and Gram-negative bacteria, such as *Staphylococcus aureus* and *Escherichia coli* (179). Furthermore, Ox-LDL can bind LOX-1 and there is considerable evidence for their pathogenic role in atherosclerosis. Based on LOX-1 mediated MAPK/NF-κB pathway activation, Ox-LDL elevates the levels of LOX-1, promotes the maturation and differentiation of DCs and induces a proinflammatory cytokine profile (174, 175). Heat shock proteins(HSP) also bind to LOX-1, and anti-LOX-1 antibody impedes such ligation thus inhibiting HSP-induced antigen cross-presentation (40). In addition, oxidized high-density lipoprotein (ox-HDL), phosphatidylserine (PS), apoptotic bodies, advanced glycation end-products (AGEs), and platelets all acts as LOX-1 ligands (**Table 1**).

LOX-1 has attracted much attention in the cardiovascular field. Altered expression of LOX-1 is linked to risks of various metabolic diseases, for example, atherosclerosis, hyperlipidemia, diabetes, obesity (180). Besides, soluble LOX-1(sLOX-1) can be released to serum after proteolytic cleavage, which acts as a promising non-invasive biomarker for many diseases such as type 2 diabetes mellitus (181). Uniquely, LOX-1 signaling also takes part in humoral responses by triggering DC-mediated

class-switched B cell to promote antibody responses and changing expressions of chemokines to facilitate B cell migration (182).

More importantly, there is a close link between metabolic dysfunction and malignant tumor with LOX-1 involved in. The prevalence of CRC is higher in patients with coronary artery disease (183) and treatment with statins, an effective lipid-lowering agent, can efficiently reduce the risk of CRC (184). Besides, increased human serum ox-LDL levels not only contribute to atherogenesis, but also correlate to increased risk of CRC (185, 186). As proven by experiments using developmentally diverse cancer cell lines, LOX-1 is crucial for maintaining the growth and transformation of tumor through NF-κB-mediated inflammatory and hypoxia responses (187). Ox-LDL binding to LOX-1 promotes the accumulation of reactive oxygen species (ROS), which contributes to the development and progression of various neoplasia, including CRC tissues (185, 188). Above all, LOX-1 is a crucial molecular bridge to connect cancers with various metabolic diseases.

More direct evidence suggests that human CRC tissues produce excessive ox-LDL and strongly upregulate LOX-1, and the overexpression of LOX-1 correlates to highly aggressive and metastatic human CRC, while metastasis and recurrence are leading causes of CRC mortality (189). The *in vitro* knockdown of LOX-1 in CRC cells impairs proliferation rate, hinders the maintenance of tumorigenicity and influences the presence of peculiar volatile organic compounds (VOCs) (189). Subsequent study using two different xenografting procedures in mice (subcutaneous and endovenous) further revealed that LOX-1 silencing affects not only the engraftment of the tumor but also the development of metastasis, where angiogenesis takes a crucial role (190). And LOX-1 also affects gene transcription through epigenetic regulation such as different histone acetylation pattern (190). The latest study that uses human CRC tissues and CRC xenograft mouse model also found the glycolytic metabolism and chemoresistance of CRC tissues were regulated *via* the upregulation of LOX-1/c-MYC/SULT2B1 axis, and the knockdown of LOX-1 downregulated SULT2B1 *via* c-MYC thus repressing glycolytic metabolism to inhibit the proliferation and chemoresistance of CRC (191). Consistent with these investigations, another recent study reported for the first time that higher serum LOX-1 levels of CRC patients determine poorer overall survival and worse prognosis (192). Serum LOX-1 actually represents an independent prognostic factor and positively correlates with many inflammatory factors, at the same time, patients with high LOX-1 expression in CRC tumor tissues also showed poor prognosis (192). LOX-1 has also been identified as a crucial player in immunosuppression in tumor microenvironment. Neutrophils with high expression of LOX-1 shows similar characteristics of myeloid-derived suppressor cell (MDSC) and exerts powerful immunosuppressive effects such as the inhibition of T cell proliferation, which contributes to the progression and recurrence of glioblastoma (193, 194).

Intriguingly, another recent study found that lower levels of LOX-1 and $CD8^+$ cytotoxic T lymphocyte (CTL) in tumor stroma were related to worse prognosis in CRC patients (195). The researchers speculated that the reasons for this phenomenon is that the CRC stromal cells that express LOX-1 were mostly $CD163^+$ M2 macrophages, whose infiltration in stroma was beneficial for CRC prognosis while harmful for several other cancers (195). Whether LOX-1 expression influences the quantity and quality of M2 macrophages in CRC microenvironment thus influencing the efficacy of anti-tumor immunity needs further evidences to elucidate.

In summary, LOX-1 not only provides an environment that facilitates tumor progression and invasion, but also mediates immunosuppressive signals to help tumor cells escape from immunosurveillance. Although there are still problems that have not been fully clarified, the current researches point out the potential to utilize LOX-1 as therapeutic target to inhibit CRC tissues growth and metastasis and repress chemoresistance. In addition, the identification and characterization of peculiar VOCs that is induced by LOX-1 may provide a simple, convenient and non-invasive biomarker for CRC diagnosis and monitoring.

Other CLRs

Although the role of Mincle in the relationship between intestinal fungal dysregulation and CRC is unclear, the ligands of Mincle hold great potential for the development of new cancer vaccine, such as promoting the lysis of mouse CRC cells (196) and enhancing the maturation and migration of DCs to trigger anti-tumor effect in CRC (197). As for Dectin-1, a recent study found that the significantly increased *Candida albicans* in the guts of CRC patients can induce the proliferation of the human intestinal epithelial cells through the Dectin-1 mediated Wnt/β-catenin signaling thus contributing to CRC development (152). But the precise effect of Dectin-1 on CRC is largely unsure.

THE ROLE OF DOWNSTREAM ADAPTOR CARD-9 IN INTESTINAL INFLAMMATION AND CARCINOGENESIS

Caspase recruitment domain 9 (CARD9), a caspase recruitment domain-containing signaling protein, functions as a central adaptor molecule to transduce the signaling of ITAM-coupled or hemITAM-bearing CLRs (e.g., Dectin-1, Dectin-2, and Mincle) in the immune response to fungi (198, 199). CARD9 not only mediates CLRs signaling by coupling the activation of Syk to the regulation of NF-κB pathway, but also widely take part in the integration of signals downstream of other PRRs, such as NLRs and TLRs (198, 199). CARD9 signaling molecule is a major player in both innate immunity and adaptive immunity to react against various pathogens properly, including fungi, bacteria, and viruses. Therefore, CARD9 is associated with many inflammatory disorders. For example, human CARD9 deficiency contributes to chronic mucocutaneous candidiasis (200) and invasive *Candida* infections in the central nervous system or digestive tract (e.g., meningoencephalitis, colitis) (201).

CARD9 is a key downstream regulatory molecule to maintain the intestinal homeostasis *via* regulating host immune system

and the intestinal flora. Many genome-wide association studies all found that CARD9 polymorphism was strongly related to CD and UC (202–204). Experiments on mice showed that CARD9-null mice had difficulty in recovering from epithelial damage with impaired production of cytokines including IL6, IL-17 and IL-22 when treated with DSS (205). And CARD9 deficiency was associated with suppressed Th17 and innate lymphoid cells (ILCs) in murine colon during *Citrobacter rodentium* infection, suggesting that CARD9 participates in an effective defense response against *C. Rodentium (*205). In addition, CARD9-null mice showed more susceptibility to colitis companied by strongly elevated fungal burdens and altered intestinal fungal composition (e.g., increased *Candida tropicalis*), which is partially due to impaired fungicidal functions of CARD9-null macrophages, thus implying an inability to accurately control intestinal fungal community is involved in the deteriorated colitis of CARD9-null mice (205–207). What is more, CARD9 gene also affects intestinal inflammation through modulating the production of microbial metabolites. Transferring the intestinal flora from CARD9-null mice to wild-type germ-free mice is proven to promote colitis and reduce IL-22 production, because the microbiota in CARD9-null mice is unable to metabolize tryptophan into the ligands of aryl hydrocarbon receptor (AHR) (207). AHR is important for inducing IL-22 production (208), a critical cytokine for the maintenance of intestinal homeostasis (209). Therefore, supplement with tryptophan-metabolizing *Lactobacillus* strains or treatment with AHR agonist is effective to attenuate intestinal inflammation (207). Consistently, both CD and UC patients shows reduced AHR ligands and defective AHR activation in their microbiota, especially for patients with CARD9 risk alleles (207). Furthermore, IBD patients with CARD9 risk alleles shows more abundant *Malassezia restricta* in the gut, which usually exists as a skin commensal fungus (210). In germ-free mice with or without bacteria colonization, increased levels of *M. restricta* alone are enough to directly exacerbate colitis, because *M. restricta* can elicit a strong proinflammatory response in a CARD9-dependent manner, implying the potential to utilize specific commensal fungi as a therapeutic target for IBD (210).

Syk-CARD9 signaling mediates a protective role in the interplay between fungal microbiota and CAC. CARD9-null mice significantly altered microbial profile, which is associated to CAC (206, 211). Upon administration with AOM-DSS, CARD9-null mice are proven to be more susceptible to CAC, whose mechanism is that defective fungicidal functions of Card9-null macrophages lead to fungal dysbiosis (especially increased *Candida tropicalis*), and *C. tropicalis* increases the number of intestinal MDSC and activates the function of MDSC (206). Antifungal treatment (fluconazole) can ameliorate CAC in CARD9-null mice together with decreased accumulation of MDSC (206). Similarly, CRC patients shows higher proportion of *C. tropicalis* and patients with higher levels of fecal fungal burden exhibit increased MDSCs in their blood and colon tissues (206). Likewise, mouse Lewis lung cancer model revealed a noncanonical CARD9/NF-κB/IDO pathway, which can limit tumor progression through inhibiting the immunosuppressive capacity of MDSCs (212). In addition to MDSCs accumulation, the deletion of CARD9 or Syk also increases susceptibility to colitis and CAC in mouse model because of another protective mechanism, microbiota/Syk/CARD9/IL-18 axis, where commensal fungi promote the activation of inflammasome and the maturation of IL-18 in a CARD9-dependent manner to influence the restitution and maintenance of intestinal epithelial barrier and the production of IFN-γ (211). Treatment with amphotericin B (AmpB) to deplete commensal fungi in wild type mice can exacerbated CAC while supplementation with IL-18 or wildtype myeloid cells in CARD9-null mice can ameliorate CAC (211).

However, CARD9 has also been shown promoting tumor effects in various types of malignant diseases, including CAC. CARD9 can promote CAC *via* CARD9/IL-1β/IL-22 axis and the IL-22 production can promote tumorigenesis *via* epithelial STAT3 activation (213). Furthermore, another study also found that CARD9 promoted liver metastasis of CRC tissues through metastasis-associated macrophage polarization *via* NF-κB pathway activation (214). Interestingly, using the mouse model of human familial adenomatous polyposis (FAP), CARD9 is revealed to exacerbate intestinal neoplasia in a sex-biased manner where male mice showed reduced viability, more tumor burden and more immune cells infiltration, implying gender differences in human CRC may involve CARD9-dependent inflammation (215).

PROSPECTIVES

Fungal dysbiosis and related immune responses contribute to the pathogenesis of IBD and CRC, which is implicated to be mediated by CLRs, especially Dectin-1, Mincle, Dectin-3 and their downstream adaptor protein CARD9. However, the downstream signaling pathways of many CLRs and detailed mechanisms of aberrant CLRs signaling affecting IBD or CRC are complex and still unclear. In particular, there are still many discrepancies and even contradictions in the current research results on the role of CLRs in IBD and CRC. There are several possible reasons for this paradox, for example, different diet in experimental animals and undiscovered crosstalk within distinct PRRs. To be specific, different diets may affect intestinal inflammation in mice by affecting their gut microbiota composition (94). And CLRs can interfere with other PRRs-mediated signal transduction, such as TLR4, so simultaneous activation of multiple PRRs may produce different effects (41). In addition, experimental dose, mouse strain, sex bias and the interaction between intestinal fungi and bacteria may also influence experimental results. All these factors need to be considered in future studies.

The improvement of next generation sequencing (NGS) and third generation sequencing (TGS) technology paves the way to further investigate intestinal microbiota. A boom in the study of intestinal bacteria is facilitated by 16S rRNA sequencing, and in the past few years, a lot of emerging fungal sequencing studies are based on internal transcribed spacer (ITS) region and 18S rRNA

(216). The combination of ITS and18S rRNA sequencing could provide a more comprehensive characterization of intestinal fungi (216). It should be noted that intestinal fungal studies that utilize metagenomics and metatranscriptomic analysis are limited till now (217). In addition, as an important turning point in microbiota research, newly-developed culture-dependent strategies, such as high-throughput culturomics combined with matrix-assisted laser desorption ionization-time of flight mass spectrometry (MALDI-TOF MS) and ITS sequencing, make up for the deficiency of sequencing research and has been applied in fungal microbiota research (218). Other cutting-edge technologies can also be applied to the study of intestinal flora, for example, genome-wide CRISPR-Cas9 screen helps researchers to find the receptors for toxins of *Enterococcus* (219).

These latest technology and research paradigms help to elucidate the molecular mechanism of intestinal microbiota-inflammation-cancer axis. Newly discovered biomarkers and targets in this axis could be utilized to develop innovative vaccines and medicines, so as to approach more efficient and more individualized treatment. For example, through taking advantage of the adjuvant capacity of Mincle agonist, conjugating model antigen with Mincle agonist is a new pathway to develop cancer vaccines, which has been proven to provoke strong anti-tumor immune responses in mice (196). Besides, a new therapeutic agent, cationic liposome TDM, shows anti-tumor effect in mouse tumor models in a Mincle-dependent manner (197). Given the powerful and diverse role of CLRs in modulating innate and adaptive immune responses in IBD and CAC, such as the role of Dectin-1 in Treg amplification and the role of DC-SIGN in tumor metastasis, CLRs is undoubtedly very promising and worth-exploring therapeutic targets.

AUTHOR CONTRIBUTIONS

ML: Writing - Original Draft & Manuscript Submission. RZ: Writing- Original Draft, Review & Editing. JL: Supervision, Resources, Funding Acquisition, Writing - Review & Editing. JNL: Supervision, Resources, Funding Acquisition, Writing - Review & Editing. All authors contributed to the article and approved the submitted version.

FUNDING

Natural Science Foundation of China (Grant Nos. 81730016 and 81900483), CAMS Innovation Fund for Medical Sciences (CIFMS2021-I2M-C&T-A-001).

REFERENCES

1. Kaplan GG. The Global Burden of IBD: From 2015 to 2025. *Nat Rev Gastroenterol Hepatol* (2015) 12(12):720–7. doi: 10.1038/nrgastro.2015.150
2. Kaplan GG, Ng SC. Understanding and Preventing the Global Increase of Inflammatory Bowel Disease. *Gastroenterology* (2017) 152(2):313–21.e2. doi: 10.1053/j.gastro.2016.10.020
3. Geremia A, Biancheri P, Allan P, Corazza GR, Di Sabatino A. Innate and Adaptive Immunity in Inflammatory Bowel Disease. *Autoimmun Rev* (2014) 13 (1):3–10. doi: 10.1016/j.autrev.2013.06.004
4. Li J, Chen D, Yu B, He J, Zheng P, Mao X, et al. Fungi in Gastrointestinal Tracts of Human and Mice: From Community to Functions. *Microbial Ecol* (2018) 75 (4):821–9. doi: 10.1007/s00248-017-1105-9
5. Popov J, Caputi V, Nandeesha N, Rodriguez DA, Pai N. Microbiota-Immune Interactions in Ulcerative Colitis and Colitis Associated Cancer and Emerging Microbiota-Based Therapies. *Int J Mol Sci* (2021) 22(21):11365. doi: 10.3390/ijms222111365
6. Gill SR, Pop M, DeBoy RT, Eckburg PB, Turnbaugh PJ, Samuel BS, et al. Metagenomic Analysis of the Human Distal Gut Microbiome. *Science* (2006) 312(5778):1355–9. doi: 10.1126/science.1124234
7. Qin J, Li R, Raes J, Arumugam M, Burgdorf KS, Manichanh C, et al. A Human Gut Microbial Gene Catalogue Established by Metagenomic Sequencing. *Nature* (2010) 464(7285):59–65. doi: 10.1038/nature08821
8. Eckburg PB, Bik EM, Bernstein CN, Purdom E, Dethlefsen L, Sargent M, et al. Diversity of the Human Intestinal Microbial Flora. *Science* (2005) 308 (5728):1635–8. doi: 10.1126/science.1110591
9. Sartor RB, Wu GD. Roles for Intestinal Bacteria, Viruses, and Fungi in Pathogenesis of Inflammatory Bowel Diseases and Therapeutic Approaches. *Gastroenterology* (2017) 152(2):327–39.e4. doi: 10.1053/j.gastro.2016.10.012
10. Ni J, Wu GD, Albenberg L, Tomov VT. Gut Microbiota and IBD: Causation or Correlation? *Nat Rev Gastroenterol Hepatol* (2017) 14(10):573–84. doi: 10.1038/nrgastro.2017.88
11. Li T-H, Liu L, Hou Y-Y, Shen S-N, Wang T-T. C-Type Lectin Receptor-Mediated Immune Recognition and Response of the Microbiota in the Gut. *Gastroenterol Rep* (2019) 7(5):312–21. doi: 10.1093/gastro/goz028
12. Janeway CA Jr. Approaching the Asymptote? Evolution and Revolution in Immunology. *Cold Spring Harb Symp Quant Biol* (1989) 54(Pt 1):1–13. doi: 10.1101/SQB.1989.054.01.003
13. Navarro-Arias MJ, Hernández-Chávez MJ, García-Carnero LC, Amezcua-Hernández DG, Lozoya-Pérez NE, Estrada-Mata E, et al. Differential Recognition of Candida Tropicalis, Candida Guilliermondii, Candida Krusei, and Candida Auris by Human Innate Immune Cells. *Infect Drug Resist* (2019) 12:783–94. doi: 10.2147/IDR.S197531
14. Geijtenbeek TBH, Gringhuis SI. Signalling Through C-Type Lectin Receptors: Shaping Immune Responses. *Nat Rev Immunol* (2009) 9(7):465–79. doi: 10.1038/nri2569
15. Kawai T, Akira S. Toll-Like Receptors and Their Crosstalk With Other Innate Receptors in Infection and Immunity. *Immunity* (2011) 34(5):637–50. doi: 10.1016/j.immuni.2011.05.006
16. Matzinger P. Tolerance, Danger, and the Extended Family. *Annu Rev Immunol* (1994) 12(1):991–1045. doi: 10.1146/annurev.iy.12.040194.005015
17. Chiba S, Ikushima H, Ueki H, Yanai H, Kimura Y, Hangai S, et al. Recognition of Tumor Cells by Dectin-1 Orchestrates Innate Immune Cells for Anti-Tumor Responses. *eLife* (2014) 3:e04177. doi: 10.7554/eLife.04177
18. Yamasaki S, Ishikawa E, Sakuma M, Hara H, Ogata K, Saito T. Mincle is an ITAM-Coupled Activating Receptor That Senses Damaged Cells. *Nat Immunol* (2008) 9(10):1179–88. doi: 10.1038/ni.1651
19. Kostarnoy AV, Gancheva PG, Lepenies B, Tukhvatulin AI, Dzharullaeva AS, Polyakov NB, et al. Receptor Mincle Promotes Skin Allergies and is Capable of Recognizing Cholesterol Sulfate. *Proc Natl Acad Sci* (2017) 114:E2758–65. doi: 10.1073/pnas.1611665114
20. Kiyotake R, Oh-hora M, Ishikawa E, Miyamoto T, Ishibashi T, Yamasaki S. Human Mincle Binds to Cholesterol Crystals and Triggers Innate Immune Responses. *J Biol Chem* (2015) 290(42):25322–32. doi: 10.1074/jbc.M115.645234
21. Daley D, Mani VR, Mohan N, Akkad N, Ochi A, Heindel DW, et al. Dectin 1 Activation on Macrophages by Galectin 9 Promotes Pancreatic Carcinoma and Peritumoral Immune Tolerance. *Nat Med* (2017) 23(5):556–67. doi: 10.1038/nm.4314
22. Sharon N, Lis H. History of Lectins: From Hemagglutinins to Biological Recognition Molecules. *Glycobiology* (2004) 14(11):53R–62R. doi: 10.1093/glycob/cwh122

23. Sharon N, Lis H. Lectins:Cell-Agglutinating and Sugar-Specific Proteins. *Science* (1972) 177(4053):949. doi: 10.1126/science.177.4053.949
24. Drickamer K. Two Distinct Classes of Carbohydrate-Recognition Domains in Animal Lectins. *J Biol Chem* (1988) 263(20):9557–60. doi: 10.1016/S0021-9258(19)81549-1
25. Zelensky AN, Gready JE. The C-Type Lectin-Like Domain Superfamily. *FEBS J* (2005) 272(24):6179–217. doi: 10.1111/j.1742-4658.2005.05031.x
26. Lee RT, Hsu T-L, Huang SK, Hsieh S-L, Wong C-H, Lee YC. Survey of Immune-Related, Mannose/Fucose-Binding C-Type Lectin Receptors Reveals Widely Divergent Sugar-Binding Specificities. *Glycobiology* (2011) 21(4):512–20. doi: 10.1093/glycob/cwq193
27. Sancho D, Reis e Sousa C. Signaling by Myeloid C-Type Lectin Receptors in Immunity and Homeostasis. *Annu Rev Immunol* (2012) 30(1):491–529. doi: 10.1146/annurev-immunol-031210-101352
28. Garred P, Genster N, Pilely K, Bayarri-Olmos R, Rosbjerg A, Ma YJ, et al. A Journey Through the Lectin Pathway of Complement—MBL and Beyond. *Immunol Rev* (2016) 274(1):74–97. doi: 10.1111/imr.12468
29. Ariizumi K, Shen G-L, Shikano S, Xu S, Ritter RIII, Kumamoto T, et al. Identification of a Novel, Dendritic Cell-Associated Molecule, Dectin-1, by Subtractive cDNA Cloning. *J Biol Chem* (2000) 275(26):20157–67. doi: 10.1074/jbc.M909512199
30. Ariizumi K, Shen G-L, Shikano S, Ritter RIII, Zukas P, Edelbaum D, et al. Cloning of a Second Dendritic Cell-Associated C-Type Lectin (Dectin-2) and Its Alternatively Spliced Isoforms *. *J Biol Chem* (2000) 275(16):11957–63. doi: 10.1074/jbc.275.16.11957
31. Geijtenbeek TBH, Torensma R, van Vliet SJ, van Duijnhoven GCF, Adema GJ, van Kooyk Y, et al. Identification of DC-SIGN, a Novel Dendritic Cell–Specific ICAM-3 Receptor That Supports Primary Immune Responses. *Cell* (2000) 100 (5):575–85. doi: 10.1016/S0092-8674(00)80693-5
32. Cohen-Kedar S, Baram L, Elad H, Brazowski E, Guzner-Gur H, Dotan I. Human Intestinal Epithelial Cells Respond to β-Glucans *via* Dectin-1 and Syk. *Eur J Immunol* (2014) 44(12):3729–40. doi: 10.1002/eji.201444876
33. Neumann K, Castiñeiras-Vilariño M, Höckendorf U, Hannesschläger N, Lemeer S, Kupka D, et al. Clec12a Is an Inhibitory Receptor for Uric Acid Crystals That Regulates Inflammation in Response to Cell Death. *Immunity* (2014) 40(3):389–99. doi: 10.1016/j.immuni.2013.12.015
34. Zhang J-G, Czabotar Peter E, Policheni Antonia N, Caminschi I, San Wan S, Kitsoulis S, et al. The Dendritic Cell Receptor Clec9A Binds Damaged Cells *via* Exposed Actin Filaments. *Immunity* (2012) 36(4):646–57. doi: 10.1016/j.immuni.2012.03.009
35. Miyake Y, Toyonaga K, Mori D, Kakuta S, Hoshino Y, Oyamada A, et al. C-Type Lectin MCL Is an FcrγCoupled Receptor That Mediates the Adjuvanticity of Mycobacterial Cord Factor. *Immunity* (2013) 38(5):1050–62. doi: 10.1016/j.immuni.2013.03.010
36. Rothfuchs AG, Bafica A, Feng CG, Egen JG, Williams DL, Brown GD, et al. Dectin-1 Interaction With Mycobacterium Tuberculosis Leads to Enhanced IL-12p40 Production by Splenic Dendritic Cells. *J Immunol* (2007) 179 (6):3463. doi: 10.4049/jimmunol.179.6.3463
37. van Vliet SJ, van Liempt E, Saeland E, Aarnoudse CA, Appelmelk B, Irimura T, et al. Carbohydrate Profiling Reveals a Distinctive Role for the C-Type Lectin MGL in the Recognition of Helminth Parasites and Tumor Antigens by Dendritic Cells. *Int Immunol* (2005) 17(5):661–9. doi: 10.1093/intimm/dxh246
38. Lambert AA, Imbeault M, Gilbert C, Tremblay MJ. HIV-1 Induces DCIR Expression in CD4(+) T Cells. *PloS Pathogens* (2010) 6(11):e1001188. doi: 10.1371/journal.ppat.1001188
39. Villadangos JA, Schnorrer P. Intrinsic and Cooperative Antigen-Presenting Functions of Dendritic-Cell Subsets *In Vivo*. *Nat Rev Immunol* (2007) 7 (7):543–55. doi: 10.1038/nri2103
40. Delneste Y, Magistrelli G, Gauchat JF, Haeuw JF, Aubry JP, Nakamura K, et al. Involvement of LOX-1 in Dendritic Cell-Mediated Antigen Cross-Presentation. *Immunity* (2002) 17(3):353–62. doi: 10.1016/S1074-7613(02)00388-6
41. del Fresno C, Iborra S, Saz-Leal P, Martínez-López M, Sancho D. Flexible Signaling of Myeloid C-Type Lectin Receptors in Immunity and Inflammation. *Front Immunol* (2018) 9. doi: 10.3389/fimmu.2018.00804
42. Rogers NC, Slack EC, Edwards AD, Nolte MA, Schulz O, Schweighoffer E, et al. Syk-Dependent Cytokine Induction by Dectin-1 Reveals a Novel Pattern Recognition Pathway for C Type Lectins. *Immunity* (2005) 22(4):507–17. doi: 10.1016/j.immuni.2005.03.004
43. Kerrigan AM, Brown GD. Syk-Coupled C-Type Lectins in Immunity. *Trends Immunol* (2011) 32(4):151–6. doi: 10.1016/j.it.2011.01.002
44. Drummond RA, Saijo S, Iwakura Y, Brown GD. The Role of Syk/CARD9 Coupled C-Type Lectins in Antifungal Immunity. *Eur J Immunol* (2011) 41 (2):276–81. doi: 10.1002/eji.201041252
45. Blank U, Launay P, Benhamou M, Monteiro RC. Inhibitory ITAMs as Novel Regulators of Immunity. *Immunol Rev* (2009) 232(1):59–71. doi: 10.1111/j.1600-065X.2009.00832.x
46. Iborra S, Martínez-López M, Cueto Francisco J, Conde-Garrosa R, Del Fresno C, Izquierdo Helena M, et al. Leishmania Uses Mincle to Target an Inhibitory ITAM Signaling Pathway in Dendritic Cells That Dampens Adaptive Immunity to Infection. *Immunity* (2016) 45(4):788–801. doi: 10.1016/j.immuni.2016.09.012
47. Pan Y-G, Yu Y-L, Lin C-C, Lanier LL, Chu C-L. Fcεri γ-Chain Negatively Modulates Dectin-1 Responses in Dendritic Cells. *Front Immunol* (2017) 8. doi: 10.3389/fimmu.2017.01424
48. Blanco-Menéndez N, del Fresno C, Fernandes S, Calvo E, Conde-Garrosa R, Kerr WG, et al. SHIP-1 Couples to the Dectin-1 hemITAM and Selectively Modulates Reactive Oxygen Species Production in Dendritic Cells in Response to Candida Albicans. *J Immunol* (2015) 195(9):4466. doi: 10.4049/jimmunol.1402874
49. Nakanishi Y, Sato T, Ohteki T. Commensal Gram-Positive Bacteria Initiates Colitis by Inducing Monocyte/Macrophage Mobilization. *Mucosal Immunol* (2015) 8(1):152–60. doi: 10.1038/mi.2014.53
50. Xavier RJ, Podolsky DK. Unravelling the Pathogenesis of Inflammatory Bowel Disease. *Nature* (2007) 448(7152):427–34. doi: 10.1038/nature06005
51. Ott SJ, Kuehbacher T, Musfeldt M, Rosenstiel P, Hellmig S, Rehman A, et al. Fungi and Inflammatory Bowel Diseases: Alterations of Composition and Diversity. *Scandinavian J Gastroenterol* (2008) 43(7):831–41. doi: 10.1080/00365520801935434
52. Li Q, Wang C, Tang C, He Q, Li N, Li J. Dysbiosis of Gut Fungal Microbiota is Associated With Mucosal Inflammation in Crohn's Disease. *J Clin Gastroenterol* (2014) 48(6):513. doi: 10.1097/MCG.0000000000000035
53. Liguori G, Lamas B, Richard ML, Brandi G, da Costa G, Hoffmann TW, et al. Fungal Dysbiosis in Mucosa-Associated Microbiota of Crohn's Disease Patients. *J Crohn's Colitis* (2016) 10(3):296–305. doi: 10.1093/ecco-jcc/jjv209
54. Hoarau G, Mukherjee PK, Gower-Rousseau C, Hager C, Chandra J, Retuerto MA, et al. Bacteriome and Mycobiome Interactions Underscore Microbial Dysbiosis in Familial Crohn's Disease. *mBio* (2016) 7(5):e01250–16. doi: 10.1128/mBio.01250-16
55. Chehoud C, Albenberg LG, Judge C, Hoffmann C, Grunberg S, Bittinger K, et al. Fungal Signature in the Gut Microbiota of Pediatric Patients With Inflammatory Bowel Disease. *Inflammatory Bowel Dis* (2015) 21(8):1948–56. doi: 10.1097/MIB.0000000000000454
56. Sokol H, Leducq V, Aschard H, Pham H-P, Jegou S, Landman C, et al. Fungal Microbiota Dysbiosis in IBD. *Gut* (2017) 66(6):1039. doi: 10.1136/gutjnl-2015-310746
57. Frau A, Ijaz UZ, Slater R, Jonkers D, Penders J, Campbell BJ, et al. Inter-Kingdom Relationships in Crohn's Disease Explored Using a Multi-Omics Approach. *Gut Microbes* (2021) 13(1):1930871. doi: 10.1080/19490976.2021.1930871
58. Qiu X, Zhang F, Yang X, Wu N, Jiang W, Li X, et al. Changes in the Composition of Intestinal Fungi and Their Role in Mice With Dextran Sulfate Sodium-Induced Colitis. *Sci Rep* (2015) 5(1):10416. doi: 10.1038/srep10416
59. Standaert–Vitse A, Jouault T, Vandewalle P, Mille C, Seddik M, Sendid B, et al. Candida Albicans Is an Immunogen for Anti–Saccharomyces Cerevisiae Antibody Markers of Crohn's Disease. *Gastroenterology* (2006) 130(6):1764–75. doi: 10.1053/j.gastro.2006.02.009
60. Joossens S, Reinisch W, Vermeire S, Sendid B, Poulain D, Peeters M, et al. The Value of Serologic Markers in Indeterminate Colitis: A Prospective Follow-Up Study. *Gastroenterology* (2002) 122(5):1242–7. doi: 10.1053/gast.2002.32980
61. Jawhara S, Thuru X, Standaert-Vitse A, Jouault T, Mordon S, Sendid B, et al. Colonization of Mice by Candida Albicans Is Promoted by Chemically Induced Colitis and Augments Inflammatory Responses Through Galectin-3. *J Infect Dis* (2008) 197(7):972–80. doi: 10.1086/528990
62. Zwolinska-Wcislo M, Brzozowski T, Budak A, Kwiecien S, Sliwowski Z, Drozdowicz D, et al. Effect of Candida Colonization on Human Ulcerative

Colitis and the Healing of Inflammatory Changes of the Colon in the Experimental Model of Colitis Ulcerosa. *J Physiol Pharmacol* (2009) 60 (1):107–18. doi: 10.1007/s12576-008-0010-x
63. Wheeler ML, Limon JJ, Bar AS, Leal CA, Gargus M, Tang J, et al. Immunological Consequences of Intestinal Fungal Dysbiosis. *Cell Host Microbe* (2016) 19(6):865–73. doi: 10.1016/j.chom.2016.05.003
64. Li X, Leonardi I, Semon A, Doron I, Gao IH, Putzel GG, et al. Response to Fungal Dysbiosis by Gut-Resident CX3CR1(+) Mononuclear Phagocytes Aggravates Allergic Airway Disease. *Cell Host Microbe* (2018) 24(6):847–+. doi: 10.1016/j.chom.2018.11.003
65. Jawhara S, Poulain D. Saccharomyces Boulardii Decreases Inflammation and Intestinal Colonization by Candida Albicans in a Mouse Model of Chemically-Induced Colitis. *Med Mycol* (2007) 45(8):691–700. doi: 10.1080/13693780701523013
66. Chen X, Yang G, Song J-H, Xu H, Li D, Goldsmith J, et al. Probiotic Yeast Inhibits VEGFR Signaling and Angiogenesis in Intestinal Inflammation. *PloS One* (2013) 8(5):e64227. doi: 10.1371/journal.pone.0064227
67. Atarashi K, Tanoue T, Oshima K, Suda W, Nagano Y, Nishikawa H, et al. Treg Induction by a Rationally Selected Mixture of Clostridia Strains From the Human Microbiota. *Nature* (2013) 500(7461):232–6. doi: 10.1038/nature12331
68. Jiang TT, Shao T-Y, Ang WXG, Kinder JM, Turner LH, Pham G, et al. Commensal Fungi Recapitulate the Protective Benefits of Intestinal Bacteria. *Cell Host Microbe* (2017) 22(6):809–+. doi: 10.1016/j.chom.2017.10.013
69. Willment JA, Marshall ASJ, Reid DM, Williams DL, Wong SYC, Gordon S, et al. The Human β-Glucan Receptor is Widely Expressed and Functionally Equivalent to Murine Dectin-1 on Primary Cells. *Eur J Immunol* (2005) 35 (5):1539–47. doi: 10.1002/eji.200425725
70. Sun WK, Lu X, Li X, Sun QY, Su X, Song Y, et al. Dectin-1 Is Inducible and Plays a Crucial Role in Aspergillus-Induced Innate Immune Responses in Human Bronchial Epithelial Cells. *Eur J Clin Microbiol Infect Dis* (2012) 31 (10):2755–64. doi: 10.1007/s10096-012-1624-8
71. Brown GD, Gordon S. A New Receptor for β-Glucans. *Nature* (2001) 413 (6851):36–7. doi: 10.1038/35092620
72. Palma AS, Feizi T, Zhang Y, Stoll MS, Lawson AM, Díaz-Rodríguez E, et al. Ligands for the β-Glucan Receptor, Dectin-1, Assigned Using "Designer" Microarrays of Oligosaccharide Probes (Neoglycolipids) Generated From Glucan Polysaccharides. *J Biol Chem* (2006) 281(9):5771–9. doi: 10.1074/jbc.M511461200
73. Brown GD. Dectin-1: A Signalling non-TLR Pattern-Recognition Receptor. *Nat Rev Immunol* (2006) 6(1):33–43. doi: 10.1038/nri1745
74. Saijo S, Fujikado N, Furuta T, S-h C, Kotaki H, Seki K, et al. Dectin-1 is Required for Host Defense Against Pneumocystis Carinii But Not Against Candida Albicans. *Nat Immunol* (2007) 8(1):39–46. doi: 10.1038/ni1425
75. Taylor PR, Tsoni SV, Willment JA, Dennehy KM, Rosas M, Findon H, et al. Dectin-1 Is Required for β-Glucan Recognition and Control of Fungal Infection. *Nat Immunol* (2007) 8(1):31–8. doi: 10.1038/ni1408
76. Goodridge HS, Reyes CN, Becker CA, Katsumoto TR, Ma J, Wolf AJ, et al. Activation of the Innate Immune Receptor Dectin-1 Upon Formation of a 'Phagocytic Synapse'. *Nature* (2011) 472(7344):471–5. doi: 10.1038/nature10071
77. Gringhuis SI, Kaptein TM, Wevers BA, Theelen B, van der Vlist M, Boekhout T, et al. Dectin-1 Is an Extracellular Pathogen Sensor for the Induction and Processing of IL-1β *via* a Noncanonical Caspase-8 Inflammasome. *Nat Immunol* (2012) 13(3):246–54. doi: 10.1038/ni.2222
78. Gringhuis SI, den Dunnen J, Litjens M, van der Vlist M, Wevers B, Bruijns SCM, et al. Dectin-1 Directs T Helper Cell Differentiation by Controlling Noncanonical NF-κb Activation Through Raf-1 and Syk. *Nat Immunol* (2009) 10(2):203–13. doi: 10.1038/ni.1692
79. Thiagarajan PS, Yakubenko VP, Elsori DH, Yadav SP, Willard B, Tan CD, et al. Vimentin Is an Endogenous Ligand for the Pattern Recognition Receptor Dectin-1. *Cardiovasc Res* (2013) 99(3):494–504. doi: 10.1093/cvr/cvt117
80. Shan M, Gentile M, Yeiser JR, Walland AC, Bornstein VU, Chen K, et al. Mucus Enhances Gut Homeostasis and Oral Tolerance by Delivering Immunoregulatory Signals. *Science* (2013) 342(6157):447–53. doi: 10.1126/science.1237910
81. Leclaire C, Lecointe K, Gunning PA, Tribolo S, Kavanaugh DW, Wittmann A, et al. Molecular Basis for Intestinal Mucin Recognition by Galectin-3 and C-Type Lectins. *FASEB J* (2018) 32(6):3301–20. doi: 10.1096/fj.201700619R
82. Rochereau N, Drocourt D, Perouzel E, Pavot V, Redelinghuys P, Brown GD, et al. Dectin-1 Is Essential for Reverse Transcytosis of Glycosylated SIgA-Antigen Complexes by Intestinal M Cells. *PloS Biol* (2013) 11(9):e1001658. doi: 10.1371/journal.pbio.1001658
83. LeibundGut-Landmann S, Gross O, Robinson MJ, Osorio F, Slack EC, Tsoni SV, et al. Syk- and CARD9-Dependent Coupling of Innate Immunity to the Induction of T Helper Cells That Produce Interleukin 17. *Nat Immunol* (2007) 8(6):630–8. doi: 10.1038/ni1460
84. Cheng S-C, van de Veerdonk FL, Lenardon M, Stoffels M, Plantinga T, Smeekens S, et al. The Dectin-1/Inflammasome Pathway Is Responsible for the Induction of Protective T-Helper 17 Responses That Discriminate Between Yeasts and Hyphae of Candida Albicans. *J Leukocyte Biol* (2011) 90(2):357–66. doi: 10.1189/jlb.1210702
85. Maloy KJ, Powrie F. Intestinal Homeostasis and its Breakdown in Inflammatory Bowel Disease. *Nature* (2011) 474(7351):298–306. doi: 10.1038/nature10208
86. Drummond RA, Dambuza IM, Vautier S, Taylor JA, Reid DM, Bain CC, et al. CD4+ T-Cell Survival in the GI Tract Requires Dectin-1 During Fungal Infection. *Mucosal Immunol* (2016) 9(2):492–502. doi: 10.1038/mi.2015.79
87. Iliev ID, Funari VA, Taylor KD, Quoclinh N, Reyes CN, Strom SP, et al. Interactions Between Commensal Fungi and the C-Type Lectin Receptor Dectin-1 Influence Colitis. *Science* (2012) 336(6086):1314–7. doi: 10.1126/science.1221789
88. Carvalho A, Giovannini G, De Luca A, D'Angelo C, Casagrande A, Iannitti RG, et al. Dectin-1 Isoforms Contribute to Distinct Th1/Th17 Cell Activation in Mucosal Candidiasis. *Cell Mol Immunol* (2012) 9(3):276–86. doi: 10.1038/cmi.2012.1
89. de Vries HS, Plantinga TS, van Krieken JH, Stienstra R, van Bodegraven AA, Festen EAM, et al. Genetic Association Analysis of the Functional C.714T>G Polymorphism and Mucosal Expression of Dectin-1 in Inflammatory Bowel Disease. *PloS One* (2009) 4(11):e7818. doi: 10.1371/journal.pone.0007818
90. Salazar-Aldrete C, Galán-Díez M, Fernández-Ruiz E, Niño-Moreno P, Estrada-Capetillo L, Abud-Mendoza C, et al. Expression and Function of Dectin-1 is Defective in Monocytes From Patients With Systemic Lupus Erythematosus and Rheumatoid Arthritis. *J Clin Immunol* (2013) 33(2):368–77. doi: 10.1007/s10875-012-9821-x
91. Yoshitomi H, Sakaguchi N, Kobayashi K, Brown GD, Tagami T, Sakihama T, et al. A Role for Fungal Beta-Glucans and Their Receptor Dectin-1 in the Induction of Autoimmune Arthritis in Genetically Susceptible Mice. *J Exp Med* (2005) 201(6):949–60. doi: 10.1084/jem.20041758
92. Tang C, Kamiya T, Liu Y, Kadoki M, Kakuta S, Oshima K, et al. Inhibition of Dectin-1 Signaling Ameliorates Colitis by Inducing Lactobacillus-Mediated Regulatory T Cell Expansion in the Intestine. *Cell Host Microbe* (2015) 18 (2):183–97. doi: 10.1016/j.chom.2015.07.003
93. Rahabi M, Jacquemin G, Prat M, Meunier E, AlaEddine M, Bertrand B, et al. Divergent Roles for Macrophage C-Type Lectin Receptors, Dectin-1 and Mannose Receptors, in the Intestinal Inflammatory Response. *Cell Rep* (2020) 30(13):4386–98.e5. doi: 10.1016/j.celrep.2020.03.018
94. Kamiya T, Tang C, Kadoki M, Oshima K, Hattori M, Saijo S, et al. β-Glucans in Food Modify Colonic Microflora by Inducing Antimicrobial Protein, Calprotectin, in a Dectin-1-Induced-IL-17F-Dependent Manner. *Mucosal Immunol* (2018) 11(3):763–73. doi: 10.1038/mi.2017.86
95. Williams SJ. Sensing Lipids With Mincle: Structure and Function. *Front Immunol* (2017) 8. doi: 10.3389/fimmu.2017.01662
96. Ishikawa E, Ishikawa T, Morita YS, Toyonaga K, Yamada H, Takeuchi O, et al. Direct Recognition of the Mycobacterial Glycolipid, Trehalose Dimycolate, by C-Type Lectin Mincle. *J Exp Med* (2009) 206(13):2879–88. doi: 10.1084/jem.20091750
97. Schoenen H, Bodendorfer B, Hitchens K, Manzanero S, Werninghaus K, Nimmerjahn F, et al. Cutting Edge: Mincle Is Essential for Recognition and Adjuvanticity of the Mycobacterial Cord Factor and its Synthetic Analog Trehalose-Dibehenate. *J Immunol* (2010) 184(6):2756. doi: 10.4049/jimmunol.0904013
98. Nagata M, Izumi Y, Ishikawa E, Kiyotake R, Doi R, Iwai S, et al. Intracellular Metabolite Beta-Glucosylceramide Is an Endogenous Mincle Ligand Possessing Immunostimulatory Activity. *Proc Natl Acad Sci* (2017) 114: E3285–94. doi: 10.1073/pnas.1618133114
99. Martinez-Lopez M, Iborra S, Conde-Garrosa R, Mastrangelo A, Danne C, Mann ER, et al. Microbiota Sensing by Mincle-Syk Axis in Dendritic Cells

Regulates Interleukin-17 and-22 Production and Promotes Intestinal Barrier Integrity. *Immunity* (2019) 50(2):446–+. doi: 10.1016/j.immuni.2018.12.020
100. Leonardi I, Iliev I, Li X, Semon A. Cx3cr1+ Mononuclear Phagocytes Control Immunity to Intestinal Fungi. *Gastroenterology* (2019) 156(3, Supplement): S101. doi: 10.1053/j.gastro.2019.01.236
101. Gong W, Guo K, Zheng T, Fang M, Xie H, Li W, et al. Preliminary Exploration of the Potential of Spliceosome-Associated Protein 130 for Predicting Disease Severity in Crohn's Disease. *Ann N Y Acad Sci* (2020) 1462(1):128–38. doi: 10.1111/nyas.14240
102. Gong W, Zheng T, Guo K, Fang M, Xie H, Li W, et al. Mincle/Syk Signalling Promotes Intestinal Mucosal Inflammation Through Induction of Macrophage Pyroptosis in Crohn's Disease. *J Crohn's Colitis* (2020) 14 (12):1734–47. doi: 10.1093/ecco-jcc/jjaa088
103. Balch SG, McKnight AJ, Seldin MF, Gordon S. Cloning of a Novel C-Type Lectin Expressed by Murine Macrophages*. *J Biol Chem* (1998) 273 (29):18656–64. doi: 10.1074/jbc.273.29.18656
104. Schick J, Schäfer J, Alexander C, Dichtl S, Murray PJ, Christensen D, et al. Cutting Edge: TNF Is Essential for Mycobacteria-Induced MINCLE Expression, Macrophage Activation, and Th17 Adjuvanticity. *J Immunol* (2020) 205(2):323. doi: 10.4049/jimmunol.2000420
105. Graham LM, Gupta V, Schafer G, Reid DM, Kimberg M, Dennehy KM, et al. The C-Type Lectin Receptor CLECSF8 (CLEC4D) Is Expressed by Myeloid Cells and Triggers Cellular Activation Through Syk Kinase. *J Biol Chem* (2012) 287(31):25964–74. doi: 10.1074/jbc.M112.384164
106. Zhao X-Q, Zhu L-L, Chang Q, Jiang C, You Y, Luo T, et al. C-Type Lectin Receptor Dectin-3 Mediates Trehalose 6,6′-Dimycolate (TDM)-Induced Mincle Expression Through CARD9/Bcl10/MALT1-Dependent Nuclear Factor (NF)-κb Activation. *J Biol Chem* (2014) 289(43):30052–62. doi: 10.1074/jbc.M114.588574
107. Zhu L-L, Zhao X-Q, Jiang C, You Y, Chen X-P, Jiang Y-Y, et al. C-Type Lectin Receptors Dectin-3 and Dectin-2 Form a Heterodimeric Pattern-Recognition Receptor for Host Defense Against Fungal Infection. *Immunity* (2013) 39(2):324–34. doi: 10.1016/j.immuni.2013.05.017
108. Preite NW, Feriotti C, de Lima DS, da Silva BB, Condino-Neto A, Pontillo A, et al. The Syk-Coupled C-Type Lectin Receptors Dectin-2 and Dectin-3 are Involved in Paracoccidioides Brasiliensis Recognition by Human Plasmacytoid Dendritic Cells. *Front Immunol* (2018) 9. doi: 10.3389/fimmu.2018.00464
109. Blankson V, Lobato-Pascual A, Saether PC, Fossum S, Dissen E, Daws MR. Human Macrophage C-Type Lectin Forms a Heteromeric Receptor Complex With Mincle But Not Dectin-2. *Scandinavian J Immunol* (2022) 95(5): e13149. doi: 10.1111/sji.13149
110. N'Diaye M, Brauner S, Flytzani S, Kular L, Warnecke A, Adzemovic MZ, et al. C-Type Lectin Receptors Mcl and Mincle Control Development of Multiple Sclerosis Like Neuroinflammation. *J Clin Invest* (2020) 130(2):838–52. doi: 10.1172/JCI125857
111. Li D, Lu L, Kong W, Xia X, Pan Y, Li J, et al. C-Type Lectin Receptor Dectin3 Deficiency Balances the Accumulation and Function of FoxO1-Mediated LOX-1+ M-MDSCs in Relieving Lupus-Like Symptoms. *Cell Death Dis* (2021) 12(9):829. doi: 10.1038/s41419-021-04052-5
112. Hütter J, Eriksson M, Johannssen T, Klopfleisch R, von Smolinski D, Gruber AD, et al. Role of the C-Type Lectin Receptors MCL and DCIR in Experimental Colitis. *PloS One* (2014) 9(7):e103281. doi: 10.1371/journal.pone.0103281
113. Wang T, Pan D, Zhou Z, You Y, Jiang C, Zhao X, et al. Dectin-3 Deficiency Promotes Colitis Development Due to Impaired Antifungal Innate Immune Responses in the Gut. *PloS Pathogens* (2016) 12(6):e1005662. doi: 10.1371/journal.ppat.1005662
114. Duan J-L, He H-Q, Yu Y, Liu T, Ma S-J, Li F, et al. E3 Ligase C-Cbl Regulates Intestinal Inflammation Through Suppressing Fungi-Induced Noncanonical NF-Kappa B Activation. *Sci Adv* (2021) 7(19):eabe5171. doi: 10.1126/sciadv.abe5171
115. Eklöw C, Makrygiannakis D, Bäckdahl L, Padyukov L, Ulfgren AK, Lorentzen JC, et al. Cellular Distribution of the C-Type II Lectin Dendritic Cell Immunoreceptor (DCIR) and its Expression in the Rheumatic Joint: Identification of a Subpopulation of DCIR+ T Cells. *Ann Rheumatic Dis* (2008) 67(12):1742. doi: 10.1136/ard.2007.076976
116. Bates EEM, Fournier N, Garcia E, Valladeau J, Durand I, Pin JJ, et al. APCs Express DCIRA Novel C-Type Lectin Surface Receptor Containing an Immunoreceptor Tyrosine-Based Inhibitory Motif. *J Immunol* (1999) 163 (4):1973–83.
117. Bloem K, Vuist IM, van den Berk M, Klaver EJ, van Die I, Knippels LMJ, et al. DCIR Interacts With Ligands From Both Endogenous and Pathogenic Origin. *Immunol Lett* (2014) 158(1):33–41. doi: 10.1016/j.imlet.2013.11.007
118. Lambert AA, Gilbert C, Richard M, Beaulieu AD, Tremblay MJ. The C-Type Lectin Surface Receptor DCIR Acts as a New Attachment Factor for HIV-1 in Dendritic Cells and Contributes to Trans- and Cis-Infection Pathways. *Blood* (2008) 112(4):1299–307. doi: 10.1182/blood-2008-01-136473
119. Bloem K, Vuist IM, van der Plas A-J, Knippels LMJ, Garssen J, Garcia-Vallejo JJ, et al. Ligand Binding and Signaling of Dendritic Cell Immunoreceptor (DCIR) Is Modulated by the Glycosylation of the Carbohydrate Recognition Domain. *PloS One* (2013) 8(6):e66266. doi: 10.1371/journal.pone.0066266
120. Meyer-Wentrup F, Cambi A, Joosten BJ, Looman MW, I Jolanda M V, Figdor CG, et al. DCIR Is Endocytosed Into Human Dendritic Cells and Inhibits TLR8-Mediated Cytokine Production. *J Leukocyte Biol* (2009) 85 (3):518–25. doi: 10.1189/jlb.0608352
121. Meyer-Wentrup F, Benitez-Ribas D, Tacken PJ, Punt CJA, Figdor CG, de Vries IJM, et al. Targeting DCIR on Human Plasmacytoid Dendritic Cells Results in Antigen Presentation and Inhibits IFN-Alpha Production. *Blood* (2008) 111(8):4245–53. doi: 10.1182/blood-2007-03-081398
122. Uto T, Fukaya T, Takagi H, Arimura K, Nakamura T, Kojima N, et al. Clec4A4 Is a Regulatory Receptor for Dendritic Cells That Impairs Inflammation and T-Cell Immunity. *Nat Commun* (2016) 7:1–15. doi: 10.1038/ncomms11273
123. Fujikado N, Saijo S, Yonezawa T, Shimamori K, Ishii A, Sugai S, et al. Dcir Deficiency Causes Development of Autoimmune Diseases in Mice Due to Excess Expansion of Dendritic Cells. *Nat Med* (2008) 14(2):176–80. doi: 10.1038/nm1697
124. Maglinao M, Klopfleisch R, Seeberger PH, Lepenies B. The C-Type Lectin Receptor DCIR Is Crucial for the Development of Experimental Cerebral Malaria. *J Immunol* (2013) 191(5):2551–9. doi: 10.4049/jimmunol.1203451
125. Tokieda S, Komori M, Ishiguro T, Iwakura Y, Takahara K, Inaba K. Dendritic Cell Immunoreceptor 1 Alters Neutrophil Responses in the Development of Experimental Colitis. *BMC Immunol* (2015) 16(1):64. doi: 10.1186/s12865-015-0129-5
126. Fournier BM, Parkos CA. The Role of Neutrophils During Intestinal Inflammation. *Mucosal Immunol* (2012) 5(4):354–66. doi: 10.1038/mi.2012.24
127. Qualls JE, Kaplan AM, van Rooijen N, Cohen DA. Suppression of Experimental Colitis by Intestinal Mononuclear Phagocytes. *J Leukocyte Biol* (2006) 80(4):802–15. doi: 10.1189/jlb.1205734
128. Gringhuis SI, den Dunnen J, Litjens M, van het Hof B, van Kooyk Y, Geijtenbeek Teunis BH. Type Lectin DC-SIGN Modulates Toll-Like Receptor Signaling *via* Raf-1 Kinase-Dependent Acetylation of Transcription Factor NF-Kb. *Immunity* (2007) 26(5):605–16. doi: 10.1016/j.immuni.2007.03.012
129. Geijtenbeek TBH, Kwon DS, Torensma R, van Vliet SJ, van Duijnhoven GCF, Middel J, et al. DC-SIGN, a Dendritic Cell–Specific HIV-1-Binding Protein That Enhances Trans-Infection of T Cells. *Cell* (2000) 100(5):587–97. doi: 10.1016/S0092-8674(00)80694-7
130. Appelmelk BJ, van Die I, van Vliet SJ, Vandenbroucke-Grauls CMJE, Geijtenbeek TBH, van Kooyk Y. Cutting Edge: Carbohydrate Profiling Identifies New Pathogens That Interact With Dendritic Cell-Specific ICAM-3-Grabbing Nonintegrin on Dendritic Cells. *J Immunol* (2003) 170 (4):1635. doi: 10.4049/jimmunol.170.4.1635
131. Singh S, Almuhanna Y, Alshahrani MY, Lowman DW, Rice PJ, Gell C, et al. Carbohydrates From Pseudomonas Aeruginosa Biofilms Interact With Immune C-Type Lectins and Interfere With Their Receptor Function. *NPJ Biofilms Microbiomes* (2021) 7(1):1–14. doi: 10.1038/s41522-021-00257-w
132. Cambi A, Gijzen K, de Vries IJM, Torensma R, Joosten B, Adema GJ, et al. The C-Type Lectin DC-SIGN (CD209) Is an Antigen-Uptake Receptor for Candida Albicans on Dendritic Cells. *Eur J Immunol* (2003) 33(2):532–8. doi: 10.1002/immu.200310029

133. Thompson A, da Fonseca DM, Walker L, Griffiths JS, Taylor PR, Gow NAR, et al. Dependence on Mincle and Dectin-2 Varies With Multiple Candida Species During Systemic Infection. *Front Microbiol* (2021) 12. doi: 10.3389/fmicb.2021.633229
134. Geijtenbeek TBH, Krooshoop D, Bleijs DA, van Vliet SJ, van Duijnhoven GCF, Grabovsky V, et al. DC-SIGN-ICAM-2 Interaction Mediates Dendritic Cell Trafficking. *Nat Immunol* (2000) 1(4):353–7. doi: 10.1038/79815
135. van Gisbergen K, Sanchez-Hernandez M, Geijtenbeek TBH, van Kooyk Y. Neutrophils Mediate Immune Modulation of Dendritic Cells Through Glycosylation-Dependent Interactions Between Mac-1 and DC-SIGN. *J Exp Med* (2005) 201(8):1281–92. doi: 10.1084/jem.20041276
136. van Gisbergen K, Ludwig IS, Geijtenbeek TBH, van Kooyk Y. Interactions of DC-SIGN With Mac-1 and CEACAM1 Regulate Contact Between Dendritic Cells and Neutrophils. *FEBS Lett* (2005) 579(27):6159–68. doi: 10.1016/j.febslet.2005.09.089
137. Nonaka M, Ma BY, Imaeda H, Kawabe K, Kawasaki N, Hodohara K, et al. Dendritic Cell-Specific Intercellular Adhesion Molecule 3-Grabbing Non-Integrin (DC-SIGN) Recognizes a Novel Ligand, Mac-2-Binding Protein, Characteristically Expressed on Human Colorectal Carcinomas. *J Biol Chem* (2011) 286(25):22403–13. doi: 10.1074/jbc.M110.215301
138. Nonaka M, Matsumoto S, Ma BY, Kido H, Kawasaki N, Kawasaki N, et al. Glycan-Dependent and -Independent Dual Recognition Between DC-SIGN and Type II Serine Protease MSPL/TMPRSS13 in Colorectal Cancer Cells. *Appl Sci* (2020) 10(8):2687. doi: 10.3390/app10082687
139. van Gisbergen K, Aarnoudse CA, Meijer GA, Geijtenbeek TBH, van Kooyk Y. Dendritic Cells Recognize Tumor-Specific Glycosylation of Carcinoembryonic Antigen on Colorectal Cancer Cells Through Dendritic Cell-Specific Intercellular Adhesion Molecule-3-Grabbing Nonintegrin. *Cancer Res* (2005) 65(13):5935–44. doi: 10.1158/0008-5472.CAN-04-4140
140. Saeland E, Belo AI, Mongera S, van Die I, Meijer GA, van Kooyk Y. Differential Glycosylation of MUC1 and CEACAM5 Between Normal Mucosa and Tumour Tissue of Colon Cancer Patients. *Int J Cancer* (2012) 131(1):117–28. doi: 10.1002/ijc.26354
141. Saunders SP, Barlow JL, Walsh CM, Bellsoi A, Smith P, McKenzie ANJ, et al. C-Type Lectin SIGN-R1 Has a Role in Experimental Colitis and Responsiveness to Lipopolysaccharide. *J Immunol* (2010) 184(5):2627. doi: 10.4049/jimmunol.0901970
142. Eriksson M, Johannssen T, von Smolinski D, Gruber A, Seeberger P, Lepenies B. The C-Type Lectin Receptor SIGNR3 Binds to Fungi Present in Commensal Microbiota and Influences Immune Regulation in Experimental Colitis. *Front Immunol* (2013) 4. doi: 10.3389/fimmu.2013.00196
143. Lightfoot YL, Selle K, Yang T, Goh YJ, Sahay B, Zadeh M, et al. SIGNR3-Dependent Immune Regulation by Lactobacillus Acidophilus Surface Layer Protein A in Colitis. *EMBO J* (2015) 34(7):881–95. doi: 10.15252/embj.201490296
144. Hanahan D, Weinberg RA. Hallmarks of Cancer: The Next Generation. *Cell* (2011) 144(5):646–74. doi: 10.1016/j.cell.2011.02.013
145. Naugler WE, Karin M. NF-κb and Cancer—Identifying Targets and Mechanisms. *Curr Opin Genet Dev* (2008) 18(1):19–26. doi: 10.1016/j.gde.2008.01.020
146. Arnold M, Sierra MS, Laversanne M, Soerjomataram I, Jemal A, Bray F. Global Patterns and Trends in Colorectal Cancer Incidence and Mortality. *Gut* (2017) 66(4):683. doi: 10.1136/gutjnl-2015-310912
147. Rubin D, Shaker A, Levin M. Chronic Intestinal Inflammation: Inflammatory Bowel Disease and Colitis-Associated Colon Cancer. *Front Immunol* (2012) 3. doi: 10.3389/fimmu.2012.00107
148. Ullman TA, Itzkowitz SH. Intestinal Inflammation and Cancer. *Gastroenterology* (2011) 140(6):1807–16.e1. doi: 10.1053/j.gastro.2011.01.057
149. Terzić J, Grivennikov S, Karin E, Karin M. Inflammation and Colon Cancer. *Gastroenterology* (2010) 138(6):2101–14.e5. doi: 10.1053/j.gastro.2010.01.058
150. Hussain SP, Amstad P, Raja K, Ambs S, Nagashima M, Bennett WP, et al. Increased P53 Mutation Load in Noncancerous Colon Tissue From Ulcerative Colitis: A Cancer-Prone Chronic Inflammatory Disease. *Cancer Res* (2000) 60(13):3333. doi: 10.1046/j.1523-5394.2000.84005.x
151. Zitvogel L, Galluzzi L, Viaud S, Vétizou M, Daillère R, Merad M, et al. Cancer and the Gut Microbiota: An Unexpected Link. *Sci Trans Med* (2015) 7(271):271ps1–ps1. doi: 10.1126/scitranslmed.3010473
152. Wang Y, Ren Y, Huang Y, Yu X, Yang Y, Wang D, et al. Fungal Dysbiosis of the Gut Microbiota Is Associated With Colorectal Cancer in Chinese Patients. *Am J Transl Res* (2021) 13(10):11287–301.
153. Gao R, Kong C, Li H, Huang L, Qu X, Qin N, et al. Dysbiosis Signature of Mycobiota in Colon Polyp and Colorectal Cancer. *Eur J Clin Microbiol Infect Dis* (2017) 36(12):2457–68. doi: 10.1007/s10096-017-3085-6
154. Flemer B, Lynch DB, Brown JMR, Jeffery IB, Ryan FJ, Claesson MJ, et al. Tumour-Associated and Non-Tumour-Associated Microbiota in Colorectal Cancer. *Gut* (2017) 66(4):633. doi: 10.1136/gutjnl-2015-309595
155. Luan C, Xie L, Yang X, Miao H, Lv N, Zhang R, et al. Dysbiosis of Fungal Microbiota in the Intestinal Mucosa of Patients With Colorectal Adenomas. *Sci Rep* (2015) 5(1):7980. doi: 10.1038/srep07980
156. Sobhani I, Bergsten E, Couffin S, Amiot A, Nebbad B, Barau C, et al. Colorectal Cancer-Associated Microbiota Contributes to Oncogenic Epigenetic Signatures. *Proc Natl Acad Sci USA* (2019) 116(48):24285–95. doi: 10.1073/pnas.1912129116
157. Khalyfa AA, Punatar S, Aslam R, Yarbrough A. Exploring the Inflammatory Pathogenesis of Colorectal Cancer. *Diseases* (2021) 9(4):79. doi: 10.3390/diseases9040079
158. Qu J, Sun Z, Peng C, Li D, Yan W, Xu Z, et al. C. *Tropicali* s Promotes Chemotherapy Resistance in Colon Cancer Through Increasing Lactate Production to Regulate the Mismatch Repair System. *Int J Biol Sci* (2021) 17(11):2756–69. doi: 10.7150/ijbs.59262
159. Zhu Y, Shi T, Lu X, Xu Z, Qu J, Zhang Z, et al. Fungal-Induced Glycolysis in Macrophages Promotes Colon Cancer by Enhancing Innate Lymphoid Cell Secretion of IL-22. *EMBO J* (2021) 40(11):e105320. doi: 10.15252/embj.2020105320
160. Kimura Y, Inoue A, Hangai S, Saijo S, Negishi H, Nishio J, et al. The Innate Immune Receptor Dectin-2 Mediates the Phagocytosis of Cancer Cells by Kupffer Cells for the Suppression of Liver Metastasis. *Proc Natl Acad Sci* (2016) 113:14097. doi: 10.1073/pnas.1617903113
161. Nonaka M, Ma BY, Murai R, Nakamura N, Baba M, Kawasaki N, et al. Glycosylation-Dependent Interactions of C-Type Lectin DC-SIGN With Colorectal Tumor-Associated Lewis Glycans Impair the Function and Differentiation of Monocyte-Derived Dendritic Cells. *J Immunol* (2008) 180(5):3347. doi: 10.4049/jimmunol.180.5.3347
162. Lu S, Bevier M, Huhn S, Sainz J, Lascorz J, Pardini B, et al. Genetic Variants in C-Type Lectin Genes are Associated With Colorectal Cancer Susceptibility and Clinical Outcome. *Int J Cancer* (2013) 133(10):2325–33. doi: 10.1002/ijc.28251
163. Jiang Y, Zhang C, Chen K, Chen Z, Sun Z, Zhang Z, et al. The Clinical Significance of DC-SIGN and DC-SIGNR, Which Are Novel Markers Expressed in Human Colon Cancer. *PloS One* (2014) 9(12):e114748. doi: 10.1371/journal.pone.0114748
164. Nikolaou S, Qiu S, Fiorentino F, Rasheed S, Tekkis P, Kontovounisios C. Systematic Review of Blood Diagnostic Markers in Colorectal Cancer. *Techniques Coloproctol* (2018) 22(7):481–98. doi: 10.1007/s10151-018-1820-3
165. Yuan M, Zhang X, Zhang J, Wang K, Zhang Y, Shang W, et al. DC-SIGN–LEF1/TCF1–miR-185 Feedback Loop Promotes Colorectal Cancer Invasion and Metastasis. *Cell Death Differentiation* (2020) 27(1):379–95. doi: 10.1038/s41418-019-0361-2
166. Silva MC, Fernandes Â, Oliveira M, Resende C, Correia A, de-Freitas-Junior JC, et al. Glycans as Immune Checkpoints: Removal of Branched N-Glycans Enhances Immune Recognition Preventing Cancer Progression. *Cancer Immunol Res* (2020) 8(11):1407–25. doi: 10.1158/2326-6066.CIR-20-0264
167. Na H, Liu X, Li X, Zhang X, Wang Y, Wang Z, et al. ovel Roles of DC-SIGNR in Colon Cancer Cell Adhesion, Migration, Invasion, and Liver Metastasis. *N J Hematol Oncol* (2017) 10:1–18. doi: 10.1186/s13045-016-0383-x
168. Sawamura T, Kume N, Aoyama T, Moriwaki H, Hoshikawa H, Aiba Y, et al. An Endothelial Receptor for Oxidized Low-Density Lipoprotein. *Nature* (1997) 386(6620):73–7. doi: 10.1038/386073a0
169. Hashimoto K, Oda Y, Nakamura F, Kakinoki R, Akagi M. Lectin-Like, Oxidized Low-Density Lipoprotein Receptor-1-Deficient Mice Show

Resistance to Age-Related Knee Osteoarthritis. *Eur J Histochem* (2017) 61 (1):49–56. doi: 10.4081/ejh.2017.2762
170. Bruneau N, Richard S, Silvy F, Verine A, Lombardo D. Lectin-Like Ox-LDL Receptor is Expressed in Human INT-407 Intestinal Cells: Involvement in the Transcytosis of Pancreatic Bile Salt-Dependent Lipase. *Mol Biol Cell* (2003) 14(7):2861–75. doi: 10.1091/mbc.e02-08-0544
171. Yoshida H, Kondratenko N, Green S, Steinberg D, Quehenberger O. Identification of the Lectin-Like Receptor for Oxidized Low-Density Lipoprotein in Human Macrophages and its Potential Role as a Scavenger Receptor. *Biochem J* (1998) 334:9–13. doi: 10.1042/bj3340009
172. Draude G, Lorenz RL. TGF-Beta 1 Downregulates CD36 and Scavenger Receptor A But Upregulates LOX-1 in Human Macrophages. *Am J Physiol-Heart Circulatory Physiol* (2000) 278(4):H1042–H8. doi: 10.1152/ajpheart.2000.278.4.H1042
173. Liang M, Zhang P, Fu J. Up-Regulation of LOX-1 Expression by TNF-Alpha Promotes Trans-Endothelial Migration of MDA-MB-231 Breast Cancer Cells. *Cancer Lett* (2007) 258(1):31–7. doi: 10.1016/j.canlet.2007.08.003
174. Nickel T, Schmauss D, Hanssen H, Sicic Z, Krebs B, Jankl S, et al. oxLDL Uptake by Dendritic Cells Induces Upregulation of Scavenger-Receptors, Maturation and Differentiation. *Atherosclerosis* (2009) 205(2):442–50. doi: 10.1016/j.atherosclerosis.2009.01.002
175. Huang D, Gao W, Lu H, Qian JY, Ge JB. Oxidized Low-Density Lipoprotein Stimulates Dendritic Cells Maturation *via* LOX-1-Mediated MAPK/NF-Kappa B Pathway. *Braz J Med Biol Res* (2021) 54(9):e11062. doi: 10.1590/1414-431x2021e11062
176. Morawietz H, Rueckschloss U, Niemann B, Duerrschmidt N, Galle J, Hakim K, et al. Angiotensin II Induces LOX-1, the Human Endothelial Receptor for Oxidized Low-Density Lipoprotein. *Circulation* (1999) 100(9):899–902. doi: 10.1161/01.CIR.100.9.899
177. Morawietz H, Duerrschmidt N, Niemann B, Galle J, Sawamura T, Holtz J. Induction of the OxLDL Receptor LOX-1 by Endothelin-1 in Human Endothelial Cells. *Biochem Biophys Res Commun* (2001) 284(4):961–5. doi: 10.1006/bbrc.2001.5044
178. Smirnova IV, Kajstura M, Sawamura T, Goligorsky MS. Asymmetric Dimethylarginine Upregulates LOX-1 in Activated Macrophages: Role in Foam Cell Formation. *Am J Physiol-Heart Circulatory Physiol* (2004) 287(2): H782–H90. doi: 10.1152/ajpheart.00822.2003
179. Shimaoka T, Kume N, Minami M, Hayashida K, Sawamura T, Kita T, et al. LOX-1 Supports Adhesion of Gram-Positive and Gram-Negative Bacteria. *J Immunol* (2001) 166(8):5108–14. doi: 10.4049/jimmunol.166.8.5108
180. Yan M, Mehta JL, Hu C. LOX-1 and Obesity. *Cardiovasc Drugs Ther* (2011) 25(5):469–76. doi: 10.1007/s10557-011-6335-3
181. Tan KCB, Shiu SWM, Wong Y, Leng L, Bucala R. Soluble Lectin-Like Oxidized Low Density Lipoprotein Receptor-1 in Type 2 Diabetes Mellitus. *J Lipid Res* (2008) 49(7):1438–44. doi: 10.1194/jlr.M700551-JLR200
182. Joo H, Li D, Dullaers M, Kim T-W, Duluc D, Upchurch K, et al. C-Type Lectin-Like Receptor LOX-1 Promotes Dendritic Cell-Mediated Class-Switched B Cell Responses. *Immunity* (2014) 41(4):592–604. doi: 10.1016/j.immuni.2014.09.009
183. Chan AOO, Jim MH, Lam KF, Morris JS, Siu DCW, Tong T, et al. Prevalence of Colorectal Neoplasm Among Patients With Newly Diagnosed Coronary Artery Disease. *Jama-J Am Med Assoc* (2007) 298(12):1412–9. doi: 10.1001/jama.298.12.1412
184. Poynter JN, Gruber SB, Higgins PDR, Almog R, Bonner JD, Rennert HS, et al. Statins and the Risk of Colorectal Cancer. *New Engl J Med* (2005) 352 (21):2184–92. doi: 10.1056/NEJMoa043792
185. Lu Jj, Mitra S, Wang XW, Khaidakov M, Mehta JL. Oxidative Stress and Lectin-Like Ox-LDL-Receptor LOX-1 in Atherogenesis and Tumorigenesis. *Antioxid Redox Signaling* (2011) 15(8):2301–33. doi: 10.1089/ars.2010.3792
186. Suzuki K, Ito Y, Wakai K, Kawado M, Hashimoto S, Toyoshima H, et al. Serum Oxidized Low-Density Lipoprotein Levels and Risk of Colorectal Cancer: A Case-Control Study Nested in the Japan Collaborative Cohort Study. *Cancer Epidemiol Biomarkers Prev* (2004) 13(11):1781–7. doi: 10.1007/s00280-004-0822-1
187. Hirsch HA, Iliopoulos D, Joshi A, Zhang Y, Jaeger SA, Bulyk M, et al. A Transcriptional Signature and Common Gene Networks Link Cancer With Lipid Metabolism and Diverse Human Diseases. *Cancer Cell* (2010) 17 (4):348–61. doi: 10.1016/j.ccr.2010.01.022
188. Keshavarzian A, Zapeda D, List T, Mobarhan S. High-Levels of Reactive Oxygen Metabolites in Colon Cancer-Tissue - Analysis by Chemiluminescence Probe. *Nutr Cancer-an Int J* (1992) 17(3):243–9. doi: 10.1080/01635589209514193
189. Murdocca M, Mango R, Pucci S, Biocca S, Testa B, Capuano R, et al. The Lectin-Like Oxidized LDL Receptor-1: A New Potential Molecular Target in Colorectal Cancer. *Oncotarget* (2016) 7(12):14765–80. doi: 10.18632/oncotarget.7430
190. Murdocca M, Capuano R, Pucci S, Cicconi R, Polidoro C, Catini A, et al. Targeting LOX-1 Inhibits Colorectal Cancer Metastasis in an Animal Model. *Front Oncol* (2019) 9. doi: 10.3389/fonc.2019.00927
191. Zhao T, Li Y, Shen K, Wang Q, Zhang J. Knockdown of OLR1 Weakens Glycolytic Metabolism to Repress Colon Cancer Cell Proliferation and Chemoresistance by Downregulating SULT2B1 *via* C-MYC. *Cell Death Dis* (2021) 13(1):4. doi: 10.1038/s41419-021-04174-w
192. Nakashima-Nakasuga C, Hazama S, Suzuki N, Nakagami Y, Xu M, Yoshida S, et al. Serum LOX-1 is a Novel Prognostic Biomarker of Colorectal Cancer. *Int J Clin Oncol* (2020) 25(7):1308–17. doi: 10.1007/s10147-020-01673-2
193. Condamine T, Dominguez GA, Youn J-I, Kossenkov AV, Mony S, Alicea-Torres K, et al. Lectin-Type Oxidized LDL Receptor-1 Distinguishes Population of Human Polymorphonuclear Myeloid-Derived Suppressor Cells in Cancer Patients. *Sci Immunol* (2016) 1(2):aaf8943. doi: 10.1126/sciimmunol.aaf8943
194. Chai E, Zhang L, Li C. LOX-1+PMN-MDSC Enhances Immune Suppression Which Promotes Glioblastoma Multiforme Progression. *Cancer Manage Res* (2019) 11:7307–15. doi: 10.2147/CMAR.S210545
195. Katayama C, Yokobori T, Ozawa N, Suga K, Shiraishi T, Okada T, et al. Low Level of Stromal Lectin-Like Oxidized LDL Receptor 1 and CD8+ Cytotoxic T-Lymphocytes Indicate Poor Prognosis of Colorectal Cancer. *Cancer Rep* (2021) 4(4):e1364. doi: 10.1002/cnr2.1364
196. Luo X, Lian Q, Li W, Chen L, Zhang R, Yang D, et al. Fully Synthetic Mincle-Dependent Self-Adjuvanting Cancer Vaccines Elicit Robust Humoral and T Cell-Dependent Immune Responses and Protect Mice From Tumor Development. *Chem Sci* (2021) 12(48):15998–6013. doi: 10.1039/D1SC05736G
197. Shiga M, Miyazaki J, Tanuma K, Nagumo Y, Yoshino T, Kandori S, et al. The Liposome of Trehalose Dimycolate Extracted From M. Bovis BCG Induces Antitumor Immunity *via* the Activation of Dendritic Cells and CD8+ T Cells. *Cancer Immunol Immunother* (2021) 70(9):2529–43. doi: 10.1007/s00262-021-02870-2
198. Ruland J. CARD9 Signaling in the Innate Immune Response. *Ann New Y Acad Sci* (2008) 1143(1):35–44. doi: 10.1196/annals.1443.024
199. Hsu Y-MS, Zhang Y, You Y, Wang D, Li H, Duramad O, et al. The Adaptor Protein CARD9 is Required for Innate Immune Responses to Intracellular Pathogens. *Nat Immunol* (2007) 8(2):198–205. doi: 10.1038/ni1426
200. Glocker E-O, Hennigs A, Nabavi M, Schaeffer AA, Woellner C, Salzer U, et al. A Homozygous CARD9 Mutation in a Family With Susceptibility to Fungal Infections. *N Engl J Med* (2009) 361(18):1727–35. doi: 10.1056/NEJMoa0810719
201. Lanternier F, Mandaviani SA, Barbati E, Chaussade H, Koumar Y, Levy R, et al. Inherited CARD9 Deficiency in Otherwise Healthy Children and Adults With Candida Species-Induced Meningoencephalitis, Colitis, or Both. *J Allergy Clin Immunol* (2015) 135(6):1558–U269. doi: 10.1016/j.jaci.2014.12.1930
202. McGovern DPB, Gardet A, Törkvist L, Goyette P, Essers J, Taylor KD, et al. Genome-Wide Association Identifies Multiple Ulcerative Colitis Susceptibility Loci. *Nat Genet* (2010) 42(4):332–7. doi: 10.1038/ng.549
203. Jostins L, Ripke S, Weersma RK, Duerr RH, McGovern DP, Hui KY, et al. Host-Microbe Interactions Have Shaped the Genetic Architecture of Inflammatory Bowel Disease. *Nature* (2012) 491(7422):119–24. doi: 10.1038/nature11582
204. Rivas MA, Beaudoin M, Gardet A, Stevens C, Sharma Y, Zhang CK, et al. Deep Resequencing of GWAS Loci Identifies Independent Rare Variants Associated With Inflammatory Bowel Disease. *Nat Genet* (2011) 43 (11):1066–U50. doi: 10.1038/ng.952
205. Sokol H, Conway KL, Zhang M, Choi M, Morin B, Cao Z, et al. Card9 Mediates Intestinal Epithelial Cell Restitution, T-Helper 17 Responses, and Control of Bacterial Infection in Mice. *Gastroenterology* (2013) 145(3):591–601.e3. doi: 10.1053/j.gastro.2013.05.047

206. Wang T, Fan C, Yao A, Xu X, Zheng G, You Y, et al. The Adaptor Protein CARD9 Protects Against Colon Cancer by Restricting Mycobiota-Mediated Expansion of Myeloid-Derived Suppressor Cells. *Immunity* (2018) 49 (3):504–14.e4. doi: 10.1016/j.immuni.2018.08.018
207. Lamas B, Richard ML, Leducq V, Pham H-P, Michel M-L, Da Costa G, et al. CARD9 Impacts Colitis by Altering Gut Microbiota Metabolism of Tryptophan Into Aryl Hydrocarbon Receptor Ligands. *Nat Med* (2016) 22 (6):598–605. doi: 10.1038/nm.4102
208. Zelante T, Iannitti RG, Cunha C, De Luca A, Giovannini G, Pieraccini G, et al. Tryptophan Catabolites From Microbiota Engage Aryl Hydrocarbon Receptor and Balance Mucosal Reactivity *via* Interleukin-22. *Immunity* (2013) 39(2):372–85. doi: 10.1016/j.immuni.2013.08.003
209. Rutz S, Eidenschenk C, Ouyang W. IL-22, Not Simply a Th17 Cytokine. *Immunol Rev* (2013) 252(1):116–32. doi: 10.1111/imr.12027
210. Limon JJ, Tang J, Li D, Wolf AJ, Michelsen KS, Funari V, et al. Malassezia Is Associated With Crohn's Disease and Exacerbates Colitis in Mouse Models. *Cell Host Microbe* (2019) 25(3):377–88.e6. doi: 10.1016/j.chom.2019.01.007
211. Malik A, Sharma D, Malireddi RKS, Guy CS, Chang T-C, Olsen SR, et al. SYK-CARD9 Signaling Axis Promotes Gut Fungi-Mediated Inflammasome Activation to Restrict Colitis and Colon Cancer. *Immunity* (2018) 49(3):515–30.e5. doi: 10.1016/j.immuni.2018.08.024
212. Qu J, Liu L, Xu Q, Re J, Xu Z, Dou H, et al. CARD9 Prevents Lung Cancer Development by Suppressing the Expansion of Myeloid-Derived Suppressor Cells and IDO Production. *Int J Cancer* (2019) 145(8):2225–37. doi: 10.1002/ijc.32355
213. Bergmann H, Roth S, Pechloff K, Kiss EA, Kuhn S, Heikenwälder M, et al. Card9-Dependent IL-1β Regulates IL-22 Production From Group 3 Innate Lymphoid Cells and Promotes Colitis-Associated Cancer. *Eur J Immunol* (2017) 47(8):1342–53. doi: 10.1002/eji.201646765
214. Yang M, Shao JH, Miao YJ, Cui W, Qi YF, Han JH, et al. Tumor Cell-Activated CARD9 Signaling Contributes to Metastasis-Associated Macrophage Polarization. *Cell Death Differ* (2014) 21(8):1290–302. doi: 10.1038/cdd.2014.45
215. Leo VI, Tan SH, Bergmann H, Cheah PY, Chew MH, Lim KH, et al. CARD9 Promotes Sex-Biased Colon Tumors in the APC(min) Mouse Model. *Cancer Immunol Res* (2015) 3(7):721–6. doi: 10.1158/2326-6066.CIR-14-0148
216. Gao B, Chi L, Zhu Y, Shi X, Tu P, Li B, et al. An Introduction to Next Generation Sequencing Bioinformatic Analysis in Gut Microbiome Studies. *Biomolecules* (2021) 11(4):530. doi: 10.3390/biom11040530
217. Zhang L, Zhan H, Xu W, Yan S, Ng SC. The Role of Gut Mycobiome in Health and Diseases. *Ther Adv Gastroenterol* (2021) 14:17562848211047130. doi: 10.1177/17562848211047130
218. Alou MT, Naud S, Khelaifia S, Bonnet M, Lagier J-C, Raoult D. State of the Art in the Culture of the Human Microbiota: New Interests and Strategies. *Clin Microbiol Rev* (2020) 34(1):e00129–19. doi: 10.1128/CMR.00129-19
219. Xiong X, Tian S, Yang P, Lebreton F, Bao H, Sheng K, et al. Emerging Enterococcus Pore-Forming Toxins With MHC/HLA-I as Receptors. *Cell* (2022). doi: 10.1016/j.cell.2022.02.002

Conflict of Interest: The authors declare that the research was conducted in the absence of any commercial or financial relationships that could be construed as a potential conflict of interest.

Publisher's Note: All claims expressed in this article are solely those of the authors and do not necessarily represent those of their affiliated organizations, or those of the publisher, the editors and the reviewers. Any product that may be evaluated in this article, or claim that may be made by its manufacturer, is not guaranteed or endorsed by the publisher.

frontiers | Frontiers in Immunology

REVIEW
published: 10 June 2022
doi: 10.3389/fimmu.2022.906122

Intestinal Uptake and Tolerance to Food Antigens

Yuhong Xiong[1,2], *Guifeng Xu*[1], *Mingwu Chen*[1*] and *Hongdi Ma*[1,2*]

[1] Department of Pediatrics, The First Affiliated Hospital of University of Science and Technology of China (USTC), Division of Life Sciences and Medicine, University of Science and Technology of China, Hefei, China, [2] Institute of Immunology, The Chinese Academy of Sciences (CAS) Key Laboratory of Innate Immunity and Chronic Disease, School of Basic Medical Sciences, Division of Life Sciences and Medicine, University of Science and Technology of China, Hefei, China

Food allergy is a growing concern due to its increasing world-wide incidence. Strict avoidance of allergens is a passive treatment strategy. Since the mechanisms responsible for the occurrence and development of food allergy have not yet been fully elucidated, effective individualized treatment options are lacking. In this review, we summarize the pathways through which food antigens enter the intestine and review the proposed mechanisms describing how the intestine acquires and tolerates food antigens. When oral tolerance is not established, food allergy occurs. In addition, we also discuss the contribution of commensal bacteria of the gut in shaping tolerance to food antigens in the intestinal tract. Finally, we propose that elucidating the mechanisms of intestinal uptake and tolerance of food antigens will provide additional clues for potential treatment options for food allergy.

Keywords: food antigens, food allergy, paracellular pathway, transcellular pathway, intestinal barrier, oral tolerance, intestinal immune system, gut microbiota

OPEN ACCESS

Edited by:
Daming Zuo,
Southern Medical University, China

Reviewed by:
Xiaoshan Shi,
Shenzhen Institutes of Advanced Technology (CAS), China
Peixiang Lan,
Huazhong University of Science and Technology, China
Chuanfeng Wu,
National Heart, Lung, and Blood Institute (NIH), United States

***Correspondence:**
Hongdi Ma
mahongdi@ustc.edu.cn
Mingwu Chen
chenmingwu01@163.com

Specialty section:
This article was submitted to Molecular Innate Immunity, a section of the journal Frontiers in Immunology

Received: *28 March 2022*
Accepted: *16 May 2022*
Published: *10 June 2022*

Citation:
Xiong Y, Xu G, Chen M and Ma H (2022) Intestinal Uptake and Tolerance to Food Antigens. Front. Immunol. 13:906122. doi: 10.3389/fimmu.2022.906122

INTRODUCTION

Globally, there is an increasing incidence of food allergy that affects the quality of life of those affected (1–3). Food allergies have been identified at all ages. Food allergy affects approximately 6% of children and 3 to 4% of adults (4). Allergies to certain foods that start in childhood can persist into adulthood, and new allergies can occur at any stage of life (5). For example, 40 to 60% of fish or shellfish allergies begin in adulthood (6). Peanut allergy affects nearly 5 million adults in the United States, and about one in six individuals with peanut allergy experience their first episode in adulthood (7).

Although food allergy has a wide incidence and is considered a substantial public health burden, its diagnosis and treatment are still inadequate due to the limitations of research into its pathogenesis (8) and the understanding of the mechanisms triggering food allergies (9). First, there are no clear and uniform diagnostic criteria. In addition, most symptoms of food allergy are not typical, such as cough, diarrhea, abdominal pain, and vomiting, which are similar to the symptoms of many other clinical diseases and are often ignored or misdiagnosed (10). Second, because of the lack of understanding of the pathogenic mechanisms of food allergy, there is a lack of safe and effective treatment options for individuals diagnosed with food allergy. The only safe and effective method for patients with a food allergy diagnosis is to strictly avoid the allergic antigens (11, 12). However, there is widespread concern that a strict and limited diet in patients with food

allergies can lead to nutritional deficiencies and growth failure in children (13). Recently, allergen-specific immunotherapy has also emerged, and involves the administration of allergic antigens orally, sublingually, or epicutaneously to induce immune tolerance to allergens. Although allergen-specific immunotherapy has made considerable progress in the treatment of food allergies, during the course of clinical treatment, allergen-specific immunotherapy has obvious limitations in efficacy, safety, and durability (14). Thus, an in-depth exploration of the pathogenic mechanism of food allergy is necessary to further improve and optimize treatment plans.

It is well-known that the primary role of the intestinal mucosa is to act as a barrier to prevent harmful substances from entering the digestive system. Furthermore, as a selective filter, the intestinal mucosa allows the necessary dietary nutrients, water, and electrolytes to be diverted from the lumen into the blood circulation of the intestine (15). Although considered as foreign antigens, food antigens are selectively filtered into the circulation by the intestinal mucosa without triggering a defense immune attack response in the intestines but induces immune tolerance. Nevertheless, the disruption of this tolerance mechanism will lead to food allergies. Herein, we focus on how food antigens pass through the intestinal barrier and how they are acquired and tolerated by the intestinal immune system. We also discuss situations in which food allergy occurs when the intestinal immune regulation is disturbed. Finally, by summarizing and discussing these studies on food allergy, we hope to provide more clues to stimulate fundamental research and clinical applications in the field of food allergy.

HOW DO FOOD ANTIGENS CROSS THE INTESTINAL BARRIER?

Structurally, the intestinal barrier can be divided into three layers. The outer layer is the mucus layer that is symbiotic with intestinal microorganisms, the central layer is a specialized single cell layer consisting of epithelial cells, and the inner layer is the lamina propria (LP) composed of innate and adoptive immune cells. The mucus layer has a Sieve-like structure, among which mucins secreted by goblet/mucinous cells cover the intestinal epithelium (16). Mucins secreted in the mucus layer can protect intestinal epithelial cells from digestive enzymes and function as a defense barrier to prevent the invasion of foreign microorganisms (17–19). The central layer is made up of intestinal epithelial cells that are considered important components of the intestinal defense system and play a key role in the transport of substances into the intestinal tract. A variety of epithelial cell subsets, including absorptive enterocytes, goblet cells, Paneth cells (20, 21), tuft cells (22), enteroendocrine cells (23), microfold cells (M cells), and epithelial stem cells, have unique and specialized characteristics and functions, which cooperatively form a sophisticated epithelial layer against numerous antigens in the lumen (24). A set of highly organized intercellular junction complexes links these intestinal epithelial cells to form intestinal paracellular barriers. These junction complexes are in dynamic balance and are divided into three types: tight junctions (TJs), adherens junctions (AJs), and desmosomes (25). Paracellular barriers composed of these junction complexes function to maintain the integrity of the intestine and also mediate the regulation of nutrients that pass through the intestine through the paracellular pathway. Beyond the mucus layer and the epithelial layer, is the LP, which contains both innate and adaptive immune cells, such as dendritic cells (DCs), macrophages, T cells, and B cells. Immune cells in the LP are involved in both immune defense and immune regulation in the intestinal microenvironment (26). The intestinal barrier composed of these three layers can effectively prevent harmful substances from entering the body. However, this barrier is not completely impenetrable. The intestinal barrier allows foreign nutrients to enter the body to meet growth needs. We will first summarize the pathways through which nutrients from ingested food pass through the intestine.

Food is digested into peptides, amino acids, polysaccharides, monosaccharides, water, electrolytes, and other nutrients through chemical and mechanical activity in the digestive tract. These nutrients, including food antigens, enter the subepithelium through two main pathways, the paracellular pathway and the transcellular pathway.

Paracellular Pathway

As mentioned above, the intercellular junction complex located in intestinal epithelial cells is the main mediator that regulates the paracellular pathway. Among the three types of epithelia junction complexes, TJs are composed of transmembrane proteins (27), which interact with each other and with the intestinal immune system, making them the main rate-limiting step in controlling the permeability of the paracellular pathway (28, 29). The TJ proteins, such as zonula occludens (ZO) (30–32), occludins (33), and claudins (34) participate in the formation of TJs and control the permeability of paracellular pathways. Small molecules derived from food nutrients, such as solutes soluble in water, cross the intestinal barrier through paracellular pathways (**Figure 1-(1)**). Paracellular pathways have the selectivity of capacity, charge, and size for the substances they transport. This pathway is highly regulated by TJs to ensure that the transport of materials across the epithelial barrier is strictly controlled. However, when the epithelial barrier is damaged, such as following destruction of TJs, the paracellular pathway becomes nonrestrictive and allows the free passage of ions, water, macromolecules, and even bacteria or viruses. This increases the intestinal permeability and leads to pathological changes (**Figure 1-(2)**). For example, food cysteine proteases degrade the TJ protein occludin, thus increasing the permeability in the paracellular pathway, which can contribute to the sensitization process of food allergies (35). Furthermore, the paracellular pathway is disrupted in patients with inflammatory bowel disease (IBD) due to the reduced expression of TJs and AJs proteins in epithelial cells in the inflammatory zone, such as ZO-1, claudin, and E-cadherin (36). Thus, the paracellular pathway plays an indispensable role in mediating materials into the intestinal subepithelium, and this process is controlled by TJs between epithelial cells. Furthermore, damage to TJs disrupts the

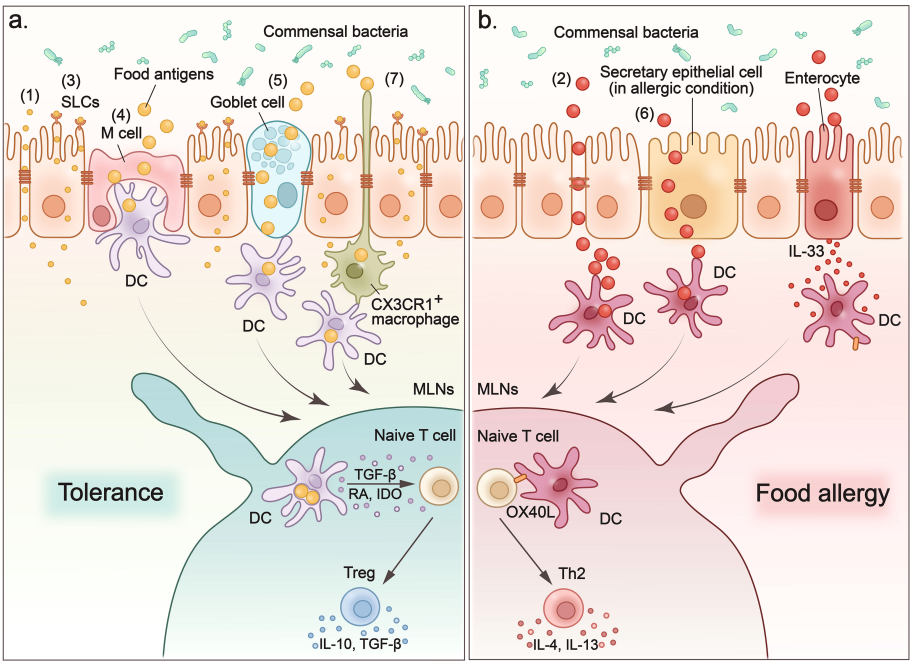

FIGURE 1 | Food antigens cross the intestinal epithelium to induce tolerance or provoke allergy. (1) Small molecules such as electrolytes and water enter the sub-epithelium *via* paracellular pathways. (2) Degradation of tight junctions increases the permeability of the paracellular pathway, which leads to non-selective and uncontrolled entry of macromolecules into the intestinal sub-epithelium and contributes to the sensitization process of food allergies. (3) Small molecules such as amino acids and glucose that are transported across the epithelium by apical brush boundary transporters such as SLCs on enterocytes. (4) M cells sample food antigens, and then present them to dendritic cells. (5) Goblet cells form goblet-cell-associated antigen passage (GAP) to enclose luminal antigens (food antigens and microbial antigens) in internal sack-like vesicles, and then transport them across entire cells to dendritic cells. (6) In food allergy mouse models, secretory epithelial cells function as conduits to allow the transport of food antigens through the epithelium of the small intestine and induce a food-induced anaphylactic reaction. (7) $CX3CR1^+$ macrophages rely on CX3CR1 expression to form dendrites to efficiently sample antigens from the intestinal lumen without disrupting the tight junctions between the cells. $CX3CR1^+$ macrophages transfer antigens they captured to $CD103^+$ DC. **(A)** When food antigens enter the intestinal sub-epithelium through above pathways, they are acquired and processed by dendritic cells. Then DCs migrate to MLNs where they present the processed food antigens and induce tolerance or food allergy. To induce oral tolerance, DCs secrete interleukin-10 (IL-10), transforming growth factor-β (TGF-β), and indoleamine 2,3-dioxygenase (IDO) to induce Tregs and promote their production of IL-10 and TGF-β to maintain tolerance. **(B)** In the case of allergy, oral antigens and adjuvants stimulate the expression of IL-33 in intestinal epithelial cells, which in turn upregulates the expression of the costimulatory molecule-OX40L on DCs. OX40L expression upregulates DCs to promote the TH2 response in the MLN and leads to more severe food allergies.

paracellular pathway, which leads to increased intestinal permeability and intestinal disorders such as food allergies and IBD.

Transcellular Pathway

Enterocytes are the main type of intestinal epithelial cells and differ greatly in structure and composition between the small intestine and the colon. In the small intestine, enterocytes have villi that protrude into the lumen. The villi increase the surface area of the intestinal mucosa for better absorption of nutrients. These cells concentrate digestive enzymes (such as pancreatic proteolytic enzymes) on their apical surface, which are involved in the chemical digestion of lipids, carbohydrates and proteins, and absorb these digested nutrients through the apical brush boundary transporters (such as the SLC1A, SLC6A, and SLC7A families) (37). As we mentioned, small molecules such as water (38) and ions (39) can enter the intestinal subepithelium *via* paracellular pathways. They can also enter the intestinal cytoplasm from the apical membrane through epithelial transporters (integral membrane protein pumps or channels) and are discharged from the basolateral membrane (**Figure 1-(3)**). For example, the sodium-dependent transport of glucose (40), alanine (41), and glutamine (42) occurs on the surface of intestinal epithelial cells. However, macromolecules can only enter the cell through vesicles, which are formed by invagination and extrusion of the apical membrane. The vesicle transfer process is called endocytosis (43), which in intestinal cells is limited to pinocytosis (44). A variety of intestinal epithelial cells are involved in these intestinal epithelial-mediated transcellular pathways. Among them, M cells and goblet cells play a pivotal role in internalizing luminal antigens into gut-associated lymphoid tissues (GALTs) and in establishing intestinal tolerance or inducing intestinal immune responses to food antigens. They indiscriminately sample lumen contents, including food antigens, and transport the intact antigens to intestinal DCs to process and present these antigens (37).

M cells are specialized epithelial cells located in the follicle-associated epithelium overlying Peyer's patches (PP) (45, 46).

Their location facilitates M cells to transcytose a wide range of substances, such as food antigens and microbes, to underlying DCs for antigen processing and presentation (47) (**Figure 1-(4)**). In addition, M cells have specialized structures that lack the typical brushlike border and have thinner calyx glycosomes, making it easier to capture large particle antigens and transcytose them by pinocytosis in the fluid phase and by receptor-mediated endocytosis (48). Besides the delivery of intact antigens into the underlying lymphoid tissue of the GALT (49, 50), M cells also participate in Ag processing and presentation based on the observation that GALT M cells express MHC class II molecules and acidic endosomal-lysosomal compartments (51). Suzuki et al. developed an M cell-targeting Ag delivery system by combining antigens OVA with pσ1 protein that is known to bind to M cells in gut and nasal-associated lymphoid tissues (NALT) to investigate the role of M cells in oral tolerance (47, 52, 53). Using this M cell-targeting antigen delivery system, the authors determined that the recombinant protein OVA-pσ1 can induce mucosal unresponsiveness through two main mechanisms: clonal deletion of Ag-specific CD4+ T cells and the induction of acquired type Tregs cells (47). However, additional studies have also reported that oral tolerance could be established even in the absence of PP or the destruction of M cells to facilitate antigen transport to the PP (54, 55). Thus, the role of M cells in the induction of oral tolerance by transporting Ags from the lumen is controversial and further studies of the mechanism are needed.

Goblet cells are specialized mucous epithelial secretory cells. The secretory products of goblet cells, including mucins, trefoil factors, and other proteins, are essential for the integrity of the intestinal barrier and the prevention against the entry of harmful antigens (56). It should be noted that another important role of goblet cells is the formation of a goblet cell-associated antigen passage (GAP) to transport luminal antigens (food antigens and microbial antigens) to antigen-presenting cells (APC) in the LP (57, 58) (**Figure 1-(5)**). Preventing the entry of harmful antigens through mucus secretion and sampling luminal substances into the intestinal immune system through GAP formation are two divergent processes for goblet cells. Molecular mechanisms have revealed that a neurotransmitter called acetylcholine can trigger both mucus release and the GAP process in goblet cells in independent signaling pathways mediated by different receptors (59). This regulation of Ach allows goblet cells to accommodate the dynamically changing demands of the mucosal environment. Goblet cells can also deliver luminal substances, including food antigens and microbial antigens, and induce intestinal tolerance through the GAP process (60). First, goblet cells capture food antigens from the lumen, enclose them in internal sack-like vesicles, and then transport them across the entire cell. Then the APCs in the LP acquire luminal antigens to induce intestinal tolerance by maintaining pre-existing Tregs in the LP, and imprinting tolerogenic properties (60). However, Noah et al. reported that in food allergic mice, secretory epithelial cells, including goblet cells, enteroendocrine cells, and Paneth cells in the small intestine function as conduits to allow the transport of food antigens through the epithelium of the small intestine to the underlying immune cells and induce a food-induced anaphylactic reaction (61) (**Figure 1-(6)**). They also found that these secretory epithelial cell antigen passages (SAP) were induced by the Th2 cytokine-IL-13 in a CD38/cADPR-dependent manner (61). Additionally, blockade of this process reduced the passage of food antigens through the epithelium of the small intestine and alleviated the induction of the food allergic reaction in the intestine (61). Finally, they confirmed that SAP formation driven by IL-13 through the PI3K/CD38/cADPR pathway is conserved in the human intestine, indicating that blockade of this process, such as by inhibiting Th2 cytokines, might represent a potential therapeutic option for food allergy.

HOW ARE FOOD ANTIGENS ACQUIRED AND TOLERATED BY THE INTESTINAL IMMUNE SYSTEM?

When food antigens enter the intestinal sub-epithelium through the above pathways, they are acquired and processed by APCs dispersed in the LP, PPs, and mesenteric lymph nodes (MLN). Oral tolerance to food antigens is often induced in MLNs (55) (**Figure 1A**). When the underlying APCs acquire the food antigens, they process them and present them to immune regulatory cells such as Treg cells in the MLN and induce tolerance (62).

Food Antigen Capture and Oral Tolerance Induction in the Intestine

As we mentioned above, food antigens can be internalized by M cells or acquired by goblet cell-associated passages. When the food antigens are captured by these specialized intestinal epithelial cells, they will be transferred to the migratory DCs in the intestinal PP (where the M cells deliver antigens to underlying DCs) (63) and LP (where the GAPs transport antigens to DCs) (57).

DCs and macrophages are the two main APCs for food antigens (64, 65). Rescigno et al. observed that DCs can penetrate the monolayers of the intestinal epithelium into the gut lumen by extending the transepithelial dendrites (66). This property provides DCs with access to antigens in the intestinal lumen. $CX3CR1^+$ macrophages have also been reported to rely on CX3CR1 expression to form dendrites to efficiently sample antigens from the intestinal lumen (67). These antigen uptake macrophages quickly transfer food antigens to $CD103^+$ DCs *via* connexin 43 in the gap junctions (67) (**Figure 1-(7)**).

In general, food antigens are collected directly by intestinal DCs or by $CX3CR1^+$ macrophages or other epithelial cells (such as the M cells and goblet cells described earlier) and are delivered to DCs (68).

When loaded with food antigens, DCs migrate to the MLNs where they present the processed food antigens and induce tolerance (**Figure 1A**). Among various subsets of DCs, $CD103^+$

DCs have been reported to play an important role in tolerance induction (67). $CD103^+$ DCs are derived from circulating monocytes that express the gut homing marker-α4β7 integrin (69). They are located in the LP of the small and large intestine. When they acquire food antigens from the lumen, they migrate to MLNs to induce oral tolerance by activating Tregs. There are several mechanisms through which $CD103^+$ DC induce Tregs. For example, intestinal $CD103^+$ DCs have been reported to secrete retinoic acid (RA) and transforming growth factor-β (TGF-β) to promote the differentiation of Foxp3+Treg cells (70, 71). $CD103^+$ DC also express indoleamine 2,3-dioxygenase (IDO), to sustain and differentiate Tregs, while inhibition of IDO *in vivo* has been reported to reduce Tregs specific to orally administered antigens and to impair the induction of oral tolerance (72).

Besides $CD103^+$ DC, resident intestinal macrophages marked with high expression of the CX3C-chemokine receptor 1 (CX3CR1) also help to maintain Foxp3 expression in Tregs in the intestine by secreting IL-10 (73, 74). These intestinal resident macrophages have been proposed to provide additional survival signals for Tregs since they express high level of MHC class II, which enables them to undergo cognate interactions with specific Treg cells (75).

In addition to Treg-mediated oral tolerance, T cell clone anergy and/or deletion are also involved in oral tolerance (76, 77). The modality of oral tolerance induction depends on the dose of food antigens (77). Low dose of antigens induce Treg mediated immune suppression, while high doses of antigens lead to anergy and deletion of antigen-specific T cells (76–78).

Intestinal Commensal Bacteria Help Establish Oral Tolerance

Intestinal commensal bacteria also provide a large number of non-self-antigens that are tolerated by the intestinal immune system (73, 79, 80). Evidence indicates that the intestinal microbiota is crucial for the development and maturation of the intestinal immune system (81, 82). In particular, intestinal commensal bacteria could help shape intestinal tolerance. In germ-free (GF) mice, the frequency of Tregs and the levels of the anti-inflammatory cytokine IL-10 produced by Tregs are markedly reduced compared to mice free of specific pathogens (83–86). In one study, 17 strains of bacteria from the human gut microbiota were identified as Treg-cell-inducing bacterial strains. Treatment of these 17 Treg cell-inducing strains could alleviate intestinal inflammation, including allergic diarrhea (87). Furthermore, the observation that food allergen sensitization is enhanced in GF mice or mice that have been treated with antibiotics suggests that commensal bacteria are essential for the establishment of oral tolerance (88). Although the mechanisms by which the intestinal microbiota regulate allergic responses to food are not yet fully defined, studies have revealed that the composition of the gut microbiota, metabolites derived from intestinal bacteria and colonization of special functional bacteria are important factors that influence intestinal tolerance to food antigens.

Mechanistically, intestinal bacteria-derived metabolites, including inosine and short-chain fatty acids (SCFAs), are considered key factors promoting Treg differentiation and improve the production of regulatory cytokines such as IL-10 (89–91). In particular, SCFAs, which are produced during the bacterial fermentation of indigestible dietary fiber, have received much attention for their immunoregulatory activity. Butyrate, one of the most abundant SCFAs in the gut, has been reported to induce functional colonic Treg cells through its function to enhance histone H3 acetylation in the promoter and conserved non-coding sequence regions of the Foxp3 locus (92). In addition, it has been reported that SCFAs, particularly acetate and butyrate, could help establish oral tolerance and prevent food allergy by enhancing retinaldehyde dehydrogenase-2 (RALDH2) activity in $CD103^+$ DC (93). RALDH2 converts vitamin A to retinoic acid, which promotes the differentiation of naive T cells into Treg cells and contributes to the establishment of oral tolerance (93, 94).

Stefka et al. reported that colonization of a Clostridia-containing microbiota can protect against sensitization to food allergens (88). Colonization of Clostridia induced early production of IL-22 by RORγt+ innate lymphoid cells (ILCs) and T cells in the intestine. This Clostridia-Induced IL-22 reduced the access of food allergen to the circulation (88).

In addition, dysbiosis of the gut microbiota leads to intolerance in the intestine. When the gut microbiota of infants allergic to milk protein was transplanted into GF mice, these recipient mice also showed an allergic response to milk-allergens (95).

PATHOGENESIS AND TREATMENT OF FOOD ALLERGY

The most important role of intestinal immune system is to distinguish innocuous food antigens and commensal microbes from pathogens. They initiate an immune response against pathogens and induce tolerance to food and commensal bacteria. However, a breakdown of the default oral tolerance to food leads to abnormal immune responses and results in food allergy (**Figure 1B**). Many factors including the genetic background, alteration of gut microbiota, food allergenicity and methods of food processing, may trigger a food allergy.

As we mentioned, the intestinal APCs, especially intestinal DCs play a pivotal role in the induction of tolerance. However, stimuli from food components or extrinsic adjuvants could activate DCs to trigger a food allergy. Although the detailed identification of stimuli and their reorganization are not very clear, it has been reported that glycoproteins from the allergenic foods could directly bind to C-type lectin receptors (CLR) on DCs to stimulate immune response to the food allergens (96). For instance, in the peanut induced allergy, the glycoprotein Ara h 1 was identified as the major peanut allergen able to bind to DC specific intercellular adhesion molecule-3-grabbing non-integrin (DC-SIGN), a C-type lectin receptor, on monocyte-derived DCs and subsequently activate DCs to induce allergic immune responses (97). Similarly, hazelnuts, walnuts, and egg whites have also been found to bind to DC-SIGN and related DC-

SIGNR to activate DCs and contribute to the development of food allergies (98, 99).

In addition, alarmins such as IL-25, IL-33, and TSLP are also involved in the development of food allergies (100, 101). Among these allergenic alarmins, intestinal epithelial cell-derived IL-33 has been reported to act on different immune cells to expand the allergenic immune response in the intestine. In an allergenic mouse model, oral Ags and adjuvants stimulate the expression of IL-33 in intestinal epithelial cells, which in turn up-regulate the expression of the costimulatory molecule-OX40L in DCs. These DCs expressing upregulated OX40L promote the Th2 response in the MLN and lead to more severe food allergies (102, 103) (**Figure 1B**). In another study, IL-33 secreted by intestinal epithelial cells was found to act on type 2 ILC (ILC2) to enhance their expansion and induce their production of IL-4 (104). The IL-33 signal-stimulated production of IL-4 by ILC2 is indispensable for oral allergic sensitization and anaphylaxis (104, 105). Furthermore, IL-33 acts directly on mast cells to potentiate antigen-driven IgE-dependent degranulation of MC and promotes oral anaphylaxis after epicutaneous sensitization (106).

Based on current understanding of the mechanisms of oral tolerance and food allergy, there have been significant advances in treatment to food allergy, such as allergen specific immunotherapy, vaccines, and non-allergen specific therapies, which provide viable options for patients with food allergies.

For allergen specific immunotherapy, patients with food allergies are treated with their specific allergens to establish the tolerance to these allergens. This process is called desensitization. There are various approaches to treating patients with allergens including oral immunotherapy (OIT), sublingual immunotherapy (SLIT), and epicutaneous immunotherapy (EPIT). Specifically, patients with allergies are treated with their allergens in increasing amounts each time until a maintenance dose is reached, and then this dose is given periodically to patients (107). Compared to other allergen-specific immunotherapies, OIT has a higher efficiency, but also has a higher risk of systemic side effects, which may even require therapeutic intervention. Clinical trials have shown that OIT directed at milk, eggs, peanuts, and wheat allergens is therapeutically effective; however, OIT directed at these allergens generally caused significant adverse effects when the dose is increased (108–110). In addition to concerns about safety, there are many factors that limit the application of allergen-specific immunotherapy. There is a lack of standardization of clinical treatment, including the type of allergen used in the treatment, the administration method, the given dose, and frequency (111, 112). Further research is needed to promote and apply allergen-specific immunotherapy in the clinical treatment of food allergies.

Since the allergenic activity of natural allergen extracts is the most concerning side effect of allergen-specific immunotherapy, and broadly limits its applicability. However, recombinant allergens with genetic modifications that can reduce allergenic activity are produced to improve the safety of the immunotherapies (113). Clinical therapy trials suggest that recombinant allergens are effective for subcutaneous immunotherapy (114–116). Based on the promising results of these clinical trials, the first recombinant allergen-based vaccines will soon be registered and available for routine clinical use in patients with allergies.

Except for allergen-specific immunotherapy, nonallergen-specific therapies for food allergies have been developed, including immune antibody therapy and prebiotics treatment. As an immune antibody therapy, omalizumab has been tested in clinical trials as a monoclonal antibody against immunoglobulin E (IgE) (117). The combination of omalizumab and OIT has achieved promising results for the treatment of food allergies (118). In the future, with an in-depth understanding of the mechanism of food allergy and the identification of therapeutic targets, more targeted antibodies, such as antibodies against Th2 cytokines, will be developed and used in the treatment of food allergy.

Since intestinal microbiosis contributes significantly to allergic states in the intestine, the manipulation of intestinal microbes holds promise for the treatment of food allergy. Preclinical evidence has shown that prebiotics have a positive effect on remission of food allergy. For example, dietary supplementation with fructo-oligosaccharides, an immunomodulatory prebiotic, significantly improved allergic intestinal inflammation in OVA23-3 TCR-transgenic mice fed with an OVA-containing diet (119). Supplements consisting of *Lactobacillus paracasei* L9 reduced allergic responses in mice allergic to β-lactoglobulin (120). Oral administration of *Lactobacillus murinus* restored the deterioration of the intestinal flora in food-allergic mice and alleviated allergic reactions (121). Although prebiotic and probiotic trials are promising in food allergy treatment, there is currently no solid evidence to support the preventive or therapeutic effects of prebiotics and probiotics in relation to clinical food allergies. Therefore, future studies should uncover more specific details and mechanisms for the treatment of food allergies, while optimal functional probiotic strains should be selected and isolated for this approach.

CONCLUSION

The incidence of food allergy worldwide has increased progressively. When food allergies are diagnosed, there are limited treatment options for patients. Strictly avoiding allergens is one of the few safe and effective treatments in clinical application. However, such treatment is considered as a passive option with significant shortcomings. The limitations of clinical treatments for food allergies are largely attributable to unclear disease mechanisms. In recent years, significant progress has been made in elucidating the mechanisms involved in food antigen uptake and oral tolerance induction in the intestine. In this review, we summarized the pathways in which food antigens cross the intestinal epithelium and the processes through which they are transferred to the sub-epithelial compartment to induce tolerance or to provoke allergic reactions in the intestine. However, more mechanistic details need to be explored regarding processes associated with the promotion of clinical manifestations associated with food antigen-triggered

anaphylaxis. More importantly, promising clinical strategies have been proposed, such as allergen-specific immunotherapy, vaccines, and non-allergen-specific therapies, which may provide additional viable options for patients with food allergies.

AUTHOR CONTRIBUTIONS

HM and YX wrote the manuscript. GX provided important advice and suggestions. HM and MC supervised the writing. All authors contributed to the article and approved the submitted version.

FUNDING

This work was supported by the National Natural Science Foundation of China (#82171783, # 81871284).

REFERENCES

1. Dunlop JH, Keet CA. Epidemiology of Food Allergy. *Immunol Allergy Clinics North Am* (2018) 38(1):13. doi: 10.1016/j.iac.2017.09.002
2. Garkaby J, Epov L, Musallam N, Almog M, Bamberger E, Mandelberg A, et al. The Sesame-Peanut Conundrum in Israel: Reevaluation of Food Allergy Prevalence in Young Children. *J Allergy Clin Immunol Pract* (2021) 9(1):200–5. doi: 10.1016/j.jaip.2020.08.010
3. Vale LS, Lobb M, Netting JM, Murray K, Clifford R, Campbell DE, et al. A Systematic Review of Infant Feeding Food Allergy Prevention Guidelines-can We AGREE? *World Allergy Organ J* (2021) 14(6):100550. doi: 10.1016/j.waojou.2021.100550
4. Gunes Bayir A, Can B, Ekingen S. Food Allergy in Children. *Bezmialem Sci* (2021) 9(3):373–9. doi: 10.14235/bas.galenos.2020.4097
5. Mandavinia M. Food Allergy in Adults Presentations, Evaluation, and Treatment. *Med Clinics North Am* (2020) 104(1):145–55. doi: 10.1016/j.mcna.2019.08.008
6. Sicherer SH, Munoz-Furlong A, Sampson HA. Prevalence of Seafood Allergy in the United States Determined by a Random Telephone Survey. *J Allergy Clin Immunol* (2004) 114(1):159–65. doi: 10.1016/j.jaci.2004.04.018
7. Warren C, Lei D, Sicherer S, Schleimer R, Gupta R. Prevalence and Characteristics of Peanut Allergy in US Adults. *J Allergy Clin Immunol* (2021) 147(6):2263–70.e5. doi: 10.1016/j.jaci.2020.11.046
8. Suaini NHA, Wang YC, Soriano VX, Martino DJ, Allen KJ, Ellis JA, et al. Genetic Determinants of Paediatric Food Allergy: A Systematic Review. *Allergy* (2019) 74(9):1631–48. doi: 10.1111/all.13767
9. Luke AK, Flessner CA. Examining Differences in Parent Knowledge About Pediatric Food Allergies. *J Pediatr Psychol* (2020) 45(1):101–9. doi: 10.1093/jpepsy/jsz091
10. Ukleja-Sokolowska N, Kuzminski A, Tykwinska M, Bartuzi Z. *In Vivo* Studies in the Diagnosis of Food Allergy - Selected Practical Aspects. *Alerg Astma Immunol* (2021) 26(1):10–7.
11. Michelet M, Balbino B, Guilleminault L, Reber LL. IgE in the Pathophysiology and Therapy of Food Allergy. *Eur J Immunol* (2021) 51(3):531–43. doi: 10.1002/eji.202048833
12. Mayorga C, Palomares F, Canas JA, Perez-Sanchez N, Nunez R, Torres MJ, et al. New Insights in Therapy for Food Allergy. *Foods* (2021) 10(5):1037. doi: 10.3390/foods10051037
13. Pavic I, Kolacek S. Growth of Children With Food Allergy. *Horm Res Paediatr* (2017) 88(1):91–100. doi: 10.1159/000462973
14. Nicolaides RE, Parrish CP, Bird JA. Food Allergy Immunotherapy With Adjuvants. *Immunol Allergy Clinics North Am* (2020) 40(1):149–73. doi: 10.1016/j.iac.2019.09.004
15. Groschwitz KR, Hogan SP. Intestinal Barrier Function: Molecular Regulation and Disease Pathogenesis. *J Allergy Clin Immunol* (2009) 124(1):3–20. doi: 10.1016/j.jaci.2009.05.038
16. Bansil R, Turner BS. The Biology of Mucus: Composition, Synthesis and Organization. *Adv Drug Deliv Rev* (2018) 124:3–15. doi: 10.1016/j.addr.2017.09.023
17. Johansson MEV, Sjovall H, Hansson GC. The Gastrointestinal Mucus System in Health and Disease. *Nat Rev Gastroenterol Hepatol* (2013) 10(6):352–61. doi: 10.1038/nrgastro.2013.35
18. Johansson MEV, Hansson GC. Immunological Aspects of Intestinal Mucus and Mucins. *Nat Rev Immunol* (2016) 16(10):639–49. doi: 10.1038/nri.2016.88
19. Schroeder BO. Fight Them or Feed Them: How the Intestinal Mucus Layer Manages the Gut Microbiota. *Gastroenterol Rep (Oxf)* (2019) 7(1):3–12. doi: 10.1093/gastro/goy052
20. Bevins CL, Salzman NH. Paneth Cells, Antimicrobial Peptides and Maintenance of Intestinal Homeostasis. *Nat Rev Microbiol* (2011) 9(5):356–68. doi: 10.1038/nrmicro2546
21. Nakamura K, Sakuragi N, Takakuwa A, Ayabe T. Paneth Cell Alpha-Defensins and Enteric Microbiota in Health and Disease. *Biosci Microb Food Health* (2016) 35(2):57–67. doi: 10.12938/bmfh.2015-019
22. Gerbe F, Jay P. Intestinal Tuft Cells: Epithelial Sentinels Linking Luminal Cues to the Immune System. *Mucosal Immunol* (2016) 9(6):1353–9. doi: 10.1038/mi.2016.68
23. Worthington JJ. The Intestinal Immunoendocrine Axis: Novel Cross-Talk Between Enteroendocrine Cells and the Immune System During Infection and Inflammatory Disease. *Biochem Soc Trans* (2015) 43:727–33. doi: 10.1042/BST20150090
24. Salim SY, Soderholm JD. Importance of Disrupted Intestinal Barrier in Inflammatory Bowel Diseases. *Inflamm Bowel Dis* (2011) 17(1):362–81. doi: 10.1002/ibd.21403
25. Turner JR. Intestinal Mucosal Barrier Function in Health and Disease. *Nat Rev Immunol* (2009) 9(11):799–809. doi: 10.1038/nri2653
26. Vancamelbeke M, Vermeire S. The Intestinal Barrier: A Fundamental Role in Health and Disease. *Expert Rev Gastroenterol Hepatol* (2017) 11(9):821–34. doi: 10.1080/17474124.2017.1343143
27. Van Itallie CM, Anderson JM. Architecture of Tight Junctions and Principles of Molecular Composition. *Semin Cell Dev Biol* (2014) 36:157–65. doi: 10.1016/j.semcdb.2014.08.011
28. Lee B, Moon KM, Kim CY. Tight Junction in the Intestinal Epithelium: Its Association With Diseases and Regulation by Phytochemicals. *J Immunol Res* (2018) 2018:2645465. doi: 10.1155/2018/2645465
29. Zuo L, Kuo WT, Turner JR. Tight Junctions as Targets and Effectors of Mucosal Immune Homeostasis. *Cell Mol Gastroenterol Hepatol* (2020) 10(2):327–40. doi: 10.1016/j.jcmgh.2020.04.001
30. Stevenson BR, Siliciano JD, Mooseker MS, Goodenough DA. Identification OF ZO-1: A High-Molecular-Weight Polypeptide Associated With the Tight Junction (Zonula Occludens) in a Variety of Epithelia. *J Cell Biol* (1986) 103(3):755–66. doi: 10.1083/jcb.103.3.755
31. Jesaitis LA, Goodenough DA. Molecular Characterization and Tissue Distribution of Zo-2, a Tight Junction Protein Homologous to Zo-1 and the Drosophila Disks-Large Tumor-Suppressor Protein. *J Cell Biol* (1994) 124(6):949–61. doi: 10.1083/jcb.124.6.949
32. Haskins J, Gu LJ, Wittchen ES, Hibbard J, Stevenson BR. ZO-3, a Novel Member of the MAGUK Protein Family Found at the Tight Junction, Interacts With ZO-1 and Occludin. *J Cell Biol* (1998) 141(1):199–208. doi: 10.1083/jcb.141.1.199
33. Furuse M, Hirase T, Itoh M, Nagafuchi A, Yonemura S, Tsukita S, et al. Occludin - a Novel Integral Membrane-Protein Localizing at Tight Junctions. *J Cell Biol* (1993) 123(6):1777–88. doi: 10.1083/jcb.123.6.1777
34. Furuse M, Fujita K, Hiiragi T, Fujimoto K, Tsukita S. Claudin-1 and -2: Novel Integral Membrane Proteins Localizing at Tight Junctions With No Sequence Similarity to Occludin. *J Cell Biol* (1998) 141(7):1539–50. doi: 10.1083/jcb.141.7.1539
35. Grozdanovic MM, Cavic M, Nesic A, Andjelkovic U, Akbari P, Smit JJ, et al. Kiwifruit Cysteine Protease Actinidin Compromises the Intestinal Barrier by

Disrupting Tight Junctions. *Biochim Biophys Acta-General Subj* (2016) 1860 (3):516–26. doi: 10.1016/j.bbagen.2015.12.005
36. Fries W, Belvedere A, Vetrano S. Sealing the Broken Barrier in IBD: Intestinal Permeability, Epithelial Cells and Junctions. *Curr Drug Targets* (2013) 14(12):1460–70. doi: 10.2174/1389450111314120011
37. Allaire JM, Crowley SM, Law HT, Chang SY, Ko HJ, Vallance BA. The Intestinal Epithelium: Central Coordinator of Mucosal Immunity. *Trends Immunol* (2018) 39(9):677–96. doi: 10.1016/j.it.2018.04.002
38. Matsuzaki T, Susa T, Shimizu K, Sawai N, Suzuki T, Aoki T, et al. Function of the Membrane Water Channel Aquaporin-5 in the Salivary Gland. *Acta Histochem Cytochem* (2012) 45(5):251–9. doi: 10.1267/ahc.12018
39. Auchere D, Tardivel S, Gounelle JC, Drueke T, Lacour B. Role of Transcellular Pathway in Ileal Ca2+ Absorption: Stimulation by Low-Ca2+ Diet. *Am J Physiol Gastrointest Liver Physiol* (1998) 275(5):G951–G6. doi: 10.1152/ajpgi.1998.275.5.G951
40. Dyer J, Hosie KB, ShiraziBeechey SP. Nutrient Regulation of Human Intestinal Sugar Transporter (SGLT1) Expression. *Gut* (1997) 41(1):56–9. doi: 10.1136/gut.41.1.56
41. Christensen HN, Liang M, Archer EG. A Distinct NA+-Requiring Transport System for Alanine Serine Cysteine and Similar Amino Acids. *J Biol Chem* (1967) 242(22):5237–46. doi: 10.1016/S0021-9258(18)99417-2
42. Rose EM, Koo JCP, Antflick JE, Ahmed SM, Angers S, Hampson DR. Glutamate Transporter Coupling to Na,K-ATPase. *J Neurosci* (2009) 29 (25):8143–55. doi: 10.1523/JNEUROSCI.1081-09.2009
43. Snoeck V, Goddeeris B, Cox E. The Role of Enterocytes in the Intestinal Barrier Function and Antigen Uptake. *Microbes Infect* (2005) 7(7-8):997–1004. doi: 10.1016/j.micinf.2005.04.003
44. Aderem A, Underhill DM. Mechanisms of Phagocytosis in Macrophages. *Annu Rev Immunol* (1999) 17:593–623. doi: 10.1146/annurev.immunol.17.1.593
45. Bockman DE, Cooper MD. Pinocytosis by Epithelium Associated With Lymphoid Follicles in Bursa of Fabricius, Appendix, and Peyers Patches - Electron-Microscopic Study. *Am J Anat* (1973) 136(4):455–77. doi: 10.1002/aja.1001360406
46. Jang MH, Kweon MN, Iwatani K, Yamamoto M, Terahara K, Sasakawa C, et al. Intestinal Villous M Cells: An Antigen Entry Site in the Mucosal Epithelium. *Proc Natl Acad Sci USA* (2004) 101(16):6110–5. doi: 10.1073/pnas.0400969101
47. Suzuki H, Sekine S, Kataoka K, Pascual DW, Maddaloni M, Kobayashi R, et al. Ovalbumin-Protein Sigma 1 M-Cell Targeting Facilitates Oral Tolerance With Reduction of Antigen-Specific CD4(+) T Cells. *Gastroenterology* (2008) 135(3):917–25. doi: 10.1053/j.gastro.2008.05.037
48. Sakhony OS, Rossy B, Gusti V, Pham AJ, Vu K, Lo DD. M Cell-Derived Vesicles Suggest a Unique Pathway for Trans-Epithelial Antigen Delivery. *Tissue Barriers* (2015) 3(1-2):e1004975. doi: 10.1080/21688370.2015.1004975
49. Neutra MR, Frey A, Kraehenbuhl JP. Epithelial M Cells: Gateways for Mucosal Infection and Immunization. *Cell* (1996) 86(3):345–8. doi: 10.1016/S0092-8674(00)80106-3
50. Gebert A, Rothkotter HJ, Pabst R. M Cells in Peyer's Patches of the Intestine. *Int Rev Cytol* (1996) 167:91–159. doi: 10.1016/s0074-7696(08)61346-7
51. Wolf JL, Bye WA. The Membranous Epithelial (M) Cell and the Mucosal Immune-System. *Annu Rev Med* (1984) 35:95–112. doi: 10.1146/annurev.me.35.020184.000523
52. Wu Y, Boysun MJ, Csencsits KL, Pascual DW. Gene Transfer Facilitated by a Cellular Targeting Molecule, Reovirus Protein Sigma 1. *Gene Ther* (2000) 7 (1):61–9. doi: 10.1038/sj.gt.3301046
53. Wu YP, Wang XH, Csencsits KL, Haddad A, Walters N, Pascual DW. M Cell-Targeted DNA Vaccination. *Proc Natl Acad Sci USA* (2001) 98 (16):9318–23. doi: 10.1073/pnas.161204098
54. Spahn TW, Fontana A, Faria AMC, Slavin AJ, Eugster HP, Zhang XM, et al. Induction of Oral Tolerance to Cellular Immune Responses in the Absence of Peyer's Patches. *Eur J Immunol* (2001) 31(4):1278–87. doi: 10.1002/1521-4141(200104)31:4<1278::AID-IMMU1278>3.0.CO;2-A
55. Spahn TW, Weiner HL, Rennert PD, Lugering N, Fontana A, Domschke W, et al. Mesenteric Lymph Nodes are Critical for the Induction of High-Dose Oral Tolerance in the Absence of Peyer's Patches. *Eur J Immunol* (2002) 32 (4):1109–13. doi: 10.1002/1521-4141(200204)32:4<1109::AID-IMMU1109>3.0.CO;2-K
56. McCauley HA, Guasch G. Three Cheers for the Goblet Cell: Maintaining Homeostasis in Mucosal Epithelia. *Trends Mol Med* (2015) 21(8):492–503. doi: 10.1016/j.molmed.2015.06.003
57. McDole JR, Wheeler LW, McDonald KG, Wang BM, Konjufca V, Knoop KA, et al. Goblet Cells Deliver Luminal Antigen to CD103(+) Dendritic Cells in the Small Intestine. *Nature* (2012) 483(7389):345–U141. doi: 10.1038/nature10863
58. Knoop KA, Gustafsson JK, McDonald KG, Kulkarni DH, Kassel R, Newberry RD. Antibiotics Promote the Sampling of Luminal Antigens and Bacteria *via* Colonic Goblet Cell Associated Antigen Passages. *Gut Microbes* (2017) 8(4):400–11. doi: 10.1080/19490976.2017.1299846
59. Gustafsson JK, Davis JE, Rappai T, McDonald KG, Kulkarni DH, Knoop KA, et al. Intestinal Goblet Cells Sample and Deliver Lumenal Antigens by Regulated Endocytic Uptake and Transcytosis. *Elife* (2021) 10:e67292. doi: 10.7554/eLife.67292
60. Kulkarni DH, Gustafsson JK, Knoop KA, McDonald KG, Bidani SS, Davis JE, et al. Goblet Cell Associated Antigen Passages Support the Induction and Maintenance of Oral Tolerance. *Mucosal Immunol* (2020) 13(2):271–82. doi: 10.1038/s41385-019-0240-7
61. Noah TK, Knoop KA, McDonald KG, Gustafsson JK, Waggoner L, Vanoni S, et al. IL-13-Induced Intestinal Secretory Epithelial Cell Antigen Passages are Required for IgE-Mediated Food-Induced Anaphylaxis. *J Allergy Clin Immunol* (2019)144(4):1058–73.e3. doi: 10.1016/j.jaci.2019.04.030
62. Liu EG, Yin XY, Swaminathan A, Eisenbarth SC. Antigen-Presenting Cells in Food Tolerance and Allergy. *Front Immunol* (2021) 11. doi: 10.3389/fimmu.2020.616020
63. Lelouard H, Fallet M, de Bovis B, Meresse S, Gorvel JP. Peyer's Patch Dendritic Cells Sample Antigens by Extending Dendrites Through M Cell-Specific Transcellular Pores. *Gastroenterology* (2012) 142(3):592–601.e3. doi: 10.1053/j.gastro.2011.11.039
64. Kelsall B. Recent Progress in Understanding the Phenotype and Function of Intestinal Dendritic Cells and Macrophages. *Mucosal Immunol* (2008) 1 (6):460–9. doi: 10.1038/mi.2008.61
65. Farache J, Zigmond E, Shakhar G, Jung S. Contributions of Dendritic Cells and Macrophages to Intestinal Homeostasis and Immune Defense. *Immunol Cell Biol* (2013) 91(3):232–9. doi: 10.1038/icb.2012.79
66. Rescigno M, Urbano M, Valzasina B, Francolini M, Rotta G, Bonasio R, et al. Dendritic Cells Express Tight Junction Proteins and Penetrate Gut Epithelial Monolayers to Sample Bacteria. *Nat Immunol* (2001) 2(4):361–7. doi: 10.1038/86373
67. Mazzini E, Massimiliano L, Penna G, Rescigno M. Oral Tolerance Can Be Established *via* Gap Junction Transfer of Fed Antigens From CX3CR1(+) Macrophages to CD103(+) Dendritic Cells. *Immunity* (2014) 40(2):248–61. doi: 10.1016/j.immuni.2013.12.012
68. Schulz O, Jaensson E, Persson EK, Liu XS, Worbs T, Agace WW, et al. Intestinal CD103(+), But Not CX3CR1(+), Antigen Sampling Cells Migrate in Lymph and Serve Classical Dendritic Cell Functions. *J Exp Med* (2009) 206(13):3101–14. doi: 10.1084/jem.20091925
69. Zeng R, Oderup C, Yuan R, Lee M, Habtezion A, Hadeiba H, et al. Retinoic Acid Regulates the Development of a Gut-Homing Precursor for Intestinal Dendritic Cells. *Mucosal Immunol* (2013) 6(4):847–56. doi: 10.1038/mi.2012.123
70. Coombes JL, Siddiqui KRR, Arancibia-Carcamo CV, Hall J, Sun CM, Belkaid Y, et al. A Functionally Specialized Population of Mucosal CD103(+) DCs Induces Foxp3(+) Regulatory T Cells *via* a TGF-Beta- and Retinoic Acid-Dependent Mechanism. *J Exp Med* (2007) 204(8):1757–64. doi: 10.1084/jem.20070590
71. Sun CM, Hall JA, Blank RB, Bouladoux N, Oukka M, Mora JR, et al. Small Intestine Lamina Propria Dendritic Cells Promote *De Novo* Generation of Foxp3 T Reg Cells *via* Retinoic Acid. *J Exp Med* (2007) 204(8):1775–85. doi: 10.1084/jem.20070602
72. Matteoli G, Mazzini E, Iliev ID, Mileti E, Fallarino F, Puccetti P, et al. Gut CD103(+) Dendritic Cells Express Indoleamine 2,3-Dioxygenase Which Influences T Regulatory/T Effector Cell Balance and Oral Tolerance Induction. *Gut* (2010) 59(5):595–604. doi: 10.1136/gut.2009.185108
73. Hadis U, Wahl B, Schulz O, Hardtke-Wolenski M, Schippers A, Wagner N, et al. Intestinal Tolerance Requires Gut Homing and Expansion of FoxP3(+)

Regulatory T Cells in the Lamina Propria. *Immunity* (2011) 34(2):237–46. doi: 10.1016/j.immuni.2011.01.016
74. Murai M, Turovskaya O, Kim G, Madan R, Karp CL, Cheroutre H, et al. Interleukin 10 Acts on Regulatory T Cells to Maintain Expression of the Transcription Factor Foxp3 and Suppressive Function in Mice With Colitis. *Nat Immunol* (2009) 10(11):1178–U61. doi: 10.1038/ni.1791
75. Mowat AM. To Respond or Not to Respond - a Personal Perspective of Intestinal Tolerance. *Nat Rev Immunol* (2018) 18(6):405–15. doi: 10.1038/s41577-018-0002-x
76. Chen YH, Inobe J, Marks R, Gonnella P, Kuchroo VK, Weiner HL. Peripheral Deletion of Antigen-Reactive T-Cells in Oral Tolerance. *Nature* (1995) 376(6536):177–80. doi: 10.1038/376177a0
77. Friedman A, Weiner HL. Induction of Anergy or Active Suppression Following Oral Tolerance is Determined by Antigen Dosage. *Proc Natl Acad Sci USA* (1994) 91(14):6688–92. doi: 10.1073/pnas.91.14.6688
78. Chen Y, Kuchroo VK, Inobe J, Hafler DA, Weiner HL. Regulatory T Cell Clones Induced by Oral Tolerance: Suppression of Autoimmune Encephalomyelitis. *Science* (1994) 265(5176):1237–40. doi: 10.1126/science.7520605
79. Kim KS, Hong SW, Han D, Yi J, Jung J, Yang BG, et al. Dietary Antigens Limit Mucosal Immunity by Inducing Regulatory T Cells in the Small Intestine. *Science* (2016) 351(6275):858–63. doi: 10.1126/science.aac5560
80. Weiss JM, Bilate AM, Gobert M, Ding Y, de Lafaille MAC, Parkhurst CN, et al. Neuropilin 1 is Expressed on Thymus-Derived Natural Regulatory T Cells, But Not Mucosa- Generated Induced Foxp3(+) T Reg Cells. *J Exp Med* (2012) 209(10):1723–42. doi: 10.1084/jem.20120914
81. Cahenzli J, Koller Y, Wyss M, Geuking MB, McCoy KD. Intestinal Microbial Diversity During Early-Life Colonization Shapes Long-Term IgE Levels. *Cell Host Microbe* (2013) 14(5):559–70. doi: 10.1016/j.chom.2013.10.004
82. Sarkar A, Yoo JY, Dutra SVO, Morgan KH, Groer M. The Association Between Early-Life Gut Microbiota and Long-Term Health and Diseases. *J Clin Med* (2021) 10(3):459. doi: 10.3390/jcm10030459
83. Atarashi K, Tanoue T, Shima T, Imaoka A, Kuwahara T, Momose Y, et al. Induction of Colonic Regulatory T Cells by Indigenous Clostridium Species. *Science* (2011) 331(6015):337–41. doi: 10.1126/science.1198469
84. Geuking MB, Cahenzli J, Lawson MAE, Ng DCK, Slack E, Hapfelmeier S, et al. Intestinal Bacterial Colonization Induces Mutualistic Regulatory T Cell Responses. *Immunity* (2011) 34(5):794–806. doi: 10.1016/j.immuni.2011.03.021
85. Russell SL, Gold MJ, Hartmann M, Willing BP, Thorson L, Wlodarska M, et al. Early Life Antibiotic-Driven Changes in Microbiota Enhance Susceptibility to Allergic Asthma. *EMBO Rep* (2012) 13(5):440–7. doi: 10.1038/embor.2012.32
86. Wang YA, Brzozowska-Prechtl A, Karten HJ. Laminar and Columnar Auditory Cortex in Avian Brain. *Proc Natl Acad Sci USA* (2010) 107 (28):12676–81. doi: 10.1073/pnas.1006645107
87. Atarashi K, Tanoue T, Oshima K, Suda W, Nagano Y, Nishikawa H, et al. T-Reg Induction by a Rationally Selected Mixture of Clostridia Strains From the Human Microbiota. *Nature* (2013) 500(7461):232–6. doi: 10.1038/nature12331
88. Stefka AT, Feehley T, Tripathi P, Qiu J, McCoy K, Mazmanian SK, et al. Commensal Bacteria Protect Against Food Allergen Sensitization. *Proc Natl Acad Sci U S A* (2014) 111(36):13145–50. doi: 10.1073/pnas.1412008111
89. Russler-Germain EV, Rengarajan S, Hsieh CS. Antigen-Specific Regulatory T-Cell Responses to Intestinal Microbiota. *Mucosal Immunol* (2017) 10 (6):1375–86. doi: 10.1038/mi.2017.65
90. Mager LF, Burkhard R, Pett N, Cooke NCA, Brown K, Ramay H, et al. Microbiome-Derived Inosine Modulates Response to Checkpoint Inhibitor Immunotherapy. *Science* (2020) 369(6510):1481–9. doi: 10.1126/science.abc3421
91. Yang WJ, Yu TM, Huang XS, Bilotta AJ, Xu LQ, Lu Y, et al. Intestinal Microbiota-Derived Short-Chain Fatty Acids Regulation of Immune Cell IL-22 Production and Gut Immunity. *Nat Commun* (2020) 11(1):4457. doi: 10.1038/s41467-020-18262-6
92. Furusawa Y, Obata Y, Fukuda S, Endo TA, Nakato G, Takahashi D, et al. Commensal Microbe-Derived Butyrate Induces the Differentiation of Colonic Regulatory T Cells. *Nature* (2013) 504(7480):446–50. doi: 10.1038/nature12721
93. Tan J, McKenzie C, Vuillermin PJ, Goverse G, Vinuesa CG, Mebius RE, et al. Dietary Fiber and Bacterial SCFA Enhance Oral Tolerance and Protect Against Food Allergy Through Diverse Cellular Pathways. *Cell Rep* (2016) 15 (12):2809–24. doi: 10.1016/j.celrep.2016.05.047
94. Jaensson E, Uronen-Hansson H, Pabst O, Eksteen B, Tian J, Coombes JL, et al. Small Intestinal CD103+ Dendritic Cells Display Unique Functional Properties That are Conserved Between Mice and Humans. *J Exp Med* (2008) 205(9):2139–49. doi: 10.1084/jem.20080414
95. Feehley T, Plunkett CH, Bao RY, Hong SMC, Culleen E, Belda-Ferre P, et al. Healthy Infants Harbor Intestinal Bacteria That Protect Against Food Allergy. *Nat Med* (2019) 25(3):448–53. doi: 10.1038/s41591-018-0324-z
96. Brown GD, Willment JA, Whitehead L. C-Type Lectins in Immunity and Homeostasis. *Nat Rev Immunol* (2018) 18(6):374–89. doi: 10.1038/s41577-018-0004-8
97. Shreffler WG, Castro RR, Kucuk ZY, Charlop-Powers Z, Grishina G, Yoo S, et al. The Major Glycoprotein Allergen From Arachis Hypogaea, Ara H 1, is a Ligand of Dendritic Cell-Specific ICAM-Grabbing Nonintegrin and Acts as a Th2 Adjuvant In Vitro. *J Immunol* (2006) 177(6):3677–85. doi: 10.4049/jimmunol.177.6.3677
98. Schnurr M, Then F, Galambos P, Scholz C, Siegmund B, Endres S, et al. Extracellular ATP and TNF-Alpha Synergize in the Activation and Maturation of Human Dendritic Cells. *J Immunol* (2000) 165(8):4704–9. doi: 10.4049/jimmunol.165.8.4704
99. Hsu S-C, Chen C-H, Tsai S-H, Kawasaki H, Hung C-H, Chu Y-T, et al. Functional Interaction of Common Allergens and a C-Type Lectin Receptor, Dendritic Cell-Specific ICAM3-Grabbing Non-Integrin (DC-SIGN), on Human Dendritic Cells. *J Biol Chem* (2010) 285(11):7903–10. doi: 10.1074/jbc.M109.058370
100. Li JN, Wang Y, Tang LH, de Villiers WJS, Cohen D, Woodward J, et al. Dietary Medium-Chain Triglycerides Promote Oral Allergic Sensitization and Orally Induced Anaphylaxis to Peanut Protein in Mice. *J Allergy Clin Immunol* (2013) 131(2):442–50. doi: 10.1016/j.jaci.2012.10.011
101. Khodoun MV, Tomar S, Tocker JE, Wang YH, Finkelman FD. Prevention of Food Allergy Development and Suppression of Established Food Allergy by Neutralization of Thymic Stromal Lymphopoietin, IL-25, and IL-33. *J Allergy Clin Immunol* (2018) 141(1):171–9.e1. doi: 10.1016/j.jaci.2017.02.046
102. Blazquez AB, Berin MC. Gastrointestinal Dendritic Cells Promote Th2 Skewing *via* OX40L. *J Immunol* (2008) 180(7):4441–50. doi: 10.4049/jimmunol.180.7.4441
103. Chu DK, Llop-Guevara A, Walker TD, Flader K, Goncharova S, Boudreau JE, et al. IL-33, But Not Thymic Stromal Lymphopoietin or IL-25, is Central to Mite and Peanut Allergic Sensitization. *J Allergy Clin Immunol* (2013) 131 (1):187–U283. doi: 10.1016/j.jaci.2012.08.002
104. Rivas MN, Burton OT, Oettgen HC, Chatila T. IL-4 Production by Group 2 Innate Lymphoid Cells Promotes Food Allergy by Blocking Regulatory T-Cell Function. *J Allergy Clin Immunol* (2016) 138(3):801–11.e9. doi: 10.1016/j.jaci.2016.02.030
105. Hammad H, Lambrecht BN. Barrier Epithelial Cells and the Control of Type 2 Immunity. *Immunity* (2015) 43(1):29–40. doi: 10.1016/j.immuni.2015.07.007
106. Galand C, Leyva-Castillo JM, Juhan Y, Han A, Lee MS, McKenzie ANJ, et al. IL-33 Promotes Food Anaphylaxis in Epicutaneously Sensitized Mice by Targeting Mast Cells. *J Allergy Clin Immunol* (2016) 138(5):1356–66. doi: 10.1016/j.jaci.2016.03.056
107. Hamad A, Burks WA. Emerging Approaches to Food Desensitization in Children. *Curr Allergy Asthma Rep* (2017) 17(5):32. doi: 10.1007/s11882-017-0700-7
108. Wood RA. Food Allergen Immunotherapy: Current Status and Prospects for the Future. *J Allergy Clin Immunol* (2016) 137(4):973–82. doi: 10.1016/j.jaci.2016.01.001
109. Wang J, Sampson HA. Safety and Efficacy of Epicutaneous Immunotherapy for Food Allergy. *Pediatr Allergy Immunol* (2018) 29(4):341–9. doi: 10.1111/pai.12869
110. Scurlock AM. Oral and Sublingual Immunotherapy for Treatment of IgE-Mediated Food Allergy. *Clin Rev Allergy Immunol* (2018) 55(2):139–52. doi: 10.1007/s12016-018-8677-0
111. Gernez Y, Nowak-Wegrzyn A. Immunotherapy for Food Allergy: Are We There Yet? *J Allergy Clin Immunol Pract* (2017) 5(2):250–72. doi: 10.1016/j.jaip.2016.12.004
112. Sampath V, Sindher SB, Pinzon AMA, Nadeau KC. Can Food Allergy be Cured? What are the Future Prospects? *Allergy* (2020) 75(6):1316–26. doi: 10.1111/all.14116

113. Valenta R, Linhart B, Swoboda I, Niederberger V. Recombinant Allergens for Allergen-Specific Immunotherapy: 10 Years Anniversary of Immunotherapy With Recombinant Allergens. *Allergy* (2011) 66(6):775–83. doi: 10.1111/j.1398-9995.2011.02565.x
114. Jutel M, Jaeger L, Suck R, Meyer H, Fiebig H, Cromwell O. Allergen-Specific Immunotherapy With Recombinant Grass Pollen Allergens. *J Allergy Clin Immunol* (2005) 116(3):608–13. doi: 10.1016/j.jaci.2005.06.004
115. Pauli G, Larsen TH, Rak S, Horak F, Pastorello E, Valenta R, et al. Efficacy of Recombinant Birch Pollen Vaccine for the Treatment of Birch-Allergic Rhinoconjunctivitis. *J Allergy Clin Immunol* (2008) 122(5):951–60. doi: 10.1016/j.jaci.2008.09.017
116. Winther L, Poulsen LK, Robin B, Melac M, Malling H. Safety and Tolerability of Recombinant Bet V 1 (Rbet V 1) Tablets in Sublingual Immunotherapy (SLIT). *J Allergy Clin Immunol* (2009) 123(2):S215–S. doi: 10.1016/j.jaci.2008.12.822
117. Arasi S, Mennini M, Cafarotti A, Fiocchi A. Omalizumab as Monotherapy for Food Allergy. *Curr Opin Allergy Clin Immunol* (2021) 21(3):286–91. doi: 10.1097/ACI.0000000000000744
118. Michelet M, Reber LL, Guilleminault L. Focus on Omalizumab in Food Allergy. *Rev Francaise D Allergol* (2021) 61(3):170–6. doi: 10.1016/j.reval.2020.12.006
119. Tsuda M, Arakawa H, Ishii N, Ubukata C, Michimori M, Noda M, et al. Dietary Fructo-Oligosaccharides Attenuate Early Activation of CD4(+) T Cells Which Produce Both Th1 and Th2 Cytokines in the Intestinal Lymphoid Tissues of a Murine Food Allergy Model. *Int Arch Allergy Immunol* (2017) 174(3-4):121–32. doi: 10.1159/000481984
120. Yang J, Ren FZ, Zhang H, Jiang L, Hao YL, Luo XG. Induction of Regulatory Dendritic Cells by Lactobacillus Paracasei L9 Prevents Allergic Sensitization to Bovine Beta-Lactoglobulin in Mice. *J Microbiol Biotechnol* (2015) 25 (10):1687–96. doi: 10.4014/jmb.1503.03022
121. Huang CH, Shen CC, Liang YC, Jan TR. The Probiotic Activity of Lactobacillus Murinus Against Food Allergy. *J Funct Foods* (2016) 25:231–41. doi: 10.1016/j.jff.2016.06.006

Conflict of Interest: The authors declare that the research was conducted in the absence of any commercial or financial relationships that could be construed as a potential conflict of interest.

Publisher's Note: All claims expressed in this article are solely those of the authors and do not necessarily represent those of their affiliated organizations, or those of the publisher, the editors and the reviewers. Any product that may be evaluated in this article, or claim that may be made by its manufacturer, is not guaranteed or endorsed by the publisher.

frontiers | Frontiers in Immunology

TYPE Original Research
PUBLISHED 02 August 2022
DOI 10.3389/fimmu.2022.922868

OPEN ACCESS

EDITED BY
Daming Zuo,
Southern Medical University, China

REVIEWED BY
Yufeng Liu,
Guangzhou First People's Hospital, China
Feng Zhang,
Sun Yat-sen University, China

*CORRESPONDENCE
Wai Ho Tang
waiho.tang@gwcmc.org
Yuan Zhang
yuan.zhang@gwcmc.org

†These authors have contributed equally to this work

SPECIALTY SECTION
This article was submitted to Molecular Innate Immunity, a section of the journal Frontiers in Immunology

RECEIVED 18 April 2022
ACCEPTED 11 July 2022
PUBLISHED 02 August 2022

CITATION
Guo M, Fan S, Chen Q, Jia C, Qiu M, Bu Y, Tang WH and Zhang Y (2022) Platelet-derived microRNA-223 attenuates TNF-α induced monocytes adhesion to arterial endothelium by targeting ICAM-1 in Kawasaki disease. *Front. Immunol.* 13:922868. doi: 10.3389/fimmu.2022.922868

Platelet-derived microRNA-223 attenuates TNF-α induced monocytes adhesion to arterial endothelium by targeting ICAM-1 in Kawasaki disease

Manli Guo[1†], Shunyang Fan[2†], Qian Chen[1], Cuiping Jia[1], Miaoyun Qiu[1], Yun Bu[1], Wai Ho Tang[1,2*] and Yuan Zhang[1*]

[1]Institute of Pediatrics, Guangzhou Women and Children's Medical Centre, Guangzhou Medical University, Guangzhou, China, [2]Heart Center, The Third Affiliated Hospital of Zhengzhou University, Zhengzhou, China

Background: Kawasaki disease (KD) is an acute vasculitis that may result in permanent coronary artery damage with unknown etiology. Endothelial cell (EC) dysfunction and platelet hyperactivity are the hallmarks of KD. Platelets are involved in the development of endothelial dysfunction. MiR-223 transferred by platelet microparticles (PMPs) has been found to involve in the functional regulation of endothelial cells in sepsis. However, the role of platelet-derived miR-223 in endothelial dysfunction has not yet been investigated in KD.

Objectives: We seek to investigate the role of platelet-derived miR-223 in endothelial dysfunction of KD vasculopathy.

Methods and results: Forty-five acute KD patients and 45 matched controls were randomly recruited in the study. When co-cultured with human coronary artery endothelial cells (HCAECs), KD platelets with higher levels of miR-223 were incorporated into HCAECs, resulting in the horizontal transfer of miR-223. Using KD platelets, PMPs, and platelet-releasate from the same amount of blood co-cultured with HCAECs, we found the increased expression of miR-223 in HCAECs was primarily derived from KD platelets, rather than PMPs or free miRNAs from platelet- releasate. KD platelet-derived miR-223 attenuated TNF-α induced intercellular cell adhesion molecule-1 (ICAM-1) expression in HCAECs. KD platelet-derived miR-223 also suppressed the monocyte adhesion to HCAECs. *In vivo*, platelet-specific miR-223 knockout (PF4-cre: miR-223$^{flox/flox}$) C57BL/6 mice and miR-223$^{flox/flox}$ C57BL/6 mice were used. Using *Lactobacillus* casei cell wall extract (LCWE) to establish KD murine model, we showed that in LCWE-injected PF4-cre: miR-223$^{flox/flox}$ mice, deficiency of platelet-miR-223 exacerbates the medial thickening of the abdominal aorta, increased ICAM-1 expression with concomitant CD45^{+} inflammatory cells infiltration into the endothelium compared to LCWE-injected miR-223$^{flox/flox}$ mice.

10.3389/fimmu.2022.922868

Conclusions: The horizontal transfer of platelet-derived miR-223 suppresses the expression of ICAM-1 in HCAECs, which at least in part attenuates leukocyte adhesion, thereby reducing endothelial damage in KD vasculitis

KEYWORDS

Kawasaki disease, endothelial cells, miR-223, platelets, ICAM-1

Introduction

Kawasaki disease (KD) is a children's acute systemic vasculitis of unknown etiology, which mainly impacts small and medium arteries, and can cause coronary aneurysms (1). In KD, a series of pathological changes occur, including endothelial injury, platelet hyperreactivity, infiltration of inflammatory cells, and vascular smooth muscle cell (VSMC) differentiation, although the relationship between these cells remains unclear (2). The current treatment for KD is the timely use of high-dose intravenous immunoglobulin (IVIG) and aspirin, for anti-inflammation and anti-platelet aggregation (3). Nevertheless, the occurrence of coronary aneurysms cannot be completely avoided, 4% of treated patients will still develop a coronary aneurysm (4). Therefore, understanding the pathogenesis of coronary arterial aneurysms will provide more effective therapy for KD patients.

The autopsy revealed that the onset of KD vasculitis was first in the luminal endothelium (1), which was characterized by numerous infiltration of inflammatory cells, edema and necrosis of endothelial cells (5). Previous studies have shown that infiltration of inflammatory cells upregulates the endothelial cell adhesion molecules (such as ICAM-1) by secreting cytokines (6), leading to the adhesion and chemotaxis of leukocytes (e.g. monocytes), further promoting endothelial damage (7, 8). Endothelial damage promotes platelet activation (9) and releases cytokines (e.g. platelet-derived growth factor-BB, PDGF-BB), which promote VSMC dedifferentiation (10). VSMC dedifferentiation plays a critical role in the coronary pathology of KD by promoting medial damage, thickening, and aneurysm formation (1). In addition, activated platelets can induce inflammatory responses in endothelial cells by releasing pro-inflammatory factors (e.g. interleukin-1β) or sheared CD40 ligands, leading to endothelial damage (11–15). Platelets are actively involved in the development of KD-induced vascular injury.

Platelets are non-nucleated cells formed by dissociation of the cytoplasm of mature megakaryocytes in the bone marrow. Early studies showed that platelets mainly play a role in thrombosis and homeostasis. Recently, accumulating evidence has shown that platelets contain a large number of miRNAs (16), as well as the subcellular mechanism of *de novo* protein synthesis (17). MicroRNA (miRNA) is a short non-coding RNA that inhibits the expression of target genes by interacting with the 3 'UTR of target mRNA (18). A previous study showed that miRNAs, such as miR-223, miR-337, and miR-199a, were differentially expressed in platelets in KD (19). MiR-223, which is abundantly expressed in platelets (20) has been found to participate in the pathological process of cardiovascular diseases (19, 21–23). For example, in atherosclerosis, miR-223 contributes to cholesterol transport, biosynthesis, and efflux by targeting several genes associated with cholesterol transport, biosynthesis, and efflux, and subsequently relieves hyperlipidemia (24). Recent studies have shown that miR-223 transferred by PMPs or platelets is involved in the functional regulation of recipient cells. In sepsis, PMPs-derived miR-223 has been shown to reduce ICAM-1-Dependent Vascular Inflammation (25). PMPs-derived miR-223 inhibited insulin-like growth factor receptor (IGF-1R), which promoted advanced glycation end products (AGEs)-induced endothelial cell apoptosis (26). In addition, platelet-derived miR-223 regulates VSMC dedifferentiation (27). Deficiency of platelet miR-223 in KD patients with aneurysms contributes to coronary artery pathology as platelet uptake fails to suppress VSMC dedifferentiation (19). Therefore, we hypothesize that platelet-derived miR-223 regulates endothelial dysfunction in KD vasculopathy.

In the present study, we now demonstrate that KD platelets with higher level of miR-223 were incorporated into HCAECs, resulting in the horizontal transfer of miR-223. KD platelet-derived miR-223 attenuates tumor necrosis factor-alpha (TNF-α) induced expression of ICAM-1 in HCAECs. In LCWE-injected PF4-cre: miR-223$^{flox/flox}$ mice, deficiency of platelet-miR-223 exacerbates the medial thickening of the abdominal aorta, increased ICAM-1 expression, with concomitant CD45^{+} inflammatory cells infiltration into the endothelium compared to LCWE-injected miR-223$^{flox/flox}$ mice. Thus, platelet-derived miR-223 contributes to attenuating the endothelial pathology of KD.

Methods

Human subjects

A total of 45 children with acute Kawasaki disease (31 males and 14 females, mean age, 48months) and 45 healthy children

(23 males and 22 females, mean age, 46 months) were randomly recruited to the study as previously described (19) (Guangzhou Women and Children Medical Center Human Investigation Committee, No. 2017102710). The diagnosis of KD meets the criteria developed in 2004 by the American Heart Association. Written informed consent was obtained from the patient's guardian or the adolescents themselves.

Animals

The animal experiments were conducted under the authorization of the Animal Care and Use Committee of Guangzhou Medical University, China (2019-384). The PF4-cre: miR-223$^{flox/flox}$ mice were created using PF4-cre mice [C57BL/6-Tg (PF4-icre) Q3Rsko/J, stock 008535] and miR-223$^{flox/flox}$ mice (C57BL/6-miR-223$^{em1(flox)Smoc}$). PF4-cre mice were purchased from Jackson Laboratory. MiR-223$^{flox/flox}$ mice were obtained from Shanghai Model Organisms Center, Inc, China. The PF4-cre: miR-223$^{flox/flox}$ mice were described below as PF4-miR-223 KO mice, miR-223$^{flox/flox}$ mice were described below as Floxed control mice.

Platelet and PMP purification

The whole blood was drawn from human subjects and centrifuged at 250g for 20 mins at room temperature to obtain platelet-rich plasma (PRP). The PRP was shifted to a new collection tube, followed by second centrifugation to absolutely spin down the residual blood cells. After treating with 100nM Prostaglandin E1 (PGE1, Sigma), the supernatant was centrifuged at 1000g for 5 mins to segregate plasma and platelets. The platelets were resuspended to 10^8 platelets/ml in HEPES-Tyrode's buffer. Platelet markers (CD41>95% positive) were used to determine the purity of platelets. The extraction method of platelet microparticles (PMPs) is described in previous studies (28). PMPs were extracted from the same amount of blood. Briefly, the platelet resuspension was slowly shaken at 10 rpm at room temperature for 4 hours. Next, platelets were centrifuged at 1000g for 5 mins. The supernatant was then centrifuged for 90 mins at 20,000 g at 18°C to obtain PMPs precipitates, and be resuspended in HEPES Tyrode's buffer in the same volume as the platelets described above. Platelet markers (CD41>90% positive) were used to determine the purity of PMPs. The supernatant containing platelet-releasate was collected and stored at -80°C.

Cell culture

Human coronary artery endothelial cells (HCAECs) were purchased from Lonza, USA, and cultured in the EBM-2 basal medium supplemented with an EGM-2 SingleQuots kit (CC-3162, Lonza, USA) containing 2% FBS and fibroblast growth factor (FGF), vascular endothelium growth factor (VEGF), human endothelial growth factor (EGF), hydrocortisone, insulin-like growth factor-1 (IGF-1), ascorbic acid, heparin. For all experiments, HCAECs were used between passages 5 to 7. The promonocytic leukemia cell line (THP-1) was purchased from FuHeng biology, China, and cultured in the RPMI1640 medium supplemented with 10% fetal bovine serum (FBS). Cells were cultured at 37°C in a humidified 5% CO2 atmosphere with the medium replaced every 48 hours. In subsequent experiments, platelets, PMPs, and the supernatant were added 100μl per dish and co-cultured with HCAECs for 24 hours. Transwell chambers with a pore size of 1μm were used, which only allowed PMPs to pass through. For cell transfection experiments, the agomiR-223/agomiR-NC or siRNA-Dicer1 (si-Dicer, GenePharma, China) were transiently transfected at a concentration of 100nM using Lipofectamine RNAiMAX (Invitrogen reagent, USA) for 24 or 48 hours. Cells were harvested for subsequent experiments. The sequences of agomiRNA or siRNA were listed in Supplementary Table 1.

Enzyme-linked immunosorbent assay (ELISA)

The levels of platelet factor 4 (PF4), β-thromboglobulin (β-TG), tumor necrosis factor-alpha (TNF-α) in human plasma were determined by platelet factor 4, PF4 ELISA Kit (CUSABIO, CSB-E07882h), β-thromboglobulin, β-TG ELISA Kit (CUSABIO, CSB-E07886h), Tumor necrosis factor-alpha, TNF-α ELISA Kit (CUSABIO, CSB-E04740h). One hundred microliters of plasma were incubated with the captured antibodies and secondary antibodies according to the instructions. The intensity was measured at 450nm and the reference was measured at 540 nm. The optical imperfections in the plate were corrected by subtracting the reading of 540 nm from 450nm. A standard curve was drawn according to the instructions to calculate the protein content of interest in each sample.

Flow cytometry

Cell expression of P-selectin (CD62P) was analyzed according to the instructions. Briefly, platelets (10^8 platelets/ml) suspended with 100μl HBSS buffer were incubated with PE anti-human CD62P antibody (BD, USA) at room temperature for 15 mins. After washing, the platelets and ECs were resuspended in HEPES-Tyrode's buffer and analyzed by BD FACSCanto™.

RNA isolation and quantitative RT-PCR

MiRNAs from platelets or HCAECs were purified using a miRNeasy mini kit (QIAGEN). According to the instructions,

the extracted RNAs were reverse-transcribed using a PrimeScript™ RT kit (Takara) and analyzed by RT-qPCR using a Hairpin-it™ miRNA qPCR quantitative kit (GenePharma). Real-time quantitative PCR (SYBR-green, TAKARA) assays were performed with an Applied Biosystems Q6 Fast Real-Time PCR System sequencer detector. Expression was normalized to the expression of small nuclear RNA U6 (snU6) or the human GAPDH housekeeping gene. The primer sequences used in RT-qPCR were listed in Supplementary Table 2.

Immunofluorescence

HCAECs were seeded into a glass-bottom culture dish at a density of 1.0×10^5 per dish. Human platelets were incubated with Cell Tracker™ Green CMFDA (Life Technology) at a concentration of 1μM in darkness for 30 mins at 37°C. After washing at least three times, the platelets were resuspended in HEPES-Tyrode's buffer at a concentration of 1.0×10^8/ml. HCAECs were co-cultured with the platelets at a 1:100 ratio. After washing with PBS buffer, cells were fixed and incubated with primary antibodies: anti-CD31 (1:100, Abcam, ab9498) or anti-ICAM-1(1:200, Abcam, ab282575) overnight at 4°C. The next day, after incubating with the secondary antibody: Alexa Fluor 594-conjugated IgG antibody (1:200, Abcam, ab150116), Fluor 488-conjugated IgG antibody (1:200, Abcam, ab150077) at 37°C for 2 hours, the cells were stained with Hoechst to visualize the nucleus. Immunofluorescence images were captured by a confocal microscope (Leica SP8). In each independent experiment, three representative images were taken for calculating the mean fluorescence intensity by ImageJ software, and used as one independent data.

For tissue sections, the slides were incubated in PBS containing 5% normal goat serum, 5% bovine serum albumin, and the primary antibody mixture at 4°C overnight. The primary antibodies used were as follows: anti-ICAM-1 (1:200, Abcam, ab222736), anti-CD31 (1:100, Abcam, ab56299), anti-CD45 (1:100, Proteintech, 60287). After incubating with each primary antibody, the slides were washed in PBS and incubated with Alexa Fluor 488-conjugated IgG secondary antibody (1:200, Abcam, ab150077) or Alexa Fluor 594-conjugated IgG secondary antibody (1:200, Abcam, ab150160) at 37°C for 2 hours. DAPI staining was performed to visualize the cell nucleus. Immunofluorescence images were taken with Leica SP8 confocal microscopy (Leica).

Transmission electron microscopy (TEM)

HCAECs were plated in 65mm Petri dishes at a density of 5×10^5 cells per dish. KD platelets were added at a ratio of 1:100 in co-culture with HCAECs for 24 hours. After washing with PBS twice, 1ml electron microscope fixative solution was added. Cells were scraped down with cell curettage and fixed at 4°C for more than 2 hours. After washing three times with 0.1M phosphoric acid buffer, cells were fixed again with 1% osmium tetroxide for 2 hours. After repeated washing with 0.1M sodium cacodylate buffer, cells were dehydrated in 30%-50%-70%-80%-95%-100%-100% ethanol successively. After uranyl acetate and lead citrate staining, ultrathin sections were examined with the transmission electron microscope FEI CM100 (Japan Electron Optics Laboratory)

Monocyte adhesion assay

HCAECs (1.0×10^5 cells per dish) were seeded and transfected as described above. As previously described (29), HCAECs were co-cultured with HC/KD platelets or transfected with agomiR-NC/agomiR-223 for 48 hours. After washing twice with PBS, cells were treated with TNF-α (2 ng/ml) for 4 hours and co-cultured with THP-1 (1.0×10^5) cells labeled with Cell Tracker™ Green CMFDA (Life Technology, 1μM, 30mins, 37°C) for 2 hours. HCAECs were gently washed with PBS and fixed with the 4% paraformaldehyde solution for 10mins, then incubated with anti-CD31 (1:100, Abcam, ab9498) at 4°C overnight. After incubating with the Alexa Fluor 594-conjugated IgG antibody (1:200, Abcam, ab150116) at 37°C for 2 hours, cells were stained with Hoechst to visualize the nucleus. Three images per sample were captured by confocal microscope (Leica SP8), and the number of adhering monocytes was calculated by ImageJ software. The average number of adhered monocytes per sample was used as one individual data for statistical analysis.

Western blotting

Total protein was extracted using Radio Immunoprecipitation Assay (RIPA) lysis buffer (Beyotime, China). Protein lysates were separated on 10% SDS-PAGE gels and transferred to PVDF membranes. After blocking with 5% skimmed milk, the membranes were incubated with primary antibodies: anti-ICAM-1(1:1000, Abcam, ab282575), anti-α-tubulin (1:2000, Abcam, ab52866) overnight at 4°C, and subsequently incubated with the secondary antibodies for an hour. The protein bands were detected using an ECL chemiluminescence kit (Beyotime, China) and quantified by ImageLab software (USA).

Ago2 immunoprecipitation

HCAECs were seeded in 65mm culture dishes (5.0×10^5 cells per dish) and transfected with agomiR-223/agomiR-NC at a concentration of 100nM for 48 hours. After harvested with RIP lysis buffer supplemented with protease and RNase inhibitors,

the cell lysates were immunoprecipitated with Ago2 (SAB4200085, SIGMA) or isotype IgG antibody-coated beads (Merck Millipore). The immunoprecipitated RNA was extracted and reverse transcribed as described in the RNA isolation and quantitative RT-PCR section.

LCWE preparation

The Lactobacillus casei cell wall extract (LCWE) was prepared as previously described (19, 30). Briefly, Lactobacillus casei (ATCC 11578) was grown in Lactobacillus MRS Broth (Difco) for 48 hours, harvested and washed with PBS. After disturbing by 2 volumes of 4% SDS/PBS at 37°C overnight, the cell wall fragment was washed 8 times with PBS to remove any SDS residue, and incubated with RNase, DNase, and trypsin. The cell wall fragment was sonicated for 2 hours at a pulse setting of 5.0 (10-s pulse/5-s pause) with cooling in an ice bath. After sonication, the cell wall fragments were spun for 20 mins at 12,000 rpm, 4°C. The supernatant was observed by centrifugation at 38,000 rpm, 4°C for 1 hour. The concentration of LCWE was determined based on the rhamnose content by using a colorimetric phenol-sulfuric assay.

KD murine model

KD murine model was prepared as previously described (19). Four hundred micrograms of LCWE or PBS were injected intraperitoneally into 4-week-old mice. The mice were sacrificed by isoflurane gaseous anesthesia two weeks after LCWE injection. The whole blood was taken directly from the right ventricle before perfusion. The abdominal aorta was taken out and embedded in the optimal cutting temperature (OCT) complex for histological analysis. The blood sample was then collected for plasma and platelet precipitation as described in Human samples.

Genotyping

Tails were clipped from mice 1-2 weeks after birth, about 2mm. Total DNA was extracted from individual tissues using the DNeasy Blood and Tissue Extraction Kit (QIAGEN). DNA pellets dissolved in water were used for PCR analysis. Primers were designed to detect alleles of WT, Floxed ctrl and recombinant PF4-miR-223 KO mice under standard PCR conditions. Primer sequences were listed in Supplementary Table 3.

HE staining

The frozen sections were dried at 37°C for 30 mins and placed in PBS for 10 mins. After being immersed in hematoxylin for 4 mins, hydrochloric acid and alcohol for 1 sec, and eosin for 1 min, the sections were fixed with neutral gum and detected by fluorescence microscope (Leica DM4). The areas of thickened medial layer were compared between groups and subjected to statistical analysis for significance.

Statistical analysis

Statistical analysis was performed using GraphPad Prism v.8.0.2 (USA). The Shapiro-Wilk normality test was used to determine the data distribution. For normally distributed data, values were presented as Mean ± SD. For two sets of data, an unpaired two-tailed Student's *t*-test was used for comparison. For multiple sets of data, analysis of One-way ANOVA was used, followed by Tukey's multiple comparisons. For non-normally distributed data, these values were expressed as Median ± interquartile range (IQR). For two sets of data analysis, the Mann-Whitney test was used, while Kruskal-Wallis and Dunn's multiple were used for multiple sets of data analysis. A difference of $P<0.05$ was considered statistically significant.

Results

KD platelets are hyperactive with increased expression of miR-223

As is known that KD is an acute febrile childhood disease characterized by multisystem vasculitis and platelets play an important role in the regulation of inflammatory diseases. We found that plasma levels of platelet factor 4 (PF4) and β-thromboglobulin (β-TG), as markers for platelet activation, were significantly increased in the KD group compared with the HC group (Figures 1A, B). Meanwhile, the surface expression of p-selectin (CD62P) in KD platelets was 2~3 fold higher than those in HC platelets (Figure 1C). These results indicated that KD platelets were highly activated. Our previous study using Genome-wide miRNA sequencing (19) showed that miR-223 was significantly increased in KD platelets. Consistently, our RT-PCR result also showed that the expression of platelet miR-223 was significantly increased in the KD group compared to the HC group (Figure 1D). These results suggest that platelets and platelet-derived miR-223 may be involved in the pathophysiological process of KD.

Activated KD platelets are internalized into HCAECs

As we recently demonstrated that activated KD platelets could be incorporated into VSMCs, we sought to investigate if KD platelets were internalized into ECs. HCAECs were co-

cultured with CMFDA green-labeled platelets for 2, 4, and 24 hours. Consistent with our previous study that activated platelets endocytosed by VSMCs (19, 27), we found that activated KD platelets were also significantly incorporated into HCAECs (Figure 2A). Three-dimensional reconstruction had shown that KD platelets were considered at the same horizontal position as the nucleus of the HCAECs (Figure 2B). The incorporation of platelets by HCAECs was further confirmed by transmission electron microscopy (Figure 2C I-III and Supplementary Figure 1). Platelets were located at the membrane of HCAECs initially (Figures 2C I-red arrow), then incorporated into the cytoplasm (Figures 2C II-red arrow), and fused with lysosomes (Figure 2C III-red arrow). Taken together, these results indicate that activated KD platelets are internalized into HCAECs.

The horizontal transfer of KD platelets derives miR-223 to HCAECs

Previous studies (31, 32) found that miR-223 was expressed in freshly isolated human vascular endothelial cells. However, the expression of miR-223 in ECs were gradually decreased until undetectable *in vitro* culture, suggesting for the exogenous source of miR-223 (31). Using THP-1 cells with high expression of miR-223 as a positive control, HCAECs were cultured with different FBS concentration or treated with VEGF, no significant expression of miR-223 was detected by RT-qPCR in HCAECs after five passages, *Ct* value >35 (Supplementary Figure 2A). However, when co-cultured with KD platelets, the intracellular level of miR-223 in HCAECs increased with incubation time (Figure 3A), and the number of co-cultured platelets (Figure 3B).

To determine if the platelet-derived miR-223 contributing to the increased level of miR-223 in HCAECs, the miR-223 expression level was first examined in HCAECs, suggesting a significantly increased level of miR-223 in HCAECs after co-culture with KD platelets (Supplementary Figure 2B). The si-Dicer was transiently transfected into HCAECs to inhibit the splicing of pre-miRNA into mature miRNA by Dicer in HCAECs. HCAECs transfected with si-Dicer showed a significant reduction of Dicer mRNA (Figure 3C). When co-cultured with KD platelets for 24 hours, either HCAECs or si-Dicer transfected HCAECs showed no statistically significant difference in miR-223 (Figure 3C). When co-cultured with RNase A-treated KD platelets for 24 hours, the level of miR-223 was significantly decreased in HCAECs (Figure 3D). These

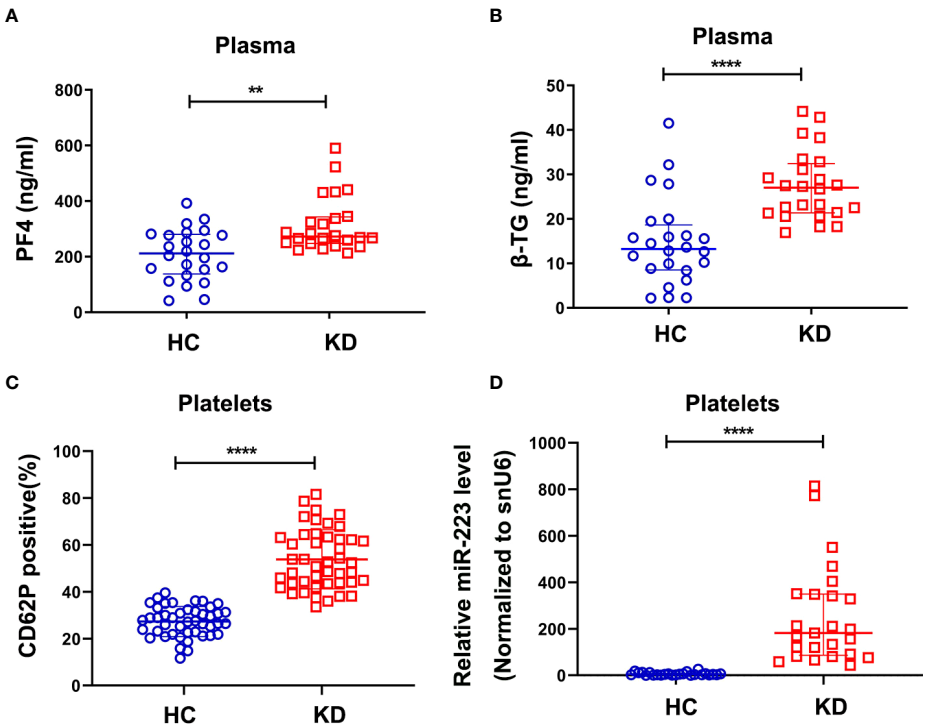

FIGURE 1
KD platelets were hyperactive and exhibit higher expression of miR-223. Plasma levels of PF4 **(A)** and β-TG **(B)** in HC and KD groups (HC: n = 24, KD: n = 24). Data are presented as median ± IQR, Mann Whitney test. **(C)** Surface expression of P-selectin (CD62P) in platelets isolated from HC and KD groups (HC: n = 45, KD: n = 45). Data are presented as mean ± SD, Unpaired *t*-test. **(D)** Relative expression of miR-223 in platelets isolated from HC and KD groups (HC: n=25, KD: n=25). Data are presented as median ± IQR, Mann Whitney test. $^{**}P < 0.01$, $^{****}P < 0.0001$. ns means no statistical difference.

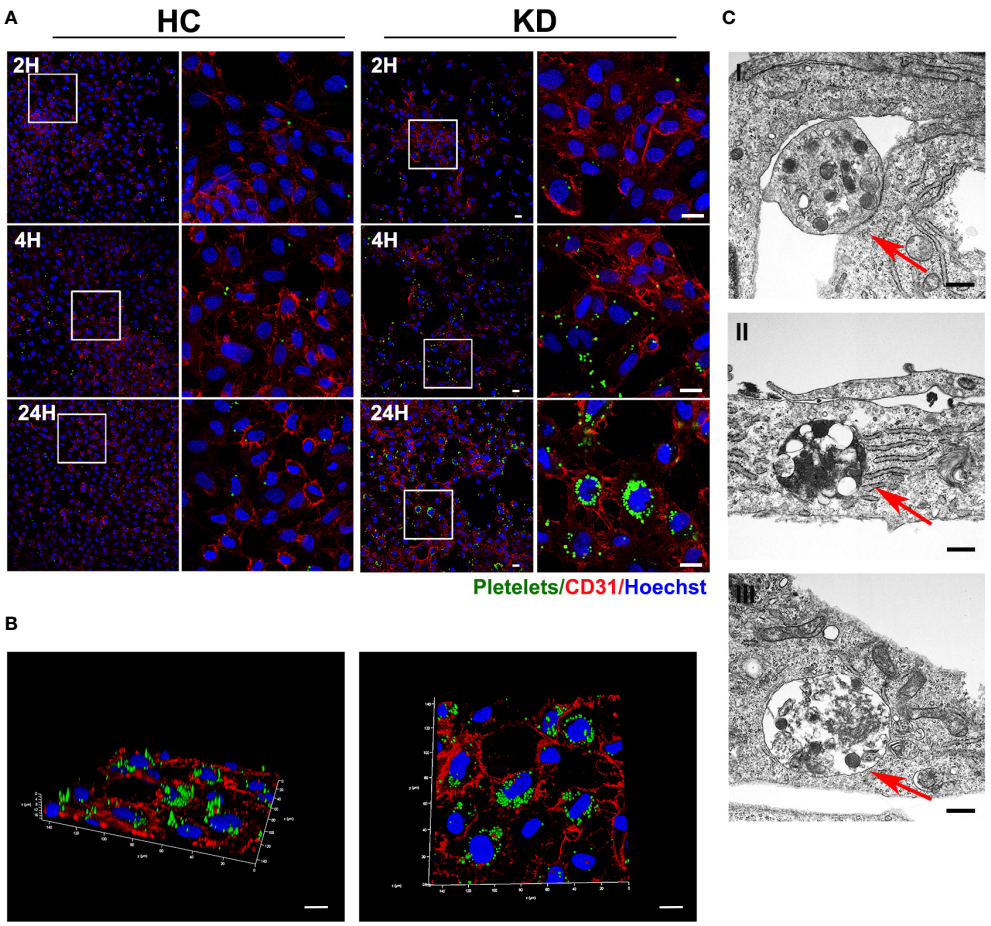

FIGURE 2
Activated KD platelets were internalized by HCAECs. **(A)** Representative immunofluorescence images of HCAECs co-cultured with CMFDA-labeled (green) HC or KD platelets for 2, 4, and 24 hours. Blue, Hoechst nuclear staining; red, CD31 in HCAECs (HC platelets: n = 6, KD platelets: n = 6). Scale bar: 20μm. **(B)** Confocal three-dimensional reconstruction of Z-stack images of HCAECs co-cultured with CMFDA-labeled KD platelets (green) for 24 hours (KD platelets: n = 6). Scale bar: 20μm. **(C)** Transmission electron microscopy of HCAECs co-cultured with KD platelets for 24h. (KD platelets: n = 3). I-III were images acquired in different fields of vision respectively. Red arrows indicated KD platelet internalized into HCAECs. Scale bar: 500nm.

results suggest that the horizontal transfer of platelet-derived miR-223 contributes to the increased level of miR-223 in HCAECs co-cultured with KD platelets.

Since platelets miRNAs can be directly released into the circulation or packaged in the PMPs. KD platelets, PMPs, and releasate from the same amount of blood were co-cultured with HCAECs for 24 hours respectively. HCAECs co-cultured with KD platelets showed significantly increased expression of miR-223. No significant difference in miR-223 level was found in HCAECs co-cultured with PMPs or supernatant containing platelet-releasate compared to the PBS group (Figure 3E). Using purified KD platelets and a transwell chamber, we found significantly increased expression of miR-223 in HCAECs after directly incubated with KD platelets (Figure 3F). These results suggest that the increased level of miR-233 in HCAECs co-cultured with KD platelets was mainly contributed by the platelet-transferred miR-223, rather than PMPs and free miRNA released by platelets.

KD platelet-derived miR-223 attenuates monocytes adhesion to HCAECs

Inflammatory factors are known to induce vascular endothelial cells inflammatory response by promoting leukocyte adhesion in vasculitis, e.g. TNF-α (33). Plasma TNF-α level was increased in patients with KD compared to healthy children (Supplementary Figure 3). TNF-α treatment was used to mimic the inflammatory state of endothelial cells *in vitro*. To investigate the functional effect of increased miR-223 level in HCAECs, we performed leukocyte adhesion assay in TNF-α-activated HCAECs. THP-1 was used as a leukocyte

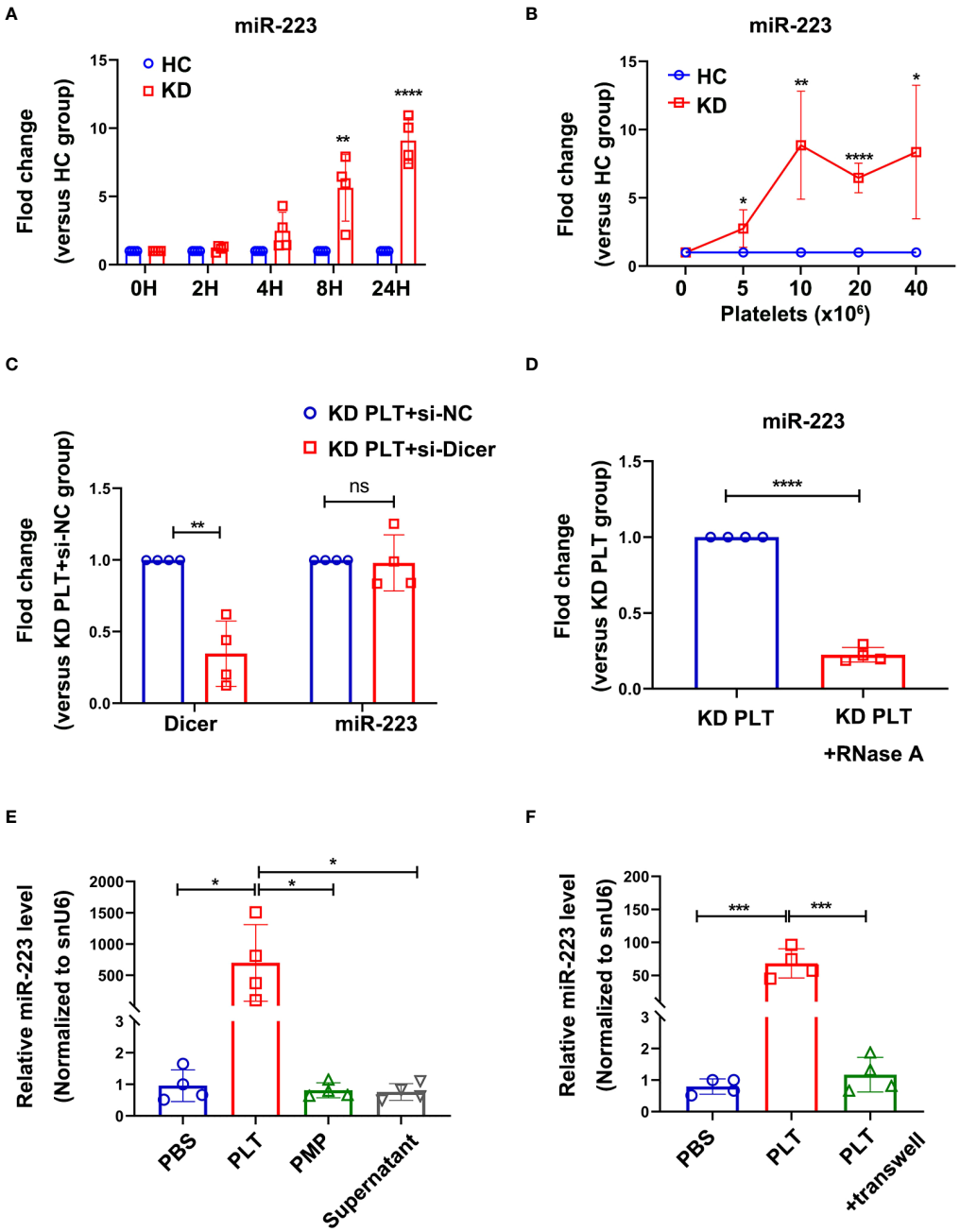

FIGURE 3
Intracellular miR-223 in HCAECs were delivered by activated KD platelets. **(A)** Level of miR-223 in HCAECs co-cultured with HC or KD platelets for 0, 2, 4, 8, and 24 hours. At each time point, the relative level of miR-223 in KD group was normalized by the HC group (n=4). Data are presented as mean ± SD, Unpaired *t*-test. **(B)** Level of miR-223 in HCAECs co-cultured with various number of platelets from HC or KD group for 24 hours. The relative level of miR-223 in KD group was normalized by each HC group (n=4). Data are presented as mean ± SD, Unpaired *t*-test. **(C)** The intracellular level of Dicer and miR-223 in HCAECs transfected with or without si-Dicer and subsequently co-cultured with KD platelets (1:100) for 24 hours. Results were presented as fold change (n=4). Data are presented as mean ± SD, Unpaired *t*-test. **(D)** The intracellular miR-223 level in HCAECs incubated with RNase A-treated (1U/ml, 1h, 37°C) KD platelets (1:100) for 24 hours. Results were presented as fold change (n=4), Unpaired *t*-test. Data are presented as mean ± SD. **(E)** The expression of miR-223 in HCAECs incubated with PLTs, PMPs, or supernatant, respectively for 24 hours (n=4). Data are presented as mean ± SD, One-way ANOVA and Tukey's multiple comparisons test. **(F)** The expression of miR-223 in HCAECs incubated with KD platelets (PLTs) with or without a transwell chamber for 24 hours (n=4). Data are presented as mean ± SD, One-way ANOVA and Tukey's multiple comparisons test. HC, HCAECs co-cultured with platelets isolated from HC; KD, HCAECs co-cultured with platelets isolated from KD patients. *P<0.05, **P < 0.01, ***P < 0.001, ****P < 0.0001. ns, no statistical difference.

representative. HCAECs were pre-transfected with agomiR-223 or agomiR-NC followed by incubation with THP-1 for 4 hours. The level of miR-223 was significantly increased after agomiR-223 transfection (Supplementary Figure 4). Using fluorescence microscopy, we evaluated green fluorescence-labeled THP-1 on the surface of HCAECs. Treatment with TNF-α increased THP-1 adherence to the HCAECs, which was attenuated by approximately 30% when HCAECs over-expressing miR-223 (Figures 4A, B). Adhesion of THP-1 to HCAECs induced by TNF-α showed no significant difference between HCAECs and HCAECs pre-cocultured with HC platelets. While pre-cocultured with KD platelets for 48h, the number of THP-1 adhesion to HCAECs showed a decreasing trend of about 40% (Figures 4C, D). Our results demonstrate that KD platelet-derived miR-223 attenuates the adhesion of monocytes to HCAECs.

KD Platelet-derived miR-223 targets ICAM-1 in HCAECs

To identify the potential targets of miR-223 in HCAECs, miRNA target prediction software (TargetScan 8.0) was used. We found that ICAM-1 harbors a conserved binding site for miR-223 within its 3' untranslated region (3' UTR) (Supplementary Figure 5A). ICAM-1 is a key endothelial receptor in the leukocyte-endothelial interaction and participates in the regulation of leukocyte adhesion to endothelial cells. A previous study using a dual-luciferase reporter assay has reported that ICAM-1 is a target gene of miR-223 in endothelial cells (29). To further determine if ICAM-1 is the target of miR-223, Ago2 immunoprecipitation was performed in HCAECs transfected with agomiR-223/agomiR-NC, and miR-223 and ICAM-1 mRNA were detected by RT-qPCR. The expression levels of miR-223 and ICAM-1 mRNA in the Ago2 complex extracted from HCAECs transfected with agomiR-223 were significantly increased, compared to cells transfected with agomiR-NC (Supplementary Figure 5B). Next, we observed the regulation of miR-223 on ICAM-1 in endothelial cells under an inflammatory state. TNF-α treatment was used to mimic the inflammatory state of HCAECs as described above. Western-blot and immunofluorescence results indicated that TNF-α treatment increased the expression of ICAM-1 in HCAECs, which was suppressed by overexpression of miR-223 by approximately 35% (Figures 5A, C). HCAECs were co-cultured with HC/KD platelets and then stimulated with TNF-α. We found that TNF-α-induced ICAM-1 expression was not significantly different between HCAECs and HCAECs pre-cocultured with HC platelets. But, the protein expression of ICAM-1 was reduced by about 30% in HCAECs pre-cocultured with KD platelets (Figures 5B, D). Taken together, our results demonstrate that KD platelet-derived miR-223 targets ICAM-1 in HCAECs.

In the LCWE-induced KD murine model, down-regulation of platelet miR-223 increases endothelial ICAM-1 expression with concomitant infiltration of inflammatory cells in abdominal aorta

To determine the role of platelet-derived miR-223 to KD vasculitis *in vivo*, the platelet-specific miR-223 knockout mice (PF4-miR-223 KO, PF4-cre: miR-223$^{flox/flox}$) were successfully constructed, LCWE was intraperitoneally injected (*i.p*) to establish KD murine model. Supplementary Figure 6A demonstrated the generation of a recombined allele upon Cre recombination in generated mice. RT-qPCR results showed that miR-223 expression in platelets was significantly decreased in PF4-miR-223 KO mice (Supplementary Figure 6B). Two weeks after LCWE injection, the murine abdominal aorta was characterized by disruption of elastin, and manifestations of medial thickening, which were significantly enhanced in the PF4-miR-223 KO mice compared to Floxed ctrl mice (Figures 6A, B). Our immunofluorescence results showed that the expression of ICAM-1 was significantly increased in the endothelium of the abdominal aorta after LCWE treatment. LCWE-injected PF4-miR-223 KO mice exhibited increased ICAM-1 expression compared to LCWE-injected Floxed ctrl mice (Figures 6C, D). Consistently, we found the infiltration of CD45$^+$ inflammatory cells was increased in the abdominal aorta of LCWE-injected KD murine model. Compared to LCWE-injected Floxed ctrl mice, LCWE-injected PF4-miR-223 KO mice exhibited increased CD45$^+$ inflammatory cells infiltration (Figures 6E, F). These results suggest that platelet-derived miR-223 inhibits endothelial ICAM-1 expression and the inflammatory cells infiltration in KD vasculopathy.

Discussion

Kawasaki disease is a childhood-acquired cardiovascular disease characterized by multi-systemic vasculitis, accompanied by a series of inflammatory responses, including inflammatory cell activation, platelet hyperactivation, and dysfunction of the endothelial cells. Necrosis of endothelial cells in the early stages of KD is critical to disturbance of the vascular barrier (5). Platelets have been found to contribute to the development of endothelial dysfunction (34). Studies have focused on the effect of platelet-derived cytokines on the formation of endothelial lesions. Here we demonstrate that KD platelet-derived miR-223 inhibits the endothelial expression of ICAM-1, at least in part contributing to attenuating the adhesion of inflammatory cells (e.g., monocytes) in KD vasculitis.

In recent years, it has been found that platelet-derived miRNAs can be released into the peripheral blood *via* encapsulation in PMPs (35). In contact with the neighboring cells, the internalized PMPs deliver miRNAs, which regulate the function of the recipient cell by post-transcriptional reprogramming (36). MiR-223, which is

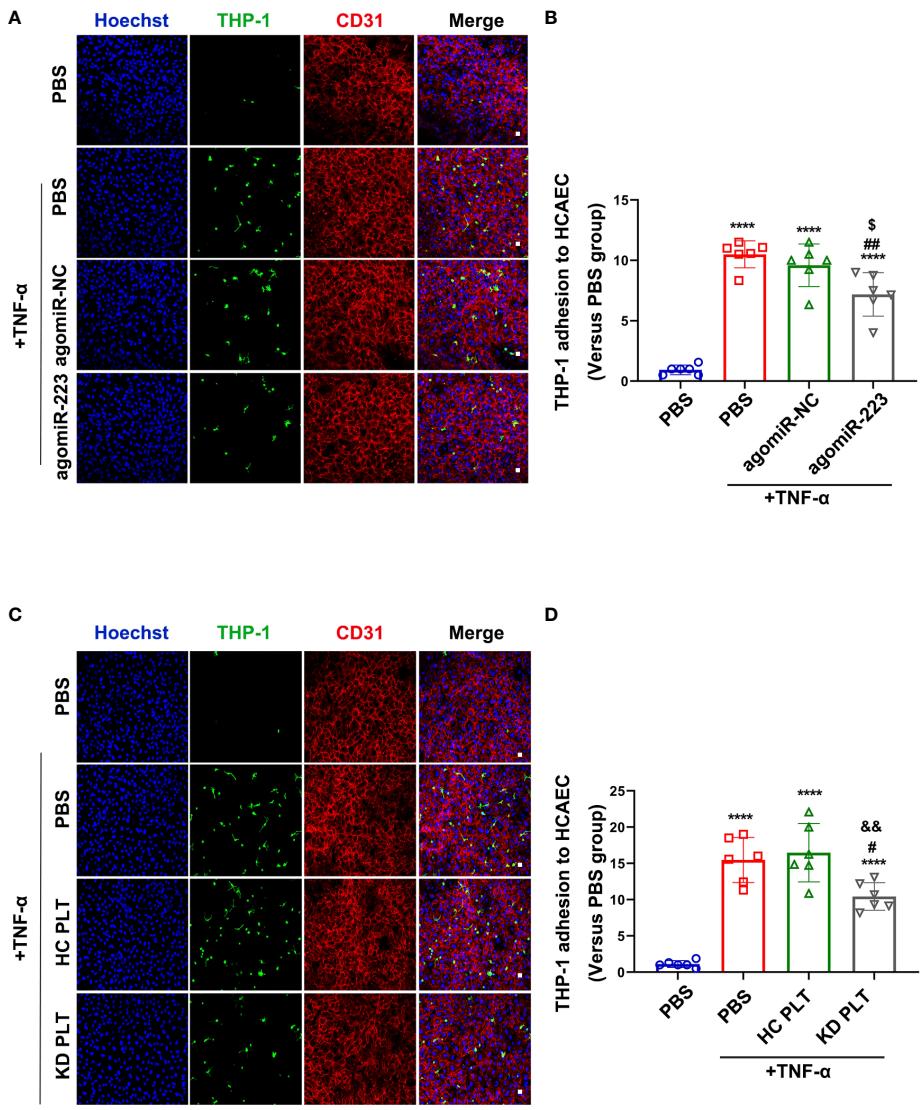

FIGURE 4
KD platelet-derived miR-223 inhibited monocyte adhesion to HCAECs. HCAECs were transfected with agomiR-223 or agomiR-NC for 48 hours followed by treatment with TNF-α (2ng/ml, 4h). **(A)** Representative immunofluorescence images of HCAECs co-cultured with CMFDA-labeled (green) THP-1 for 2 hours. Blue, Hoechst nuclear staining; red, CD31 in HCAECs (n = 6). Scale bar: 20μm. **(B)** The number of CMFDA-labeled THP-1 adhered to the surface of HCAECs. Results were presented as fold change(n = 6). Data are presented as mean ± SD, One-way ANOVA and Tukey's multiple comparisons test. HCAECs were co-cultured with HC or KD platelets for 48 hours followed by treatment with TNF-α (2ng/ml, 4 hours). **(C)** Representative immunofluorescence images of HCAECs co-cultured with CMFDA-labeled (green) THP-1 for 2 hours. Blue, Hoechst nuclear staining; red, CD31 in HCAECs (n = 6). Scale bar: 20μm. **(D)** The number of CMFDA-labeled THP-1 adhered to the surface of the HCAECs. Results were presented as fold change (n = 6). Data are presented as mean ± SD, One-way ANOVA and Tukey's multiple comparisons test. $^{****}P < 0.0001$ vs. PBS group; $^{\#}P < 0.05$, $^{\#\#}P < 0.01$ vs. PBS+TNF-α group; $^{\$}P < 0.05$ vs. agomiR-NC+TNF-α group; $^{\&\&}P < 0.01$ vs. HC PLT+TNF-α group.

abundantly expressed in human platelets, is encapsulated in PMPs and released upon thrombin stimulation (28). Co-incubation of HUVECs with PMPs increased the level of miR-223 in HUVECs and inhibited IGF-1R expression, which promoted the endothelial cell apoptosis after incubation with late glycosylation end products (26). In addition, platelet internalization was recently identified as a novel pathway for miRNA delivery (19, 27, 37). It has been reported that platelets were internalized into the hepatocyte. Following this internalization, platelets transfer RNA to the hepatocyte, which stimulated hepatocyte proliferation (37). Our recent study has demonstrated that the horizontal transfer of platelet-derived miR-223 increased the level of miR-223 in VSMCs, which suppressed VSMC dedifferentiation by inhibiting platelet-derived growth factor receptor β (PDGFRβ) in VSMCs (27). Consistently, we found platelets from KD patients with coronary aneurysms showed a significant decrease in miR-223 expression, compared with platelets

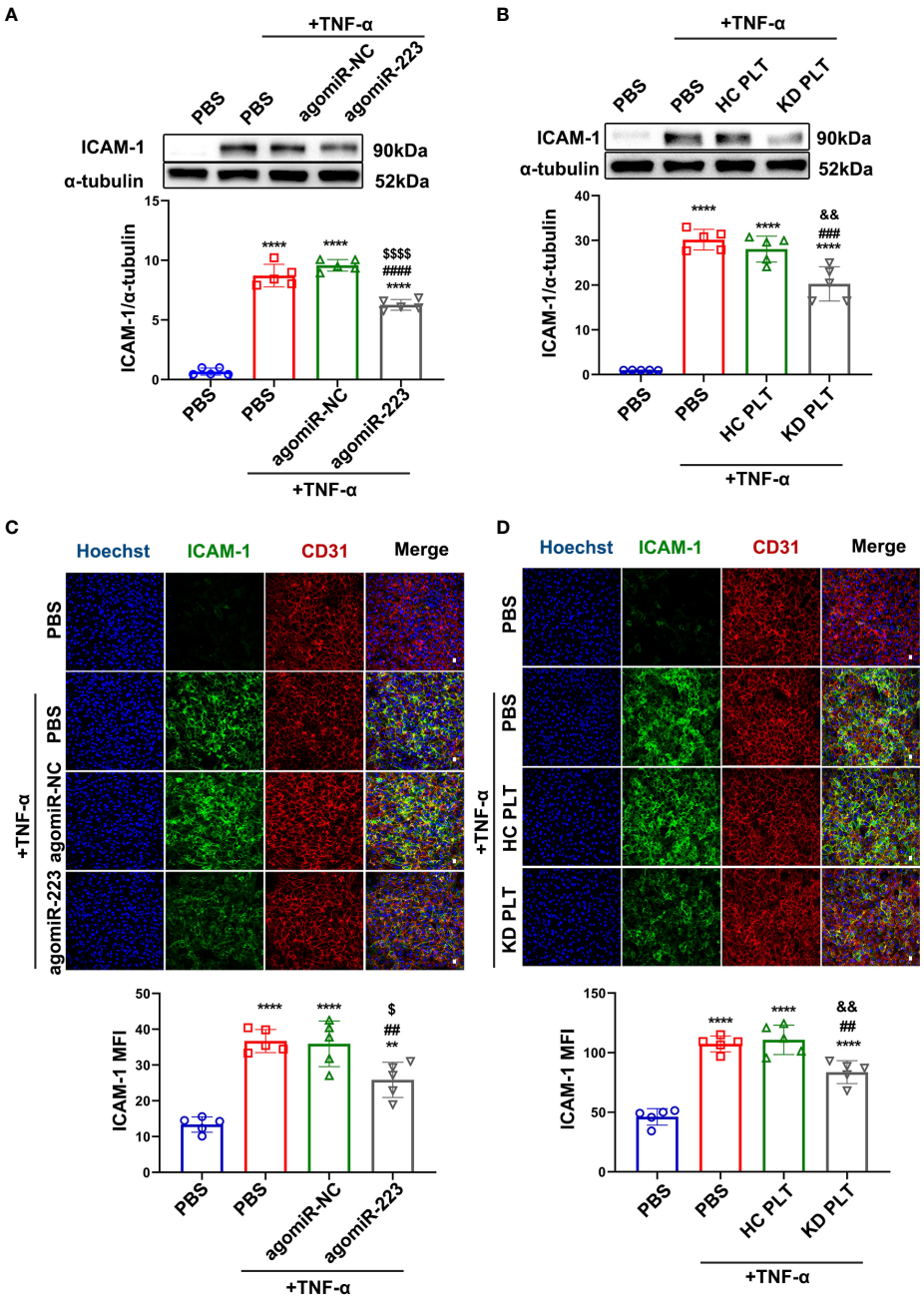

FIGURE 5
KD platelet-derived miR-223 attenuated TNF-α-induced ICAM-1 expression in HCAECs. **(A)** Expression of ICAM-1 in HCAECs transfected with agomiR-223/agomiR-NC for 48 hours followed by treatment with TNF-α (2ng/ml, 4 hours) was determined by Western blot analysis (n = 5). Data are presented as mean ± SD, One-way ANOVA and Tukey's multiple comparisons test. **(B)** Expression of ICAM-1 in HCAECs and HCAECs co-cultured with HC or KD platelets for 48 hours followed by treatment with TNF-α (2ng/ml, 4 hours) was determined by Western blot analysis (n = 5). Data are presented as mean ± SD, One-way ANOVA and Tukey's multiple comparisons test. **(C)** Representative immunofluorescence images and quantification of ICAM-1 in HCAECs transfected with agomiR-NC/agomiR-223 for 48 hours followed by TNF-α treatment. Green, ICAM-1; blue, Hoechst nuclear staining; red, CD31 in HCAECs (n = 5). Scale bar: 20μm. Data are presented as mean ± SD, One-way ANOVA and Tukey's multiple comparisons test. **(D)** Representative immunofluorescence images and quantification of ICAM-1 in HCAECs and HCAECs co-cultured with HC or KD platelets for 48 hours followed by TNF-α treatment. Green, ICAM-1; blue, Hoechst nuclear staining; red, CD31 in HCAECs (n = 5). Scale bar: 20μm. Data are presented as mean ± SD, One-way ANOVA and Tukey's multiple comparisons test. $^{**}P < 0.01$, $^{****}P < 0.0001$ vs. PBS group; $^{\#\#}P < 0.01$, $^{\#\#\#}P < 0.001$, $^{\#\#\#\#}P < 0.0001$ vs. PBS+TNF-α group; $^{\$}P < 0.05$, $^{\$\$\$\$}P < 0.0001$ vs. agomiR-NC+TNF-α group; $^{\&\&}P < 0.01$ vs. HC PLT+TNF-α group.

10.3389/fimmu.2022.922868

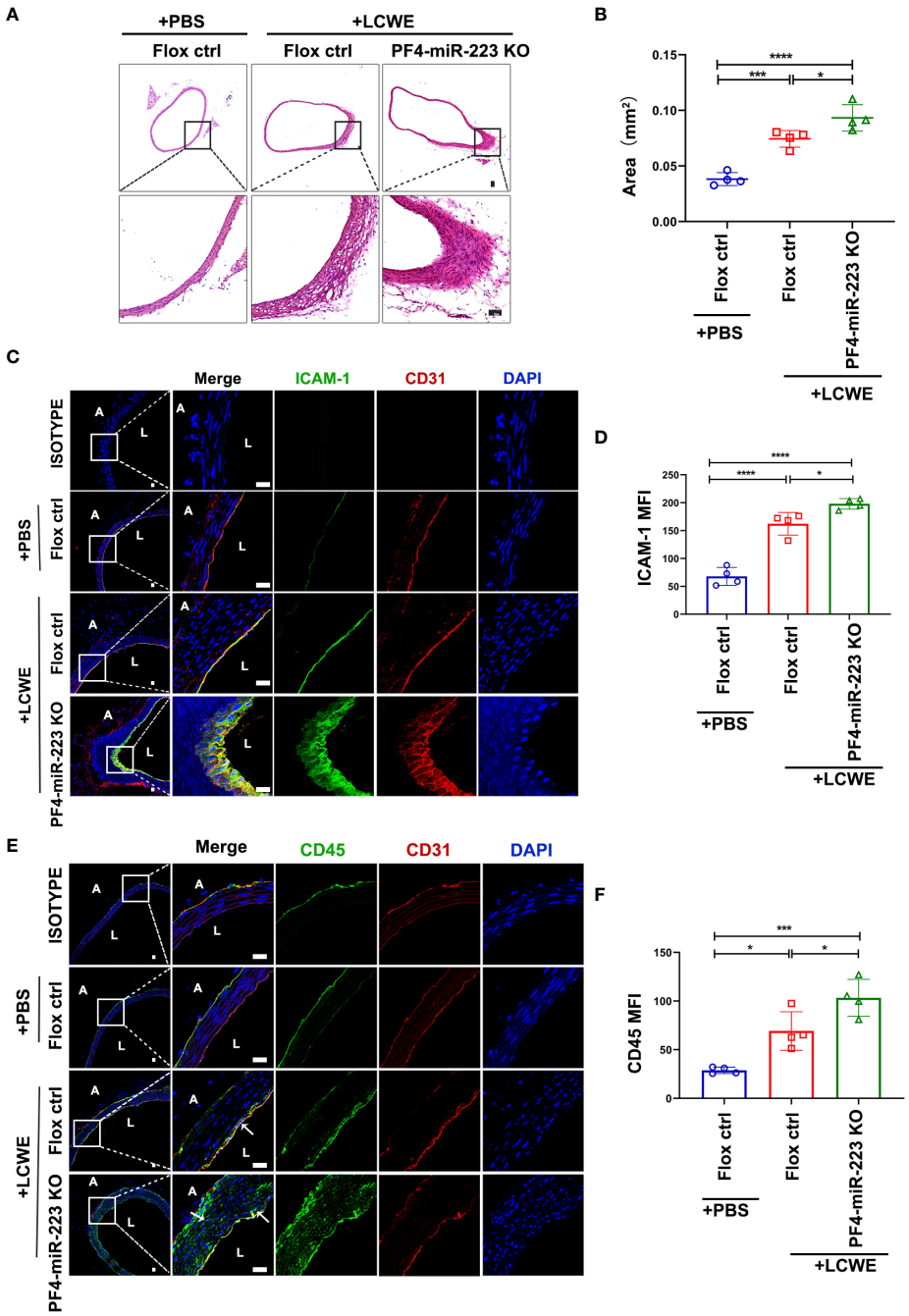

FIGURE 6
In LCWE-induced KD murine model, deficiency of platelet-miR-223 exacerbated the medial thickening, increased ICAM-1 expression with concomitant $CD45^+$ inflammatory cells infiltration in the endothelium of abdominal aorta. LCWE or PBS was administrated *i.p.* for two weeks. The abdominal aorta tissues were collected, and continuous cross-sections were performed for H&E staining and immunofluorescence analysis. **(A)** Representative H & E-stained sections of PBS or LCWE injected mice were shown. n = 4, Scale bar: 50μm. **(B)** Quantification of the media layer areas of abdominal aorta in each group was shown. n = 4, Data are presented as mean ± SD, One-way ANOVA and Tukey's multiple comparisons test. **(C)** Representative immunofluorescence images of sections from PBS or LCWE-injected mice. CD31 was stained as red, ICAM-1 as green, and the nucleus visualized as blue (DAPI). n = 4, Scale bars: 20μm. **(D)** Quantification of ICAM-1 expression in abdominal aorta tissues was shown (n = 4). Data are presented as mean ± SD, One-way ANOVA and Tukey's multiple comparisons test. **(E)** Representative immunofluorescence images of sections from PBS or LCWE-injected mice. CD31 was stained as red, CD45 as green, and the nucleus visualized as blue (DAPI). n = 4, Scale bars: 20μm. **(F)** Quantification of CD45 expression in abdominal aorta tissues was shown (n = 4). Data are presented as mean ± SD, One-way ANOVA and Tukey's multiple comparisons test. L, lumen; A, adventitia; Flox ctrl: miR-223 $^{flox/flox}$ mice.PF4-miR-223 KO, PF4-cre: miR-223 $^{flox/flox}$ mice. $^*P < 0.05$, $^{***}P < 0.001$, $^{****}P < 0.0001$.

from KD patients without coronary aneurysms (19). Deficiency of platelet miR-223 in KD patients with aneurysms contributes to coronary artery pathology as platelet uptake fails to suppress VSMC dedifferentiation. Thus, platelet-derived miR-223 was identified as a protective role in KD-induced arterial aneurysms. In the present study, our results showed that KD platelets with a higher level of miR-223 were incorporated into HCAECs, resulting in the horizontal transfer of miR-223. Using KD platelets, PMPs, and platelet-releasate from the same amount of blood co-cultured with HCAECs, we found the increased expression of miR-223 in HCAECs was primarily derived from KD platelets, rather than PMPs or free miRNAs from platelet releasate. Since miR-223 targets ICAM-1, the horizontal transfer of platelet-derived miR-223 contributes to the downregulation of ICAM-1 in HCAECs. Our results provide evidence for the regulatory function of horizontal transfer of platelet-derived miRNAs.

It is well known that ICAM-1 is a key endothelial receptor contributing to leukocyte-EC interactions and plays a critical role in inflammatory responses (38, 39). Adhesion of leukocytes, particularly monocyte adhesion and migration to ECs, is critical for the development of vasculitis (40). ICAM-1 is generally expressed at low basal levels in endothelial cells, but its expression is upregulated by inflammatory cytokines (41). Clinical studies have shown that the circulating levels of ICAM-1 expression are increased in the KD and positively correlated with disease severity (42, 43), but the underlying mechanism remains elusive. ICAM-1 was identified as one of the target genes of miR-223 (29). Studies on sepsis showed that TNF-α induced expression of ICAM-1 in endothelial cells was partially attenuated by miR-223 transferred by PMPs (25). However, studies on the involvement of miR-223 regulating ICAM-1 in endothelial cells were limited to *in vitro* studies (25, 44). Our results show that KD platelet-derived miR-223 also attenuates TNF-α induced expression of ICAM-1 in HCAECs. In LCWE-injected PF4-miR-223 KO mice, deficiency of platelet-miR-223 exacerbates the medial thickening of the abdominal aorta, increased ICAM-1 expression with concomitant $CD45^+$ inflammatory cells infiltration into the endothelium compared to LCWE-injected Floxed ctrl mice, suggesting that platelet-derived miR-223 play an important role in endothelial pathology of KD.

There are some limitations in this study. First, platelet-derived miR-223 only partially attenuates TNF-α induced expression of ICAM-1, suggesting that other mechanisms may be involved. Wang et al. demonstrated that miR-223 exerted a protective effect by targeting IL6ST in KD-induced endothelial injury (45). Another study showed that miR-223 regulated EC proliferation by targeting IGF-1R in KD (31). Furthermore, Maruyama et al. proposed that miR-223 plays an important role in KD vasculitis by targeting NLRP3 (46). These studies suggest that miR-223 plays an important protective role in KD vasculitis. Our study demonstrates that platelet-derived miR-223 at least in part contributes to KD vasculopathy by targeting ICAM-1. Second, in PF4-miR-223 KO mice, miR-223 expression in platelets was decreased by 80%, in comparison with those from Floxed ctrl mice. We think impure platelet preparation may contribute to the incomplete knockout of miR-223 in platelets. Third, due to the

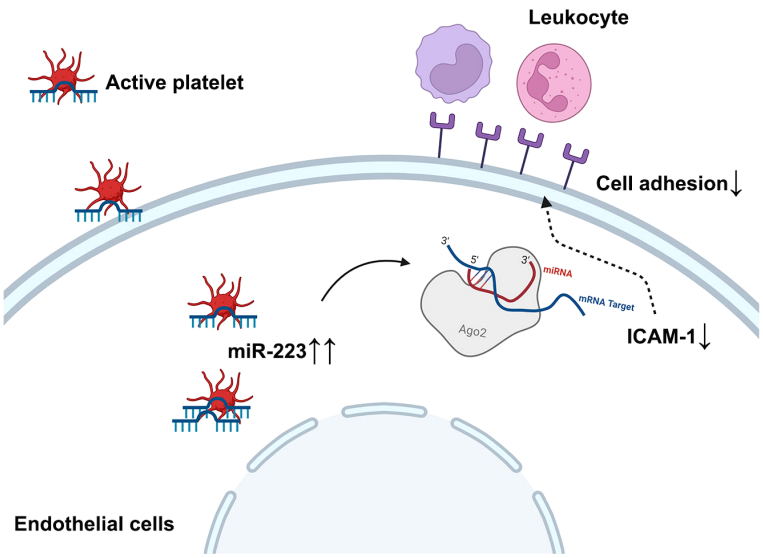

FIGURE 7
Schematic figure of the working model diagram of the regulatory function of platelet-derived miR-223 in endothelial cells. In the case of KD, platelets are hyperactive and internalized into HCAECs. The horizontal transfer of platelet derives miR-223 to HCAECs, which suppress the expression of ICAM-1 in HCAECs and partially attenuates leukocyte adhesion, thereby reducing further endothelial damage in KD vasculitis. ICAM-1, intercellular cell adhesion molecule-1.

limitation amount of blood samples, not all patient plasma were used for ELISA detection; Forth, in our recent study (19), TNF-α was detected to induce the expression of miR-223 *via* regulating the activity of Dicer, which further cleaves pre-miR-223 into mature miR-223 (47), suggesting the important role of TNF-α in KD platelet hyperreactivity. Other pro-inflammatory cytokines, such as interleukin-1β (IL-1β), were also found to contribute to KD vasculopathy (48), so further studies are warranted to explore the role of platelet-derived miR-223 in IL-1β induced vasculopathy.

In summary, we demonstrate that the horizontal transfer of platelet-derived miR-223 suppresses the expression of ICAM-1 in HCAECs, which at least in part attenuates leukocyte adhesion, thereby reducing endothelial damage in KD vasculitis (Figure 7). Platelet-derived miR-223 may serve as a brake for inflammatory cell infiltration into the endothelium. Thus, miR-223 level in platelets may serve as a potential prognostic marker for KD vasculopathy.

Data availability statement

The original contributions presented in the study are included in the article/supplementary material. Further inquiries can be directed to the corresponding authors.

Ethics statement

The studies involving human participants were reviewed and approved by Guangzhou Women and Children Medical Center Human Investigation Committee, No. 2017102710. Written informed consent to participate in this study was provided by the participants' legal guardian/next of kin. The animal study was reviewed and approved by Animal Care and Use Committee of Guangzhou Medical University, China (2019-384).

Author contributions

MG and YZ conceptualized this study. MG, SF, QC, CJ, MQ, YB, YZ, and WT determined the methodology. MG, SF, QC, CJ, and YZ performed the investigations. MG and YZ wrote the original draft. SF, MQ, YB, and WT wrote, reviewed, and edited the draft. YZ and WT supervised the overall study. All authors contributed to the article and approved the submitted version.

Funding

This work was supported by the National Natural Science Foundation of China (Grant No. 81902144, 82022033, 81970437, 81903605, 31900527), the Ministry of Science and Technology of the People's Republic of China (Grant No. QN20200131001), the Guangzhou science and technology project (Grant No. 201904010483), and Guangzhou Medical University (Grant No. 02-410-2206047).

Conflict of interest

The authors declare that the research was conducted in the absence of any commercial or financial relationships that could be construed as a potential conflict of interest.

Publisher's note

All claims expressed in this article are solely those of the authors and do not necessarily represent those of their affiliated organizations, or those of the publisher, the editors and the reviewers. Any product that may be evaluated in this article, or claim that may be made by its manufacturer, is not guaranteed or endorsed by the publisher.

Supplementary material

The Supplementary Material for this article can be found online at: https://www.frontiersin.org/articles/10.3389/fimmu.2022.922868/full#supplementary-material

References

1. Shulman ST, Rowley AH. Kawasaki Disease: Insights into pathogenesis and approaches to treatment. *Nat Rev Rheumatol* (2015) 11(8):475–82. doi: 10.1038/nrrheum.2015.54

2. Amano S, Hazama F, Kubagawa H, Tasaka K, Haebara H, Hamashima Y. General pathology of Kawasaki disease. on the morphological alterations corresponding to the clinical manifestations. *Acta Pathol Jpn* (1980) 30(5):681–94. doi: 10.1111/j.1440-1827.1980.tb00966.x

3. Friedman KG, Gauvreau K, Hamaoka-Okamoto A, Tang A, Berry E, Tremoulet AH, et al. Coronary artery aneurysms in Kawasaki disease: Risk factors for progressive disease and adverse cardiac events in the us population. *J Am Heart Assoc* (2016) 5(9):e003289. doi: 10.1161/jaha.116.003289

4. Newburger JW, Takahashi M, Gerber MA, Gewitz MH, Tani LY, Burns JC, et al. Diagnosis, treatment, and long-term management of Kawasaki disease: A statement for health professionals from the committee on rheumatic fever, endocarditis and Kawasaki disease, council on cardiovascular disease in the young, American heart association. *Circulation* (2004) 110(17):2747–71. doi: 10.1161/01.CIR.0000145143.19711.78

5. Orenstein JM, Shulman ST, Fox LM, Baker SC, Takahashi M, Bhatti TR, et al. Three linked vasculopathic processes characterize Kawasaki disease: A light and

transmission electron microscopic study. *PLoS One* (2012) 7(6):e38998. doi: 10.1371/journal.pone.0038998

6. Pober JS, Sessa WC. Evolving functions of endothelial cells in inflammation. *Nat Rev Immunol* (2007) 7(10):803–15. doi: 10.1038/nri2171

7. Nonoyama S. Immunological abnormalities and endothelial cell injury in Kawasaki disease. *Acta Paediatr Jpn* (1991) 33(6):752–5. doi: 10.1111/j.1442-200x.1991.tb02604.x

8. Hernandez GE, Iruela-Arispe ML. The many flavors of Monocyte/Macrophage–endothelial cell interactions. *Curr Opin Hematol* (2020) 27(3):181–9. doi: 10.1097/MOH.0000000000000573

9. Sakurai Y. Autoimmune aspects of Kawasaki disease. *J Investig Allergol Clin Immunol* (2019) 29(4):251–61. doi: 10.18176/jiaci.0300

10. Shi N, Chen SY. Smooth muscle cell differentiation: Model systems, regulatory mechanisms, and vascular diseases. *J Cell Physiol* (2016) 231(4):777–87. doi: 10.1002/jcp.25208

11. Massberg S, Brand K, Gruner S, Page S, Muller E, Muller I, et al. A critical role of platelet adhesion in the initiation of atherosclerotic lesion formation. *J Exp Med* (2002) 196(7):887–96. doi: 10.1084/jem.20012044

12. Hermann A, Rauch BH, Braun M, Schror K, Weber AA. Platelet Cd40 ligand (Cd40l)–subcellular localization, regulation of expression, and inhibition by clopidogrel. *Platelets* (2001) 12(2):74–82. doi: 10.1080/09537100020031207

13. Henn V, Slupsky JR, Grafe M, Anagnostopoulos I, Forster R, Muller-Berghaus G, et al. Cd40 ligand on activated platelets triggers an inflammatory reaction of endothelial cells. *Nature* (1998) 391(6667):591–4. doi: 10.1038/35393

14. Urbich C, Dernbach E, Aicher A, Zeiher AM, Dimmeler S. Cd40 ligand inhibits endothelial cell migration by increasing production of endothelial reactive oxygen species. *Circulation* (2002) 106(8):981–6. doi: 10.1161/01.cir.0000027107.54614.1a

15. Nording HM, Seizer P, Langer HF. Platelets in inflammation and atherogenesis. *Front Immunol* (2015) 6:98. doi: 10.3389/fimmu.2015.00098

16. Landry P, Plante I, Ouellet DL, Perron MP, Rousseau G, Provost P. Existence of a microrna pathway in anucleate platelets. *Nat Struct Mol Biol* (2009) 16(9):961–6. doi: 10.1038/nsmb.1651

17. Weyrich AS, Schwertz H, Kraiss LW, Zimmerman GA. Protein synthesis by platelets: Historical and new perspectives. *J Thromb Haemost* (2009) 7(2):241–6. doi: 10.1111/j.1538-7836.2008.03211.x

18. Ha M, Kim VN. Regulation of microrna biogenesis. *Nat Rev Mol Cell Biol* (2014) 15(8):509–24. doi: 10.1038/nrm3838

19. Zhang Y, Wang Y, Zhang L, Xia L, Zheng M, Zeng Z, et al. Reduced platelet mir-223 induction in Kawasaki disease leads to severe coronary artery pathology through a mir-223/Pdgfrβ vascular smooth muscle cell axis. *Circ Res* (2020) 127(7):855–73. doi: 10.1161/circresaha.120.316951

20. Dahiya N, Sarachana T, Vu L, Becker KG, Wood WH3rd, Zhang Y, et al. *Platelet MicroRNAs: An Overview. Transfus Med Rev* (2015) 29(4):215–9. doi: 10.1016/j.tmrv.2015.08.002

21. Wang K, Long B, Liu F, Wang JX, Liu CY, Zhao B, et al. A circular rna protects the heart from pathological hypertrophy and heart failure by targeting mir-223. *Eur Heart J* (2016) 37(33):2602–11. doi: 10.1093/eurheartj/ehv713

22. Taibi F, Metzinger-Le Meuth V, Massy ZA, Metzinger L. Mir-223: An inflammatory oncomir enters the cardiovascular field. *Biochim Biophys Acta* (2014) 1842(7):1001–9. doi: 10.1016/j.bbadis.2014.03.005

23. Shan Z, Qin S, Li W, Wu W, Yang J, Chu M, et al. An endocrine genetic signal between blood cells and vascular smooth muscle cells: Role of microrna-223 in smooth muscle function and atherogenesis. *J Am Coll Cardiol* (2015) 65(23):2526–37. doi: 10.1016/j.jacc.2015.03.570

24. Vickers KC, Landstreet SR, Levin MG, Shoucri BM, Toth CL, Taylor RC, et al. Microrna-223 coordinates cholesterol homeostasis. *Proc Natl Acad Sci U.S.A.* (2014) 111(40):14518–23. doi: 10.1073/pnas.1215767111

25. Szilagyi B, Fejes Z, Rusznyak A, Fenyvesi F, Pocsi M, Halmi S, et al. Platelet microparticles enriched in mir-223 reduce icam-1-Dependent vascular inflammation in septic conditions. *Front Physiol* (2021) 12:658524. doi: 10.3389/fphys.2021.658524

26. Pan Y, Liang H, Liu H, Li D, Chen X, Li L, et al. Platelet-secreted microrna-223 promotes endothelial cell apoptosis induced by advanced glycation end products *Via* targeting the insulin-like growth factor 1 receptor. *J Immunol* (2014) 192(1):437–46. doi: 10.4049/jimmunol.1301790

27. Zeng Z, Xia L, Fan X, Ostriker AC, Yarovinsky T, Su M, et al. Platelet-derived mir-223 promotes a phenotypic switch in arterial injury repair. *J Clin Invest* (2019) 129(3):1372–86. doi: 10.1172/jci124508

28. Laffont B, Corduan A, Ple H, Duchez AC, Cloutier N, Boilard E, et al. Activated platelets can deliver mrna regulatory Ago2*Microrna complexes to endothelial cells *Via* microparticles. *Blood* (2013) 122(2):253–61. doi: 10.1182/blood-2013-03-492801

29. Tabet F, Vickers KC, Cuesta Torres LF, Wiese CB, Shoucri BM, Lambert G, et al. Hdl-transferred microrna-223 regulates icam-1 expression in endothelial cells. *Nat Commun* (2014) 5:3292. doi: 10.1038/ncomms4292

30. Lee Y, Wakita D, Dagvadorj J, Shimada K, Chen S, Huang G, et al. Il-1 signaling is critically required in stromal cells in Kawasaki disease vasculitis mouse model: Role of both il-1alpha and il-1beta. *Arterioscler Thromb Vasc Biol* (2015) 35(12):2605–16. doi: 10.1161/ATVBAHA.115.306475

31. Chu M, Wu R, Qin S, Hua W, Shan Z, Rong X, et al. Bone marrow-derived microrna-223 works as an endocrine genetic signal in vascular endothelial cells and participates in vascular injury from Kawasaki disease. *J Am Heart Assoc* (2017) 6(2):e004878. doi: 10.1161/jaha.116.004878

32. Shi L, Fisslthaler B, Zippel N, Frömel T, Hu J, Elgheznawy A, et al. Microrna-223 antagonizes angiogenesis by targeting B1 integrin and preventing growth factor signaling in endothelial cells. *Circ Res* (2013) 113(12):1320–30. doi: 10.1161/circresaha.113.301824

33. Kevil CG, Bullard DC. Roles of Leukocyte/Endothelial cell adhesion molecules in the pathogenesis of vasculitis. *Am J Med* (1999) 106(6):677–87. doi: 10.1016/s0002-9343(99)00132-1

34. Davì G, Patrono C. Platelet activation and atherothrombosis. *N Engl J Med* (2007) 357(24):2482–94. doi: 10.1056/NEJMra071014

35. Randriamboavonjy V, Fleming I. Platelet communication with the vascular wall: Role of platelet-derived microparticles and non-coding rnas. *Clin Sci (Lond)* (2018) 132(17):1875–88. doi: 10.1042/CS20180580

36. Mussbacher M, Pirabe A, Brunnthaler L, Schrottmaier WC, Assinger A. Horizontal microrna transfer by platelets - evidence and implications. *Front Physiol* (2021) 12:678362. doi: 10.3389/fphys.2021.678362

37. Kirschbaum M, Karimian G, Adelmeijer J, Giepmans BN, Porte RJ, Lisman T. Horizontal rna transfer mediates platelet-induced hepatocyte proliferation. *Blood* (2015) 126(6):798–806. doi: 10.1182/blood-2014-09-600312

38. Rahman A, Fazal F. Hug tightly and say goodbye: Role of endothelial icam-1 in leukocyte transmigration. *Antioxid Redox Signal* (2009) 11(4):823–39. doi: 10.1089/ARS.2008.2204

39. Bui TM, Wiesolek HL, Sumagin R. Icam-1: A master regulator of cellular responses in inflammation, injury resolution, and tumorigenesis. *J Leukoc Biol* (2020) 108(3):787–99. doi: 10.1002/JLB.2MR0220-549R

40. van Gils JM, Zwaginga JJ, Hordijk PL. Molecular and functional interactions among monocytes, platelets, and endothelial cells and their relevance for cardiovascular diseases. *J Leukoc Biol* (2009) 85(2):195–204. doi: 10.1189/jlb.0708400

41. Sumagin R, Sarelius IH. A role for icam-1 in maintenance of leukocyte-endothelial cell rolling interactions in inflamed arterioles. *Am J Physiol Heart Circ Physiol* (2007) 293(5):H2786–98. doi: 10.1152/ajpheart.00720.2007

42. Liu F, Ding Y, Yin W. [Expression of sicam-1 in children with intravenous immunoglobulin-resistant Kawasaki disease]. *Zhongguo Dang Dai Er Ke Za Zhi* (2013) 15(12):1109–12. doi: 10.7499/j.issn.1008-8830.2013.12.018

43. Furukawa S, Imai K, Matsubara T, Yone K, Yachi A, Okumura K, et al. Increased levels of circulating intercellular adhesion molecule 1 in Kawasaki disease. *Arthritis Rheum* (1992) 35(6):672–7. doi: 10.1002/art.1780350611

44. Li J, Tan M, Xiang Q, Zhou Z, Yan H. Thrombin-activated platelet-derived exosomes regulate endothelial cell expression of icam-1 *Via* microrna-223 during the thrombosis-inflammation response. *Thromb Res* (2017) 154:96–105. doi: 10.1016/j.thromres.2017.04.016

45. Wang X, Ding YY, Chen Y, Xu QQ, Qian GH, Qian WG, et al. Mir-223-3p alleviates vascular endothelial injury by targeting Il6st in Kawasaki disease. *Front Pediatr* (2019) 7:288. doi: 10.3389/fped.2019.00288

46. Maruyama D, Kocaturk B, Lee Y, Abe M, Lane M, Moreira D, et al. Microrna-223 regulates the development of cardiovascular lesions in lcwe-induced murine Kawasaki disease vasculitis by repressing the Nlrp3 inflammasome. *Front Pediatr* (2021) 9:662953. doi: 10.3389/fped.2021.662953

47. Elgheznawy A, Shi L, Hu J, Wittig I, Laban H, Pircher J, et al. Dicer cleavage by calpain determines platelet microrna levels and function in diabetes. *Circ Res* (2015) 117(2):157–65. doi: 10.1161/CIRCRESAHA.117.305784

48. Jia C, Zhang J, Chen H, Zhuge Y, Chen H, Qian F, et al. Endothelial cell pyroptosis plays an important role in Kawasaki disease *Via* Hmgb1/Rage/Cathespin b signaling pathway and Nlrp3 inflammasome activation. *Cell Death Dis* (2019) 10(10):778. doi: 10.1038/s41419-019-2021-3

frontiers | Frontiers in Immunology

TYPE Original Research
PUBLISHED 24 August 2022
DOI 10.3389/fimmu.2022.944591

OPEN ACCESS

EDITED BY
Zhi-Bin Zhao,
Guangdong Provincial People's Hospital, China

REVIEWED BY
Chuntao Yang,
Guangzhou Medical University, China
Jing Lao,
Five Branches University, United States

*CORRESPONDENCE
Yanyan Liu
799042406@qq.com
Yuyao Wu
yaoyaovermeil@hotmail.com
Suiping Huang
gzdoctorhsp@126.com

†These authors share first authorship

SPECIALTY SECTION
This article was submitted to Molecular Innate Immunity, a section of the journal Frontiers in Immunology

RECEIVED 15 May 2022
ACCEPTED 28 July 2022
PUBLISHED 24 August 2022

CITATION
Ji S, You Y, Peng B, Zhong T, Kuang Y, Li S, Du L, Chen L, Sun X, Dai J, Huang S, Wu Y and Liu Y (2022) Multi-omics analysis reveals the metabolic regulators of duodenal low-grade inflammation in a functional dyspepsia model.
Front. Immunol. 13:944591.
doi: 10.3389/fimmu.2022.944591

Multi-omics analysis reveals the metabolic regulators of duodenal low-grade inflammation in a functional dyspepsia model

Shuai Ji[1†], Yanting You[1†], Baizhao Peng[1†], Tianyu Zhong[1†], Yuxiang Kuang[2], Shasha Li[2], Lijing Du[3], Liqian Chen[1], Xiaomin Sun[1], Jiaojiao Dai[1], Suiping Huang[2*], Yuyao Wu[4*] and Yanyan Liu[1*]

[1]School of Traditional Chinese Medicine, Southern Medical University, Guangzhou, China, [2]The Second Clinical College of Guangzhou University of Chinese Medicine, Guangzhou, China, [3]School of Pharmacy, Shanghai Jiao Tong University, Shanghai, China, [4]Integrated Hospital of Traditional Chinese Medicine, Southern Medical University, Guangzhou, China

Several gastrointestinal phenotypes and impairment of duodenal mucosal barrier have been reported in clinical studies in patients with functional dyspepsia (FD). Due to the preferential colonization of the mucosa, intestinal microbes and their metabolites are commonly involved in host metabolism and immune responses. However, there are no studies on the intertwined correlation among multi-level data. For more comprehensive illustrating, a multi-omics analysis focusing on the duodenum was performed in the FD rat model. We found that differential microbiomes in the duodenum were significantly correlated with the biosynthesis of lipopolysaccharide and peptidoglycan. The innate immune response-related genes, which were upregulated in the duodenum, were associated with the TLR2/TLR4-NFκB signaling pathway. More importantly, arachidonyl ethanolamide (anandamide, AEA) and endocannabinoid analogues showed linear relationships with the FD phenotypes. Taken together, multi-level data from microbiome, transcriptome and metabolome reveal that AEA may regulate duodenal low-grade inflammation in FD. These results suggest an important cue of gut microbiome–endocannabinoid system axis in the pathogenesis of FD.

KEYWORDS

multi-omics, innate immune, inflammation, endocannabinoid, functional dyspepsia

Introduction

Studies have shown that the prevalence of FD is approximately 16% in the general population, although with potential regional and diagnosis-related variations (1). The principles of treatment with a better biopsychosocial understanding of the gut–brain axis

have been highlighted (2). A recent study reported that the vagal gut-brain signaling regulates both the cerebral pain perception and the structural plasticity of FD in a "bottom-up" manner (3); however, this may not have a high clinical translational potential. Clinical data have confirmed that duodenal barrier disruption does exist in the patients with FD (4). The potential damage-associated molecular patterns (DAMPs), but not the pathogens themself, can enter though impaired intestinal barrier, resulting in the host innate immune responses and a low-grade inflammatory condition (5).

The endocannabinoid system, especially the arachidonyl ethanolamide (AEA), was first proposed to be a regulator of energy balance and gastrointestinal load with brainstem-duodenum neural connections (6). Earlier studies have proved that AEA has a crucial role in the physiological regulation of gastric emptying (7). Also, the dysregulation of peripheral AEA is involved in the modulation of small intestinal motility, with a high level in the duodenum (8). However, no studies have investigated whether AEA is involved in the pathophysiological processes of FD.

In this study, we introduce a combined approach including multi-omics data of microbiome, untargeted metabolome and transcriptome to explore the mechanisms underlying FD pathogenesis. Microbial disturbances and predicted metabolic enzymes associated with the biosynthesis of lipopolysaccharide and peptidoglycan are detected in the duodenum. The duodenal protein-coding genes related to host innate immune response are associated with the Toll-like receptor (TLR) signaling and NK-κB-mediated inflammatory signaling pathways. Interestingly, AEA and several endocannabinoid analogues identified in the duodenal with distinct metabolic patterns are significantly correlated with the phenotypes found in FD. These results provide strong evidence that the "gut microbiome–endocannabinoid system axis" in the duodenum is a novel biomarker and therapeutic target for the treatments of functional gastrointestinal disorders.

Results

Compromised gastrointestinal motor function and impaired duodenal mucosal barrier were accompanied with reduction of immune organs index in the rat model of FD

The experimental workflow is illustrated in Figure 1A. Using the classical method, gavage of iodoacetamide for six consecutive days at young age significantly altered body weight in adult rats (Figure 1B). Compared to the control group, the gastrointestinal transit rate was significantly lower in the model group (Figure 1C). However, no significant signs of duodenal damage were observed between the groups (Figure 1D) but only a small amount of incomplete tight junctions (Figure 1E). With further increasing pressure (air injection volume), the model group had higher scores on gastrointestinal sensitivity measures compared with the control group (Figure 1F). An additional trans-endothelial electrical resistance (TEER) experiment was conducted to investigate the duodenal barrier phenotypes in detail. A significant reduction of TEER was observed in the model group (Figure 1G). As shown in Figure 1H, a higher lactulose/mannitol (L/M) ratio in the model group was indicative of increased permeability and impairment of absorption. Similarly, the plasma content of D-lactate was significantly increased in the model group (Figure 1I).

Immunofluorescence staining showed that the duodenal expressions of E-cadherin and β-catenin were significantly decreased in the model group (Figures 2A-D). As shown in Figures 2E-H, the relative protein expressions of desmocollin 2 (DSC2), tight junction protein 1 (ZO-1) and occludin (OCLN) were markedly reduced in the model group. Moreover, significant decreases in the relative mRNA expressions of *Dsc2*, *Cln3*, *Tjp1* and *Ocln* were observed in the model group (Figures 2I-L). Concomitantly, indexes of spleen and thymus were decreased in the model group, indicating the compromise of immune function (Figures 2M, N).

Duodenal microbiome regulated the biosynthesis of lipopolysaccharide and peptidoglycan in the rat model of FD

As for now, no available data on the characteristics of duodenal microbiome of FD. For reference, we performed a pooled analysis including two studies on the fecal microbiome of FD following the same modelling approach. After removing the batch effect, reanalysis of external datasets (BioProject ID: PRJNA575916, PRJNA719295) was conducted using the QIIME pipeline, which was the same for the subsequent analysis. The groups did not differ significantly in both alpha- and beta-diversity from each other. Nevertheless, function prediction of faecal microbiome suggests that the lipopolysaccharide biosynthesis was markedly elevated in the model group (Supplemental Figure 1).

With focus on the duodenal microbial environment, we analysed the microbial composition and further predicted the metabolic enzymes of microbiome in our own experimental data. Similar to the previous results, no significant differences were found between the groups for both alpha- and beta-diversity (Figure 3A; Supplemental Figure 2). Differentially microbial species (the relative abundance of OTUs) were determined using DESeq2. Among these, *Pasteurellaceae*, *Lachnospiraceae*, *Muribaculaceae* identified to the family level and *Akkermansia* identified to the genus level were enriched in the control group, while *Bacillaceae*, *Prevotellaceae*, *Erysipelotrichaceae* identified to the family level, *Bacillus*, *Methylobacterium*, *Turicibacter*, *Dubosiella*, *Fusicatenibacter* identified to the genus level and *Idiomarina_marina*, *Bacillus_firmus* identified to the species level were enriched in

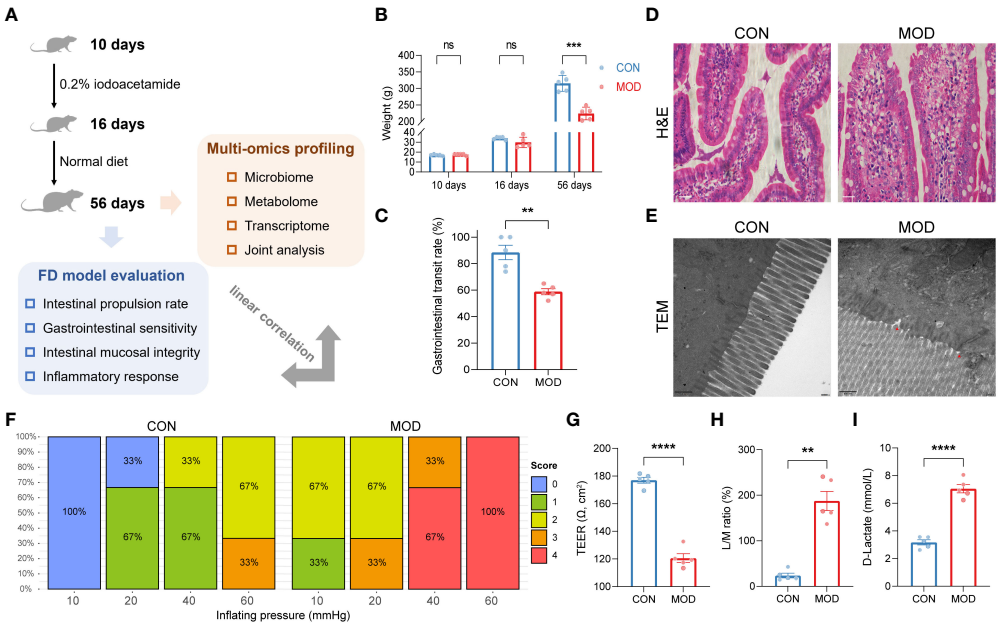

FIGURE 1
Phenotypes found in the rat model of FD. **(A)** A schematic diagram of the multi-omics analysis. **(B)** Changes in body weights (*** $p < 0.001$ by two-way ANOVA with correction of two-stage linear step-up procedure of Benjamini, Krieger and Yekutieli, ns indicates not significant). **(C)** Gastrointestinal transit rate. **(D)** H&E-stained duodenum. Scale bar, 20 μm. **(E)** TEM analysis of duodenum. Scale bar, 500 nm. Two red triangles indicate incomplete tight junctions. **(F)** Behavioral testing of GD (10 to 60 mmHg) and pain score (0-4). **(G)** TEER of duodenal epithelial barrier (**** $p < 0.0001$ by unpaired t test with Welch's correction). **(H)** Urine L/M ratio (** $p < 0.01$ by Mann Whitney test). **(I)** Plasma content of D-lactate (**** $p < 0.0001$ by unpaired t test with Welch's correction). The circles on the bar plots represent individual values with mean ± SEM (bars) (n = 3 or 5 rats/group).

the model group (Figure 3B). The detailed information of differential microbiome was summarized in Supplemental Table 1. Based on the PICRUSt2 analysis, we selected potential metabolic enzymes involved in the biosynthesis of lipopolysaccharide and peptidoglycan of duodenal microbiome (Supplemental Figure 3; Supplemental Table 2). Most of enzymes were elevated in the model group, although only a few of them reached statistical significance (Figure 3C). Spearman correlation coefficients between every two variables were calculated and were presented in Figure 3C; details were summarized in Supplemental Table 3.

The upregulated innate immune response-related transcript profiles of the duodenum were associated with the proinflammatory toll-like receptor signaling pathway

Given the potential DAMPs, we further explored the innate immune specific transcriptional signature of the duodenal mucosa. A total of 64 differentially expressed genes were upregulated in the control group while 835 further genes were significantly upregulated in the model group (Figure 4A). Based on these results, differentially expressed genes were filtered for innate immune responses using the InnateDB database. In total, 101 genes were significantly upregulated and only one was downregulated in the model group (Figure 4B). Details were presented in Supplemental Table 4. These protein-coding genes were matched with the STRING database for further interaction and enrichment analysis. PPI network was established and illustrated in Figure 4C. Then, subnetwork was established using MCL clustering (Figure 4D). Functional enrichment analysis indicated that the duodenal innate immune responses to lipopolysaccharide and peptidoglycan, which highlighted the importance of Toll-like receptor signaling and NK-κB-mediated proinflammatory effects.

TLR2/TLR4-NFκB signaling and proinflammatory cytokines were elevated in the duodenum

Immunohistochemical stain highlighted the increased $CD3^+$ T lymphocyte, mast cell and eosinophil populations in the duodenum of the model group (Figures 5A-D). Western Blot analysis demonstrated significant elevations in the relative protein expressions of Toll-like receptor 4 (TLR4) and

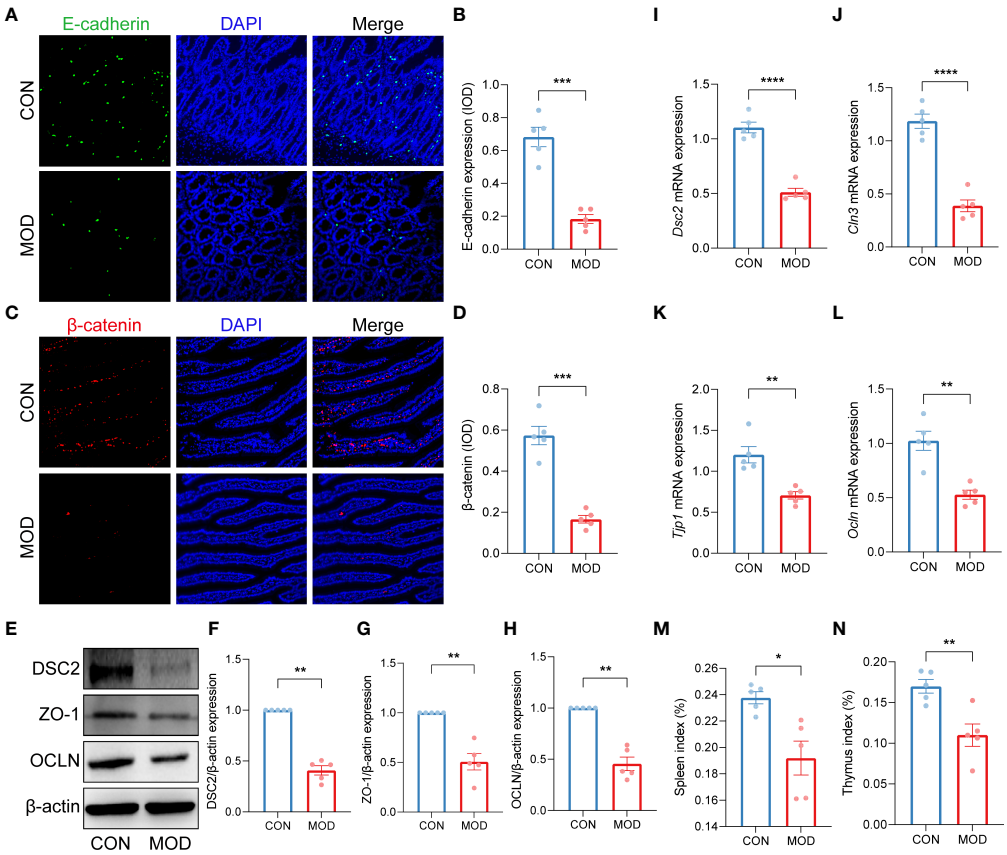

FIGURE 2
Impaired duodenal mucosal barrier was accompanied with decreased immune organs index. **(A-D)** Duodenal immunofluorescence staining **(A, C)** and the relative expression (IOD) of E-cadherin **(B)** and β-catenin **(D)** (*** $p < 0.001$ by unpaired t test with Welch's correction). **(E-H)** The WB bands **(E)** and scaled normalized protein expressions of DSC2 **(F)**, ZO-1 **(G)** and OCLN **(H)** (** $p < 0.01$ by Mann Whitney test). **(I-L)** The relative mRNA expression of *Dsc2* **(I)**, *Cln3* **(J)**, *Tjp1* **(K)** and *Ocln* **(L)** (** $p < 0.01$, **** $p < 0.0001$ by unpaired t test with Welch's correction). **(M, N)** Indexes of spleen **(M)** and thymus **(N)** (* $p < 0.05$, ** $p < 0.01$ by unpaired t test with Welch's correction). The circles on the bar plots represent individual values with mean ± SEM (bars) ($n = 5$ rats/group).

inhibitor of NFκB kinase subunits alpha and beta (IKKα+IKKβ) in the model group, but only NF-κB p65 subunit was significantly increased (Figures 5E-H). In addition, the relative mRNA expressions of *Tlr2*, *Tlr4* and *Rela* were markedly increased in the model group (Figures 5I-K). Subsequently, the levels of proinflammatory cytokines IL-1β, IL-6 and TNF-α were significant elevated in the model group (Figures 5L-N).

The rat model of FD demonstrated a distinct metabolic pattern in the duodenum

In order to explore the factors that might mediate duodenal low-grade inflammation in the rat model of FD, we next performed untargeted metabolomics analysis of these duodenal tissues. Data were acquired in both positive and negative ion modes, respectively. In the positive ion mode, representative chromatograms of the control and model group were shown (Supplemental Figures 4A, B). After preprocessing the raw data, all samples with QC were analyzed using PCA (Supplemental Figure 4C). The OPLS-DA model was then established (Supplemental Figure 4D). Hotelling's T^2, Residuals Normal Probability and Permutation tests were used to evaluate the model (Supplemental Figures 4E-G). The VIP scores and correlation coefficients were acquired based on the OPLS-DA model (Supplemental Figure 4H). The same analysis for the negative ion mode was shown in Supplemental Figure 5. With additional thresholds, a total of 36 differential metabolites were enriched in the control group and 18 differential metabolites were enriched in the model group (Figure 6). The detailed information of metabolites was summarized in Supplemental Table 5.

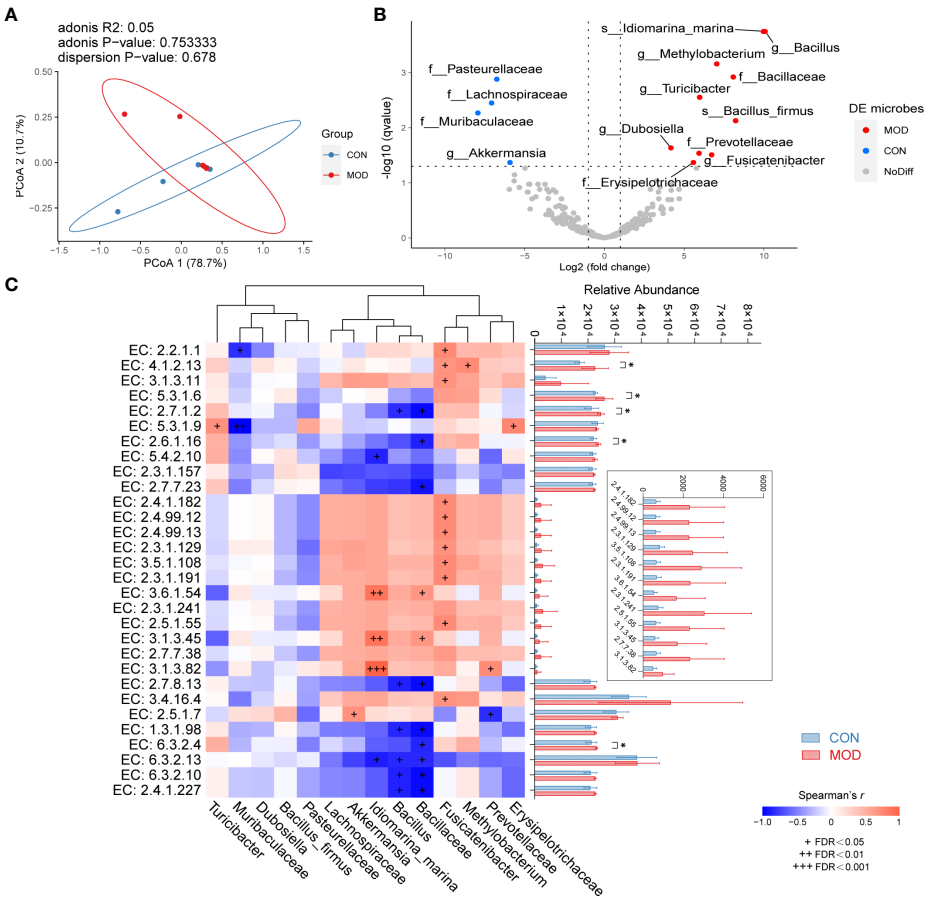

FIGURE 3
Microbial features of duodenum. **(A)** Weighted UniFrac PCoA with an adonis test. **(B)** Differential microbiome with DESeq2 analysis. The left dots (blue) indicate the microbiome enriched in control group; the right dots (red) are representative of the microbiome enriched in model group. **(C)** Spearman correlations of differential microbiome and predicted functional enzymes (Spearman's $r > 0.6$ with + FDR < 0.05, ++ FDR < 0.01 or +++ FDR < 0.001 represent significant). The right side indicates multiple comparison of relative abundance of enzymes with Fisher's LSD (mean ± SEM, * $p < 0.05$ represent significant) ($n = 5$ rats/group).

Arachidonyl ethanolamide and endocannabinoid analogues showed linear relationships with phenotypes found in FD

To integrate multi-level omics data, we conducted the mantel test when differential duodenal metabolites were used as environmental factors. As illustrated in Figure 7, AEA was the best explanatory variable for all the three profiles (the innate immune response-related genes: Mantel's r = 0.503, p = 0.018; the microbial 16S OTUs: Mantel's r = 0.310, p = 0.046; the DAMPs-related ECs: Mantel's r = 0.468, p = 0.017). Details for calculation were summarized in Supplemental Table 6.

Next, linear regression models were performed to present linear relationships between the relative abundance of AEA and phenotypes found in the rat model of FD. In gastrointestinal motor function, AEA was negatively linear correlated with the gastrointestinal transit rate (Figure 8A). With regards to permeability and absorption, AEA was positively linear correlated with L/M ratio and the content of D-lactate, and was negatively linear correlated with TEER (Figures 8B-D). In terms of duodenal mucosal barrier, AEA was negatively linear corelated with the relative protein expressions of E-cadherin and β-catenin and the relative mRNA expressions of DSC2, OCLN and CLN3 (Figures 8E-I). Additionally, AEA was positively linear correlated with the relative amounts of mast cells, the relative mRNA expressions of TLR2, TLR4 and NFκB, and the levels of proinflammatory cytokines IL-1β, IL-6 and TNF-α (Figures 8J-P). Aside from AEA, several endocannabinoid analogues, such as myristoyl ethanolamide (MEA), oleoyl ethanolamide (OEA), palmitoleoyl ethanolamide (PEA) and stearoyl ethanolamide (SEA), were also used to established linear regression models (Supplemental Figures 6-9). Instead, OEA, PEA and SEA were opposite to AEA described above.

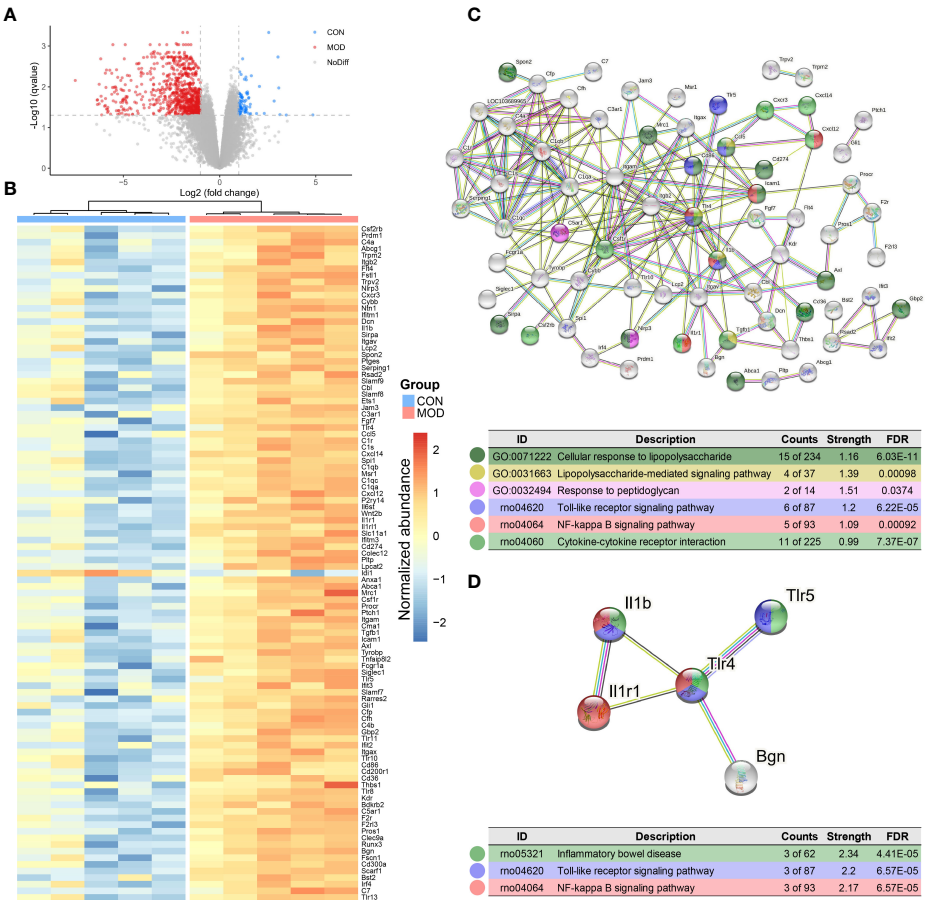

FIGURE 4
Transcriptome analysis of duodenum. **(A)** Differential expressed genes with DESeq2 analysis. Dotted line: BH FDR < 0.05 and |log2(FC)| > 1 represent significant (the control group: high expression in blue; the model group: high expression in red). **(B)** Selected differential genes based on InnateDB database. **(C)** PPI network based on innate immune response-related protein-coding genes (interaction score > 0.7 and hiding disconnected nodes). **(D)** The subnetwork clustering with MCL algorithm. Color-coded dots were clustered with GO and KEGG pathway enrichment analysis (n = 5 rats/group).

Discussion

Short-term gavage of iodoacetamide was firstly reported in 2008 by Liu and co-workers as the most classical modeling approach (9). Afterward, pharmacological and nonpharmacological therapies, including drug molecules, natural products and electroacupuncture, were extensively studied (10–12). The heterogeneity of FD has been demonstrated with different pathophysiological mechanisms under varied symptom conditions (13). Single-setting studies lack representativeness and comprehensiveness to understand the disease itself. Current review highlights the importance of the application of multi-omics methods such as the metabolomics data and the integration of these multiple layers in relation to phenotypes found in complex diseases (14). Unfortunately, no previous studies have compared and assessed the intertwined characteristics using a multi-omics approach.

A recent study with a large sample size reported FD and other gastrointestinal disorders shares several commonalities in a wide spectrum of pathophysiology, which increases the difficulty of treatment against a specific disease (15). Compared to a global exploration, it is more important to profile the comprehensive features locally. One study has demonstrated that TEER and the expression of ZO-1 are significantly decreased in patients with abdominal symptoms of FD. And the level of IL-1β elevated in the patients is negatively correlated with both of above measures (16). Another clinical study using confocal laser endomicroscopy visually confirmed that the impairment of duodenal mucosal barrier was an important pathogenesis factor in FD (4). Similar to these results, we also found that TEER was significantly decreased and the same trend as the relative mRNA expressions of tight junction proteins in the rat model of FD. Moreover, an elevated trend of the levels of proinflammatory

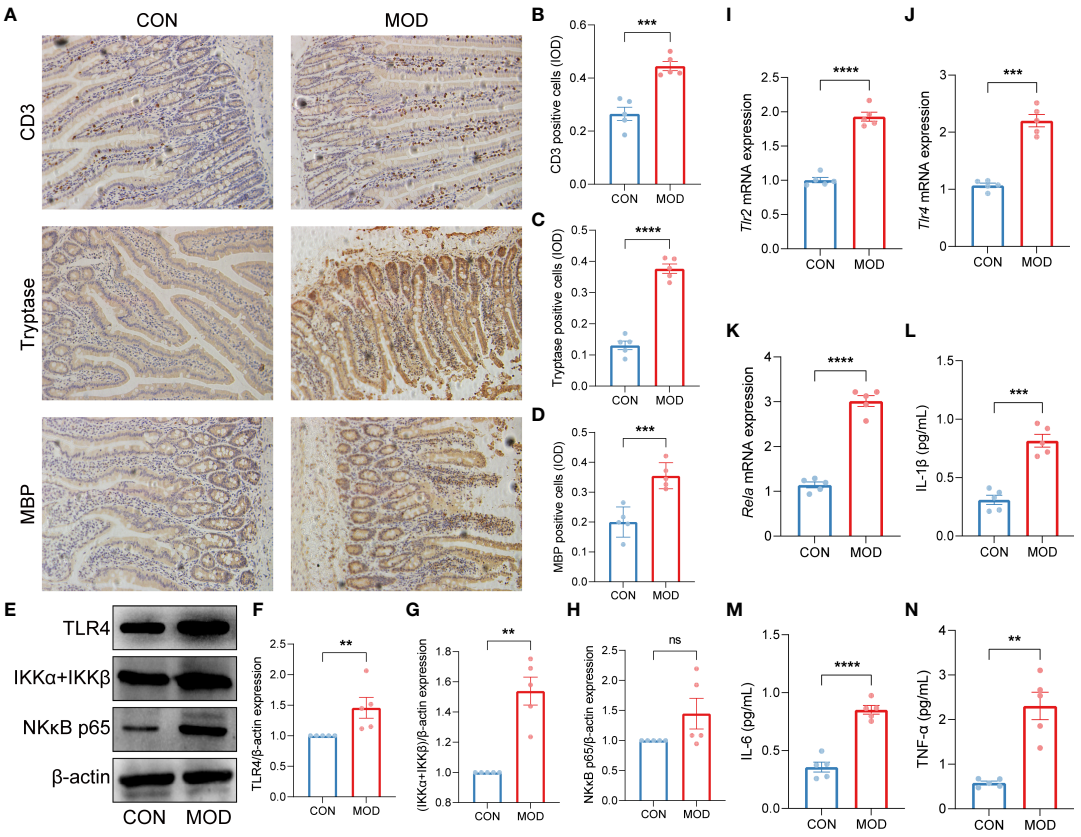

FIGURE 5
Validation of innate immune cells-mediated TLR2/TLR4-NFκB signaling pathway. **(A-D)** Duodenal immunohistochemical staining **(A)** and the relative expression (IOD) of CD3-labeled T lymphocytes **(B)**, tryptase-labeled mast cells **(C)** and MBP-labeled eosinophils **(D)** (*** $p < 0.001$, **** $p < 0.0001$ by unpaired t test with Welch's correction). **(E-H)** The WB bands **(E)** and scaled normalized protein expressions of TLR4 **(F)**, IKKα + IKKβ **(G)** and NK-κB p65 **(H)** (** $p < 0.01$ by Mann Whitney test, ns indicates not significant). **(I-K)** The relative mRNA expressions of *Tlr2* **(I)**, *Tlr4* **(J)** and *Rela* **(K)** (*** $p < 0.001$, **** $p < 0.0001$ by unpaired t test with Welch's correction). **(L-N)** The plasma contents of proinflammatory cytokines IL-1β **(L)**, IL-6 **(M)** and TNF-α **(N)** (IL-1β and IL-6: *** $p < 0.001$, **** $p < 0.0001$ by unpaired t test with Welch's correction; TNF-α: ** $p < 0.01$ by Mann Whitney test) ($n = 5$ rats/group).

cytokines IL-1β, IL-6 and TNF-α in the clinical samples were in line with our *in vivo* study data. The activation of T lymphocyte and eosinophilia with increased peripheral proinflammatory cytokines IL-1β, IL-6 and TNF-α are identified as the main features of FD (17). The duodenal hyperplasia of mast cells and eosinophils have been reported as the pathophysiological phenomena overlapping irritable bowel syndrome and FD as demonstrated in a cross-sectional study (18). As an administration of corticotropin-release hormone, the mast cell-eosinophil signalling increases small intestinal permeability (19). In addition, mast cells and eosinophilia in activation statue have been observed to cluster around intestinal submucosal plexus neurons, which alter the neuronal responsiveness of intestine and delayed gastric emptying (20, 21).

In terms of the initial triggers involved in the pathophysiological process, one view emphasizes the eating-related symptoms and the dietetic management of FD (22). The duodenal microbes support the digestive functions of small intestine with the actions of fermentation and non-host functional enzymes, which prevent inappropriate activation of immune responses towards foods (23). Beneficial immune and microbial regulation and the treatment of FD with specific probiotics have also been demonstrated to be effective and safe (24). The colonized microbes serve as a signalling hub that incorporate environmental exposure and signals, regulating the host's metabolism and innate immune system (25). On the other hand, host innate immunity regulates the microbial distribution along the gastrointestinal tract. Importantly, the microbiome located in duodenal mucosa indicate a greater sensitivity to the innate immune responses compared to other intestinal sites (26). The duodenal microenvironment has emerged as an important player in the pathophysiological mechanisms of FD, in which both locally microbial community disorder, host and microbial metabolism and host innate immunity are involved (27). These

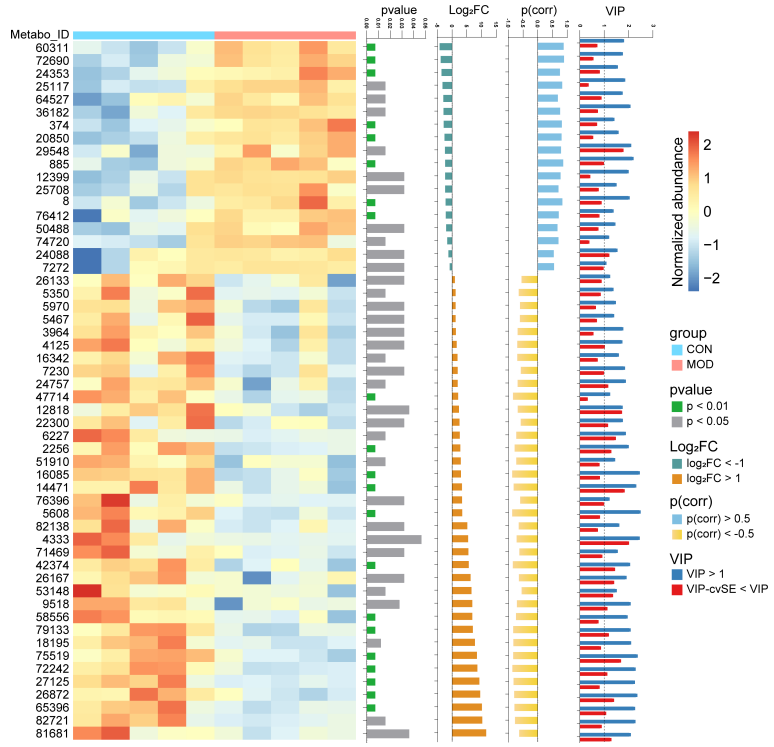

FIGURE 6
Metabolome analysis of duodenum. Differential metabolites were identified with thresholds of $p < 0.05$, |log2(FC)| > 1, |p(corr)| > 0.5 and VIP > 1 with cvSE of VIP less than the VIP value (n = 5 rats/group). The compound names corresponding to the Metabo_ID from top to bottom are as follows. 60311: Glycolithocholic acid; 72690: Taurolithocholate; 24353: Decanoyl-L-carnitine; 25117: Sphingosine; 64527: Glycodeoxycholic acid; 36182: Arachidonyl Ethanolamide; 374: Tyramine; 20850: C17 Sphingosine; 29548: Taurocholic acid; 885: Benzyl sulfate; 12399: Myristoyl Ethanolamide; 25708: Sphinganine; 8: 3-Hydroxybutyric acid; 76412: Taurodeoxycholate; 50488: Palmitoylcarnitine; 74720: Tricaprylin; 24088: Phytosphingosine; 7272: N,N-Dimethyltetradecylamine; 26133: 7-Sulfocholic acid; 5350: FA 18:2+O; 5970: Eicosapentaenoic acid; 5467: 9-HODE; 3964: gamma-Linolenic acid; 4125: Linoleic acid; 16342: Cholic acid; 7230: FA 18:2+2O; 24757: LPE(18:2/0:0); 47714: 7-Ketolithocholic acid; 12818: Lithocholic acid; 22300: Andrastin C; 6227: Arachidonic acid; 2256: Biotin; 51910: 6,7-Diketolithocholic acid; 16085: 3-Oxocholic acid; 14471: Murocholic acid; 76396: Taurochenodeoxycholate; 5608: FA 18:1+1O; 82138: LPC(18:1/0:0); 4333: Oleic acid; 71469: LPE(18:1/0:0); 42374: 3-Ketocholanic Acid; 26167: Oleoyl Ethanolamide; 53148: Hyocholic acid; 9518: N,N-Dimethyltetradecylamine-N-oxide; 58556: Stearoyl-L-Carnitine; 79133: LPC(17:0/0:0); 18195: Palmitoleoyl Ethanolamide; 75519: LPC(16:0/0:0); 72242: LPC(15:0/0:0); 27125: Docosahexaenoic acid; 26872: Stearoyl Ethanolamide; 65396: LPE(16:0/0:0); 82721: LPC(18:0/0:0); 81681: LPC(18:2/0:0).

imbalances may in part be mediated by specific microbiome-associated metabolites (28). A recent study showed that the metabolic functional prediction of oral and gastric microbiome based on 16S rRNA sequencing data. Among these, purine metabolism, biosynthesis of lipopolysaccharide and amino acid related enzymes were enriched in saliva microbiome, while peptidases and associated processing at the gastric level. However, metabolic function of duodenal microbiome has not been reported (29).

Previous clinical data showed that increased fasting plasma AEA has a significant negative correlation with the duodenal expression of ZO-1. There was a similar, although non-significant, trend in the relationship between AEA and the relative mRNA expression of TLR4 and the content of TNF-α, while an opposite trended association between AEA and ZO-1 (30). Another clinical study using positron emission tomography have demonstrated the higher availability of endocannabinoid 1 (CB1) receptor in the different cerebral regions of patients with FD, indicating that the dysfunction of endocannabinoid system is involved in the disease process (31). Additionally, enteroendocrine cells in duodenum also contain the main mRNA transcripts that encode endocannabinoids and biosynthesis-associated fatty acids (32). In healthy populations, pre-treatment with the CB1 receptor antagonist inhibited the gastric accommodation reflex but not compliance, distension and nutrient tolerance (33). The application of endocannabinoid receptor antagonist *in vitro* significantly decreased TEER and the relative mRNA expressions of ZO-1 and OCLN (34). Animal study has also proved that addition of endocannabinoid receptor antagonist elevates the intestinal permeability (35). Some notions have been substantiated that AEA can be synthesized from mast cells (36) and lymphocytes (37). Furthermore, CB1

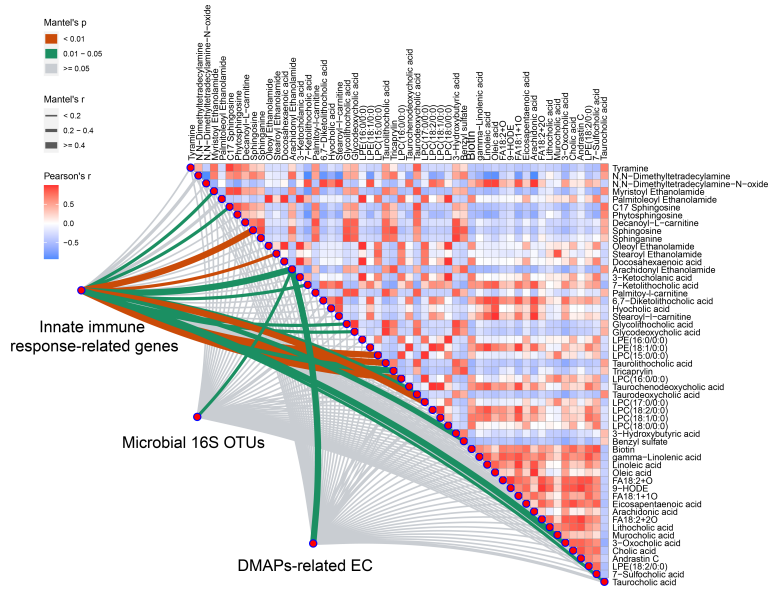

FIGURE 7
Variations of microbiome with DAMPs-related enzymes and duodenal metabolites have significant relationship with innate immune response-related genes expression. Integrated analysis of multi-omics data was performed using Mantel test. AEA was selected from all the three profiles (Mantel's $p < 0.05$ represent significant) ($n = 5$ rats/group).

receptor is expressed on the surface of mast cells (38), while both CB1 and CB2 receptors on eosinophils (39, 40) and T lymphocytes (41, 42). As the gate opener assisting actions of DAMPs, AEA exerts negative effects on the intestinal barrier, presenting the gut microbiota-endocannabinoid system axis in relation to the host metabolism (5). In contrast, several endocannabinoid analogues have been recognised as the key gate keepers. With the region-specific actions, intestinal OEA plays a major role in gut physiological processes in the host (43). As the natural agonist of peroxisome proliferator-activated receptor-α (PPARα) with a high affinity, OEA effectively relieves peripheral inflammatory conditions (44). Similarly, the PEA of leukocytes actives PPARα at the early stage of LPS-induced inflammation in a PPARα-dependent manner (45, 46). The reduced levels of OEA, PEA and SEA also disturbed lipid and fatty acid metabolism, resulting in proinflammatory responses (47). Taken together, the specific alternation of intestinal immunity has associations with endocannabinoid system, microbial community and host metabolism (48). Nevertheless, research study on the intertwined correlation among the above three layers has not been reported.

Our study has some shortcomings. Due to technical limitations, clarified protein-coding genes of duodenal microbiome could not be confirmed. Verification studies on host endocannabinoid system are needed, which are currently on-going. Further studies at the cellular level, and clinical data are also needed to suggest how the endocannabinoid system regulates the cause-effect relationship between microbial metabolic function and host innate immune response.

In conclusion, this study provides multi-omics evidence to suggest that duodenal microbiome regulate the biosynthesis of lipopolysaccharide and peptidoglycan; and the host endocannabinoid system acts as the potential regulator of duodenal DAMPs-mediated low-grade inflammation in the rat model of FD.

Methods

Animal model

The rat model of FD was developed as described previously (9). In brief, acclimatization lasted one week after the quarantine period of 3 days. In the model group, the oral gavage with 200μl of 0.1% iodoacetamide solution (dissolved in 2% sucrose aqueous solution) was administered once daily for 6 days, while the control group was given normal 2% sucrose aqueous solution at the same time. All the rats were fed on a standard chow up to 8 weeks of age. The duodenal tissues of additional two rats from each group were examined using transmission electron microscopy. Another three rats from each group were used for the assessment of behavioural response to gastric distention due to any potential confounders related to proinflammatory responses.

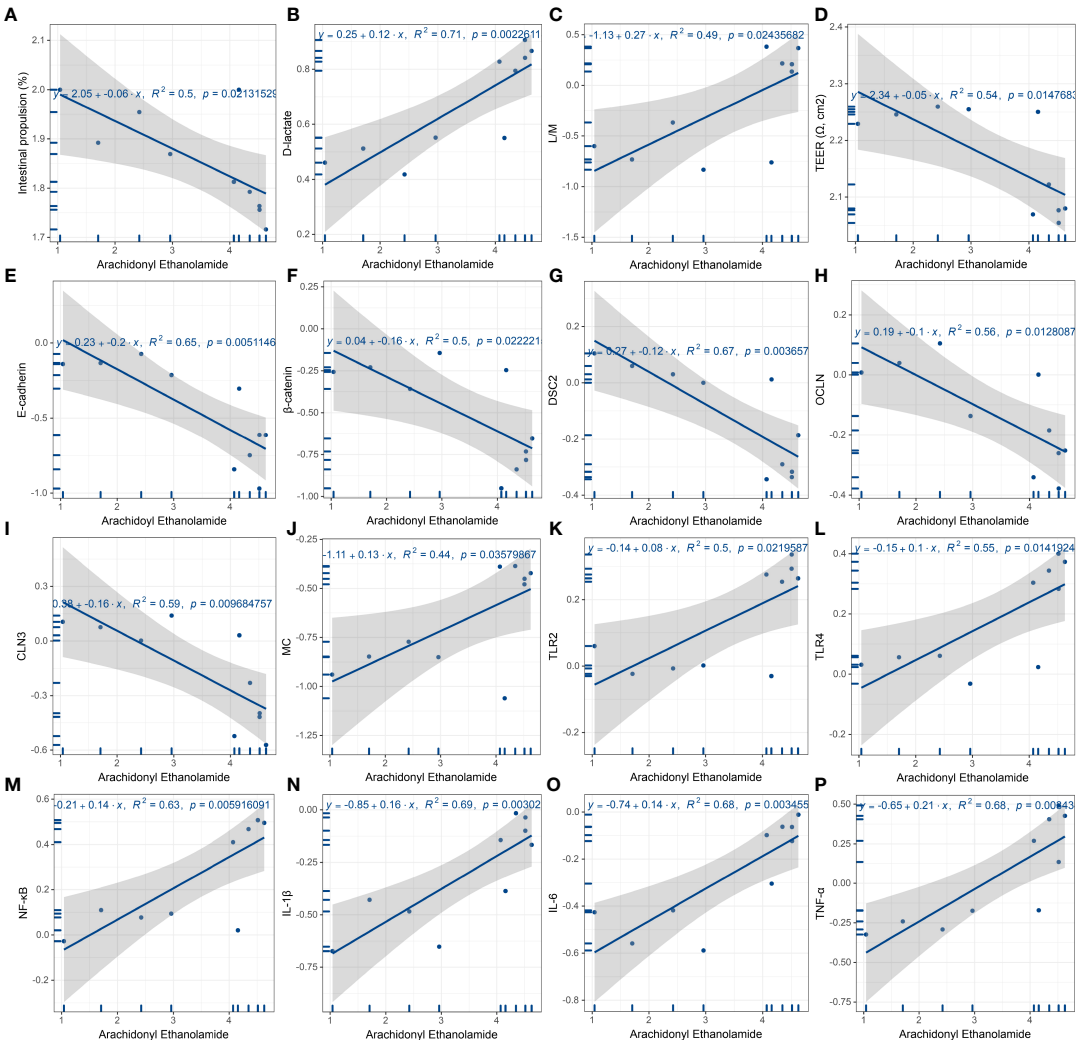

FIGURE 8
Linear regression analysis of AEA and features of FD. **(A)** Gastrointestinal motor function. AEA was negatively linear correlated with the gastrointestinal transit rate. **(B-D)** Duodenal permeability and absorption. AEA was positively linear correlated with L/M ratio **(B)** and the content of D-lactate **(C)**, while negatively linear correlated with TEER **(D)**. **(E-I)** Duodenal mucosal barrier. AEA was negatively linear corelated with the relative protein expressions of E-cadherin **(E)** and β-catenin **(F)** and the relative mRNA expressions of *Dsc2* **(G)**, *Ocln* **(H)** and *Cln3* **(I)**. **(J-P)** Innate immune cells and proinflammatory signaling. AEA was positively linear correlated with the relative amounts of mast cells **(J)**, the relative mRNA expressions of *Tlr2* **(K)**, *Tlr4* **(L)** and *Rela* **(M)**, and the contents of proinflammatory cytokines IL-1β **(N)**, IL-6 **(O)** and TNF-α **(P)** (All data are log10 transformed. $p < 0.05$ represent significant) ($n = 5$ rats/group).

Behavioral response to gastric balloon distention

The balloon fabrication procedure, implantation surgery and behavioral response to GD were performed according to previous study (9). After 24-hour fasting, 8-week-old rats of model group were anaesthetized with 10% chloral hydrate intraperitoneally. Balloons with surface sterilization should not obstruct the pylorus. Behavioral testing of GD was performed on day 6 after surgery. The rats of model group were allowed an hour to acclimate to the individual plastic environment. The inflating pressure was slowly increased to 20, 40, 60, 80 mmHg for 20 seconds with 5 minutes rest, respectively. The behavioral response to GD was graded into 0–4 rating scale as described previously.

Gastrointestinal transit

The calculation of gastrointestinal transit referenced the previous study (49). Briefly, all the rats were gavaged with a charcoal marker (mixtures of 20% charcoal and 5% gum arabic,

1mL/100g body weight) into the stomach after 24-hour fasting. Following the formula, the gastrointestinal transit rate (%) = migration distance of charcoal marker/whole length of the small intestine × 100%. Each measurement was repeated three times and the mean value was taken.

Trans-endothelial electrical resistance

A Ussing chamber was used to measure the TEER as described previously (50) with some modifications. Fresh duodenum tissues (1cm long × 0.5cm wide) were cleaned and rapidly put into Krebs-Ringer buffer with constant carbogenation (O_2/CO_2, 95/5%) at 37°C. The parameters were set as stable voltage of 5mV and polar constant-current pulses of 16 mA every 60 s with a 200 ms duration. Measurements were recorded every 30 min within 2 h.

Quantitation of lactulose and mannitol

Duodenal permeability was assessed by L/M ratio using high performance liquid chromatography (HPLC) Agilent 1260 (Agilent Technologies, Santa Clara, CA, USA) with a Waters C18 column (Waters, Milford, USA), referring to previous literature (51) with adjustment according to our laboratory experience.

Immune organ index

The innate immune-related organs (thymus and spleen) were collected and freshly weighed. Excess liquid was blotted off using filter paper to reduce computational error. The immune organ index was calculated by the following formula: organ index (%) = organ weight/body weight × 100%.

Quantitation of D-lactate and cytokines

Plasma D-lactate and proinflammatory cytokines were quantized using enzyme-linked immunosorbent assays (ELISA). EnzyChrom™ D-Lactate Assay Kit was purchased from BioAssay Systems (Hayward, CA). Rat IL-1 beta ELISA Kit (ab255730), IL-6 ELISA Kit (ab234570) and TNF alpha ELISA Kit (ab236712) were purchased from Abcam (Shanghai, China). Establishment of standard curves and specific experimental steps followed the instructions of above ELISA kits. The optical density (OD) values of D-Lactate and cytokines (IL-1β, IL-6 and TNF-α) were respectively read at 565 and 450 nm.

Immunohistochemical and immunofluorescence staining

IHC. A portion of the duodenum tissue was processed for paraffin embedding. Immunohistochemical staining for CD3 (52), mast cell tryptase (53) and eosinophil MBP (54) were performed as described previously. Anti-CD3 (ab5690) and anti-mast cell tryptase (ab2378) antibodies were purchased from Abcam (Shanghai, China). Anti-eosinophil major basic protein antibody (MBP) [BMK-13] (ARG22591) was purchased from arigo Biolaboratories (Shanghai, China).

IF. Immunofluorescent labeling of duodenal sections with antibodies against β-Catenin (55) and E-cadherin (56) was performed as previous studies. β-Catenin (D10A8) XP® Rabbit mAb (#8480), E-Cadherin (4A2) Mouse mAb (#14472), anti-mouse IgG (H+L), F(ab')2 Fragment (Alexa Fluor® 488 Conjugate) (#4408), anti-rabbit IgG (H+L), F(ab')2 Fragment (Alexa Fluor® 555 Conjugate) (#4413) were purchased from Cell Signaling Technologies (Shanghai, China).

For each specimen, three random visual fields as well as three duplications were observed. The integrated optical density (IOD) was calculated using Image-Pro Plus 6.0 software.

Transmission electron microscopy analysis

For intuitively observing tight junctions between epithelial cells, additional fresh duodenum tissues (chopped in $1mm^3$ pieces) of each group were fixed with pre-cooled 2.5% glutaraldehyde. Standard procedures of TEM and image processing referred to previous study (57).

16S rRNA sequencing

After 24-hour fasting, duodenum tissues with contents were aseptically retrieved. Considering microbiome located in the crypt-villus structure, duodenum tissues and contents were mixed with the homogenate. The sodium dodecyl sulfate (SDS) with grinding-based method was used to extract genomic DNA. After purifying with GeneJET Gel Extraction Kit (Thermofisher), PCR product was collected to generate libraries of the V4 region (PCR primers: 515F/806R (58)) using Ion Plus Fragment Library Kit 48 rxns (Thermofisher). Sequencing was performed on the Ion S5™XL platform (Thermofisher). Raw SE400 reads were filtered with Cutadapt (V1.9.1, http://cutadapt.readthedocs.io/en/stable/). Chimeras were identified and removed with vsearch (V1.7.0, https://github.com/torognes/vsearch). Clean reads obtained as described above were clustered using Uparse (Uparse

v7.0.1001, http://drive5.com/uparse/) to obtain operational taxonomic units (OTUs) with a threshold of 97% similarity. Species annotation was performed on the representative sequences of OTUs using Mothur (https://mothur.org/), on which SSUrRNA database of SILVA (Release 132) (http://www.arb-silva.de/) was used with a threshold of 0.8~1). Multiple sequence alignment was conducted to investigate phylogenetic relationship by MUSCLE (v3.8.31, http://www.drive5.com/muscle/). Alpha and beta diversity metrics were analyzed using QIIME (V1.9.1) pipeline. Functional enzymes and KEGG pathways prediction was analyzed using PICRUSt2 (https://github.com/picrust/picrust2). The publicly available datasets can be download through NCBI SRA database (BioProject ID: PRJNA575916, PRJNA719295). In-house raw data are also available for download (BioProject ID: PRJNA835600).

Transcriptome sequencing

Total RNA was extracted with Trizol (Invitrogen). The magnetic beads with Oligo (dT) were used to enrich mRNA. Concentration and purity were determined based on 260/280nm UV absorbance ratios and the integrity was then measured by Agilent 2100 bioanalyzer. The transcriptome libraries were obtained using NEBNext® Ultra™ RNA Library Prep Kit for Illumina® (NEB). Sequencing was performed on the Hiseq 4000 (Illumina) platform. After filtering, clean reads were aligned to the reference genome using HISAT2 (https://daehwankimlab.github.io/hisat2/). Transcripts were then assembled with StringTie (http://ccb.jhu.edu/software/stringtie/). The resulting read counts were converted to FPKM value. The genes in relation to innate immunity were selected based on the InnateDB database (https://www.innatedb.ca/). The PPI network was established with STRING (http://string-db.org) with a minimum required interaction score > 0.7. A subnetwork was then clustered with a MCL algorithm. In-house raw data are available for download through NCBI SRA database (BioProject ID: PRJNA835595).

Untargeted metabolome

Sample preprocessing steps and TOF MS paraments were the same as our previous described (59). The UPLC gradient was programmed with some modifications. Raw data was converted to abf using abfconvert. Based on MS-DIAL (V4.24) software, peak detection, deconvolution, samples alignment, compounds identification and computation of missing values were performed using an in-house method.

Western blot

A BCA assay was used to measure the concentration of total protein extracted from homogenized duodenum tissues. Western blot was performed following standard procedures. Briefly, 20μl denatured protein each well was loaded onto SDS-PAGE. After electrophoresis, the proteins were electroblotted to a PVDF membrane. Incubations of the primary and secondary antibodies were performed overnight at 4°C and for one hour at room temperature, respectively. Anti-Tight Junction Protein 1 (ZO-1) antibody (NBP1-85047) was purchased from Novus (Shanghai, China). Anti-Occludin (OCLN) (ab167161), anti-Claudin 3 (CLN3) (ab15102), anti-Desmocollin 2 (DSC2) (ab230039), anti-Toll-like receptor 4 (TLR4) (ab217274), anti-IKK alpha + IKK beta (ab178870), anti-NK-κB p65 (ab16502) and anti-beta Actin (ab8227) antibodies were purchased from Abcam (Shanghai, China). After washing with TBST three times for 10 min, ECL detection, exposure and development were performed. Protein band intensity was measured and quantified by Image Lab software.

Quantitative PCR

Purified mRNA described above was reverse transcribed to first-strand cDNA using an Evo M-MLV One Step RT-qPCR Kit (Accurate Biotechnology). Templates were collected following the condition of 37°C for 15 min and 85°C for 5 s. A SYBR® Green Premix Pro Taq HS qPCR Kit (Accurate Biotechnology) was used to amplification following the condition of one cycle for 30 s at 95°C and 40 cycles for 5 s at 95°C, 30 s at 60°C. PCR product was quantified using comparative ΔCt method (relative quantification, RQ). Primers information was summarized in Supplemental Table 7.

Statistics

Welch-corrected t test and Mann-Whitney test were conducted using GraphPad Prism (9.2.0). In beta diversity, adonis statistics were performed based on QIIME pipeline. With thresholds of BH FDR < 0.05 and $|\log2(FC)| > 1$, differential expressed microbiome and genes were identified by DESeq2 (https://git.bioconductor.org/packages/DESeq2). For metabolomics data, multivariate analysis was performed using MetaboAnalyst (v5.0) and SIMCA (V14.1). Compounds with multiple thresholds of $p < 0.05$, $|\log2(FC)| > 1$, $|p(corr)| > 0.5$ and VIP > 1 with cross-validation standard error (cvSE) of VIP less than the VIP value were selected as differential metabolites. Mantel test was performed to established connections with multi-omics data with Pearson correlation coefficient. The

Spearman correlation coefficient was used to analyze the correlations between microbiome and functional enzymes with a threshold of $p < 0.05$.

Study approval

All animal experiments were followed the standards of the Guide for the Care and Use of Laboratory Animals (National Research Council. 2011. Guide for the care and use of laboratory animals, 8th ed. National Academies Press, Washington, DC) and were approved by the Institutional Animal Care and Use Committee of Guangdong Provincial Hospital of Chinese Medicine (Ethics Approval Number: 2017007-2).

Data availability statement

The datasets presented in this study can be found in online repositories. The names of the repository/repositories and accession number(s) can be found in the article/Supplementary Material.

Ethics statement

The animal study was reviewed and approved by the Institutional Animal Care and Use Committee of Guangdong Provincial Hospital of Chinese Medicine.

Author contributions

Acquiring and analyzing data were contributed by SJ and YY. Conducting experiments was contributed by BP, TZ, YK, LD and LC. Designing research was contributed by YY, SH, YW and YL. Funding acquisition was contributed by YL and JD. Investigation was contributed by YW, SL, SH and YW. Providing reagents was contributed by SL, SH and YW. Supervision was contributed by XS, JD, SH and YL. Writing the manuscript was contributed by SJ and BP. All authors reviewed and edited the manuscript.

Funding

This work was supported by the Key Project of National Natural Science Foundation of China (81830117), the National Natural Science Foundation of China (81873205 and 81904037), the Natural Science Foundation of Guangdong Province, China (2019A1515010400, 2021A1515110990), the Science and Technical Plan of Guangzhou, Guangdong, China (201903010069), and the Innovation Team and Talents Cultivation Program of the National Administration of Traditional Chinese Medicine (ZYYCXTD-C-202001).

Acknowledgments

We also thank Professor Hiu Yee Kwan for the language revision.

Conflict of interest

The authors declare that the research was conducted in the absence of any commercial or financial relationships that could be construed as a potential conflict of interest.

Publisher's note

Supplementary material

The Supplementary Material for this article can be found online at: https://www.frontiersin.org/articles/10.3389/fimmu.2022.944591/full#supplementary-material

References

1. Ford AC, Mahadeva S, Carbone MF, Lacy BE, Talley NJ. Functional dyspepsia. *Lancet* (2020) 396(10263):1689–702. doi: 10.1016/S0140-6736(20)30469-4

2. Black CJ, Drossman DA, Talley NJ, Ruddy J, Ford AC. Functional gastrointestinal disorders: advances in understanding and management. *Lancet* (2020) 396(10263):1664–74. doi: 10.1016/S0140-6736(20)32115-2

3. Cordner ZA, Li Q, Liu L, Tamashiro KL, Bhargava A, Moran TH, et al. Vagal gut-brain signaling mediates amygdaloid plasticity, affect, and pain in a functional dyspepsia model. *JCI Insight* (2021) 6(6):e144046. doi: 10.1172/jci.insight.144046

4. Nojkov B, Zhou S-Y, Dolan RD, Davis EM, Appelman HD, Guo X, et al. Evidence of duodenal epithelial barrier impairment and increased pyroptosis in patients with functional dyspepsia on confocal laser endomicroscopy and "Ex vivo" mucosa analysis. *Am J Gastroenterol* (2020) 115(11):1891–901. doi: 10.14309/ajg.0000000000000827

5. Cani PD, Plovier H, Van Hul M, Geurts L, Delzenne NM, Druart C, et al. Endocannabinoids–at the crossroads between the gut microbiota and host metabolism. *Nat Rev Endocrinol* (2016) 12(3):133–43. doi: 10.1038/nrendo.2015.211

6. Di Marzo V, Ligresti A, Cristino L. The endocannabinoid system as a link between homoeostatic and hedonic pathways involved in energy balance regulation. *Int J Obes (Lond).* (2009) 33 Suppl 2:S18–24. doi: 10.1038/ijo.2009.67

7. Di Marzo V, Capasso R, Matias I, Aviello G, Petrosino S, Borrelli F, et al. The role of endocannabinoids in the regulation of gastric emptying: alterations in mice fed a high-fat diet. *Br J Pharmacol* (2008) 153(6):1272–80. doi: 10.1038/sj.bjp.0707682

8. Izzo AA, Piscitelli F, Capasso R, Aviello G, Romano B, Borrelli F, et al. Peripheral endocannabinoid dysregulation in obesity: relation to intestinal motility and energy processing induced by food deprivation and re-feeding. *Br J Pharmacol* (2009) 158(2):451–61. doi: 10.1111/j.1476-5381.2009.00183.x

9. Liu L-S, Winston JH, Shenoy MM, Song G-Q, Chen JDZ, Pasricha PJ. A rat model of chronic gastric sensorimotor dysfunction resulting from transient neonatal gastric irritation. *Gastroenterology* (2008) 134(7):2070–9. doi: 10.1053/j.gastro.2008.02.093

10. Liu LS, Shenoy M, Pasricha PJ. The analgesic effects of the GABAB receptor agonist, baclofen, in a rodent model of functional dyspepsia. *Neurogastroenterol Motil.* (2011) 23(4):356–61.e160-1. doi: 10.1111/j.1365-2982.2010.01649.x

11. Zhao J, Zhao L, Zhang S, Zhu C. Modified liu-Jun-Zi decoction alleviates visceral hypersensitivity in functional dyspepsia by regulating EC cell-5HT3r signaling in duodenum. *J Ethnopharmacol* (2020) 250:112468. doi: 10.1016/j.jep.2019.112468

12. Ouyang X, Li S, Zhou J, Chen JD. Electroacupuncture ameliorates gastric hypersensitivity *via* adrenergic pathway in a rat model of functional dyspepsia. *Neuromodulation* (2020) 23(8):1137–43. doi: 10.1111/ner.13154

13. Vanheel H, Farré R. Changes in gastrointestinal tract function and structure in functional dyspepsia. *Nat Rev Gastroenterol Hepatol* (2013) 10(3):142–9. doi: 10.1038/nrgastro.2012.255

14. Wörheide MA, Krumsiek J, Kastenmüller G, Arnold M. Multi-omics integration in biomedical research - a metabolomics-centric review. *Anal Chim Acta* (2021) 1141:144–62. doi: 10.1016/j.aca.2020.10.038

15. Garcia-Etxebarria K, Carbone F, Teder-Laving M, Pandit A, Holvoet L, Thijs V, et al. A survey of functional dyspepsia in 361,360 individuals: Phenotypic and genetic cross-disease analyses. *Neurogastroenterol Motil.* (2021) 34(6):e14236. doi: 10.1111/nmo.14236

16. Komori K, Ihara E, Minoda Y, Ogino H, Sasaki T, Fujiwara M, et al. The altered mucosal barrier function in the duodenum plays a role in the pathogenesis of functional dyspepsia. *Dig Dis Sci* (2019) 64(11):3228–39. doi: 10.1007/s10620-019-5470-8

17. Burns G, Carroll G, Mathe A, Horvat J, Foster P, Walker MM, et al. Evidence for local and systemic immune activation in functional dyspepsia and the irritable bowel syndrome: A systematic review. *Am J Gastroenterol* (2019) 114(3):429–36. doi: 10.1038/s41395-018-0377-0

18. Walker MM, Talley NJ, Prabhakar M, Pennaneach'h CJ, Aro P, Ronkainen J, et al. Duodenal mastocytosis, eosinophilia and intraepithelial lymphocytosis as possible disease markers in the irritable bowel syndrome and functional dyspepsia. *Aliment Pharmacol Ther* (2009) 29(7):765–73. doi: 10.1111/j.1365-2036.2009.03937.x

19. Wallon C, Yang PC, Keita AV, Ericson AC, McKay DM, Sherman PM, et al. Corticotropin-releasing hormone (CRH) regulates macromolecular permeability *via* mast cells in normal human colonic biopsies in vitro. *Gut* (2008) 57(1):50–8. doi: 0.1136/gut.2006.117549

20. Cirillo C, Bessissow T, Desmet A-S, Vanheel H, Tack J, Vanden Berghe P. Evidence for neuronal and structural changes in submucous ganglia of patients with functional dyspepsia. *Am J Gastroenterol* (2015) 110(8):1205–15. doi: 10.1038/ajg.2015.158

21. Liebregts T, Adam B, Bredack C, Gururatsakul M, Pilkington KR, Brierley SM, et al. Small bowel homing T cells are associated with symptoms and delayed gastric emptying in functional dyspepsia. *Am J Gastroenterol* (2011) 106(6):1089–98. doi: 10.1038/ajg.2010.512

22. Duncanson K, Burns G, Pryor J, Keely S, Talley NJ. Mechanisms of food-induced symptom induction and dietary management in functional dyspepsia. *Nutrients* (2021) 13(4):1109. doi: 10.3390/nu13041109

23. Oliphant K, Allen-Vercoe E. Macronutrient metabolism by the human gut microbiome: major fermentation by-products and their impact on host health. *Microbiome* (2019) 7(1):91. doi: 10.1186/s40168-019-0704-8

24. Wauters L, Slaets H, De Paepe K, Ceulemans M, Wetzels S, Geboers K, et al. Efficacy and safety of spore-forming probiotics in the treatment of functional dyspepsia: a pilot randomised, double-blind, placebo-controlled trial. *Lancet Gastroenterol Hepatol* (2021) 6(10):784–92. doi: 10.1016/S2468-1253(21)00226-0

25. Thaiss CA, Zmora N, Levy M, Elinav E. The microbiome and innate immunity. *Nature* (2016) 535(7610):65–74. doi: 10.1038/nature18847

26. Gu M, Samuelson DR, de la Rua NM, Charles TP, Taylor CM, Luo M, et al. Host innate and adaptive immunity shapes the gut microbiota biogeography. *Microbiol Immunol* (2022) 66(6):330–41. doi: 10.1111/1348-0421.12963.

27. Wauters L, Talley NJ, Walker MM, Tack J, Vanuytsel T. Novel concepts in the pathophysiology and treatment of functional dyspepsia. *Gut* (2020) 69(3):591–600. doi: 10.1136/gutjnl-2019-318536

28. Burns GL, Hoedt EC, Walker MM, Talley NJ, Keely S. Physiological mechanisms of unexplained (functional) gastrointestinal disorders. *J Physiol* (2021) 599(23):5141–61. doi: 10.1113/JP281620

29. Cervantes J, Michael M, Hong B-Y, Springer A, Guo H, Mendoza B, et al. Investigation of oral, gastric, and duodenal microbiota in patients with upper gastrointestinal symptoms. *J Investig Med* (2020) jim-2020-001642. doi: 10.1136/jim-2020-001642.

30. Little TJ, Cvijanovic N, DiPatrizio NV, Argueta DA, Rayner CK, Feinle-Bisset C, et al. Plasma endocannabinoid levels in lean, overweight, and obese humans: relationships to intestinal permeability markers, inflammation, and incretin secretion. *Am J Physiol Endocrinol Metab* (2018) 315(4):E489–95. doi: 10.1152/ajpendo.00355.2017

31. Ly HG, Ceccarini J, Weltens N, Bormans G, Van Laere K, Tack J, et al. Increased cerebral cannabinoid-1 receptor availability is a stable feature of functional dyspepsia: a [F]MK-9470 PET study. *Psychother Psychosom.* (2015) 84(3):149–58. doi: 10.1159/000375454

32. Sykaras AG, Demenis C, Case RM, McLaughlin JT, Smith CP. Duodenal enteroendocrine I-cells contain mRNA transcripts encoding key endocannabinoid and fatty acid receptors. *PloS One* (2012) 7(8):e42373. doi: 10.1371/journal.pone.0042373

33. Ameloot K, Janssen P, Scarpellini E, Vos R, Boesmans W, Depoortere I, et al. Endocannabinoid control of gastric sensorimotor function in man. *Aliment Pharmacol Ther* (2010) 31(10):1123–31. doi: 10.1111/j.1365-2036.2010.04259.x

34. Muccioli GG, Naslain D, Bäckhed F, Reigstad CS, Lambert DM, Delzenne NM, et al. The endocannabinoid system links gut microbiota to adipogenesis. *Mol Syst Biol* (2010) 6:392. doi: 10.1038/msb.2010.46

35. Matias I, Gonthier M-P, Orlando P, Martiadis V, De Petrocellis L, Cervino C, et al. Regulation, function, and dysregulation of endocannabinoids in models of adipose and beta-pancreatic cells and in obesity and hyperglycemia. *J Clin Endocrinol Metab* (2006) 91(8):3171–80. doi: 10.1210/jc.2005-2679

36. Bisogno T, Maurelli S, Melck D, De Petrocellis L, Di Marzo V. Biosynthesis, uptake, and degradation of anandamide and palmitoylethanolamide in leukocytes. *J Biol Chem* (1997) 272(6):3315–23. doi: 10.1074/jbc.272.6.3315

37. Maccarrone M, De Petrocellis L, Bari M, Fezza F, Salvati S, Di Marzo V, et al. Lipopolysaccharide downregulates fatty acid amide hydrolase expression and increases anandamide levels in human peripheral lymphocytes. *Arch Biochem Biophys* (2001) 393(2):321–8. doi: 10.1006/abbi.2001.2500

38. Sugawara K, Zákány N, Hundt T, Emelianov V, Tsuruta D, Schäfer C, et al. Cannabinoid receptor 1 controls human mucosal-type mast cell degranulation and maturation in situ. *J Allergy Clin Immunol* (2013) 132(1):182–93. doi: 10.1016/j.jaci.2013.01.002

39. Small-Howard AL, Shimoda LMN, Adra CN, Turner H. Anti-inflammatory potential of CB1-mediated cAMP elevation in mast cells. *Biochem J* (2005) 388(Pt 2):465–73. doi: 10.1042/BJ20041682

40. Chouinard F, Lefebvre JS, Navarro P, Bouchard L, Ferland C, Lalancette-Hébert M, et al. The endocannabinoid 2-arachidonoyl-glycerol activates human neutrophils: critical role of its hydrolysis and *de novo* leukotriene B4 biosynthesis. *J Immunol* (2011) 186(5):3188–96. doi: 10.4049/jimmunol.1002853

41. Castaneda JT, Harui A, Kiertscher SM, Roth JD, Roth MD. Differential expression of intracellular and extracellular CB(2) cannabinoid receptor protein by human peripheral blood leukocytes. *J Neuroimmune Pharmacol* (2013) 8(1):323–32. doi: 10.1007/s11481-012-9430-8

42. Sánchez López AJ, Román-Vega L, Ramil Tojeiro E, Giuffrida A, García-Merino A. Regulation of cannabinoid receptor gene expression and endocannabinoid levels in lymphocyte subsets by interferon-β: a longitudinal study in multiple sclerosis patients. *Clin Exp Immunol* (2015) 179(1):119–27. doi: 10.1111/cei.12443

43. Izzo AA, Sharkey KA. Cannabinoids and the gut: new developments and emerging concepts. *Pharmacol Ther* (2010) 126(1):21–38. doi: 10.1016/j.pharmthera.2009.12.005

44. Lo Verme J, Fu J, Astarita G, La Rana G, Russo R, Calignano A, et al. The nuclear receptor peroxisome proliferator-activated receptor-alpha mediates the anti-inflammatory actions of palmitoylethanolamide. *Mol Pharmacol* (2005) 67(1):15–9. doi: 10.1124/mol.104.006353

45. Solorzano C, Zhu C, Battista N, Astarita G, Lodola A, Rivara S, et al. Selective n-acylethanolamine-hydrolyzing acid amidase inhibition reveals a key role for endogenous palmitoylethanolamide in inflammation. *Proc Natl Acad Sci USA* (2009) 106(49):20966–71. doi: 10.1073/pnas.0907417106

46. Zhu C, Solorzano C, Sahar S, Realini N, Fung E, Sassone-Corsi P, et al. Proinflammatory stimuli control n-acylphosphatidylethanolamine-specific phospholipase d expression in macrophages. *Mol Pharmacol* (2011) 79(4):786–92. doi: 10.1124/mol.110.070201

47. Geurts L, Everard A, Van Hul M, Essaghir A, Duparc T, Matamoros S, et al. Adipose tissue NAPE-PLD controls fat mass development by altering the browning process and gut microbiota. *Nat Commun* (2015) 6:6495. doi: 10.1038/ncomms7495

48. Everard A, Geurts L, Caesar R, Van Hul M, Matamoros S, Duparc T, et al. Intestinal epithelial MyD88 is a sensor switching host metabolism towards obesity according to nutritional status. *Nat Commun* (2014) 5:5648. doi: 10.1038/ncomms6648

49. Bashashati M, Storr MA, Nikas SP, Wood JT, Godlewski G, Liu J, et al. Inhibiting fatty acid amide hydrolase normalizes endotoxin-induced enhanced gastrointestinal motility in mice. *Br J Pharmacol* (2012) 165(5):1556–71. doi: 10.1111/j.1476-5381.2011.01644.x

50. Vanheel H, Vicario M, Vanuytsel T, Van Oudenhove L, Martinez C, Keita ÅV, et al. Impaired duodenal mucosal integrity and low-grade inflammation in functional dyspepsia. *Gut* (2014) 63(2):262–71. doi: 10.1136/gutjnl-2012-303857

51. Hansen LBS, Roager HM, Søndertoft NB, Gøbel RJ, Kristensen M, Vallès-Colomer M, et al. A low-gluten diet induces changes in the intestinal microbiome of healthy Danish adults. *Nat Commun* (2018) 9(1):4630. doi: 10.1038/s41467-018-07019-x

52. Yousef MM, Yantiss RK, Baker SP, Banner BF. Duodenal intraepithelial lymphocytes in inflammatory disorders of the esophagus and stomach. *Clin Gastroenterol Hepatol* (2006) 4(5):631–4. doi: 10.1016/j.cgh.2005.12.028

53. Hahn HP, Hornick JL. Immunoreactivity for CD25 in gastrointestinal mucosal mast cells is specific for systemic mastocytosis. *Am J Surg Pathol* (2007) 31(11):1669–76. doi: 10.1097/PAS.0b013e318078ce7a

54. Zuberi RI, Ge XN, Jiang S, Bahaie NS, Kang BN, Hosseinkhani RM, et al. Deficiency of endothelial heparan sulfates attenuates allergic airway inflammation. *J Immunol* (2009) 183(6):3971–9. doi: 10.4049/jimmunol.0901604

55. Perreault N, Katz JP, Sackett SD, Kaestner KH. Foxl1 controls the wnt/beta-catenin pathway by modulating the expression of proteoglycans in the gut. *J Biol Chem* (2001) 276(46):43328–33. doi: 10.1074/jbc.M104366200

56. Berkhout M, Gosens MJEM, Brouwer KM, Peters WHM, Nagengast FM, van Krieken JHJM, et al. Loss of extracellular e-cadherin in the normal mucosa of duodenum and colon of patients with familial adenomatous polyposis. *Hum Pathol* (2006) 37(11):1389–99. doi: 10.1016/j.humpath.2006.05.018

57. Zhang L, Wei X, Zhang R, Si D, Petitte JN, Ahmad B, et al. A novel peptide ameliorates LPS-induced intestinal inflammation and mucosal barrier damage *via* its antioxidant and antiendotoxin effects. *Int J Mol Sci* (2019) 20(16):3974. doi: 10.3390/ijms20163974

58. Caporaso JG, Lauber CL, Walters WA, Berg-Lyons D, Lozupone CA, Turnbaugh PJ, et al. Global patterns of 16S rRNA diversity at a depth of millions of sequences per sample. *Proc Natl Acad Sci USA* (2011) 108 Suppl 1:4516–22. doi: 10.1073/pnas.1000080107

59. Ji S, Han S, Yu L, Du L, You Y, Chen J, et al. Jia wei xiao yao San ameliorates chronic stress-induced depression-like behaviors in mice by regulating the gut microbiome and brain metabolome in relation to purine metabolism. *Phytomedicine* (2022) 98:153940. doi: 10.1016/j.phymed.2022.153940

frontiers | Frontiers in Immunology

TYPE Original Research
PUBLISHED 31 August 2022
DOI 10.3389/fimmu.2022.900963

OPEN ACCESS

EDITED BY
Zhi-Bin Zhao,
Guangdong Provincial People's Hospital, China

REVIEWED BY
Qingjun Pan,
Affiliated Hospital of Guangdong Medical University, China
Pankaj Sharma,
Boston Children's Hospital and Harvard Medical School, United States
Pan Su,
Houston Methodist Research Institute, United States

*CORRESPONDENCE
Guobao Wang
nfyywanggb@163.com

†These authors have contributed equally to this work and share first authorship

SPECIALTY SECTION
This article was submitted to Molecular Innate Immunity, a section of the journal Frontiers in Immunology

RECEIVED 21 March 2022
ACCEPTED 08 August 2022
PUBLISHED 31 August 2022

CITATION
Zhang W, Yuan Y, Li X, Luo J, Zhou Z, Yu L and Wang G (2022) Orange-derived and dexamethasone-encapsulated extracellular vesicles reduced proteinuria and alleviated pathological lesions in IgA nephropathy by targeting intestinal lymphocytes.
Front. Immunol. 13:900963.
doi: 10.3389/fimmu.2022.900963

Orange-derived and dexamethasone-encapsulated extracellular vesicles reduced proteinuria and alleviated pathological lesions in IgA nephropathy by targeting intestinal lymphocytes

Wang Zhang[1†], Ye Yuan[1†], Xiang Li[1], Jiao Luo[1], Zhanmei Zhou[1], Lei Yu[2] and Guobao Wang[1*]

[1]Renal Division, Nanfang Hospital, Southern Medical University, National Clinical Research Center for Kidney Disease, State Key Laboratory of Organ Failure Research, Guangzhou, China, [2]Department of Anatomy, School of Basic Medical Sciences, Southern Medical University, Guangzhou, China

Current evidence highlights the critical role of the gut-kidney axis in the pathogenesis of IgA nephropathy (IgAN). However, few attempts have been made to explore targeted intestinal immunity therapy. This research aims to develop an oral intestine targeting medication based on extracellular vesicles (EVs) and investigate its therapeutic efficacy in IgAN. EVs were isolated from orange juice and electroporated with dexamethasone sodium phosphate (DexP). After oral administration, EVs-DexP was picked up by lymphocytes in the submucosal area of ileocecum. EVs-DexP outperformed DexP not only in suppressing lymphocyte stimulation *in vitro* but also in alleviating renal pathological lesions in the IgAN mouse model. Clinical improvement was accompanied by a reducing IgA secreted by the intestine and a decreasing IgA + B220 + lymphocytes in Peyer's patches. The present study develops a cost-effective, biofriendly EVs-based glucocorticoid strategy for IgAN.

KEYWORDS

IgA nephropathy (IgAN), intestine immunity, extracellular vesicle (EV), immunosuppressive therapy, Peyer's patches

Introduction

IgA nephropathy (IgAN) is the most common primary glomerulonephritis worldwide, especially in Asia, with heterogeneous clinical and pathological phenotypes. It is estimated that 20–40% of IgAN patients develop ESRD within 20 years from the time of diagnosis (1). The recent IgAN landmark trials of STOP-IgAN (2)and TESTING (3) raised deep concern about the issue of corticosteroids/immunosuppressive therapy-related infection, despite potential benefits of preventing renal progression (4).

The gut-kidney axis in IgA nephropathy has been comprehensively reviewed by Coppo (5), who concluded that genetic background, B cell activity, IgA synthesis, gut-associated lymphoid tissue intestinal immunity(GALT), and diet may all have a role in the development and progression of IgA nephropathy. Peyer's patches (PPs), the inductive sites producing immunocompetent primed B cells, are supposed to be a key element in IgA production. Nevertheless, limited attempts have been performed to explore intestinal immunity targeted therapy in IgAN.

The past decade has witnessed dramatic progress in nanotechnology combined with modern medicine. Extracellular vesicles (EVs), characterized by nanoscale sizes ranging from 30 to 200 nm and a (phospho) lipid bilayer structure, have recently gained much interest as promising candidates for drug delivery. They are nanoparticles derived from a variety of cells and found in almost all biological fluids (6), mediating physiological and pathological processes. However, heterogeneous origination and composition, inconsistent stability in circulation and metabolism, and low quantities yield by mammalian cells (7) challenged their role as drug carriers in clinical application. Plant-derived nanoparticles emerged as feasible natural drug carriers considering a stable physicochemical property, biosafety, and large-scale production (8).

Herein, we set out to isolate EVs from oranges and evaluate the capacity of this plant-derived nanoparticle as an oral drug delivery vehicle. Our findings that EVs were taken up by ileocecal lymphocytes after oral administration further inspired us to load dexamethasone sodium phosphate (DexP), one of the highly potent glucocorticoids, into EVs and investigate its immunosuppressive effect *in vitro* and therapeutic efficacy in the IgAN mouse model. Our findings would provide a novel bio-friendly approach to treat IgAN *via* regulating intestinal immunity.

Materials and methods

EVs isolation

Orange juice was squeezed and filtered by gravity through a Whatman filter paper. Collect the filtrate 125mL and dilute the sample using protease inhibitor and PBS to a final volume of 250mL. The protease inhibitor cocktail, a mix of 1.67mL 1M sodium azide, 2.5mL of 100mM PMSF, and 0.5mL of 1mM leupeptin stock solutions, was immediately added as recommended by Christopher, etc. (9) Then low-velocity centrifugation was performed at room temperature: centrifuge at 4,000 × g for 20 min to remove cells and large debris, then at 8,000 × g for 20 min, followed by 15,000 × g for 20 min to remove cellular debris. Filter the supernatant by 0.45μm syringe filter. The next step was high-velocity ultracentrifugation at 4°C: centrifuge the supernatant in polycarbonate ultracentrifuge tube at 170,000 × g for 90 min to pellet the crude extracellular vesicles fraction. Carefully discard the supernatant and resuspend the pellet in a small volume of PBS. Then vortex it rigorously for at least 10 min to break all aggregation and obtain a suspension of primary nanovesicles.

Quantification

Particle number was measured by nanoparticle tracking analysis (NTA) using ZetaView Particle Metrix. EVs were lyophilized and weighed up, and total proteins were measured using BCA assay.

Particle size and surface charge

Collected samples were diluted to avoid inter-particle interaction. Size distribution and zeta potential were assessed by Zetasizer Nano ZS (Malvern Instruments, UK).

Transmission electron microscopy

EVs pellets were resuspended in PBS and spotted onto a carbon-coated copper grid. The excess liquid was removed, and filter paper was used to drain the grid; a drop was negatively stained with 3% phosphotungstic acid and loaded onto the grid for 5 minutes. The grid was then dried at room temperature. Finally, the samples were observed under a HITACHI H-7650 transmission electron microscope operated at 80kV.

Lipidomic analysis

EVs samples in chloroform/methanol/water (1/1/1, v/v/v) solution were vortexed for 30 mins and centrifuged at 1,500 × g for 10 mins. Organic phage was collected and transferred to a new tube and lyophilized using nitrogen. Dried metabolites were reconstituted in 400μl isopropanol/methanol (1/1, v/v) solution, vortexed, centrifuged at 23,500 × g for 10 min at 4°C, and the supernatant was analyzed using liquid chromatograph-mass spectrometry (LC-MS) (Thermo, Ultimate 3000LC, Orbitrap Elite). A Kinetex C18 column (100 × 2.1mm, 1.9μm) and the

following gradient: 0-2 min 30% mobile phase B; 2-2.1min 55% B; 2.1-12 min 65% B;12-18 min 85% B; 18-25 min100% B; 25-30 min 30% B, was applied for the experiment. Mobile phase A was acetonitrile/water (3:2, v/v), 10mM ammonium formate and 0.1% formic acid. Mobile phase B was acetonitrile/isopropanol (1:9, v/v), 10mM ammonium formate and 0.1% formic acid. The flow rate was 0.3 ml/min, and the column was at 45°C. The MS data files were processed using Thermo package software Lipid Search for producing a list of lipid names and peak areas.

Drug encapsulation

A mixture of EVs and dexamethasone sodium phosphate (DexP) in different proportions were gently blended in 0.5ml of electroporation buffer (125mM NaCl, 5mM KCl, 1.5mM CaCl2, 10mM glucose, 20mM HEPES, pH 7.4) at 4°C. After electroporation at 300 V for 15ms in 0.2cm electroporation cuvettes by a Gene Pulser II Electroporator (Bio-Rad, USA), the mixture was incubated at 37°C for 30 min to ensure the plasma membrane of the EVs fully recovered. Residual DexP and electroporation buffer were removed by Milli-Q water using a regenerated cellulose dialysis membrane (Spectra/Por 4 Dialysis Membranes, Carl Roth) with 6-8kDa molecular weight cut-off (MWCO). Change the Milli-Q water every 4 hours, and the duration of dialysis is 24 hours. The retained EVs were incubated with 1% Triton-X 100 (SigmaAldrich, Schnelldorf, Germany)9 for 4 hours on ice for lysing. Then the lysate was subjected to intermittent sonication for 10 minutes to ensure the (phospho) lipid bilayer of EVs was fully ruptured. The amount of encapsulated DexP was measured by detecting the absorbance at 242nm using UV-spectrophotometry. Entrapment Efficiency (%EE) = (total amount of DexP added - unencapsulated DexP “)/total amount of DexP added] *100%.

Toxicity

For cytotoxicity assays, cells (3×10^5/well) were cultivated on 96-well plates, then added with the indicated concentration of drugs in 10% FBS RPMI 1640 containing 5 ug/ml ConA and 3U/ml IL-2. Cell proliferation was detected after 24-hour incubation with cell counting kit-8 (DOJINDO Laboratories, CK04) at 450 nm. *In vivo*, wild-type female BALB/c mice (5- or 6-week-old) were treated daily with EVs (80 mg/kg b. wt.) for two weeks. Serum levels of alanine aminotransferase (ALT) creatinine (Cr) and urea nitrogen (BUN) were analyzed by the AU480 Chemistry System (Beckman Coulter System).

Stability

The stability of EVs was examined in acidic solution (0.01M hydrochloric acid, PH=2), alkaline solution (0.1M sodium bicarbonate, PH=8), and artificial gastric and intestinal fluid respectively. The artificial gastric fluid solution was prepared according to Polish Pharmacopoeia IX by the dissolution of 2.0g NaCl and 3.2g pepsin in quadruple-distilled water. Then, 80 mL of 1M hydrochloric acid was added to adjust the pH, then supplemented with quadruple-distilled water to 1000mL. Artificial intestinal juice was prepared by dissolving 6.8g of potassium dihydrogen phosphate into 500mL of distilled water, using 0.1 M NaHCO3 solution to adjust the PH to 6.8. Then 10g of pancreatin was mixed, and distilled water was supplemented to 1000mL.

In vivo distribution of EVs

Orange-derived EVs were labeled with near-infrared fluorescent dye Dil (20 μM) by incubation at 37°C for 30 min, followed by centrifugation at 10,000×g for 30 min to remove unbound dye. Mice that had been fasted for 24 hours were gastrically given 200ul Dil-labeled EVs (80 mg/kg EVs protein) and were euthanized at 0h, 2h, 4h, and 6h following gavage. Imaging *ex vivo* was performed on the stomach, gut, spleen, liver, kidney, and bladder. Fluorescence intensities were assessed using Carestream MS FX Pro *In Vivo* Imaging System with customized wavelength filters for excised organs. The relative intensities were measured and compared with an equal amount of unlabeled EVs treated control.

Isolation of Peyer’s patches lymphocytes

Intestinal Peyer’s patch lymphocytes were collected as described previously (10). Briefly, euthanize the mouse and aseptically remove the small intestine from the duodenum to the cecum. PPs are excised from the intestines and gently forced through a steel mesh grid. Gravity sediment the resulting cell suspension through 4°C CMF/HEPES for 10 minutes, discard the debris pellet and collect the supernatant. Pellet cells by centrifuging 20 min at 850 × g, in a swinging-bucket rotor, 4°C. Resuspend pellet and subject to Percoll fractionation. Lymphocytes will be recovered from a distinct band formed at the interface of the 100% and 40% Percoll.

Flow cytometric characterization of Peyer’s patch lymphocytes

Murine PPs lymphocytes were isolated and cultured for 24h in 12-well plates with a cell count of $0.5\text{-}1\times10^7$ in 3ml cell suspension per well. For viability assay, lymphocytes were stimulated with 0.5ug/ml ConA and 3U/ml IL-2 in each well for 24h. The inhibitory effect of EVs (0.5ug/well), DexP (0.1ug/ml), and EVs-DexP (0.6ug EVs electroporated with 0.3ug DexP) were then

determined. The following antibodies were used for FACS analysis: Fixable Viability Stain 780(BD Horizon™, 565388); PE Hamster Anti-Mouse CD3(BD Pharmingen™, 553063); FITC Rat Anti-Mouse CD4 (BD Pharmingen™, 553729); APC Hamster Anti-Mouse CD69(BD Pharmingen™, 560689); FITC Rat Anti-Mouse IgA (Invitrogen, 11-4204-82); PE Rat Anti-Mouse CD45R/B220(BD Pharmingen™, 553089). Cells were analyzed using a FACScan (Becton Dickinson, San Jose, California, USA).

The IgAN mouse model and treatments

Male Balb/c mice, 6- or 8-week-old (weight 25 ± 5g), were obtained from the Laboratory Animal Center (Southern Medical University, China). The routine urine test was checked after one week of pre-feeding. Balb/c mice were fed standard food and had free access to distilled water. On the 13th week, all Balb/c mice were killed.

Twenty-four mice were randomized into four groups:

Control group (n =6): mice were given oral acidified water on alternative days until death. After 6 weeks and on the 9th week, they were injected *via* tail veins with saline with the same quantity and time as the model group.

IgAN model group (n =6): mice were orally given 0.1% bovine serum albumin (BSA) (Sigma Chemical Co., St. Louis, MO, USA) with acidified water (6 mM HCl), 0.4mL for each, on alternate days. After 6 weeks, each mouse was injected *via* tail veins with 0.1 ml 1% BSA buffer solution at a fixed time, once a day, for 3 days. From the 9th week on, the mice were injected with staphylococcal enterotoxin B (SEB) (the Academy of Military Medical Sciences, Beijing, China), diluted by sterile saline with 0.4 mg/kg, once a week, for 3 weeks.

DexP treatment group (n =6): from the 6th week on, each IgAN mouse was intragastrical given DexP 1.6mg/kg every other day until the end of the 12th week.

EVs-DexP treatment group (n =6): from the 6th week on, each IgAN mouse was intragastrical given EVs-DexP (100ug EVs and 40ug DexP were electroporated) every other day until the end of the 12th week.

Spot-urine sample was collected, and urinary albumin/creatinine ratio (ACR) was evaluated before and after treatment using a QuantiChrom™ Protein Creatinine Ratio Assay Kit (DPCR-100, Bioassay Systems, Hayward, CA, USA). Serum creatinine and aminotransferase levels were measured with commercial kits according to the manufacturer's instructions. Kidney tissues were fixed with 10% paraformaldehyde and embedded in paraffin. They were cut into 3μm tissue sections and stained with PAS methods. The stained renal tissue sections were examined and scored by pathologists under an optical microscope.

All mouse care and experiments were approved by the Institutional Animal Care and Use Committee (IACUC) of Nanfang Hospital. All experimental procedures and animal care were carried out under the guidance of the Ethics Committee to minimize the suffering of animals.

Immunohistochemistry and immunofluorescence staining

For IHC staining, formalin-fixed and paraffin-embedded small intestine sections were incubated with primary antibodies against IgA (Abcam, ab97234) and analyzed using streptavidin peroxidase detection system (Maixin) according to the manufacturer's protocol. DAB (Maixin) was used as an HRP-specific substrate. Staining intensity for IgA was ranked using a 5-point scale from 0 (unstained) to 4 (very intensively stained). The histopathological evaluations were performed by three independent pathologists. Every group and tissue examination were blinded.

The kidney and small intestine tissue for IF staining was cut into frozen sections and fixed with acetone for 1 min. After fixation, they were blocked with 2% bovine serum albumin diluted by PBS at room temperature for 1 h. They were washed with PBS three times and incubated with FITC-labelled goat anti-mouse IgA (Abcam, ab97234) at 37°C for 40min. After washing with PBS three times, they were mounted with anti-quenching tablets and observed under a confocal microscope. Cell nuclei were stained with DAPI. Images were quantified by counting the number of positive nuclei and divided by the total number of nuclei.

Statistical analysis

All data were analyzed by the SPSS18.0 statistical software. A two-tailed, unpaired, or paired Student t-test was used to compare the variables of two groups, and one-way or two-way ANOVA was performed for multi-group comparisons. With homogeneity of variance between two groups, the LSD test was used. With the heterogeneity of variance between groups, the Games-Howell test was employed. Co-localization of IF and the analysis of mean of interest of domain (IOD) in IHC staining were calculated with Image-Pro Plus. $P < 0.05$was noted statistically different. Statistical details are included in the respective figure legends.

Results

Preparation and characterization of DexP-packaging EVs

Extracellular vesicles were isolated from orange juice using the ultra-high-speed centrifugation method (Figure 1A). Negatively stained cup-shaped membrane nanovesicles of 100

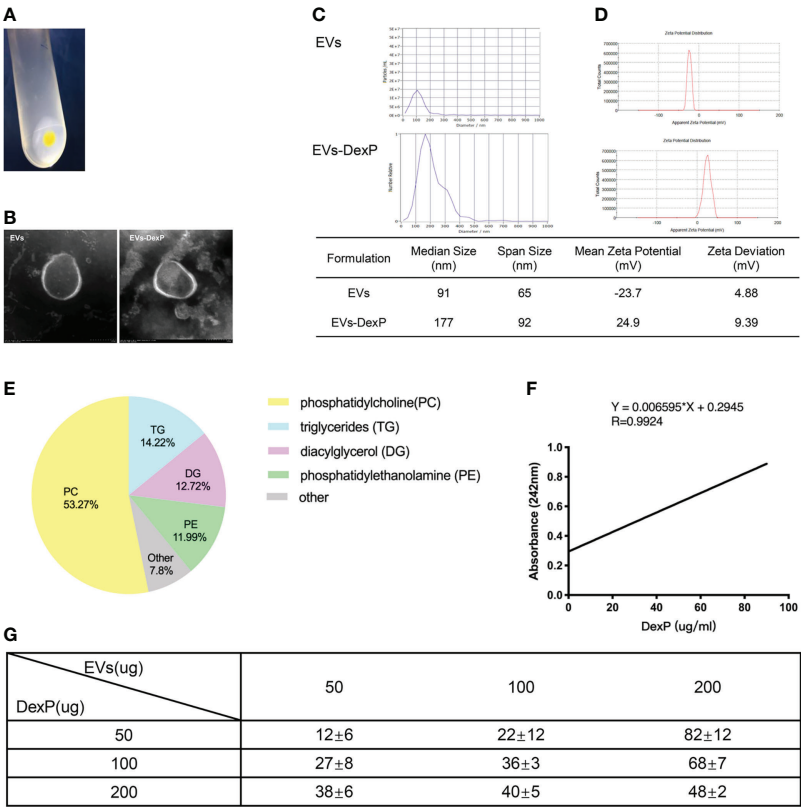

Formulation	Median Size (nm)	Span Size (nm)	Mean Zeta Potential (mV)	Zeta Deviation (mV)
EVs	91	65	-23.7	4.88
EVs-DexP	177	92	24.9	9.39

G

EVs(ug) / DexP(ug)	50	100	200
50	12±6	22±12	82±12
100	27±8	36±3	68±7
200	38±6	40±5	48±2

FIGURE 1
Characterization of EVs and EVs-DexP. **(A)** EVs pellets extracted from orange juice by ultra high-speed centrifugation. **(B)** Electron microscopic image of EVs and EVs-DexP. **(C)** Size distribution of EVs and EVs-DexP. **(D)** Zeta potential of EVs and EVs-DexP. **(E)** LC-MS-based lipid profiling of orange-derived EVs. **(F)** The standard curve was determined by varying concentrations of DexP and its corresponding absorbance at 242 nm using a UV-spectrophotometer. **(G)** Entrapment Efficiency (EE) at different concentrations of DexP and EVs *via* electroporation (time constant=10 ms and voltage=300V). EE (%) = (total amount of DexP added - unencapsulated DexP)/total amount of DexP added *100%.

to 150 nm were discovered using electron microscopy (Figure 1B). By BCA quantification, we obtained 5.65 ± 0.51mg of total protein in 758.4 ± 30.3mg pellets from 100ml juice. There were 1.1×10^{11} particles in 100μg/ml EVs suspension, and the median size of EVs was 91nm according to NTA (Figure 1C). Zeta potential ranging -23.7 ± 4.88 were examined by dynamic light scattering (DLS) (Figure 1D). Orange-derived EVs had 53.27% phosphatidylcholine and comparatively low triglycerides (14.2%), diacylglycerol (12.7%), and phosphatidylethanolamine (12.0%), according to LC-MS lipid profiling (Figure 1E).

Electroporation is a process in which a hydrophilic pore is formed in the cellular membrane in a condition of an external electric field, allowing chemicals, DNA, RNA, or drugs to flow through. Membrane integrity quickly recovers after drug loading into the vesicle interior through transient holes. Because dexamethasone is lipid-soluble and EVs are made up of a (phospho) lipid bilayer, it's challenging to encapsulate Dex intravesicular rather than sandwiched between double-membrane structures or residing at their bilayer surface. Thus, we chose its water-soluble pro-drug dexamethasone phosphate (DexP) to be encapsulated, which is known to be processed in phagocyte lysosomes to deliver active dexamethasone into the cell cytoplasm. After drug loading, EVs still maintained the integrity of the double membrane structure (Figure 1B), with the size increased from 91 to 177nm (Figure 1C) and the mean zeta potential changed to 24.9 mV (Figure 1D). We investigated the encapsulation efficiency (EE) at various concentrations of EVs and DexP in a 200ul electroporation buffer system with a time constant of 10ms and a voltage of 300V. We firstly constructed the standard curve of absorbance values for different DexP concentrations in electroporation buffer (Figure 1F), and ecapulated DexP content was calculated accrording to the detected absorbance at 242nm using UV-spectrophotometry after the EVs membrane was ruptured. When 50ug or 100ug DexP is introduced, EE raises as the amount of EVs increases from 50ug to 200ug. When the amount of DexP was larger than or equal to the amount of EVs at 200ug, however, the proportional increase was reduced. When the EVs: DexP concentration ratio was 1:2 or even 1:4, the

optimal encapsulation efficiency was calculated to be 70-80% (Figure 1G).

Stability, safety, and distribution of orally administered EVs

To test physicochemical stability, we incubated EVs in different PH environments and simulated gastrointestinal fluids for two hours (Figure 2A). The size of EVs slightly increased both in an acidic solution (PH=2) and in an alkaline solution (PH=8). EVs surface at neutral PH or in an acid environment was negatively charged, but weakly positive charged in an alkaline environment. Of note, incubation in gastric and intestinal enzymatic solution did not affect the heterogeneity of diameter and stability of the colloidal dispersion. In terms of drug safety, mice administrated with EVs preserved good hepatic or renal function, either orally or intravenously (Figures 2B–D).

To trace the biodistribution of EVs *in vivo*, we labeled EVs with the lipophilic dye Dil and performed FRI *ex vivo* scans of the gastrointestinal tract and other organs. Fluorescence accumulated predominantly in the ileocecum 2 to 4 hours after gavage (Figure 2E). Immunofluorescence colocalization results demonstrated that Dil-labeled EVs were co-stained with submucosa $CD4^+$T cells, $CD11b^+$ follicular dendritic cells, and $CD11c^+$macrophages in the jejunum (Figure 2F) and ileum (Figure 2G).

EVs-DexP inhibits lymphocytes activation *in vitro*

Flow cytometry revealed that DexP and EVs-DexP could considerably inhibit ConA stimulation on PPs lymphocytes (Figure 3A), although the difference between ConA+DexP and ConA or ConA+EVs was not statistically significant (ConA+DexP vs. ConA+EVs: g58.48 vs. 63.55, p=0.1265). EVs-DexP presented a more significant suppressing effect compared to DexP in that the proportion of $CD4^+CD69^+$ cells was dramatically reduced by EVs-DexP (ConA+DexP vs. ConA+EVs-DexP: 58.48% vs. 50.98%, p=0.0175). In addition, the CCK-8 experiment showed similar results (Figure 3B).

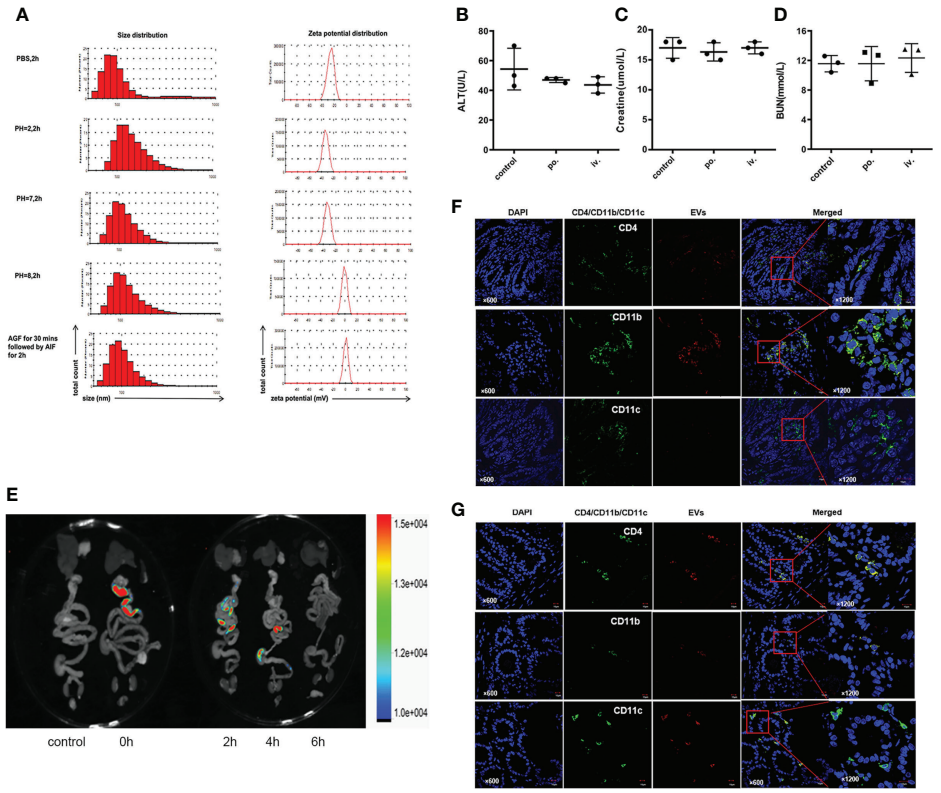

FIGURE 2
Stability and safety of EVs. **(A)** Size and zeta potential of EVs in different PH solutions and artificial gastrointestinal fluid. **(B–D)** Impact of EVs on liver and kidney function through oral and intravenous administration. Oral is abbreviated as po.; intravenous is abbreviate as iv.**(E)** Biodistribution of Dil-labeled EVs after gavage in the mouse. **(F, G)** Colocalization of Dil-labeled and $CD4^+$T cells, $CD11b^+$ follicular dendritic cells, and $CD11c^+$macrophages in jejunum and ileum. Representative staining images of CD4, CD11b, CD11c (green), EVs (red) and DAPI(blue); scale bars, 10μm.

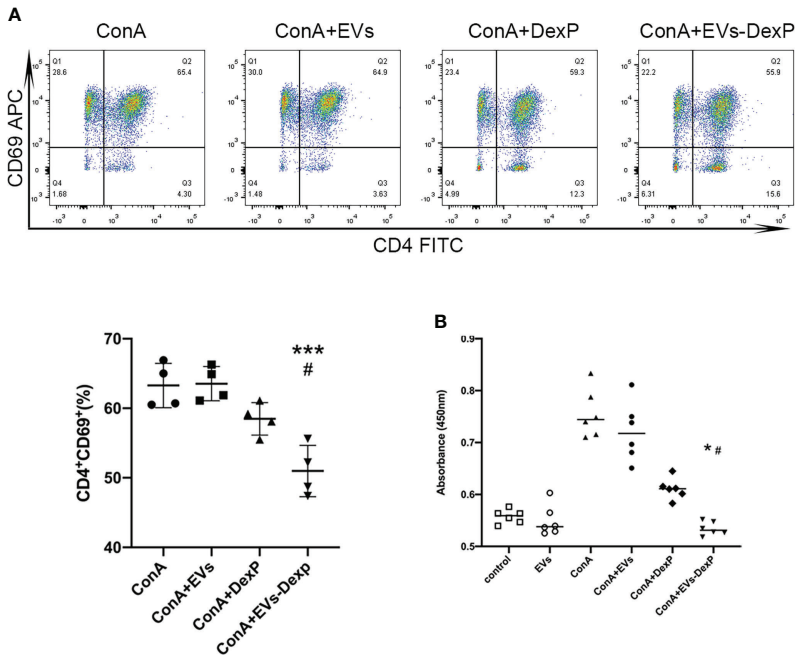

FIGURE 3
EVs-DexP inhibits lymphocytes activation *in vitro*. **(A)** Flow cytometry analysis of $CD4^+CD69^+$ population after the DexP or EVs-DexP treatment of PPs lymphocytes activated by ConA. From left to right, living cells, $CD3^+$ cells, $CD4^+CD69^+$cells are detected. **(B)** CCK-8 assay showing the effect of EVs, DexP and EVs-DexP on PPs lymphocyte proliferation after co-culture for 24h. Data are presented as mean ± SD, * p<0.05 vs. ConA+EVs, *** p<0.001 vs. ConA+EVs, # p<0.05 vs. ConA+DexP; one-way ANOVA.

Therapeutic efficacy of EVs-DexP in IgAN mice

In this study, we successfully constructed an IgAN mouse model using oral bovine serum albumin combined with intravenous staphylococcal enterotoxin B. The urinary albumin/creatinine ratio (ACR) was significantly higher after modeling (control vs. IgAN: 22.4 vs. 173.3 ug/mg, p<0.001) (Figure 4A). Light microscopy revealed mild to moderate mesangial cell proliferation, as well as immunofluorescence presenting granular deposition of IgA in the mesangial area, as shown in the second row of graphs in Figure 4E.

During IgAN modeling, DexP or EVs-DexP was given every other day from the beginning of the 6th week to the end of the 12th week. Both DexP and EVs-DexP treatment reduced urine protein to varied degrees, as shown in Figure 4B by the ACR difference before and after treatment (IgAN vs. DexP treatment: 173.3 vs.126.1 ug/mg, p=0.420; IgAN vs. EVs-DexP treatment: 173.3 vs. 84.3 ug/mg, p=0.037). EVs-DexP seemed to alleviate proteinuria to a more considerable extent than DexP despite no significant statistical difference in ACR (DexP treatment vs. EVs-DexP treatment: 126.1 vs. 84.3ug/mg, p=0.523) (Figure 4B). Hepatic aminotransferase (Figure 4C) and serum creatine (Figure 4D) fluctuated within normal limits in the course of modeling and treatment.

As seen in Figure 4F, the IgAN mice displayed diffuse mild to moderate mesangial cell proliferation with focal segmental hyperplasia and occasional sclerosis, graded as Lee's grade III. DexP treatment resulted in less extent of mesangial proliferation and IgA intensity than IgAN counterparts, especially the IgAN mice given EVs-DexP only displayed mild segmental mesangial proliferation with faint IgA deposition, scoring Lee's grade I-II.

EVs-DexP decreased intestinal IgA^+ lymphocytes

IgA-secreting plasma cells have been discovered to derive from the antigen-specific IgA-committed B cells in PPs. IgA can be expressed in activated B lymphocytes, plasmablasts, and mature plasma cells. B220 is a surface antigen molecule primarily expressed on B lymphocytes (IgA^+ $B220^+$cells) and fades when B cells develop into mature plasma cell (IgA^+B220^- cells). We then examined the immunophenotype alterations of lymphocytes in PPs of each group. As seen in Figure 5, the ratio of IgA^+ $B220^+$ in PPs was much higher in the IgAN group, whereas DexP and EVs-DexP were able to drastically lower this ratio (IgAN vs. DexP treatment: 8.37% vs. 6.44%, p=0.275; IgAN vs. EVs-DexP treatment: 8.37% vs. 3.98%, p=0.016). However, the difference in the ratio of IgA^+B220^+ cells in PPs was marginal

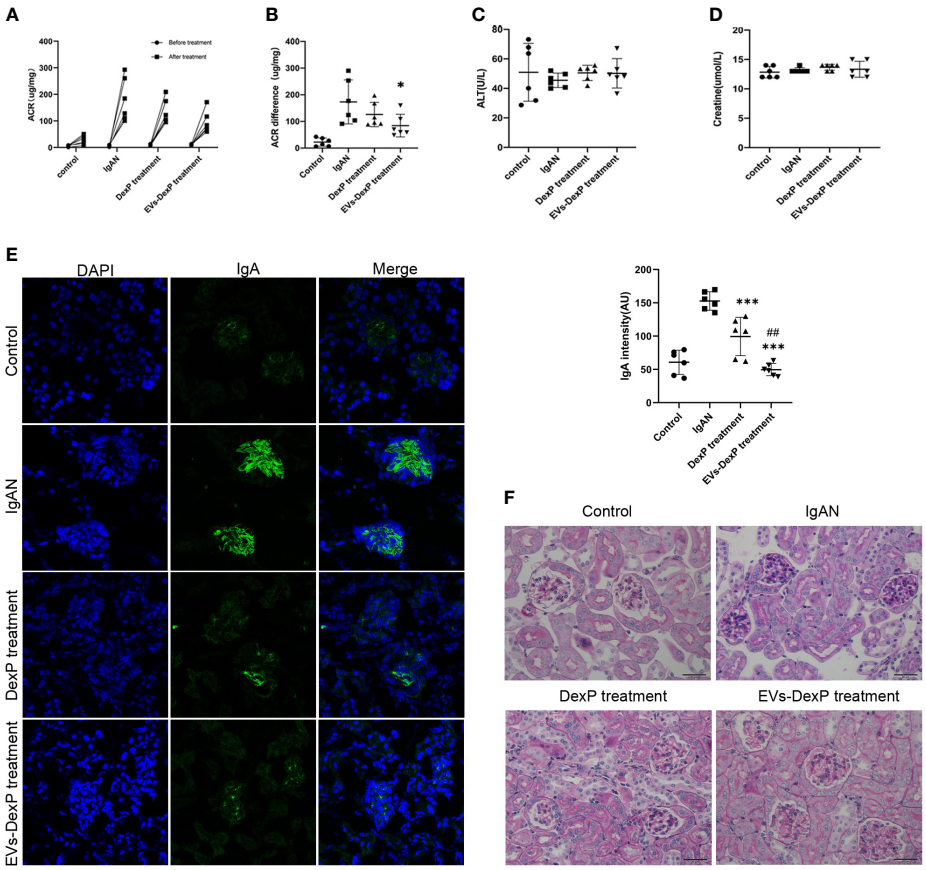

FIGURE 4
Improved therapeutic efficacy of EVs-DexP in IgAN mice. Twenty-four mice were randomized into four groups: control, IgAN model, IgAN receiving DexP treatment, and IgAN receiving EVs-DexP treatment. n=6 mice per group. **(A, B)** Spot-urine sample was collected before modeling and at the end of 12 weeks for urinary albumin/creatinine ratio(ACR) analysis. **(C, D)** Hepatic aminotransferase and serum creatine levels were measured at the end of 12 weeks. **(E)** Confocal images of immunofluorescence. IgA-FITC (green), DAPI was used to stain the nuclei (blue); scale bars, 75μm. **(F)** PAS staining images of glomerular; scale bars, 20μm. * p<0.05 vs. IgAN mice; ***p<0.001 vs. IgAN mice; ## p<0.01 vs. DexP treatment; one-way ANOVA.

between the two treatment groups (DexP vs. EVs-DexP: 6.44% vs. 3.98%, p=0.216).

EVs-DexP reduced intestinal IgA synthesis

LIGHT is a costimulatory molecule expressed on activated T cells. In the PPs of IgAN mice, the percentage of $LIGHT^+CD4^+$ cells were decreased by both DexP and EVs-DexP (IgAN vs. DexP treatment: 21.05% vs. 11.97%, p<0.0001; IgAN vs. EVs-DexP treatment: 21.05% vs. 7.31%, p<0.0001). EVs-DexP exhibited stronger suppressive effect than DexP (DexP vs. EVs-DexP treatment: 11.97% vs. 7.31%, p=0.0318) (Figure 6A). Immunohistochemistry of the intestine (PPs removed for flow cytometry assay) revealed that IgA staining of the IgAN group was much stronger than the other two treatment groups, and EVs-DexP could significantly reduce IgA production (Figure 6B).

Discussion

In this study, we successfully developed an extracellular vesicles-based delivery system encapsulated with dexamethasone (EVs-DexP), which displayed advantages over DexP in alleviating renal IgA deposition, reducing intestinal IgA production, accompanied by decreased ratio of IgA^+B220^+ lymphocytes in Peyer's patches.

Clinical observations elicited interest in mocosal immunity in patients with IgAnephropathy that those who experience episodes of gross hematuria often have a history of upper respiratory or intestinal preceding infection. Inflammatory bowel diseases such as ulcerative colitis and Crohn's disease

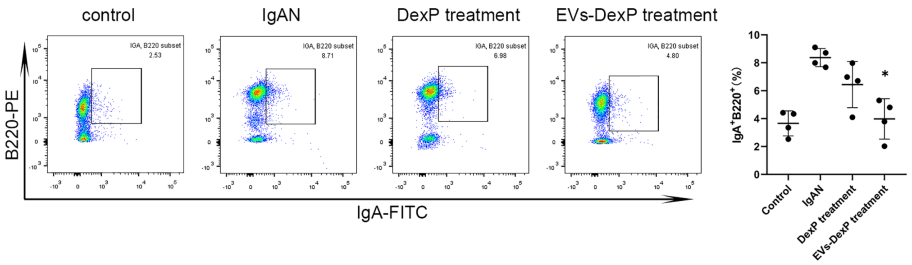

FIGURE 5
Effect of EVs-DexP on IgA$^+$lymphocytes immunophenotype in PPs. Flow cytometry analysis of the ratio of IgA$^+$ B220$^+$ cells in PPs from different intervention groups of IgAN mice. n=4 mice per group.* p<0.05 vs. IgAN mice; one-way ANOVA.

are often combined with IgA nephropathy (11, 12).Besides, IgAN susceptibility loci can be divided into two categories according to the relationship with the intestinal disease (13, 14): the first category share with inflammatory disease (IBD) susceptibility loci such as HLA-DQ/DR, CARD9 and HORMAD2; the second involves genes encoding for the maintenance of intestinal immune barrier integrity and regulation of intestinal mucosal immune response such as DEFA, TNFSF13, VAV3, ITGAM-ITGAX and PSMB8. Based on a better knowledge of mucosal immunity, B cell activation, and complement activation in IgA nephropathy, several clinical studies of targeted treatments are currently underway. B cell–depleting therapy with rituximab, which was originally developed for the treatment of rheumatoid arthritis and B cell malignancies, is an appealing therapeutic option, especially because B cells may be involved in the production of galactose-deficient IgA1 and its antibodies in IgA nephropathy. Despite the fact that rituximab effectively reduced CD19$^+$B cells, it did not improve eGFR or reduce proteinuria when compared to supportive therapy.

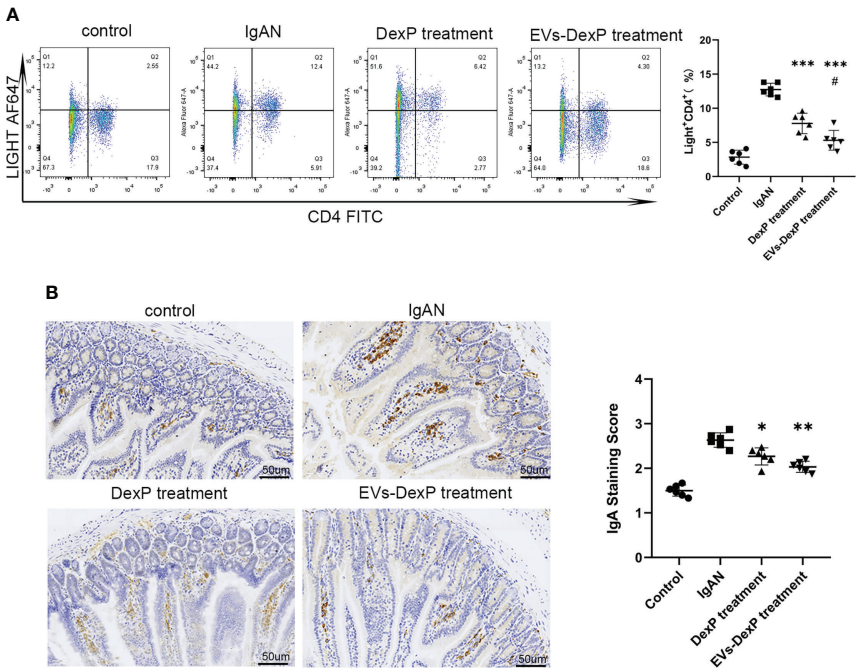

FIGURE 6
Effect of EVs-DexP on intestinal IgA production. **(A)** Flow cytometry analysis of the ratio of LIGHT$^+$CD4$^+$ cells in PPs from different intervention groups of IgAN mice. **(B)** Immunohistochemical staining intensity of IgA in the intestine; scale bars, 50μm. Data are presented as mean ± SD of six independent mice per group. *p<0.05 vs. IgAN mice, **p<0.01 vs. IgAN mice,*** p<0.001 vs. IgAN mice; # p<0.05 vs. DexP treatment; one-way ANOVA.

Furthermore, neither the serum levels nor the antibodies of galactose-deficient IgA1 were lowered (15). Interestingly, rituximab had no beneficial benefits in patients with ulcerative colitis (16), comparable to the results in IgA nephropathy. More notably, a novel enteric capsule formulation of the locally acting glucocorticoid budesonide (Nefecon) has gained much interest in phase 2a (17) and 2b (18) trials, in light of its considerable effect on urine albumin excretion through inhibiting intestinal immune activity. It was made to release the active component in the distal part of the ileum and the proximal part of the colon, where the Peyer's patches are located. In addition, this targeted release corticosteroids for IgA nephropathy were well tolerated when compared to systemic corticosteroids. The failure of rituximab and the clinical success of Nefecon in IgA nephropathy suggests a relationship between rituximab-resistant mucosal B cells and the continued production of IgA1, and supports the significance of mucosal immunity in IgA nephropathy.

Glucocorticoids have been a cornerstone of treatment for inflammatory and autoimmune renal disease. Because the available clinical evidence (2, 3) suggests a significant risk of toxicity associated with high-dose corticosteroid therapy in IgAN, the KDIGO guidelines state that "clinical benefit of corticosteroids in IgAN is not established and should be given with extreme caution or avoided entirely in the situations". The challenge for improving IgAN treatment is to strike a balance between efficacy and risk of systemic steroid-based regimens. Dexamethasone (Dex) is one of the highly potent glucocorticoids applied to treat a broad spectrum of allergic, hematologic, and autoimmune diseases. Regarding its long half-life (36-54 hours) and significant adrenal suppression, Dex is rarely prescribed to treat glomerulonephritis compared to short-acting prednisone or methylprednisone. However, low dosage and local application have been proven to exert its anti-inflammation effect while alleviating adverse effects occurring in systemic administration, such as infection, osteoporosis, and hyperglycemia.

Extracellular vesicles are a highly heterogeneous class of vesicles released by all types of cells for the purpose of mediating intercellular communication. EVs are taken up by the target cells when utilized as drug delivery vehicles. Edible plant nanoparticles (19) were reported to be similar in sizes and structures to mammalian derived EVs, possessing a stable physicochemical property, biosafety, and large-scale production. Therefore, they have garnered growing interest as promising new candidates in the field. Ju et al. (20) published the first report that grape exosome-like nanoparticles can penetrate the intestinal mucus barrier, be taken up by mice intestinal stem cells. Wang et al. (21)illustrated that grapefruit-derived nanovesicles were preferentially taken up by intestinal macrophages and ameliorated DSS-induced mouse colitis. Oral administration provides lots of advantages over other administration methods, the most compelling of which is a reduction in systemic exposure. We found that orange-derived EVs maintained their stability in the gastrointestinal tract, which is crucial for the oral delivery approach applied to treat other diseases that require steroid minimization. Following gavage, orange-derived EVs accumulated in the ileocecum of mice, where they were picked up by dendritic cells and monocytes located in the submucosal PPs. This motivated us to design a targeted oral formulation for IgAN that acts on intestinal lymphocytes.

Therefore, we attempted to encapsulate orange-derived EVs with water-soluble DexP. *In vitro*, we confirmed that EVs-DexP had a more potent suppressive effect on stimulated lymphocytes than DexP. Notably, in the IgAN mouse model, as compared to the free DexP, EVs-DexP displayed advantages over DexP in reducing proteinuria and alleviating mesangial hyperplasia and IgA deposition, even though albuminuria following therapy was not statistically significant in both groups. Munagala and colleagues (22) identified bovine milk as a scalable source of exosomes capable of delivering chemotherapeutic agents. In their report, drug-loaded exosomes showed much greater effectiveness in cell culture experiments and against lung tumor xenografts *in vivo* when compared to a free drug. Subsequently, they demonstrated that milk-derived exosome loading with antitumor agents might serve as an alternative to conventional intravenous treatment to boost efficacy and minimize toxicity (23, 24). In accordance with the findings of earlier studies (25), we assume that exosomes improve the benefit/risk ratio of medications by enhancing their bioavailability, selectivity, and effectiveness in the target tissue while reducing the required doses and minimizing adverse effects to healthy tissues.

As the induction site of mucosal immunity, PPs are lymph nodes structured into a subepithelial dome rich in $CD11c^+$ dendritic cells, T cell-rich interfollicular zones, and B cell-rich follicles with a high frequency of IgA^+ cells. B lymphocytes undergo allotype conversion to IgA^+ B lymphocytes in PPs when they are at rest. Unlike the spleen and other lymph nodes, IgA secreting B lymphocytes in PPs do not directly differentiate into mature plasma cells in PPs, but rather leave at plasma blast stage, lose their B lymphocytes label, enter into lymphocyte recycling, and eventually reach the lamina propria of the small intestine, where they develop further into mature plasma cells (26). Following EVs-DexP exposure, IgA^+B220^+ lymphocytes in PPs decreased, and the intestine secreted less IgA. As a consequence, we reasoned that EVs-DexP reduced proteinuria and IgA deposition was directly related to decreased intestinal IgA production by dampening the activation of IgA^+ B cells in PPs.

The synthesis of IgA in mucosal areas is initiated by T lymphocyte-dependent B cell responses or T-cell independent mechanisms. The IgA produced in a T-dependent manner is like a general response establishing specific immunity induced by pathogens with protective high-affinity. The IgA produced by B-lymphocytes in a T-independent context is often against

commensal bacteria sharing an interspecies reactivity. LIGHT (homologous to lymphotoxin, exhibits inducible expression, competes with herpesvirus glycoprotein D for HVEM on T cells), a member of the TNF superfamily (TNFSF14), is a proinflammatory cytokine and potent costimulatory molecule (27)expressed on activated T cells (28). Previous findings establish a crucial role for LIGHT in T cell activation *via* direct stimulation of neighboring T cells (27). Wang et al. demonstrate a direct contribution of T cell-mediated mucosal immunity in the development of IgAN (29). In their study, LIGHT transgenic mice acquired intestinal inflammation with dysregulated polymeric IgA production, transportation, and clearance caused by T cells. This model produced elevated levels of polymeric IgA, anti-DNA IgG, and IgA antibodies, as well as IgA and C3 mesangial deposition accompanied by proteinuria and hematuria, highlighting a direct role of T-cell-mediated mucosal immunity to IgAN pathogenesis. In mice with a human LIGHT transgene expressed under the control of the CD2 promoter (30), T lineage cells constitutively express the transgene-derived LIGHT, and as a result, the mice developed inflammation and tissue destruction. The inflammation in the intestine was particularly severe. This correlated with other changes in the mucosal immune system, such as selective increases in lamina propria B cells and increases in serum IgA, despite decreases in B lymphocytes elsewhere. The T cell-mediated terminal differentiation of plasma cells to IgA secretion are up-regulated during inflammation. Similar to the previous reports, our findings demonstrated that the IgAN animals had a higher ratio of $LIGHT^+CD4^+$ cells and IgA^+B220^+ cells, and that EVs-DexP repressed both, indicating that intestinal IgA production was reduced *via* a T-cell-dependent mechanism.

Conclusions

In conclusion, our research revealed the stability, safety, and capacity to target intestine lymphocytes of orange-derived EVs as an oral drug delivery vehicle. Notably, EVs encapsulated with DexP displayed advantages over free DexP in inhibiting lymphocyte activation, reducing proteinuria, and alleviating renal pathological lesions in IgAN animals. Given their potential use in clinical practice, further investigation on dose-response, pharmacokinetics, and adverse effects analysis is warranted. In that oranges are a widely available and economically reliable source for EVs, and dexamethasone is a common and highly potent glucocorticoid, the EVs-DexP oral formulation is expected to serve as an alternative for steroid-based therapy, enhancing efficacy while minimizing systematic exposure. Our findings contribute to a better understanding of the importance of intestine immune in the development of IgAN.

Data availability statement

The original contributions presented in the study are included in the article/Supplementary Material. Further inquiries can be directed to the corresponding author.

Ethics statement

The animal study was reviewed and approved by the Institutional Animal Care and Use Committee (IACUC) of Nanfang Hospital.

Author contributions

WZ and GW conceptualized and supervised the study. WZ and YY performed experiments and wrote the manuscript. XL and LY isolated EVs and performed characterization analysis and drug loading. JL and ZZ performed renal tissue sectioning, staining, and pathology scoring. All authors contributed to the article and approved the submitted version.

Funding

The research was funded by the National Natural Science Foundation of China (No. 81870489).

Conflict of interest

The authors declare that the research was conducted in the absence of any commercial or financial relationships that could be construed as a potential conflict of interest.

Publisher's note

Supplementary material

The Supplementary Material for this article can be found online at: https://www.frontiersin.org/articles/10.3389/fimmu.2022.900963/full#supplementary-material

SUPPLEMENTARY FIGURE 1
Graphical abstract. We obtained a considerable amount of EVs from oranges as an oral drug delivery vehicle targeting intestinal lymphocytes. EVs encapsulated with DexP displayed advantages over free DexP in inhibiting lymphocyte activation, reducing proteinuria, and alleviating renal pathological lesions in IgAN animals. EVs-DexP oral formulation is likely to serve as an alternative for traditional steroid-based therapy for IgAN, improving efficacy while minimizing systematic exposure.

SUPPLEMENTARY FIGURE 2
FACS gating strategy of $CD4^+CD69^+$ population after the DexP or EVs-DexP treatment of PPs lymphocytes activated by ConA.

SUPPLEMENTARY FIGURE 3
FACS gating strategy of IgA^+B220^+ cells in PPs.

SUPPLEMENTARY FIGURE 4
FACS gating strategy of $LIGHT^+CD4^+$ cells in PPs.

References

1. Coppo R. Clinical and histological risk factors for progression of IgA nephropathy: An update in children, young and adult patients. *J Nephrol* (2017) 30(3):339–46. doi: 10.1007/s40620-016-0360-z

2. Schena FP, Manno C. Intensive supportive care plus immunosuppression in IgA nephropathy. *N Engl J Med* (2016) 374(10):992. doi: 10.1056/NEJMc1600141

3. Lv J, Zhang H, Wong MG, Jardine MJ, Hladunewich M, Jha V, et al. Effect of oral methylprednisolone on clinical outcomes in patients with IgA nephropathy: The TESTING randomized clinical trial. *JAMA* (2017) 318(5):432–42. doi: 10.1001/jama.2017.9362

4. Magistroni R, D'Agati VD, Appel GB, Kiryluk K. New developments in the genetics, pathogenesis, and therapy of IgA nephropathy. *Kidney Int* (2015) 88 (5):974–89. doi: 10.1038/ki.2015.252

5. Coppo R. The intestine-renal connection in IgA nephropathy. *Nephrol Dial Transplant* (2015) 30(3):360–6. doi: 10.1093/ndt/gfu343

6. Kalluri R, LeBleu VS. The biology, function, and biomedical applications of exosomes. *Science* (2020) 367(6478):eaau6977. doi: 10.1126/science.aau6977

7. de Jong OG, Kooijmans SAA, Murphy DE, Jiang L, Evers MJW, Sluijter JPG, et al. Drug delivery with extracellular vesicles: From imagination to innovation. *Acc Chem Res* (2019) 52(7):1761–70. doi: 10.1021/acs.accounts.9b00109

8. Zhang M, Viennois E, Xu C, Merlin D. Plant derived edible nanoparticles as a new therapeutic approach against diseases. *Tissue Barriers* (2016) 4(2):e1134415. doi: 10.1080/21688370.2015.1134415

9. Stanly C, Fiume I, Capasso G, Pocsfalvi G. Isolation of exosome-like vesicles from plants by ultracentrifugation on Sucrose/Deuterium oxide (D2O) density cushions. *Methods Mol Biol* (2016) 1459:259–69. doi: 10.1007/978-1-4939-3804-9_18

10. Lefrancois L, Lycke N. Isolation of mouse small intestinal intraepithelial lymphocytes, peyer's patch, and lamina propria cells. *Curr Protoc Immunol* (2001) Chapter 3:Unit 3.19. doi: 10.1002/0471142735.im0319s17

11. Ambruzs JM, Walker PD, Larsen CP. The histopathologic spectrum of kidney biopsies in patients with inflammatory bowel disease. *Clin J Am Soc Nephrol* (2014) 9(2):265–70. doi: 10.2215/CJN.04660513

12. Wijarnpreecha K, Thongprayoon C, Panjawatanan P, Thamcharoen N, Pachariyanon P, Nakkala K, et al. Celiac disease and the risk of kidney diseases: A systematic review and meta-analysis. *Dig Liver Dis* (2016) 48(12):1418–24. doi: 10.1016/j.dld.2016.08.115

13. Kiryluk K, Li Y, Scolari F, Sanna-Cherchi S, Choi M, Verbitsky M, et al. Discovery of new risk loci for IgA nephropathy implicates genes involved in immunity against intestinal pathogens. *Nat Genet* (2014) 46(11):1187–96. doi: 10.1038/ng.3118

14. Gharavi AG, Kiryluk K, Choi M, Li Y, Hou P, Xie J, et al. Genome-wide association study identifies susceptibility loci for IgA nephropathy. *Nat Genet* (2011) 43(4):321–7. doi: 10.1038/ng.787

15. Lafayette RA, Canetta PA, Rovin BH, Appel GB, Novak J, Nath KA, et al. A randomized, controlled trial of rituximab in IgA nephropathy with proteinuria and renal dysfunction. *J Am Soc Nephrol* (2017) 28(4):1306–13. doi: 10.1681/ASN.2016060640

16. Ben-Horin S. Randomised placebo-controlled trial of rituximab (anti-CD20) in active ulcerative colitis. *Gut* (2012) 61(2):327. doi: 10.1136/gutjnl-2011-300398

17. Smerud HK, Barany P, Lindstrom K, Fernstrom A, Sandell A, Pahlsson P, et al. New treatment for IgA nephropathy: Enteric budesonide targeted to the ileocecal region ameliorates proteinuria. *Nephrol Dial Transplant* (2011) 26 (10):3237–42. doi: 10.1093/ndt/gfr052

18. Fellstrom BC, Barratt J, Cook H, Coppo R, Feehally J, de Fijter JW, et al. Targeted-release budesonide versus placebo in patients with IgA nephropathy (NEFIGAN): A double-blind, randomised, placebo-controlled phase 2b trial. *Lancet* (2017) 389(10084):2117–27. doi: 10.1016/S0140-6736(17)30550-0

19. Mu J, Zhuang X, Wang Q, Jiang H, Deng ZB, Wang B, et al. Interspecies communication between plant and mouse gut host cells through edible plant derived exosome-like nanoparticles. *Mol Nutr Food Res* (2014) 58(7):1561–73. doi: 10.1002/mnfr.201300729

20. Ju S, Mu J, Dokland T, Zhuang X, Wang Q, Jiang H, et al. Grape exosome-like nanoparticles induce intestinal stem cells and protect mice from DSS-induced colitis. *Mol Ther* (2013) 21(7):1345–57. doi: 10.1038/mt.2013.64

21. Wang B, Zhuang X, Deng ZB, Jiang H, Mu J, Wang Q, et al. Targeted drug delivery to intestinal macrophages by bioactive nanovesicles released from grapefruit. *Mol Ther* (2014) 22(3):522–34. doi: 10.1038/mt.2013.190

22. Munagala R, Aqil F, Jeyabalan J, Gupta RC. Bovine milk-derived exosomes for drug delivery. *Cancer Lett* (2016) 371(1):48–61. doi: 10.1016/j.canlet.2015.10.020

23. Munagala R, Aqil F, Jeyabalan J, Agrawal AK, Mudd AM, Kyakulaga AH, et al. Exosomal formulation of anthocyanidins against multiple cancer types. *Cancer Lett* (2017) 393:94–102. doi: 10.1016/j.canlet.2017.02.004

24. Agrawal AK, Aqil F, Jeyabalan J, Spencer WA, Beck J, Gachuki BW, et al. Milk-derived exosomes for oral delivery of paclitaxel. *Nanomedicine* (2017) 13 (5):1627–36. doi: 10.1016/j.nano.2017.03.001

25. Lepeltier E, Rijo P, Rizzolio F, Popovtzer R, Petrikaite V, Assaraf YG, et al. Nanomedicine to target multidrug resistant tumors. *Drug Resist Update* (2020) 52:100704. doi: 10.1016/j.drup.2020.100704

26. Craig SW, Cebra JJ. Peyer's patches: an enriched source of precursors for IgA-producing immunocytes in the rabbit. *J Exp Med* (1971) 134(1):188–200. doi: 10.1084/jem.134.1.188

27. Wang J, Lo JC, Foster A, Yu P, Chen HM, Wang Y, et al. The regulation of T cell homeostasis and autoimmunity by T cell-derived LIGHT. *J Clin Invest* (2001) 108(12):1771–80. doi: 10.1172/JCI13827

28. Mauri DN, Ebner R, Montgomery RI, Kochel KD, Cheung TC, Yu GL, et al. LIGHT, a new member of the TNF superfamily, and lymphotoxin alpha are ligands for herpesvirus entry mediator. *Immunity* (1998) 8(1):21–30. doi: 10.1016/s1074-7613(00)80455-0

29. Wang J, Anders RA, Wu Q, Peng D, Cho JH, Sun Y, et al. Dysregulated LIGHT expression on T cells mediates intestinal inflammation and contributes to IgA nephropathy. *J Clin Invest* (2004) 113(6):826–35. doi: 10.1172/JCI20096

30. Shaikh RB, Santee S, Granger SW, Butrovich K, Cheung T, Kronenberg M, et al. Constitutive expression of LIGHT on T cells leads to lymphocyte activation, inflammation, and tissue destruction. *J Immunol* (2001) 167(11):6330–7. doi: 10.4049/jimmunol.167.11.6330

Frontiers in Immunology

Explores novel approaches and diagnoses to treat immune disorders.

The official journal of the International Union of Immunological Societies (IUIS) and the most cited in its field, leading the way for research across basic, translational and clinical immunology.

Discover the latest Research Topics

See more →

Frontiers

Avenue du Tribunal-Fédéral 34
1005 Lausanne, Switzerland
frontiersin.org

Contact us

+41 (0)21 510 17 00
frontiersin.org/about/contact